LRGP-CNRS UMR 7274

Laboratoire Réactions et Génie des Procédés

Centre National de la recherche scientifique

Ressources Procédés Produits Environnement

THÈSE

Présentée pour obtenir le grade de

Docteur en Génie des Procédés et des Produits

le 15 Mai 2018 à Nancy

Par

Antonio AGUILERA MIGUEL

TRANSFERT DE MATIÈRE DANS LES MILIEUX COMPLEXES.
INGÉNIERIE INVERSE: DE LA PROPRIÉTÉ D'USAGE AU MATÉRIAU

Directeur: Pr. Christophe CASTEL

Codirecteurs: Pr. Véronique SADTLER et Dr. Philippe MARCHAL

Composition du Jury:

Examinateur: Dr. Véronique SCHMITT

Rapporteurs: Pr. Raffaella OCONE et Pr. Jack LEGRAND

Résumé élargi

La maîtrise des phénomènes de transfert de masse est une condition impérative pour l'élaboration et l'utilisation des produits formulés. L'objectif principal de cette thèse est le développement d'une ingénierie inverse appliquée à l'ingénierie des produits chimiques. Contrairement à l'ingénierie prospective, l'ingénierie inverse est généralement définie comme le processus d'examen d'un système déjà mis en œuvre afin de le représenter sous une forme ou un formalisme différent et à un niveau d'abstraction plus élevé. La notion clé est celle de représentation, qui peut être associée au concept de modèle au sens large du terme. L'objectif de ces représentations est de mieux comprendre l'état actuel d'un système, par exemple pour le corriger, le mettre à jour, le mettre à niveau, en réutiliser des parties dans d'autres systèmes, ou même le réinventer complètement. Le concept existe depuis longtemps avant les ordinateurs ou la technologie moderne, et remonte probablement à l'époque de la révolution industrielle.

Traditionnellement, l'ingénierie inverse a consisté à prendre des produits et à les disséquer physiquement pour découvrir les secrets de leur conception. Ces secrets étaient alors généralement utilisés pour fabriquer des produits similaires ou meilleurs. Elle est généralement menée pour obtenir les connaissances, les idées et la philosophie de conception manquantes lorsque ces informations ne sont pas disponibles. Dans certains cas, l'information appartient à quelqu'un qui n'est pas disposé à la partager. Dans d'autres cas, l'information a été perdue ou détruite. De toute évidence, l'application la plus connue de l'ingénierie inverse est le développement de produits concurrents. Ce qui est intéressant, c'est qu'il n'est pas aussi populaire dans l'industrie qu'on pourrait s'y attendre. C'est principalement parce qu'on pense qu'il s'agit d'un processus tellement complexe qu'il n'a tout simplement pas de sens sur le plan financier, ainsi qu'un processus long et sujet aux erreurs.

Au cours de la dernière décennie, l'utilisation croissante de nombreuses technologies nouvelles en tant que systèmes de livraison contrôlée a donné lieu à des essais et des erreurs coûteux pour la mise au point de systèmes nouveaux et efficaces. Afin de faciliter une conception et une optimisation plus rationnelle, face à l'ensemble des possibilités existantes, toute solution d'ingénierie inverse qui pourrait semi-automatiser le développement du produit apporterait une aide précieuse aux utilisateurs (scientifiques et éducateurs). Cela faciliterait l'importance essentielle de choisir les bons matériaux pour l'application correcte.

L'objectif de la thèse est de développer une méthodologie pour l'ingénierie de conception du produit basée sur l'ingénierie inverse afin de déterminer la formulation optimale à partir d'une propriété d'utilisation finale donnée, ici la libération contrôlée. La thèse est divisée en quatre chapitres, suivis d'une conclusion finale et de perspectives.

Le premier chapitre est consacré à l'approche de l'ingénierie inverse. L'ingénierie des produits chimiques est définie par la conversion des besoins des clients en produits chimiques en maîtrisant la formulation et les interactions avec le processus. Les objectifs de l'ingénierie des produits chimiques tels que définis dans la littérature peuvent être décrits en cinq étapes : 1) conversion des besoins des consommateurs aux spécifications techniques ; 2) modélisation et optimisation, conception assistée par ordinateur ; 3) capacités prédictives pour les propriétés physiques avec l'utilisation de la thermodynamique appliquée ; 4) cadre systématique et intégré pour la conception de nouveaux produits ; 5) cadre pour lier la découverte de produits aux efforts de R-D.

Un état de l'art des technologies de libération contrôlée est présenté dans ce chapitre. Différents nanoporteurs pharmaceutiques polymériques peuvent être utilisés : micelles polymères, nanocapsules, nanogels polymères, polymères, polymères ramifiés (dendrimères), nanoparticules hybrides à noyaux poreux. Pour les applications alimentaires, le type de capsules dépend de la nature des composés encapsulés. Pour les composés hydrophobes, on peut utiliser des émulsions (micro-émulsions, émulsions de Pickering) ou des supports lipidiques nanostructurés. Pour les composés hydrophiles, hydrogels, liposomes, colloïdosomes, colloïdosomes sont les différentes possibilités d'encapsulation. Il y a quatre principaux mécanismes de libération : contrôlé par diffusion, contrôlé par solvant, contrôlé par réaction chimique et contrôlé par stimuli.

La prédiction de la libération contrôlée dépend bien sûr du mécanisme en cause. Certaines équations empiriques existent, comme l'équation de Peppas. Le modèle de Hopfenberg est également un modèle empirique, capable de prendre en compte la dissolution, le gonflement et le clivage de la chaîne polymère. Un complément du dernier modèle est le modèle Cooney, qui tient compte de la géométrie des capsules. Le dernier modèle empirique est basé sur des réseaux neuronaux artificiels. Les modèles mécanistes sont généralement basés sur des équations de transfert de masse.

La deuxième loi de Fick est la base des phénomènes de diffusion. Si l'intégrité des capsules demeure, certaines expressions donnant la cinétique de la libération du médicament peuvent être trouvées dans la littérature, soit pour les réservoirs de médicaments, soit pour les dispositifs monolithiques. Pour les phénomènes de gonflement des polymères, la diffusion de l'eau dépend également de la deuxième loi de Fick, tout comme pour la diffusion du médicament. En cas de gonflement du polymère et de dissolution du médicament, le modèle de couche séquentielle est appliqué. La deuxième loi de Fick est utilisée avec des coefficients de diffusion non constants, qui sont décrits par une dépendance exponentielle de type Fujita, à la fois pour la diffusion de l'eau et de la drogue. Pour la dissolution, la cinétique de perte de masse du polymère est également prise en compte. Enfin, pour l'érosion/dégradation

des polymères, deux types de phénomènes d'érosion, en surface ou en volume, peuvent se produire en fonction de la cinétique de clivage de la chaîne polymère par rapport à la cinétique de pénétration de l'eau. La cinétique de libération tient compte du front d'érosion. Le clivage de la chaîne polymère est un processus aléatoire qui pourrait être simulé par l'approche de Monte Carlo. Le processus de transport de masse est représenté par la deuxième loi de Fick tridimensionnelle.

La conclusion du chapitre est la description du cadre de rétro-ingénierie. Elle commence par le domaine d'application (profil de produit cible) et les principes actifs correspondants. Ensuite, la deuxième étape est l'étude de la thermodynamique et des équilibres de phase, suivie d'un traitement de formulation pour obtenir un système dispersé avec des caractéristiques spécifiques. Ensuite, on procède à la modélisation théorique et à la simulation de la cinétique de libération. La dernière étape est le travail expérimental afin de tester la meilleure solution et de vérifier et améliorer les simulations.

Le chapitre 2 est consacré à l'établissement d'un modèle de transfert de masse sans paramètres d'ajustement. Le modèle de système est l'émulsion, car il est adapté à la réalisation de systèmes de distribution. Une partie de ce chapitre correspond à un article publié dans Colloïdes et Surfaces A. L'objectif de l'article est d'étudier la stabilisation de l'huile hautement concentrée dans les émulsions aqueuses (jusqu'à 94%) par des dextrans modifiés hydrophobiquement. Ces stabilisateurs permettent une longue stabilité sur l'échelle de temps malgré une cinétique plus lente, des tailles de gouttelettes plus élevées et des tensions de surface plus élevées que les autres stabilisateurs commerciaux.

Les objectifs du chapitre sont de modéliser un système pour les applications d'administration en considérant les émulsions hautement concentrées comme système modèle. Pour le flux de masse, la résistance au transfert de masse est localisée dans la couche de tensioactif, caractérisée par la perméabilité, et dans le film en phase continue autour de la gouttelette, caractérisé par un coefficient de transfert de masse. La perméabilité est obtenue à partir du produit entre la perméabilité d'une couche de désordre et un facteur représentant la diminution de la perméabilité due à l'ordre interfacial. Un domaine de variation est donné pour le coefficient de transfert de masse interfaciale dans le cas où l'épaisseur du film en phase continue est inconnue, ce qui est souvent le cas. Le coefficient de diffusion peut être estimé à partir de l'équation de Stokes-Einstein ou d'équations empiriques. Le coefficient de partage à l'équilibre thermodynamique peut être calculé à partir des coefficients d'activité.

Ces propriétés thermodynamiques peuvent être estimées à partir de techniques de conception moléculaire assistée par ordinateur (CAMD). Différentes techniques ont été utilisées dans ce travail. Parmi eux, il y a le modèle UNIFAC (Functional-group Activity Coefficients), qui permet de prédire le coefficient d'activité en phase liquide. Le modèle a une contribution

combinatoire au coefficient d'activité due aux différences de taille et de forme des molécules, et une contribution résiduelle due aux interactions énergétiques. Un modèle UNIFAC modifié (Dortmund) est proposé pour tenir compte des composés de taille très différente en changeant empiriquement la partie combinatoire. En raison de certains inconvénients du modèle UNIFAC, modifié ou non, en raison de l'absence de certains paramètres d'interaction binaires, l'utilisation du COSMOS-RS (Conductor-like Screening Model for Real Solvents) est utile pour l'évaluation de l'interaction moléculaire dans les liquides et, ensuite, pour fournir des données supplémentaires pour le modèle UNIFAC modifié. Le modèle ainsi obtenu est appelé Révision et extension 6 du modèle modifié d'UNIFAC (Dortmund). La prédiction de l'équilibre liquide-liquide permet de calculer les deux compositions de phase au moyen d'une méthode itérative de bissection, y compris le calcul des coefficients d'activité et l'intégration d'un bilan massique.

La méthode VABC (Atomic and Bond Contributions of van der Waals volume) est utilisée pour le calcul des volumes moléculaires. La viscosité du mélange liquide est calculée par un modèle UNIFAC modifié (UNIFAC-VISCO). Le volume molaire liquide au point d'ébullition normal est calculé (méthode Tyn et Callus) à partir du volume critique, qui est calculé par une méthode de contribution de groupe (méthode Joback). Le modèle de transfert de masse tient compte de la diffusion dans la gouttelette, à travers le film interfacial et dans la phase continue et l'équation résultante est basée sur la seconde loi de Fick.

Le troisième chapitre est consacré à la simulation. La première partie consiste en une vue d'ensemble du modèle ab-initio développé dans la thèse pour prédire la libération d'un principe actif à partir de l'eau dans des émulsions fortement concentrées dans l'huile avec les modèles détaillés au chapitre 2. Le modèle ab initio est développé sur MATLAB pour prédire le débit instantané de l'ingrédient actif dans les deux phases et son profil de pourcentage cumulatif.

Une analyse des structures moléculaires d'éventuels produits chimiques candidats est ensuite donnée afin de créer une cartographie des matériaux avec lesquels travailler. L'ingrédient actif choisi est l'acide mandélique. La phase dispersée est l'eau avec parfois une certaine quantité d'électrolyse (NaCl), ce qui augmente la stabilité de l'émulsion. Pour la phase continue, quatre huiles différentes ont été choisies, deux n-alcanes saturés (dodécane et hexadécane) et deux esters d'acides gras (myristate d'isopropyle et palmitate d'isopropyle). Trois types différents d'agents tensioactifs ont été choisis, avec un HLB (équilibre hydrophile-lipophile) approprié par rapport aux huiles choisies. Ce sont : un ester d'acide gras de sorbitane (monooléate de sorbitane, SPAN 80), un acide gras polyglycérisé (polyricinoléate de polyglycérol, PGPR) et un éther alkylique de polyéthylène glycol (polyoxyéthylène glycol-2-oléyléther, BRIJ 93).

Une bonne initiative consiste à proposer une analyse de sensibilité des variables. Le modèle ab-initio est utilisé pour réaliser des expériences virtuelles et le plan d'expériences virtuel (VDOE) permet de revoir l'interaction entre les variables du processus. Un plan factoriel de 64 combinaisons est d'abord analysé. Le diagramme de Pareto montre que le facteur le plus influent est la fraction de masse en phase dispersée, suivie du choix du surfactant. Au contraire, la concentration de l'ingrédient actif et le diamètre des gouttelettes ont une influence moins importante et peuvent être négligés pour des analyses futures.

Pour une analyse plus approfondie, seules quatre variables (fraction de masse en phase dispersée, rapport huile-surfactant, type d'huile, type d'huile, type de surfactant) ont été conservées pour une conception factorielle de 300 combinaisons. Le coefficient de diffusion diminue linéairement avec la fraction de masse en phase dispersée, qui est le facteur d'influence le plus important. Le rapport huile-surfactant n'a pas d'effet. L'huile de palmitate et le SPAN 80 donnent le coefficient de diffusion le plus bas. De plus, les interactions les plus prononcées de la fraction de masse dispersée sont liées au choix de l'huile ou de l'agent tensioactif, en particulier pour les faibles fractions.

Le dernier chapitre donne la validation expérimentale. Le premier point est la comparaison des coefficients de distribution prévus et expérimentaux. Les résultats montrent que la meilleure prédiction est donnée par la révision et l'extension 6 du modèle UNIFAC modifié (Dortmund). On sait que le modèle classique de l'UNIFAC est davantage consacré à l'équilibre vapeur-liquide. Un problème est le fait que, pendant les expériences, une troisième phase (un film nuageux) apparaît à l'interface. Cette troisième phase n'est pas prise en compte dans le modèle, et peut perturber la détermination de l'ingrédient actif, qui se fait par une conférence sur l'absorption des UV. Cependant, la présence de sel permet d'améliorer la prédiction, car le film interfacial devient plus étroit. La prédiction est également moins bonne pour le tensioactif BRIJ 93, mais il semble très compliqué de donner une raison justifiant ce fait en raison de déviations expérimentales.

La prédiction par la méthode UNIFAC-VISCO des viscosités du mélange est en accord avec les viscosités expérimentales pour la diminution avec l'augmentation du rapport huile/factant. Les viscosités sont largement plus élevées avec le tensioactif PGPR, mais les valeurs prévues et expérimentales présentent des différences significatives, peut-être dues à la formation de micelles dans ce cas.

Pour la comparaison de la cinétique de libération, les émulsions ont été préparées avec des diamètres de gouttelettes allant de 8 à 19 (μm). Une comparaison entre les courbes de libération prévue et expérimentale est faite pour les différentes phases huileuses et les surfactants. Certaines similitudes et différences apparaissent. La comparaison entre le coefficient de diffusion prévu et le coefficient de diffusion expérimental montre qu'un

meilleur accord est obtenu pour les émulsions préparées avec des huiles de dodécane et d'hexadécane avec SPAN 80® et PGPR® comme surfactants. Une discussion sur la raison de ce résultat devrait être utile pour la mise en œuvre de cette approche à d'autres systèmes. Les écarts entre les coefficients de diffusion expérimental et prédit sont relativement bien corrélés avec les écarts observés pour les modules de stockage expérimental et prédit.

La dernière partie du chapitre est un rapport d'analyse en composantes principales pour visualiser l'importance des variables. Le film interfacial et le coefficient de partage ont un rôle clé. La viscosité de la phase continue a un effet sur la cinétique de libération, qui pourrait être contrôlée par l'ajout d'épaississants. Certaines différences entre les prédictions et les expériences peuvent s'expliquer par la grande perméabilité de certains tensioactifs, comme par exemple le BRIJ 93®, car, dans ce cas, un transfert de masse rapide à travers la couche de tensioactif pourrait modifier les paramètres structurels en un temps plus court, conduisant alors à des instabilités non prises en compte dans le modèle.

Cette thèse est la première étape d'un projet à long terme sur la rétroingénierie appliquée à la conception de produits. Quelle est la formulation optimale pour obtenir une propriété d'utilisation finale? Cette question peut être résolue en utilisant la méthodologie développée dans ce travail pour les émulsions hautement concentrées, en ajoutant des critères commerciales. Des modèles constitutifs ont été établis pour prédire le transfert de masse de la matière active en fonction des paramètres de formulation, y compris des techniques assistées par ordinateur comme la modélisation moléculaire, ou des modèles UNIFAC pour les prévisions d'équilibre liquide-liquide et pour l'estimation de la viscosité des mélanges. L'approche d'ingénierie inverse est vraiment très intéressante pour l'ingénierie de conception de produits pour le criblage rapide possible des différentes variables influençant la cinétique de libération. Une perspective importante est d'appliquer la même méthodologie à d'autres systèmes de dissémination contrôlée.

Acknowledgements

Firstly, I would like to express my sincere gratitude to my supervisors *Christophe Castel*, *Véronique Sadtler* and *Philippe Marchal* for the continuous support of my Ph.D study and related research, for their patience, motivation, and immense knowledge. Their guidance helped me in all the time of research and writing of this thesis. I could not have imagined having better advisors and mentors for my Ph.D study.

My sincere thanks also goes to *Lionel Choplin*, who provided me an opportunity to join their team, and who gave access to the laboratory and research facilities. Without its precious support, together with *Josiane Moras*, it would have not been possible to conduct this research. A very special gratitude goes out to the *Ministère de l'Enseignement Supérieur de la Recherche et de la l'Innovation*, for helping and providing the funding for the work.

To *Charly Koenig* and *Herve Simonaire*, who helped me on the design of the pilot plant and during troubleshooting, to *Sébastien Kiesgen de Richter* and co-workers from LEMTA laboratory, who allowed me to use their technique of incoherent polarized steady light transport (AIPSLT) for emulsion characterization in my work. I extend my deepest appreciation for their helpful and expert advice, guidance, and encouragement.

I am also very indebted to *Edeluc López-Gonzalez*, *Hala Fersadou* and *Emilio Paruta-Tuarez*, because their previous work in the laboratory inspired me and helped me for the development of my thesis in the beginning.

I thank my fellow labmates; *Eve Masurel, Yaoh, Katja Huys, Mégane Poirson, Anne-Laure Bagard, Arvind Krishnan, Jiaqi Dong, Darkhan Zholtayev, Aikumis Serikbayeva, Caroline Bottelin, Assia Saker, Benjamin Lhuizière* and *Martin Meulders* for all the stimulating discussions and accompaniment, specially *Mahbub Morshed* for the sleepless nights we were working together before deadlines, and generally to all of them for the fun we have had in the last years. Also I thank my colleagues and professors from the University of Huelva. In particular, I am grateful to *Crispulo Gallegos* for enlightening me the first glance of research during my life, and being my mentor since I left the university.

Last but not the least, I would like to thank my family: my parents *Antonio* and *Mª Carmen*, and to my sisters *Alicia* and *Mª Carmen* for supporting me spiritually throughout writing this thesis and my life in general.

I would like to dedicate my dissertation to my loving parents: Antonio and Mª Carmen. They have inspired me throughout my lifetime and always inspired me to follow my passion. I am certain that I would have not been able to achieve the goals in my life without having them as a constant role model. I would like also to convey how much my grandfather Antonio meant to me when I was a kid and his unwavering love truly showed to me how amazing the human spirit can be. Today I still feel his presence within me and I know that he is still guiding me everyday through the journey of life .

Declaration

I hereby declare that except where specific reference is made to the work of others, the contents of this dissertation are original and have not been submitted in whole or in part for consideration for any other degree or qualification in this, or any other university. This dissertation is my own work and contains nothing which is the outcome of work done in collaboration with others, except as specified in the text and Acknowledgements.

Antonio AGUILERA MIGUEL

Table of contents

List of figures

List of tables

Chapter 1

TOWARDS A REVERSE ENGINEERING APPROACH

'To understand how something works, you must first take it apart and unravel its secrets. Only then, you can build something better. The process is called reverse engineering. In the future, corporations will rely on it to gain access to the competitive secrets', John Woo

1.1 Introduction

Mastery of mass transfer phenomena is an imperative condition into formulated products elaboration and their use. The main objective of this thesis is the development of a reverse engineering applied to chemical product engineering. "In contrast with forward engineering, reverse engineering is commonly defined as the process of examining an already implemented system in order to represent it in a different form or formalism and at a higher abstraction level" [29]. "The key notion is the one of representation, that can be associated to the concept of model in the large sense of the word. The objective of such representations is to have a better understanding of the current state of a system, for instance to correct it, update it, upgrade it, reuse parts of it in other systems, or even completely re-engineer it" [30].

The idea of reverse engineering has been around since some time before PCs or present day innovation, and most likely goes back to the times of the industrial revolution. Generally, reverse engineering has been tied in with taking items and physically dismembering them to reveal the privileged insights of their design. Such privileged insights were then normally used to make similar or better products. It is normally directed to acquire missing learning, thoughts, and outline logic when such data is inaccessible. "In some cases, the information is owned by someone who is not willing to share them. In other cases, the information has been

lost or destroyed. Clearly, the most well-known application of reverse engineering is for the purpose of developing competing products. The interesting point is that it is not really as popular in the industry as one would expect. This is primarily because is thought to be such a complex process that it just does not make sense financially, as well as a time-consuming and error-prone process" [31].

In the past decade, the growing use of numerous novel technologies as controlled-delivery systems has prompted a costly trial-and-error development of new and effective systems. In order to facilitate a more rational design and optimization, facing the set of existing possibilities, any reverse engineering solution that could semiautomate the product development would bring precious help to the users (formulation scientists and educators). This would facilitate the essential importance of choosing the right materials for the correct application. Starting from a final usage property (for example: a desired flow release) the main goal of this work is to develop a product design methodology which allow us to determine the optimal features for a formulation to prepare: phases in presence, composition, interface type, size and distribution of current objects, phase equilibria, diffusion within phases and evolutionary character of the material. The overall structure of this dissertation takes the form of five chapters:

- In this introductory chapter, current research challenges in chemical product design are discussed. A review of the controlled delivery technologies and their mechanisms for mass transfer is outlined. Current tools of mathematical modeling for prediction of controlled release are examined. After this, a reverse engineering framework for chemical product design is proposed.

- The second chapter begins by laying out the theoretical dimensions of the research, and looks at how to model the diffusion in a highly structured emulsion system and to handle different equilibria models between phases.

- The third chapter is concerned with the simulation. The main idea is to develop simulation tools for prediction of mass transfers within different materials. Sensitivity studies of parameters, including results obtained from modeling will allow for the establishment of a cartography.

- The fourth chapter presents different experimental validations and conclusions for tying up the theoretical and experimental parts from previous chapters.

- The final chapter of conclusions draws upon the entire thesis. It gives a brief summary and critique of the findings, and includes a discussion of the implication of the findings to future research into this area.

1.2 Research challenges in chemical product design

Chemical product design can be seen as the operational and concrete task of converting consumer needs and new technologies into new chemical products. This is a fundamental objective for modern corporations. "Confronting an inexorably focused and dynamic market, the capacity to consistently recognize client needs, and make items that address such issues is basic to business achievement" [32]. New product development combines strategic and organizational actions with technical effort; the former dealing with the management of the development process, strategic placement and launch of a new product; the latter being chiefly concerned with the design of the product and its manufacturing process.

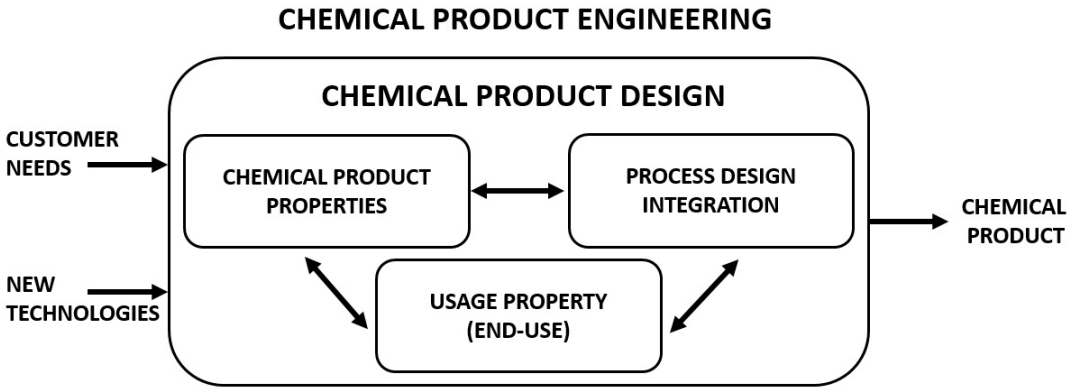

Fig. 1.1 Structure for chemical product engineering.

Chemical product engineering, designates the framework of knowledge, approaches, methodologies and tools employed to analyze, develop and produce the whole range of chemical products. "The ultimate aim of chemical product engineering is the translation of phenomelogical laws and models, expressed by property, process and usage functions, into comercial product technology" [33]. This requires the comprehension of the connection between plainly visible macroscopic and miscroscopic properties, and the capacity to combine issues over length and time scales spreading over many orders of magnitude.

From a practical point of view, the design of a new chemical product involves the embodiment of property, process and usage functions [32] (Fig. 1.1). "One first tries to find a candidate product that exhibits certain desirable or targeted behavior and then tries to find a process that can manufacture it with the specified qualities" [34]. The candidate may be a single chemical, a mixture, or a formulation of active ingredients and additives" . Examples of chemical products, such as functional chemicals (solvents, refrigerants, lubricants, etc.), agrochemicals (pesticides, insecticides, etc.), pharmaceuticals & drugs, cosmetics & personal care products, home and office products, etc., can be found everywhere.

Table 1.1 Typical forms of formulated products [23]

Physical Form	Product Form	Examples
Solid	Composites	Bar of soap
	Capsules	Whale oil capsule
	Tablets	Aspirine tablet
	Solid foams	Styrofoam
	Powders and Granules (bulk)	Powdered detergent
Semi-solid	Pastes	Toothpaste
	Creams	Pharmaceutical cream
Liquid	Liquid foams	Shaving foam
	Macromolecular solutions	Dishwashing liquid
	Microemulsions	Hair conditioner
	Dilute emulsions and suspensions	Writting ink
	Solutions	Perfume
Gas	Aerosols	Hair spray

Multifunctional products whose structure (in the range 0.1-100 μm) are specifically designed and manufactured to provide the functionality desired by customers [32]. These products, which include shaped and bulk solids, semisolids, liquids and gases (Table 1.1) have been termed formulated products, structured or dispersed systems, or chemical-based consumer products. These formulated products (e.g., pharmaceutical, cosmetic and food consumer goods) now represent a large fraction of the business. They can be defined as combined systems (typically with 4 to 50 components) designed to meet end-use requirements. They are often multifunctional (because they accomplish more than one function valued by the customer) and microstructured or engineered (since their properties derives significantly from their microstructure) [33]. The extent of the area has likewise extended to join items that are not unadulterated mixes, blends or specific materials. For example, devices that do a physical or compound change, or customer merchandise whose usefulness is given by a synthetic/physical innovation.

The performance and end-use properties of a chemical product depend on its composition, ingredients' properties, microstructure and the circumstances under which it is used [32]. Its microstructure is determined not only by the product recipe, but also by the process conditions used in its manufacture. Understanding the relations between materials, process, usage properties and different product spaces, is crucial for chemical product design. The product structure often has a preponderant influence over functionality and end-use properties. The desired product structure requires selection of the proper product ingredients, but it is often determined largely by the manufacturing process .

As Costa (2006) identified, the research challenges currently faced in chemical product engineering and design are diverse. They can be organized in terms of five generic objectives covering the development of: (1) tools to convert problem representation spaces from customer needs to technical specifications; (2) modeling and optimization approaches for chemical product design; (3) predictive capabilities for physical properties; (4) systematic approaches supporting chemical product design, and (5) frameworks to effectively link product discovery to R&D efforts. [32].

1. **Tools to convert problem representation spaces from customer needs to technical specifications**; The improvement of chemical products requires the transformation of client prerequisites into a totally specified product and its manufacturing procedure, and, thus, needs the interpretation of data between representational spaces (Fig. 1.2). The properties, process and usage properties are three of the principle columns supporting this interpretation procedure. A fruitful and quickly developing area of chemical product engineering research is the enhanced comprehension of the connection between performance, composition, ingredient properties, manufacturing variables and usage variables for frameworks of pertinence to chemical products. This is a troublesome and intriguing issue for multiphase and metastable systems with structured microstructures, for example, froths, colloids and gels, which are of specific significance in chemical product.

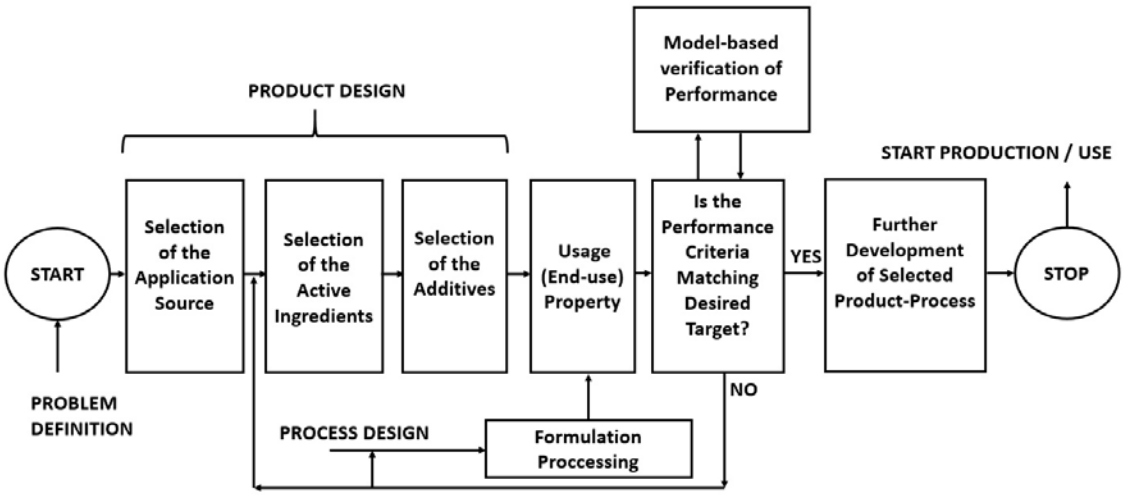

Fig. 1.2 Chemical product design as a translation of information between representational spaces.

2. **Modeling and optimization approaches for chemical product design**; Chemical engineering has focused on the development of models and optimization formulations for manufacturing processes. The background of knowledge available in this field has to be adapted and extended to address chemical product design and the integration of chemical product and process design [32]. Computer-aided molecular/mixture design (CAMD) is a promising topic of research in this field. "Essentially, it is the optimization-based solution of the inverse problem of finding a compound or a mixture of compounds possessing a set of previously specified properties" [35]. Much research work has been done in this area and a large number of references in this topic can be found, among which is the book by Achenie et al. (2002), which provides one of the first extended reviews on the subject [1].

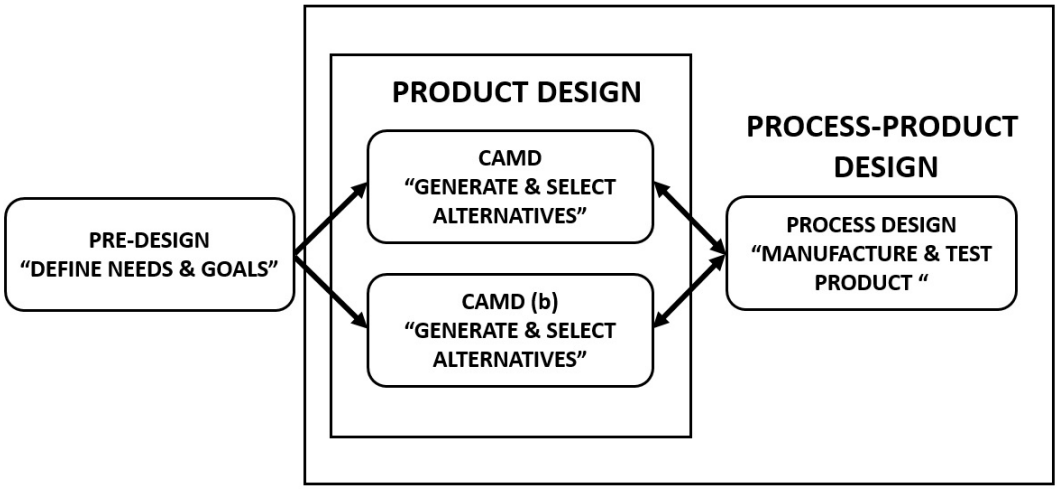

Fig. 1.3 Steps of the design process related to product design. Adapted from [1].

3. **Predictive capabilities for physical properties**; Closely related to CAMD is the need to develop capabilities to accurately predict the physical properties for compounds and mixtures [35] (Fig. 1.4). "In fact, the effective resolution of the inverse problem of finding a compound or mixture matching a set of prespecified functionalities involves the prediction of the properties associated with candidate solutions" [32]. There is a serious gap between current thermodynamic modeling capabilities to describe commodity chemicals and the understanding of more complex chemical products, such as formulated products [36]. Thus, applied thermodynamics is a promising research area in the context of chemical product engineering [37].

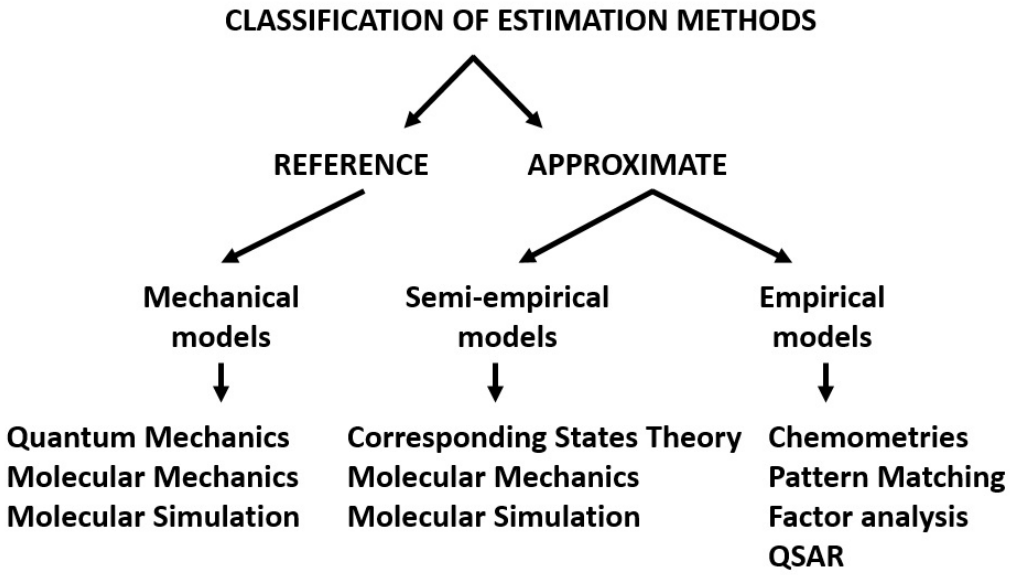

Fig. 1.4 Classification of property estimation methods. Adapted from [1].

4. **Systematic approaches supporting chemical product design**; The chemical process industries have been launching successful chemical products for a long time. However, "such products have traditionally been developed through costly and time-consuming trial-and-error design procedures" [32]. The development of a systematic and integrated framework based on identified tools, methodologies, workflow and data-flow for the inter-related activities involved in the design of new products has been recognized as one of the main research challenges in the context of chemical product engineering [38, 39]. Such a framework would not only have potential industrial application, but would also provide a significant contribution to the effective teaching of chemical product engineering [32] .

5. **Frameworks to effectively link product discovery to R&D efforts**; The optimal planning of R&D efforts and scheduling approaches aimed at a better coordination of the pipeline of new products have been emerging as an interesting research field supporting effective product discovery [39–42],

1.3 State-of-the-art of controlled release technologies

It is becoming increasingly difficult to ignore the need for optimization of the incorporation or release of active ingredients (AIs) in formulated products within food [5], pharmaceutical [2], and cosmetic [43] industries among others. The steady increase in the number of scientific publications on this topic clearly shows the importance of this problem [44].

For example, in pharmaceuticals (Fig. 1.5), "one of the main goals of release kinetics control is to maintain the drug level in blood within the therapeutic window, between the minimum effective concentration (MEC) and the minimum toxic concentration (MTC). When a drug is administered as a single large dose, the drug level is elevated above MTC, causing toxic side effects, and then rapidly drops below the MEC" [45]. Multiple dosing with a certain interval may reduce the fuctuation of drug levels in plasma but can face patient non-compliance issues. Therefore, it is desirable to develop drug carriers that provide sustained or controlled release of a drug with a low dosing frequency. [2]. For this purpose, a constant drug release rate (zero-order drug release profile) is frequently pursued [45]. On the other hand, an excessive attenuation in drug release can compromise therapeutic effectiveness of a system; therefore, pulsatile or stimuli-responsive drug release is also explored to achieve timely drug release [46].

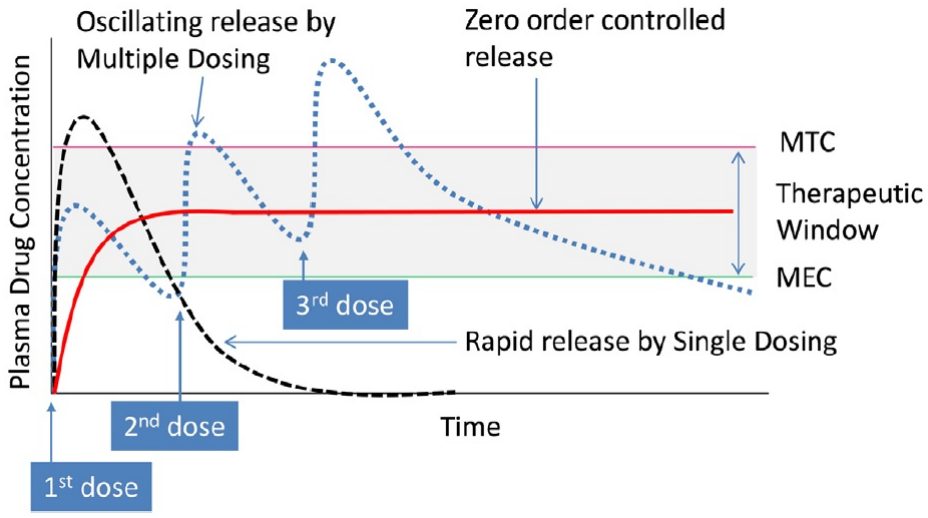

Fig. 1.5 Plasma drug concentration profiles obtained by single dosing (short dashed line), multiple dosing (dotted line), and zero order controlled release (solid line). Taken from [2].

.

In cosmetics, the transdermal delivery or local release, allows for delivery of the largest fraction of active compound molecules at the site of action [3]. The administration is easy and offers a controlled release without pain [43]. The active ingredient donor, or vehicle, is usually a cream, ointment or polymer matrix formulation, or a device containing that formulation, such as a transdermal patch. The transfer from the vehicle into the skin (dermal delivery), and eventually through it into the blood circulation system (transdermal delivery) (Fig. 1.6), depends to some extent on the vehicle properties (though in some cases it is dominated by skin resistance), and thus an appropriate design of the vehicle may be essential to control drug delivery and attain the desired therapeutic effect [16].

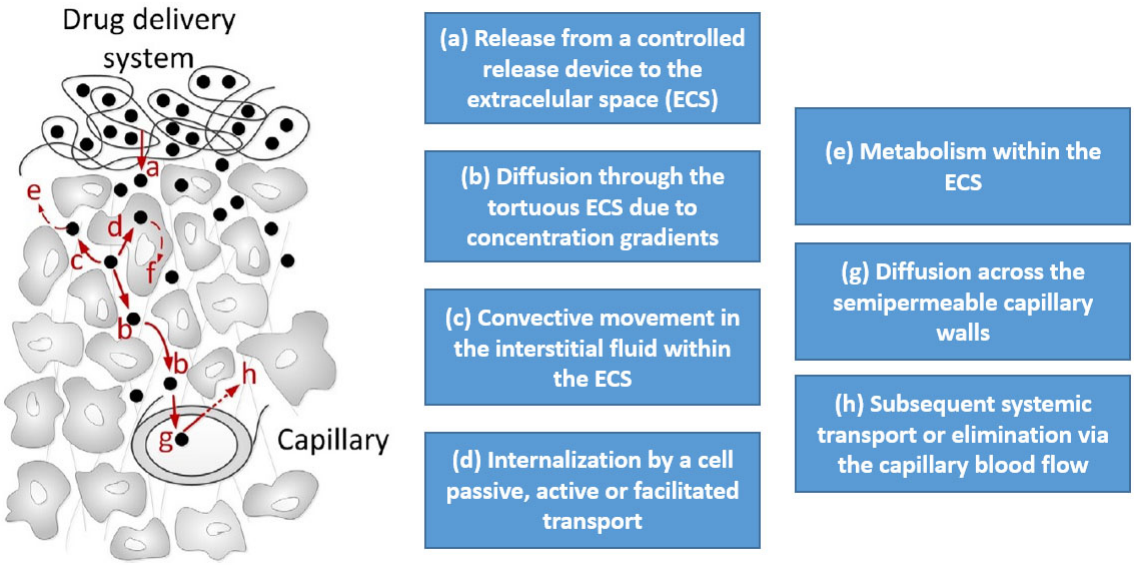

Fig. 1.6 Mechanisms of transport and elimination of an agent during controlled release from a polymeric device into a local region of tissue. The solid circles represent the therapeutic agent and the arrows represent the modes of transport and reactions that occur after release from the device (top). Taken from [3].

In food applications, the nutritional value of foods and beverages can be enhanced by incorporation of vitamins and nutraceuticals [47]. The concentration and bioavailability of flavor, scent or color agents affect sensory reactions to foods [48]. Antimicrobials and preservatives extends shelf-life [49]. However, many of these compounds have low solubility in foodstuffs, or are highly sensitive to environmental degradation agents such as free radicals, pH, and enzymes [5]. Their encapsulation concentrates the active ingredient in a protective environment, that of the carrier's interior, while also allowing control over the release profile [50].

1.3.1 Carriers developed for controlled release

To develop and design carriers with desirable release kinetics, a reasonable understanding of the mechanisms by which a carrier retains and releases an active ingredient is required. Also, it is essencial to know the effects of composition or morphology on the release, as well as current techniques for preparation. The progress in synthetic polymer chemistry has allowed the precise design of hybrid and multifunctional colloidal particles, which differ in type, size and shape, thus enhancing their possible applications as target-oriented carriers of low and high molar mass active species [4]. As Kowalczuk (2014) pointed out, pharmaceutical nanocarriers can be divided into five types differing in aspects such as structural flexibility, accesible functional groups and stability : a) polymeric micelles (PMs) from amphiphilic block copolymers that self-associate in aqueous solutions ; b) polymeric nanocapsules (PNCPs), in which the ingredient is encapsulated within the polymeric membrane ; c) polymeric nanogels (PNGs), cross-linked hydrogel nanoparticles with excellent acceptability because of the higher water content ; d) highly branched polymers, mainly dendrimers (DDs), three dimensional synthetic macromolecules in which atoms are arranged in many branches along a central backbone of carbon atoms ; and e) hybrid nanoparticles with porous cores (HNPCs). The different types are shown in Fig. 1.7.

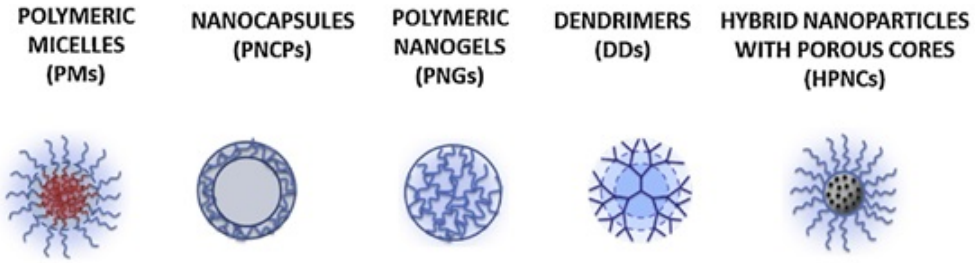

Fig. 1.7 Examples of polymeric nanocarriers used for the loading and release of active compounds. Taken from [4].

These products play a central role in varied applications such as drug delivery [51–54], medical imaging [55, 56], personal care [57, 58], microfluidics [59] and nanotechnology [60]. Nevertheless, in hindsight analysis of the progress made to date, one wonders what caused such frenzy over nanotechnology or nanoparticles in the first place. There was no evidence that nanoparticles would be better drug delivery systems than other formulations. Nanoparticles were simply assumed to have different properties from those of micro/macro particles simply because of their huge surface area. "Nanoparticles with enormous surface area may be useful for certain applications, such as increasing the dissolution rate of poorly soluble drugs, but other than that, no substantial advantages have been observed" [44].

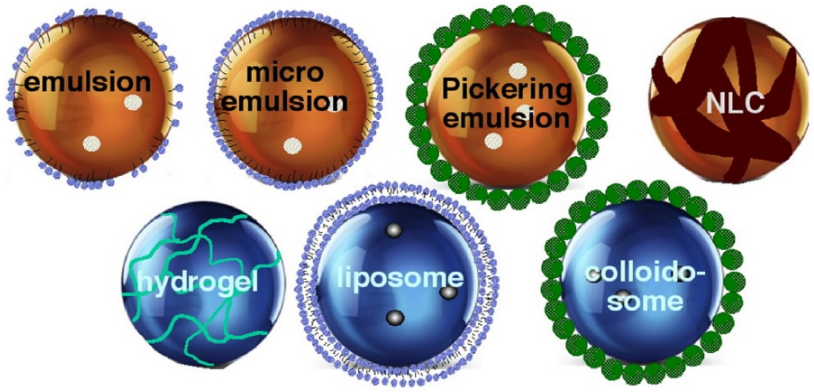

Fig. 1.8 Carriers for encapsulation of active compounds in food applications. Top: Particles with a hydrophobic core. Bottom: Particles for encapsulation of hydrophilic compounds. Blue denotes aqueous medium, light brown a liquid lipid (or oil) phase, and dark brown a solid lipid phase. Green spheres are colloidal particles, and small blue molecules are emulsifiers. Taken from [5].

In food applications, examples of carriers at nano and also microscale can be found. Most are designed to increase the effective solubility of hydrophobic compounds in aqueous-based systems or hydrophobic ones in oil-based solutions. Fig. 1.8 depicts some of the carriers that are commonly used or studied for encapsulation and release in food-related applications. As Dan (2016) mentions, hydrophobic compound encapsulation utilizes cores that may be liquid (emulsions and microemulsions), solid (solid lipid nanoparticles-SLNs), or a mix of solid and liquid domains (nano-structured lipid carriers-NLCs). Particles for encapsulation of hydrophilic substances are composed of an aqueous core, delineated from the surrounding continuous phase by a shell. This include nano-hydrogels, liposomes and colloidosomes. In both categories, the carriers are stabilized by either emulsifying molecules (emulsions) or by colloidal particles-CPs (pickering emulsions).

Each product of carrier for controlled release requires detailed studies and optimization of their stability, size distribution, functionalities and loading capacity. "They are usually complex systems whose properties and performance are determined not only by composition but also by structure at a nano or microscale, making the design task more challenging" [5]. The properties and synthesis methods of these products have been extensively discussed elsewhere [4, 21], and are outside the scope of this review. The purpose of this section was to give a general overview of the main carriers developed for controlled release technology. As one can see, carriers come in many varieties. Because of the interdependence of the topics, it results more interesting to categorize the carriers based on the release mechanisms as it follows.

1.3.2 General analysis of release mechanisms

Due to the major importance of drug controlled release into pharmaceutical industries, the ensemble of release mechanisms can be well examined within this field. Lee (2015) highlighted the mechanisms by which a drug escapes a carrier. The release was classified into four categories [2]: diffusion, solvent, chemical reaction, and stimuli controlled release, as briefly summarized below (Fig. 1.9). Depending on the type of drug, incorporated drug dose, types and amounts of excipients, preparation technique, environmental conditions during drug release as well as geometry and dimensions of the drug delivery, one or more of the following phenomena (Fig. 1.9) might be involved in the control of drug release from a dosage form [9].

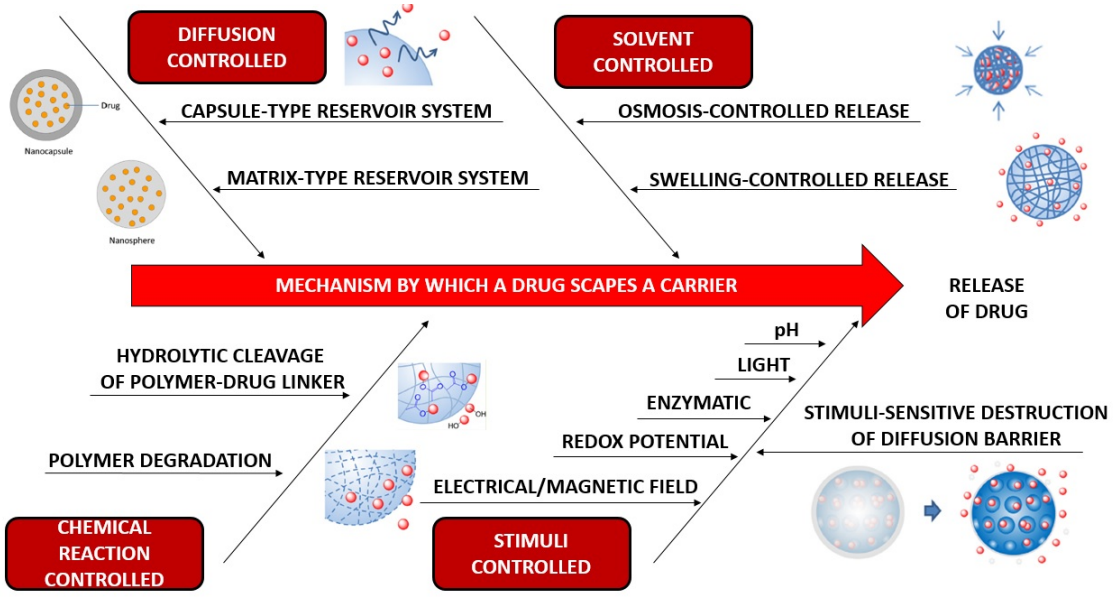

Fig. 1.9 Mechanisms typically involved in drug delivery systems. Adapted from [2].

Diffusion-controlled

Diffusional mass transport is almost always involved in the control of drug release out of a dosage form. In various cases, drug diffusion is the predominant step, in others it 'only' plays a major role, e.g. in combination with polymer swelling or polymer degradation/matrix erosion. In certain cases, it even plays only a minor role. For each type of drug delivery system and type of release conditions the given, so-called '*initial and boundary*' conditions need to be considered. The '*initial conditions*' concern the initial distribution of the diffusing

species in the system. The mathematical treatment is much simpler if this distribution is homogeneous. The '*boundary conditions*' concern the conditions for diffusion at the boundaries of the drug delivery system. If the device dimensions are constant with time (no significant swelling or dissolution/erosion), the boundaries are called '*stationary*'. In contrast, in case of time-dependent device dimensions, the boundary conditions are called '*moving*'. If the device swells significantly, the boundaries are moving outwards; if the system dissolves/erodes significantly, they move inwards. In case of '*perfect sink conditions*' the drug concentration in the surrounding bulk fluid can be considered negligible. Furthermore, if the release medium is well stirred, the liquid unstirred boundary layer surrounding the device is generally thin. If the mass transfer resistance within the drug delivery system for drug diffusion is much higher than the mass transfer resistance in this liquid boundary layer, the latter can generally be neglected. [10]

Solvent-controlled

Solvent transport into a drug carrier can influence the drug release behavior from the carrier. The solvent-controlled release includes osmosis-controlled release and swelling-controlled release [61]. Osmosis-controlled release occurs in a carrier covered with a semi-permeable polymeric membrane, through which water can flow from outside of the carrier (with a low drug concentration) to the drug-loaded core (with a high drug concentration). This mechanism results in a zero-order release profile as long as a constant concentration gradient is maintained across the membrane [62]. When glassy hydrophilic polymeric systems are placed in an aqueous solution including body fluids, water diffuses into the system. The water uptake results in the swelling of the polymeric particles followed by drug release (swelling-controlled release). The drug release rate is determined by the diffusion rate of water and the chain relaxation rate of polymers [63]. The swelling-controlled systems consist of polymeric materials with three dimensionally crosslinked network such as hydrogels, where the mesh size plays a central role in controlling the drug release behavior [64]. The swelling-controlled systems may achieve a zero-order drug release depending on the initial drug distribution in the system [65] or polymer composition [66].

Chemical reaction-controlled

Drug carriers comprising biodegradable polymers such as polyesters, polyamides, poly(amino acids), and polysaccharides release drugs via hydrolytic and/or enzymatic degradation of ester, amide, and hydrazone bonds in their backbones [67–69] . Matrices made of polymers like poly(lactic-co-glycolic acid) (PLGA), polylactic acid (PLA), and polycaprolactone

(PCL) undergo bulk degradation, resulting in simultaneous degradation of entire matrices. On the other hand, those made of polyanhydrides and poly(orthoesters) tipically erode from the surface into the core (surface degradation) as the polymer degradation occurs faster than water diffusion into the matrix [70]. However, in a small dimension matrix like nanoparticles, where the distance of water diffusion is short and the domain size of crystallization is restricted, the polymer degradation is substantially accelerated, and these polymers do not necessarily follow the typical surface erosion behavior but show a sign of bullk degradation (constant particle size during polymer degradation) [71]. Drug release kinetics is determined by the degradation rate of polymers, which depends on their molecular weight, end groups, monomer, composition, and crystallinity [72]. "Biodegradable polymeric systems are preferable, because they are disintigrated into compounds that are readily removed from the body without causing long-term side effects" [2]. From drug polymer conjugates, a drug is released from the carrier via hydrolytic or enzymatic cleavage of the linkage between the drug and the polymer. The rate of cleavage controls the drug release kinetics [73]. "Enzymatically cleavable drug-polymer conjugates may be used for target-specific drug delivery, if the enzyme is concentrated in target issues" [74].

Stimuli-controlled release

Responsive polymer materials can adapt to surrounding environments, regulate transport of ions and molecules, change wettability and adhesion of different species on external stimuli, or convert chemical and biochemical signals into optical, electrical, thermal and mechanical signals, and vice versa [2]. "These materials are playing an increasingly important part in a diverse range of applications, such as drug delivery, diagnostics, tissue engineering and smart optical systems, as well as biosensors, microelectromechanical systems, coatings and textiles" [6]. Drug release from stimuli-responsive nanocarriers is controlled by internal or external stimuli such as temperature, pH, ionic strength, sound, and electric or magnetic fields [46]. As it is possible to localize the stimuli, these carriers have been explored for target-specific drug delivery [2]. pH-sensitive carriers have been developed for tumor-specific drug delivery and to increase the contrast between intracellular and extracellular drug release [75]. In thermosensitive drug carriers, drug release is caused by temperature-induced phase transition of the polymer [76]. Because of the complexity and interdependence of the topics, it is difficult to categorize the published articles. A global classification as shown in Fig. 1.10 may be useful in understanding the wide domain of transformations (reversible and irreversible) of stimuli-responsive nanocarriers based on polymers, colloids and surfaces.

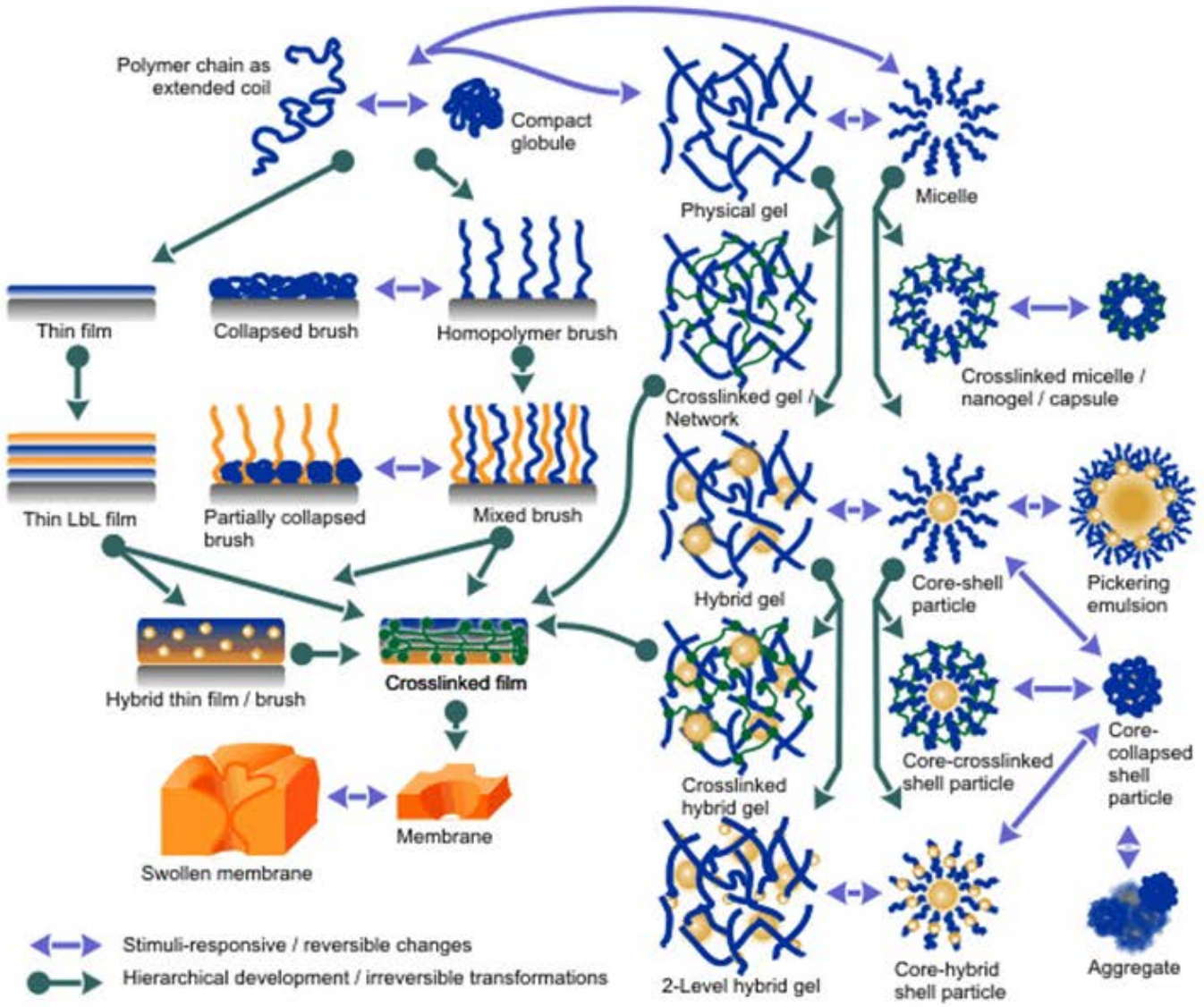

Fig. 1.10 Stimuli-responsive nanostructures based on polymers, colloids and surfaces Taken from [6].

1.4 Current tools for prediction of controlled release

Mathematical modeling of drug delivery and predictability of drug release is a field of steadily increasing academic and industrial importance with an enormous future potential. Because of the noteworthy advances in information technology, the '*in-silico*' or '*ab-initio*' optimization of novel delivery systems can be required to essentially enhance in precision and effortlessness of utilization. Comparable to other fields (e.g., aeronautics and aviation), computer simulations are probably going to wind up plainly a necessary piece of future innovative work in pharmaceutical innovation. "It is just an issue of time when numerical projects will be routinely used to help optimizing the plan of novel dosage products" [9]. Considering the desired type of administration, drug dose to be incorporated and targeted drug release profile, mathematical predictions will allow for good estimates of the required composition, geometry, dimensions and preparation procedure of the respective dosage forms.

In this way, one of the real main thrusts for the utilization of mathematical modeling in drug delivery is to spare time and to diminish costs: the quantity of required experimental tests to build up as well as the optimization of a current drug delivery product can altogether be diminished. Moreover, the quantitative examination of the physical, chemical, and conceivably natural phenomena, which are associated with the control of drug release, offers another central preferred standpoint: the basic understanding on the release mechanisms can be illustrated. "This knowledge is not only of academic interest, but a pre-requisite for an efficient improvement of the safety of the new pharmaco-treatments (particularly for highly potent drugs with narrow therapeutic windows)" [9]. Moreover, potential difficulties experienced during production can be significantly more productively addressed if the system is not dealt as a '*black box*', but there is an intensive comprehension of how drug release is controlled. It is definitive to know which product properties are critical to give a desired performance.

As Siepmann (2008) reviewed, up to date, numerous mathematical theories have been described in the literature [77–79, 64], but most of them still lack in accuracy and/or easiness of application. The pioneer of mathematical modeling of drug delivery is consireded to be Professor Takeru Higuchi. In 1961, he published his famous equation allowing for a simple and surprising description of drug release from an ointment base exhibiting a considerable initial excess of dissolved drug within an inert matrix with film geometry [80, 81]. This was the beginning of the quantitative treatment of drug release from pharmaceutical dosage forms. Numerous models have been proposed since then, including '*empirical/semi-empirical*' as well as '*mechanistic realistic theories*'. In the first case, the mathematical treatment is (at least partially) purely descriptive and not based on real physical, chemical and/or biological

phemonena. Consequently, no or very limited insight into the underlying drug release mechanisms can be gained. Furthermore, the predictive power of empirical/semi-empirical models is often low [9]. This kind of models may for example be valuable if diverse types of drug release profiles are to be compared utilizing a particular parameter (e.g., a release rate constant for experimental design). However, extraordinary alert must be paid if mechanistic conclusions are drawn or quantitative predictions made. An exception are approaches based on artificial neural networks (ANNs), which can show good predictive power.

In contrast, mechanistic mathematical theories are based on real phenomena, such as diffusion, dissolution, swelling, erosion, precipitation and/or degradation [82–88]. This type of models allows for the determination of system-specific parameters that can offer deeper insight into the underlying drug release mechanisms. For instance, the relative importance of several processes that are involved (e.g., drug diffusion and polymer swelling) can be estimated. The dosage form is not treated as a '*black box*', but as a real drug delivery system where the mechanisms of which can be understood [9]. For product development such mechanistic realistic mathematical models consider the quantitative prediction of the impacts of formulation and manufacture parameters (e.g., the underlying tablet heigth and radius) on the subsequent release. Accordingly, the required composition, size, shape and manufacture procedure of a novel dose frame with wanted properties turn out to be hypothetically predictable. In addition, challenges experienced during production are substantially less demanding to address while having a reasonable thought of how the system functions.

1.5 Empirical and semi/empirical mathematical models

1.5.1 Peppas equation

A very frequently used and easy-to-apply model to describe drug release is the so-called Peppas equation, or power law [24]:

$$\frac{M_t}{M_\infty} = kt^n \tag{1.1}$$

Here, M_t and M_∞ are the absolute cumulative amount of drug released at time t and infinite time, respectively; k is a constant incorporating structural and geometric characteristics of the system, and n is the release exponent, which might be indicative of the mechanism of drug release. Nicholas Peppas was the first to introduce this equation in the field of drug delivery [24]. A release exponent of 0.5 can serve as an indication for diffusion controlled drug release, but only if all assumptions these particular solutions are based on are fulfilled (film geometry with negligible edge effects, time- and position-independent diffusion coefficients

Table 1.2 Release exponent n of the Peppas equation [24] and release mechanisms from controlled delivery systems of different geometry. Taken from [9].

Drug release mechanism	Exponent, n		
	Thin film	Cylinder	Sphere
Fickian diffusion	0.5	0.43	0.43
Anomalous transport	0.5<n<1.0	0.45<n<0.89	0.43<n<0.85
Polymer swelling	1.0	0.89	0.85

in a non-swellable and insoluble matrix former) [9]. For other device geometries and pure drug diffusion control, different release exponent values have been derived [89, 90]. In contrast, if polymer swelling is the solely release rate controlling mechanism and in the case of a delivery system with film geometry, zero order drug release kinetics is observed, corresponding to a release exponent of n=1. But again, none of the model assumptions for this particular must be violated. For other geometries than that of thin films with negligible edge effects, different n-values can serve as indicators for purely swelling controlled drug delivery (Table 1.2). Release exponents that are in between these extreme values for the respective device geometry indicate so-called '*anomalous*' transport, thus, an overlapping of different types of phenomena, potentially including drug diffusion and polymer swelling [9].

1.5.2 Hopfenberg model

Hopfenberg [91] proposed an interesting semi-empirical model allowing for a quantitative description of drug release from degradable drug delivery systems exhibiting a release which is proportional to the (time-dependent) surface area of the device. All mass transfer processes that are involved in the control of drug release are assumed to add up to a single zero order process (characterized by a rate constant, k_0), which is confined to the surface area of the system. This zero order process might correspond to one single physical or chemical phenomenon, but it might also result from the superposition of several processes, such as dissolution, swelling and/or polymer chain cleavage. The Hopfenberg model can for instance be applied to surface eroding polymer matrices for which a zero order surface detachment of the drug is the rate limiting release step [9]. The general equation is as follows:

$$\frac{M_t}{M_\infty} = 1 - \left(1 - \frac{k_0 t}{c_0 a}\right)^n \tag{1.2}$$

Here, M_t and M_∞ are the cumulative absolute amounts of drug released at time t and at infinite time, respectively; c_0 denotes the uniform initial drug concentration within the

system; and a is the radius of a cylinder or sphere or the half-thickness of a slab; n is a '*shape factor*' representing spherical (n=3), cylidrical (n=2) or slab geometry (n=1). The model ignores edge and end effects.

1.5.3 Cooney model

A more detailed analysis for spheres and cylinders undergoing surface erosion was presented by Cooney [7]. Also his model is based on the assumption that there is one single zero order kinetics process, which is confined to the surface of the drug delivery system. As in the Hopfenberg model the release rate is assumed to be proportional to the surface area of the device, which is time- dependent. For a cylinder with the initial length L_0 and initial diameter D_0, the following equation was derived quantifying the drug release rate f as a function of time t:

$$f = \frac{(D_0 - 2Kt)^2 + 2(D_0 - 2Kt)(L_0 - 2Kt)}{D_0^2 + 2D_0L_0} \tag{1.3}$$

Where K is a constant. Fig. 1.11 illustrates the effects of the ratio "initial length:initial diameter" (L_0/D_0) of a cylinder on the resulting relative drug release rate versus time. When L_0/D_0 aproaches zero (film geometry) the curves transform into a horizontal line with a constant relative drug release of 1. It is interesting to note that for disc-like cylinders (ratios of $L_0/D_0 < 1$, curves numbered 0.1, 0.2 and 0.5), the relative drug release rate remains finite up to complete drug release. In contrast, for rod-like cylinders ($L_0/D_0 > 1$, curves numbered 1, 2, 5 and infinity), the relative drug release rate approaches zero at late time points.

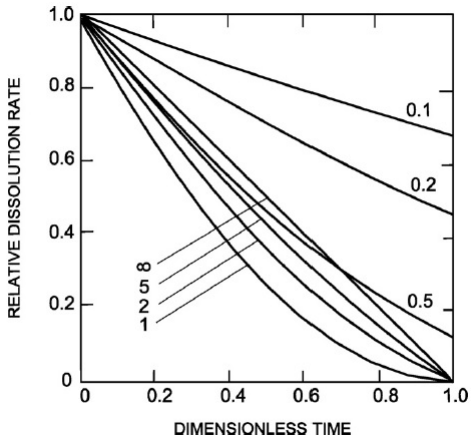

Fig. 1.11 Effects of the ratio "initial length:initial diameter" (L_0/D_0) of a cylinder on the resulting relative dissolution rate (or relative drug release rate) versus time according to the semi-empirical Cooney model. Taken from [7].

1.5.4 Artificial neural networks

Also artificial neural networks (ANNs) can be used to model drug delivery [8, 92]. The basic principle of this type of mathematical analysis is illustrated in Fig. 1.12. An ANN consists of one input layer, one output layer and one or more hidden intermediate layers. Each layer is composed of several units, corresponding to '*neurons*'. The input layer encompasses n input values of causal factors, e.g. the drug loading, compression force or excipient content. The output layer can for instance consist of constants describing the drug release profile. As illustrated, the units of neighboring layers are interconnected, the links corresponding to '*synapses*'. The strength of these links can vary, they are also called '*weights*'. Upon definition of the model structure a set of experimental results (consisting of input and output values) is used to '*train*' the network, that is to define the optimal equations and weights allowing for the calculation of the output values based on the input values. Thus, ANNs can be considered as nonlinear regression analysis tools. Once the system is '*trained*', it can be used to make quantitative predictions for the output values based on new input values. This type of analysis was used by Takahara [8] to simulate the effects of the amounts of microcrystalline cellulose and hydroxypropyl methylcellulose as well as of the compression pressure used to prepare trapidil-loaded matrix tablets on the resulting drug release kinetics. Ibric [93] applied ANNs to study acetylsalicylic acid release from Eudragit RS-based matrix tablets, whereas theophylline release from coated pellets was analyzed by Ghaffari [94] using this type of mathematical modeling approach. A further interesting application of neural networks in drug delivery was presented by Shao [95], predicting drug release from and tablet tensile strength of immediate release formulations.

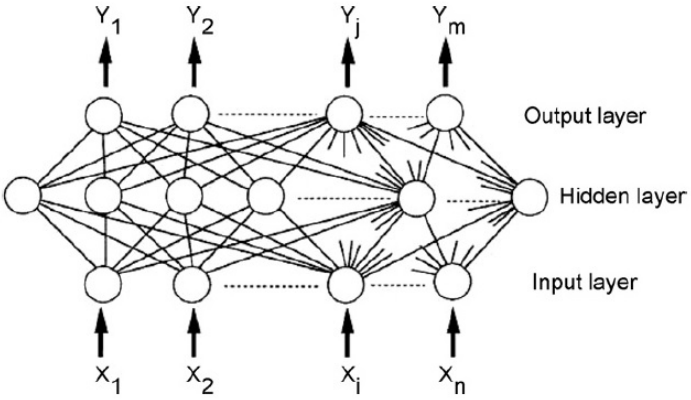

Fig. 1.12 Basic principle of mathematical modeling using artificial neural networks (ANNs): X_i represents the input value of causal factors, n is the number of causal factors, Y_i denotes the output value of responses and m the number of responses. Taken from [8].

1.6 Mechanistic realistic theories

1.6.1 Theories based on Fick's law of diffusion

Diffusion-controlled drug release is typically shown in a capsule-type reservoir system, in which a drug is dissolved or dispersed in a core surrounded by a polymeric membrane [96]. Drug diffusion is driven by the difference in its concentration across the membrane. Here, the drug first dissolves in the core, then diffuses through the membrane [9]. Matrix-type nanospheres, where drug molecules are dispersed throughout the polymer matrix, also show a diffusion-controlled release profile. In the matrix-type systems, there is no membrane that serves as a diffusion barrier; therefore, this system usually shows high initial release, followed by a decreasing release rate with the increasing diffusion distance for drug molecules located interior of the carrier [2]. In order to quantify diffusional mass transport, Fick's laws of diffusion can be used [97]:

Fick's first law of diffusion:

$$F = -D \cdot \frac{\partial c}{\partial x} \tag{1.4}$$

where F is the rate of transfer per unit area of section (flux); c is the concentration of the diffusing species and D denotes the diffusion coefficient (also called diffusivity).

Fick's second law of diffusion (which can be derived from Fick's first law and mass balance considerations):

$$\frac{\partial c}{\partial x} = D \cdot \left(\frac{\partial^2 c}{\partial x^2} + \frac{\partial^2 c}{\partial y^2} + \frac{\partial^2 c}{\partial z^2} \right) \tag{1.5}$$

where c is the concentration of the diffusing species; t denotes time, D is the diffusion coefficient and x, y and z are the three spatial (Cartesian) coordinates.

A very important aspect when solving Fick's second law of diffusion is the fact whether or not the diffusion coefficient of the diffusing species is constant or not. The mathematical treatment is much simpler if D is constant. Reasons for time- and position- dependent diffusion coefficient might include matrix erosion, polymer swelling and/or degradation. In these cases, generally no 'analytical solutions' of Fick's law can be derived (no '*exact*' solutions quantifying the amount of drug released as a function of time), but 'numerical solutions' ('*approximate*' solutions) can be used [9]. Notwithstanding, if drug release is simply diffusion controlled with constant diffusion coefficients, the numerical treatment can be fairly direct. As Siepmann describes in his review [9] of mathematical modeling, different types of systems can be distinguished (Fig. 1.13), including: (i) reservoir devices consisting of a drug depot, which is surrounded by a release rate controlling barrier membrane (often

polymer-based), and (ii) monolithic systems, also called "*one-block*" systems, because there is no local separation between a drug reservoir and a release rate controlling barrier.

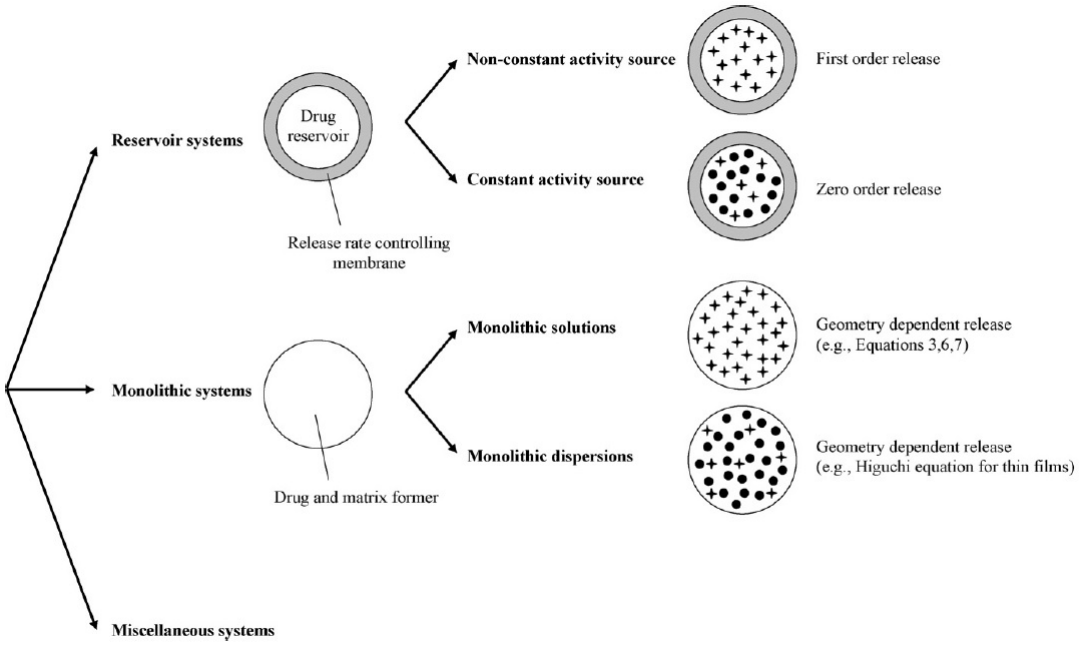

Fig. 1.13 Classification system for primarily diffusion controlled drug delivery systems. Stars represent individual drug molecules, black circles drug crystals and/or amorphous aggregates. Only spherical dosage forms are illustrated, but the classification is applicable to any type of geometry. Taken from [9].

For both types of systems two subclasses can be distinguished: the initial drug concentration is either below or above drug solubility in the device. In the case of a reservoir device (Fig. 1.14) with an initial drug concentration below drug solubility (e.g., a polymer-coated tablet or pellet with a low drug loading), released drug molecules are not replaced and the drug concentration at the inner membrane's surface continuously decreases with time (non-constant activity source). If the membrane does not swell or dissolve, if perfect sink conditions are provided throughout the release period and if the drug permeability through the barrier remains constant, first order release kinetics results, irrespective of the geometry of the device [98]:

$$\frac{\partial M_t}{\partial t} = \frac{ADKC_t}{l} = \frac{ADK}{l} \cdot \frac{M_0 - M_t}{V} \tag{1.6}$$

Where M_t represents the absolute cumulative amount of drug released at time t; C_t denotes the concentration of the drug in the release medium at time t; M_0 is the initial amount of drug within the dosage form; V the volume of the drug reservoir, A the total surface area of the device, and l the thickness of the membrane; K represents the partition coefficient of

the drug between the membrane and the reservoir, and D the diffusion coefficient of the drug within the membrane.

Fig. 1.14 Representations of reservoir devices (drug depot surrounded by a release rate controlling barrier membrane) at different geometries (slab, sphere, cylinder). Taken from [9]. Note that equations kinetics 1.6 and 1.7 are irrespective of the device geometry.

In contrast, if the initial drug concentration exceeds the drug solubility in a reservoir device, released molecules are replaced by the (partial) dissolution of drug crystals/amorphous aggregates, resulting in constant drug concentrations (saturated solutions) at the inner membrane's surface (constant activity source) [9]. If the properties of the release rate controlling barrier (including its thickness and permeability for the drug) remain constant and if perfect sink conditions are provided throughout the release period, zero order release kinetics result as long as drug excess is provided, irrespective of the geometry of the system [98]:

$$\frac{\partial M_t}{\partial t} = \frac{AJ_{lim}}{l} = \frac{ADKC_s}{l} \tag{1.7}$$

where M_t is the amount of drug release at time t; $\delta M_t/\delta t$ denotes the steady state release rate at time t; A is the total surface area of the device, J_{lim} the membrane-limiting flux, l the thickness of the membrane, D the diffusion coefficient of the drug within the membrane, K the partition coefficient of the drug between the membrane and the reservoir, and C_s the solubility of the drug in the reservoir. However, in practice often deviations from these '*ideal*' systems are observed, for instance the film coatings show crack formation due to significant hydrostatic pressure built up within the device or due to membrane swelling and/or (partial) dissolution [99]. This renders the numerical treatment considerably more muddled and yet there is a critical absence of mechanistic realistic mathematical theories considering these features.

In the case of monolithic devices, the system geometry significally affects the resulting drug release kinetics. If the initial drug concentration is below drug solubility, the drug molecules are individualized/dissolved within the carrier material (monolithic solution). Otherwise, dissolved drug molecules co-exist with amorphous aggregates and/or drug crystals (monolithic dispersions). In the case of monolithic solutions and in the absence of significant

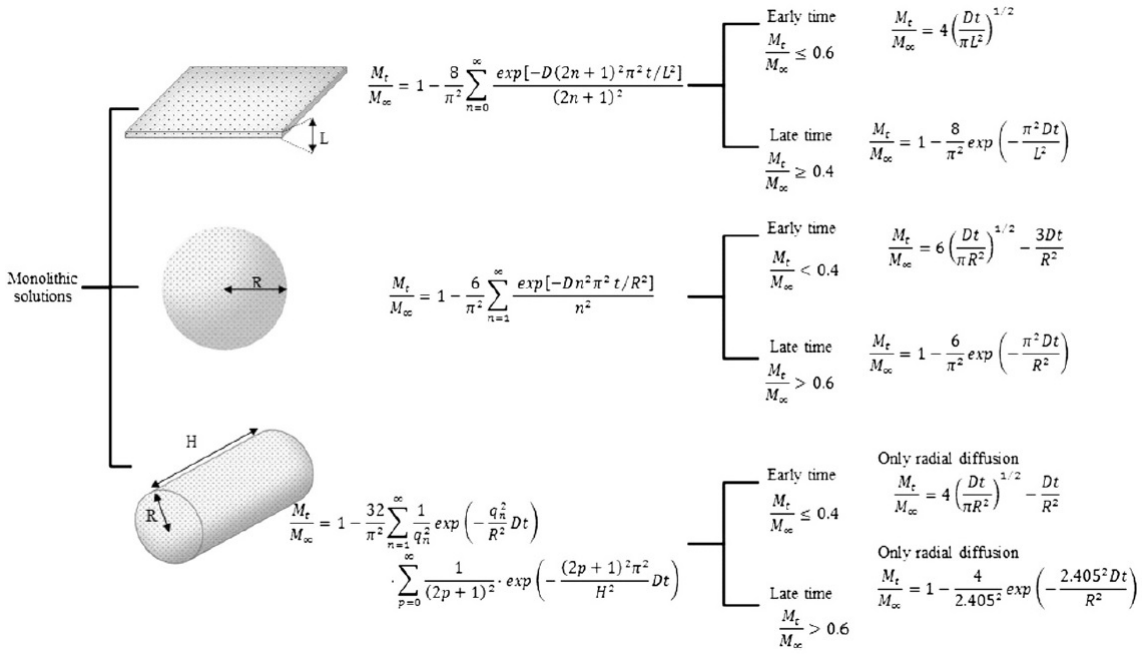

Fig. 1.15 Overview on the mathematical equations, which can be used to quantify drug release from monolithic solutions (initial drug concentration<drug solubility). The "*exact*" equations are valid during the entire release periods, the indicated early and late time approximations are only valid during parts of the release periods. Taken from [10].

changes in the carrier matrix during drug release (e.g., constant porosity, no swelling, time-independent permeability for the drug) and if perfect sink conditions are maintained throughout the release period and if drug release is primarily controlled by diffusion through the carrier matrix, the resulting release can be calculated as showed in Fig. 1.15 , depending on the system's geometry [9].

Where M_t and M_∞ denote the absolute cumulative amounts of drug released at time t and infinity, respectively; n and p are dummy variables, D the diffusion coefficient of the drug within the matrix former, L (in the case of thin films with negligible edge effects [97]) is the thickness of the film, R (in the case of spherical dosage forms [97]) the radius of the sphere, (in the case of cylinders considering axial as well as radial mass transport [100] the radius of the cylinder, H denote the height of the cylinder and q_n are the roots of the Bessel function of the first kind of zero order $[J_0(g_n) = 0]$. To avoid the use of infinite series of exponential functions, early and late time approximations have been proposed for these equations [98].

For monolithic dispersions (Fig. 1.16) the mathematical description becomes even more complex. For the simplest geometry of thin films with negligible edge effects, Takeru Higuchi published the famous square root of time relationship between the amount of drug released

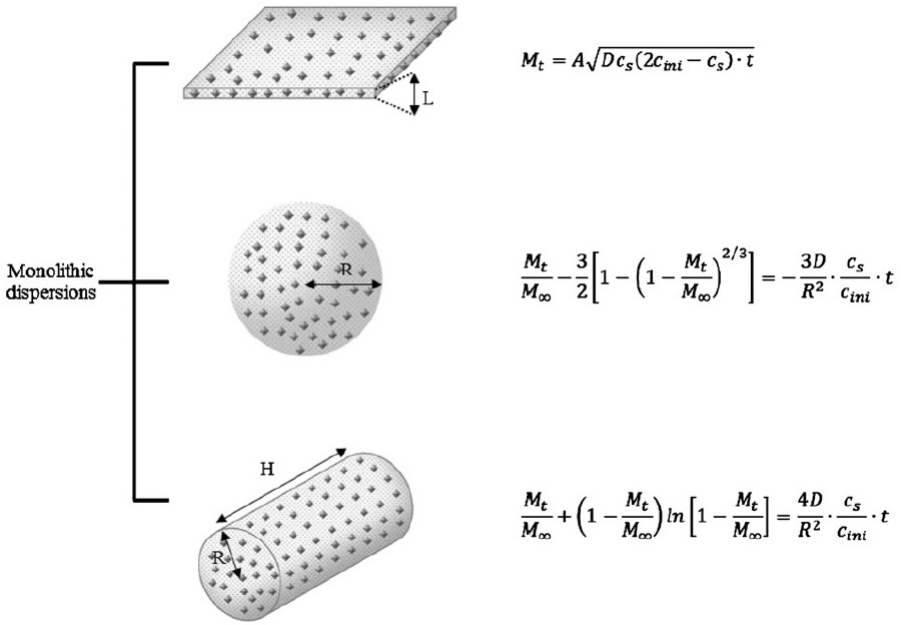

Fig. 1.16 Overview on the mathematical equations, which can be used to guantify drug release from monolithic dispersions (initial drug concentration > drug solubility). The variables are explained in the text. Taken from [10].

from a thin ointment film with a large excess of drug (initial drug concentration » drug solubility in the carrier material) in 1961 [80, 81]:

$$\frac{M_t}{A} = \sqrt{DC_s(2C_{ini} - C_s)\cdot t} \tag{1.8}$$

where M_t is the cumulative absolute amount of druf released at time t, A is the surface area of the film exposed to the release medium, D is the drug diffusivity in the carrier material, and C_{ini} and C_s represent the initial drug concentration and the solubility of the drug in the carrier material, respectively. An important advantage of this equation its simplicity. However, when applying it to controlled drug delivery systems, all the assumptions Higuchi based this equation on must be fulfilled, including: (i) drug concentration much higher than drug solubility, (ii) device geometry of a thin film with negligible edge effects, (iii) size of the drug particles much smaller than film thickness, (iv) no swelling or dissolution of the carrier material, (v) drug diffusivity is constant (not dependent on time or position) and (vi) perfect sink conditions are maintained throughout the experiment.

For monolithic dispersions with other geometries than that of a thin film with negligible edge effects, the reader is referred to the literature [101]. If both, diffusion through the inner device matrix as well as diffusion through a surrounding barrier membrane are of importance

for drug release (Fig. 1.13, '*miscellaneous*' systems), the mathematical modeling is also more complex and geometry dependent. Again, the reader is referred to the literature for more details [102].

1.6.2 Theories considering polymer swelling

If polymer swelling is of importance of the control of drug release, e.g. as in the case of hydroxypropyl methylcellulose (HPMC)-based matrix tablets, the transition of the macromolecules from the glassy (less mobile) to the rubbery (more mobile) state has to be considered in the model [103]. The two most important consequences of significant polymer sweeling in a controlled release matrix system are: (i) the length of the diffusion pathways increases, resulting in decreasing drug concentration gradients (being the driving forces for diffusion) and, thus, potentially decreasing drug release rates; (ii) the mobility of the macromolecules significantly increases, resulting in increased drug mobility and, thus potentially increasing drug release rates [9]. Fig. 1.17 schematically shows the physical phenomena which can be engaged with the control of drug release from a swellable delivery system.

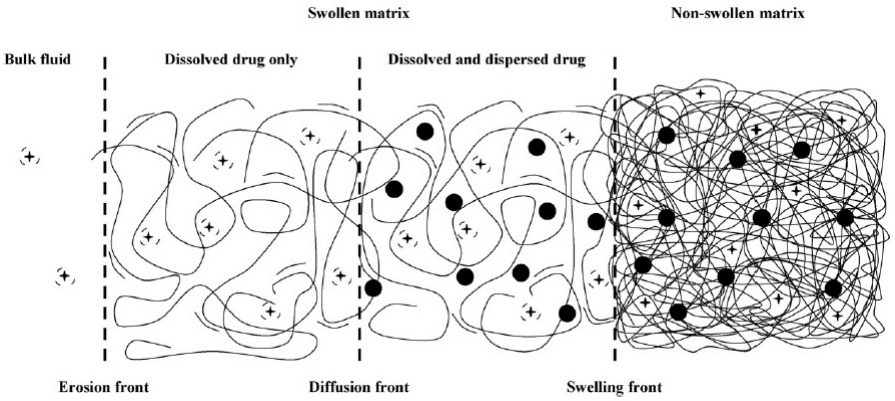

Fig. 1.17 Schematic presentation of a swelling controlled drug delivery system containing dissolved and dispersed drug (stars and black circles, respectively), exhibiting the following moving boundaries: (i) an '*erosion front*', separating the bulk fluid from the delivery system; (ii) a '*diffusion front*', separating the swollen matrix containing dissolved drug only and the swollen matrix containing dissolved and dispersed drug; and (iii) a '*swelling front*', separating the swollen and non-swollen matrix. Taken from [11].

This might represent a cross-section through half of a matrix tablet which is exposed to an aqueous bulk fluid in radial direction. On the right hand side, the inner tablet core is still dry and in the glassy state (non-swollen), on the left hand side the bulk fluid is located. Upon contact with the release medium, water diffuses into the system. With increasing water content, the mobility of the polymer chains (and, thus, also drug molecules) increases.

As soon as a certain, polymer-specific water concentration is reached, the macromolecular mobility steeply increases. This phenomenon is called '*polymer chain relaxation*' or '*glassy-to-rubbery-phase-transition*'. The front at which this process takes place is called '*swelling-front*', which separates the swollen from non-swollen matrix. Importantly, this is not a stationary boundary but a moving one. The front that separates the swollen matrix containing only dissolved drug from the swollen matrix that contains both, dissolved and non-dissolved drug, is called '*diffusion front*' (Fig. 1.17). Importantly also, this front is moving. Furthermore, a third front can be distinguished, which separates the drug delivery system from the release medium and which is also moving. In the case of water-soluble matrix formers, this front is called '*erosion front*' [9].

A very interesting example of mechanistic realistic mathematical theory allowing for the quantification of drug release from swellable polymer films has been proposed by Korsmeyer et al. [12]. It allows for a simultaneous consideration of the diffusion of water into the device and drug out of the system as well las of polymer swelling. To account for the increase in water and drug mobility with increasing water content of the polymer matrix, a Fujita-type exponential relationship was chosen [104] and shown to be appropriate for the prediction of different types of transport behaviors. Dimensional changes in the films are accounted for by allowing each spatial increment to expand according to the amount of water that diffused in. At early time points, the swelling is restricted to one dimension by the glassy core of the sample. At later time points, when enough water has penetrated into the core of the system to plasticize it, the sample relaxes to an isotropically swollen state. Afterwards, swelling is three-dimensional. Under these conditions, water (subscript 1) diffusion can be described as follows:

$$\frac{\partial C_1}{\partial \tau} = \frac{\partial}{\partial \xi} \cdot \left(D_1 \cdot \frac{\partial C_1}{\partial \xi} \right) \tag{1.9}$$

where D_1 is the diffusion coefficient of water, and C_1 is the normalized water concentration:

$$C_1 = \frac{C_w}{C_{w,e}} \tag{1.10}$$

Here, C_w is the water concentration in the film at a particular position, and $C_{w,e}$ is the equilibrium water concentration in the system. Time t is scaled according to the water diffusivity in the fully swollen system, $D_{1,s}$, and the dry thickness of the film, L_0:

$$\tau = \frac{tD_{1,s}}{L_0^2} \tag{1.11}$$

The spatial coordinate x is normalized with respect to the dry thickness of the thin film:

$$\xi = \frac{x}{L_0} \tag{1.12}$$

To describe drug diffusion (subscript 2), the following equations are used:

$$\frac{\partial C_2}{\partial \tau} = \frac{\partial}{\partial \xi} \cdot \left(D_2 \cdot \frac{\partial C_2}{\partial \xi} \right) \tag{1.13}$$

$$C_2 = \frac{C_s}{C_{s,i}} \tag{1.14}$$

Here, D_2 is the diffusion coefficient of the drug, and C_2 is the normalized drug concentration; C_s denotes the drug concentration in the film, and $C_{s,i}$ the initial drug concentration in the system. The following boundary conditions are considered:

$$C_1(0,\tau) = C_1(\xi,\tau) = 1 \tag{1.15}$$

$$C_2(0,\tau) = C_2(\xi,\tau) = 0 \tag{1.16}$$

Where 0 and ξ are the two surfaces of the thin film. Please note that ξ describes the continuously moving outside surface of the film. The following initial conditions are considered:

$$C_1(\xi,0) = 0 \tag{1.17}$$

$$C_2(\xi,0) = 1 \tag{1.18}$$

Due to the complexitiy of this set of partial differential equations, the latter was solved numerically. As it can be seen in Fig. 1.18, good agreement between theory and experiment was obtained when fitting this model to sets of experimentally measure theophylline release kinetics from (hydroxyethyl methacrylate-co-N-vinyl-2-pyrrolidone) copolymer-based films.

1.6.3 Theories considering polymer swelling and drug dissolution

In practice, regularly considerably more more processes are simultaneously involved in the control of drug release from oral controlled release matrix tablets. Generally, the matrix former is water-soluble. Thus, also polymer dissolution must be taken into account [9]. Different comprehensive mathematical theories have been proposed aiming to describe this

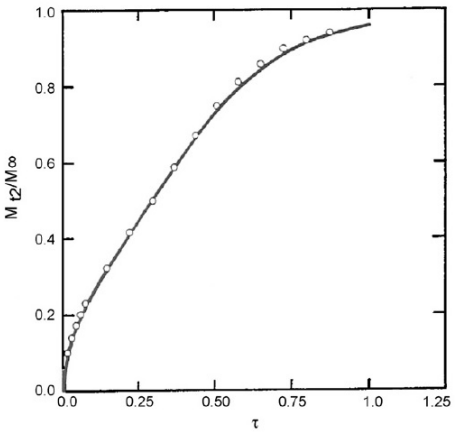

Fig. 1.18 Fit of the Korsmeyer-Peppas model to experimentally determined theophylline release kinetics from hydroxyethyl methacrylate-co-N-vinyl-2-pyrrolidone copolymers-based films (curve = theory, symbols = experiment). Taken from [12].

type of drug delivery systems [105, 77]. In the following, only one example will briefly be described. The reader is referred to the literature for more details [105, 77]. The so-called '*sequential layer model*' [106] takes into account the diffusion of water and drug with time- and position- dependent diffusivities, moving boundary conditions, the swelling of the system, polymer and drug dissolution, and radial and axial mass transfer within cylindrical tablets. The model was successfully fitted to drug release kinetics from matrices based on hydroxypropyl methylcellulose (HPMC) and HPMC derivatives.

Because the polymer dissolution must be taken into account, the complexity of partial differential equations increases, and numerical solution is required. Water and drug diffusion are considered based on Fick's second law of diffusion for cylindrical geometry, taking into account axial and radial mass transport and concentration-dependent diffusivities [97]:

$$\frac{\partial C_k}{\partial t} = \frac{1}{r}\left\{\frac{\partial}{\partial r}\cdot\left(rD_k\cdot\frac{\partial C_k}{\partial r}\right)+\frac{\partial}{\partial \theta}\cdot\left(\frac{D_k}{r}\cdot\frac{\partial C_k}{\partial \theta}\right)+\frac{\partial}{\partial z}\cdot\left(rD_k\cdot\frac{\partial C_k}{\partial z}\right)\right\} \tag{1.19}$$

Here, C_k and D_k are the concentration and diffusion coefficient of the diffusing species ($k = 1$ for water, $k = 2$ for the drug), respectively; r denotes the radial coordinate, z is the axial coordinate, θ is the angular coordinate (Fig. 1.19a), and t represents time. Analogous to the Korsmeyer-Peppas model described above, a Fujita-type [104] exponential dependence of the water and drug diffusion coefficients on the water content of the system is taken into account:

$$D_k = D_{kcrit} \cdot exp\left\{-\beta_k \cdot \left(1 - \frac{C_1}{C_{1crit}}\right)\right\} \tag{1.20}$$

where β_1 and β_2 are dimensionless constants characterizing this concentration-dependence. Also D_{1crit} and D_{2crit} denote the diffusion coefficients of water and drug at the interface tablet/release medium, where polymer chain disentaglements occurs [105]. Ideal mixing is assumed (no volume contraction upon mixing drug, polymer and water), and the total volume of the system at any time point is given by the sum of the volumes of the single components. The calculation of the new tablet dimensions is based on a mass balance considering drug, polymer and water. Polymer dissolution is taken into account using the reptation theory [107]: Above a certain critical water concentration (C_{1crit}), the polymer chains at the surface of the tablet start to disentagle and diffuse through the liquid, unstirred layer surrounding the device into the bulk fluid (release medium). A dissolution rate constant, k_{diss}, is considered characterizing the polymer mass loss velocity, which is normalized to the actual surface area of the system:

$$M_{pt} = M_{p0} - k_{diss} A_t t \tag{1.21}$$

Here, M_{pt} and M_{p0} are the dry polymer matrix mass at time t, and $t = 0$, respectively; A_t denotes the surface area of the device at time t. The initial conditions reflect the fact that the matrix is dry and the drug uniformly distributed throughout the device at $t = 0$. The boundary conditions are defined as follows: The water concentration at the surface of the matrix, C_{1crit} is calculated from the critical polymer disentaglement concentration. The drug concentration at the surface of the tablet is assumed to be equal to zero (perfect sink condition). In order to reduce computation time, the origin of the coordinate system is placed at the center of the cylinder, resulting in two symmetry planes for the drug and water concentration profiles (Fig. 1.19 b). Thus, only the concentration profiles within a quarter of the tablet need to be calculated. Due to the complexity of the resulting set of partial equations, also in this case a numerical solution is required.

Fig. 1.20 shows an example for a practical application of this mathematical model: The theoretically predicted effects of the initial radius of HPMC-based matrix tablets (with an initial height of 2.6 mm, composition: 50% drug and 50% HPMC) on the resulting relative and absolute release of theophylline into phosphate buffer pH 7.4 is illustrated. The curves show the theoretically predicted drug release profiles. Then, in a second step, the respective drug release rates were determined experimentally (symbols in Fig. 1.20). As it can be seen, good agreement between theory and experiment was obtained in all cases.

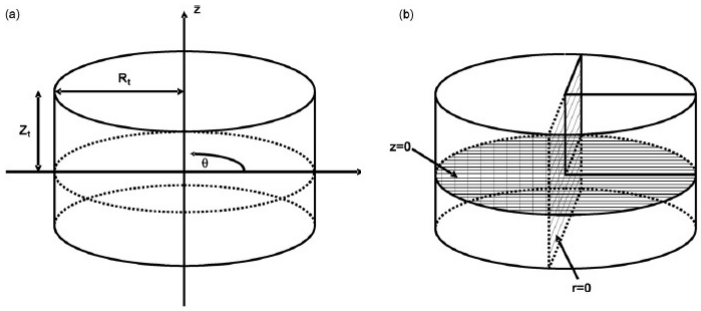

Fig. 1.19 Mathematical modeling of drug release from HPMC-based matrix tablets: (a) scheme of a cylindrical tablet for mathematical analysis, with (b) symmetry planes in axial and radial direction for the water and drug concentration profiles (R_t and Z_t represent the time dependent radius and half-height of the cylinder, respectively. Taken from [9].

1.6.4 Theories considering polymer erosion/degradation

Polymer degradation is the chain scission process by which polymer chains are cleaved into oligomers and monomers. In contrast, erosion is defined as the process of material loss from the polymer bulk. Such materials may be monomers, oligomers, parts of the polymer backbone or even parts of the polymer bulk. Thus, the degradation of water-insoluble polymers is part of their erosion process [9]. Dependind on the relative rates of water peneteration into such systems and of polymer chain cleavage, two extreme types of erosion can be distinguished: surface (or heterogeneous) erosion and bulk (or homogeneous) erosion. In the first case, the polymer chain cleavage is much faster than the water penetration into the system. Consequently, the degradation process is mostly restricted to the outermost polymer layers and the erosion predominantly affects the surface, and not the inner parts of the device. In contrast, if water penetration is much more rapid than polymer chain cleavage, the entire system is rapidly wetted and degradation occurs throughout the device (bulk erosion) [61]. Generally, drug delivery systems which are based on polymers with highly reactive bonds (e.g. polyanhydrides) in their backbone structure undergo surface erosion, whereas devices that are based on polymers with less reactive functional groups [e.g., poly(lactic-co-glycolic acid)(PLGA)] tend to be bulk eroding" [9].

An interesting mathematical theory for surface eroding drug delivery systems with film geometry was proposed by Lee in 1980 [13]. It is an analytical solution that is valid for different '*drug loading:drug solubility*' ratios. As illustrated in Fig. 1.21 a, the movements of two fronts are considered: a diffusion front, and an erosion front. Here, R denotes the time-dependent position of the diffusion front, and S the time-dependent position of the erosion front; A is the initial drug concentration within the delivery system, which is above drug solubility, C_s (monolithic dispersion); C_b represents the drug concentration in the well

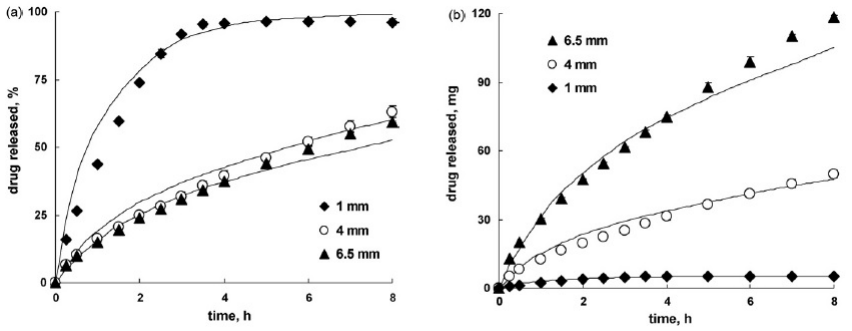

Fig. 1.20 Practical application of the '*sequential layer model*': Theoretically predicted effects of the initial tablet radius on the release patterns of theophylline from HPMC-based matrix tablets in phosphate buffer pH 7.4 and experimental verification: (a) relative amount of drug released and (b) absolute amount of drug released versus time (37°C), initial tablet height = 2.6 mm, initial tablet radius indicated in the figures, 50% (w/w) initial drug loading) (curves: predicted values, symbols: independent experimental data). Taken from [9].

stirred release medium, and x the position (with $x = 0$ at the center and $x = a$ at the surface of the film). It is assumed that the erosion front moves at a constant velocity, that edge effects are negligible and that perfect sink conditions are maintained throughout the experiment. Under these conditions, Lee derived the following equations for a quantitative description of drug release:

$$\frac{M_t}{M_\infty} = \delta + \tau\frac{Ba}{D} - \delta\frac{C_s}{A}\cdot\left(\frac{1}{2} + \frac{a_3}{6}\right) \tag{1.22}$$

$$a_3 = \frac{A}{C_s} + \delta h - \sqrt{\left(\frac{A}{C_s} + \delta h\right)^2 - 1 - 2\delta h} \tag{1.23}$$

$$h = \frac{1}{2}\cdot\frac{Ba}{D}\cdot\left(1 - \frac{A}{C_s}\right) \tag{1.24}$$

Here, M_t and M_∞ are the cumulative absolute amounts of drug released at time t and at infinite time, respectively; δ denotes the relative separation between the diffusion and erosion fronts [$\delta = (S-R)/a$]; B is the surface erosion rate constant with the dimensions of a velocity; a represents the half-thickness of the film, D the drug diffusivity within the system, and τ is the dimensionless time ($\tau = Dt/a^2$). The parameter Ba/D is a measure for the relative contribution of erosion and diffusion to drug release. The calculated effects on the '*initial drug loading:drug solubility*' ratio ($A : C_s$) on the resulting drug release patterns are illustrated in Fig. 1.21 b. In this example, the relative contributions of erosion and diffusion are kept constant (= 1). As it can be seen, the relative drug release rate decreases with

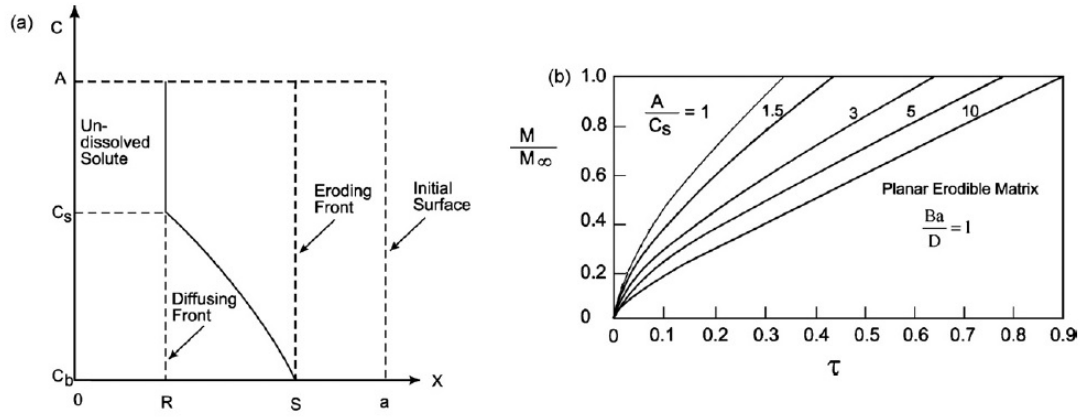

Fig. 1.21 Modeling drug release from surface eroding monolithic dispersions with film geometry: (a) scheme of the drug concentration profile within the system according to Lee (1980). Two moving fronts are considered: a diffusion front and an erosion front. (b) Calculated drug release profiles as a function of the '*initial drug loading:drug solubility*' ratio (A/C_s).The parameter Ba/D serves as a measure for the relative contribution of erosion and diffusion. Taken from [13].

increasing A/C_s ratio. The model predicts that the release approaches zero order kinetics when the initial drug loading becomes much higher than drug solubility in the matrix.

As polymer chain cleavage is a random process, Monte Carlo simulations can effectively be used to simulate polymer degradation. Zygourakis [108] was the first to propose this type of theories allowing for a quantitative description of drug release from surface eroding polymer matrices. The basic idea is to represent polymer matrix cross-sections by two-dimensional grids. Each pixel represents one of the system's components: drug, polymer and potentially filler and pores. To simulate drug or polymer '*dissolution*' a so-called '*life expectancy*' is defined for each type of pixel. As soon as a pixel comes into contact with water, its '*lifetime*' starts to decrease. Once the '*lifetime*' expires, the pixel is assumed to '*dissolve*' instantaneously. Importantly, different '*life expectancies*' can be defined for the involved system compounds, taking into account differences in their dissolution rates [14].

As example, an approach combining Monte Carlo simulations with diffusional transport was used to quantify drug release from spherical poly(lactic-co-glycolic acid) (PLGA)-based microparticles [109]. For the mathematical analysis, the latter are divided into concentric rings of equal volume (Fig. 1.22, the rings are described upon rotation of the pixels shown in Fig. 1.22 b around the z-axis). Due to the symmetry planes at the $r = 0$ and $z = 0$ planes (in the case of homogeneous initial drug and polymer distribution), it is sufficient to calculate the mass transport phenomena in only one quarter of the two-dimensional circle shown in

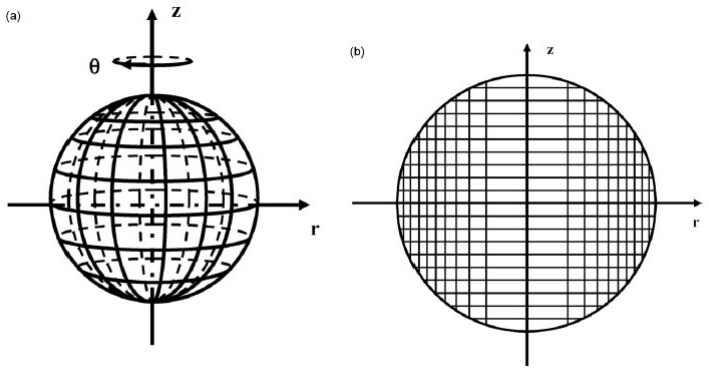

Fig. 1.22 Schematic presentation of a spherical PLGA-based microparticle for mathematical analysis: (a) three-dimensional geometry; (b) two-dimensional cross-section with two-dimensional pixel grid. Upon rotation of the latter around the z-axis, rings of identical volume are described. Taken from [14].

figures 1.22 b and 1.23 a. At $t = 0$ each ring represents either drug or non-degraded polymer. Due to the identical volume of the polymer rings it is reasonable to assume that each of them contains a similar number of cleavable ester bonds. Thus, the probability with which a ring representing non-degraded polymer degrades upon its first contact with water is similar for all rings. As described above, life time expectancies are assigned to all polymer pixels (rings), reflecting the degradation rate of the macromolecules. Importantly, knowing the status of each pixel (ring) ('*non-eroded polymer*' or '*pore*') at each time point, the microparticle porosities in radial and axial direction (depending on time and position) can be calculated (Fig. 1.23 b). Based on these porosity values, the position- and direction-dependent drug diffusivities within the spheres can be calculated as a function of the exposure time to the release medium. This information is essential for the accurate calculation of the diffusional mass transport processes using Fick's second law [97].

$$\frac{\partial C}{\partial t} = \frac{1}{r}\left\{\frac{\partial}{\partial r}\cdot\left(rD\cdot\frac{\partial C}{\partial r}\right)+\frac{\partial}{\partial \theta}\cdot\left(\frac{D}{r}\cdot\frac{\partial C}{\partial \theta}\right)+\frac{\partial}{\partial z}\cdot\left(rD\cdot\frac{\partial C}{\partial z}\right)\right\} \tag{1.25}$$

Here, c and D are the concentration and diffusion coefficient of the drug; r denotes the radial coordinate, z the axial coordinate, and θ the angle perpendicular to the r-z-plane. In addition, the limited solubility of the drug within the system is taken into account: Only drug which is soluble under the given conditions is considered to be available for diffusion. Taking into account the given initial and boundary conditions (initial homogeneous drug distribution and perfect sink conditions), the set of partial differential equations is solved numerically, using finite differences. Based on these calculations, system-specific parameters can be determined and the dominant physical and chemical phenomena in each of the release

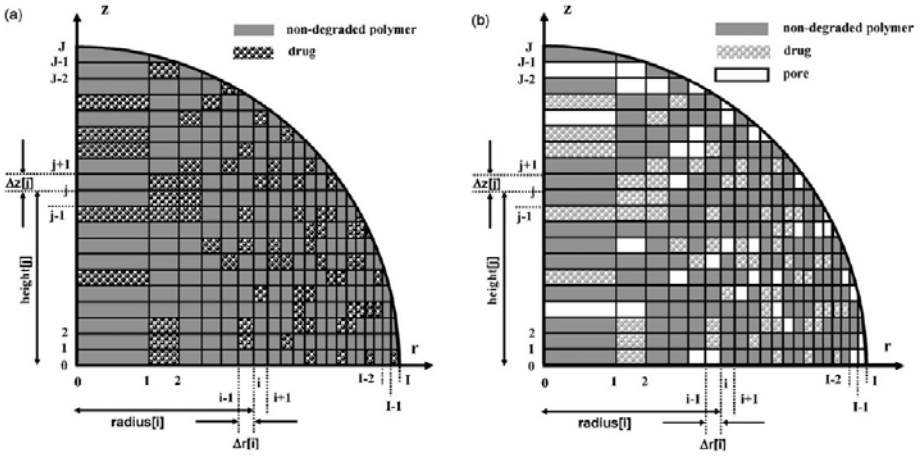

Fig. 1.23 Principle of a Monte Carlo-based approach to simulate polymer degradation and diffusional drug release from PLGA-based microparticles. Schematic structure of the system (one quarter of the two-dimensional grid shown in Fig. 1.22b: (a) at time t=0 (before exposure to the release medium) and (b) during drug release. Gray, dotted and white pixels represent non-degraded polymer, drug and pores, respectively. Taken from [14].

periods be identified. For instance, it can be shown that this specific system the initial '*burst release*' is primarily controlled by pure drug diffusion. Furthermore, the model allows for quantitative predictions of the effects of formulation and processing parameters, including the initial microparticle size and drug loading. Importantly, good agreement between theory and experiment was obtained (Fig. 1.24).

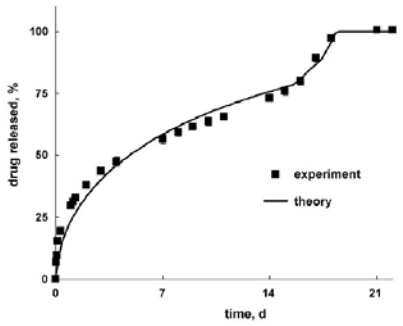

Fig. 1.24 Fit of a mechanistic realistic mathematical theory based on Monte Carlo simulations and considering diffusional mass transport as well as limited local drug solubility to experimentally determined drug release from 5-fluouracil-loaded, PLGA-based microparticles in phosphate buffer pH 7.4: experimental results (symbols) and fitted theory (curve). Taken from [14].

1.7 A reverse engineering methodology

1.7.1 Motivation

The research brings together chemists, physicists, and biologists. A lot of effort has been made to develop an '*ideal*' carrier. This promising scientific field is one of the fastest growing. However, it is unlikely that there will be one general theory that is applicable to any type of delivery system. It is much more likely that there will be a broad spectrum of different mathematical models, applicable to specific types of devices differing in geometry, active ingredient and excipient type. The literature on the subject of mathematical modeling is enormous and therefore difficult to distill into some globally useful steps. Cause of this problematic issue, one of the main concerns nowadays is the need for a systematic approach to controlled release product design, but also for efficient and reliable strategies to manage the associated complexities, such as multidisciplinary problem, multiscale models, multicriteria optimization, multiple source of data and many more.

The process of obtaining useful higher-level representations of systems is called reverse engineering (RE), and remains a complex but very valuable goal to achieve. The application of RE principles and techniques in order to generate relevant model-based views of systems, facilitates their understanding and manipulation. In this context, the application of RE metholodogies [30] is practically used in order to (1) discover initial models from elements composing a given system and (2) understand (process) these models to generate relevant views (i.e., derived models) on this system. However, generic and extensible solutions potentially addressing several kinds of scenarios relying on different technologies are still missing or incomplete. Clearly, given that RE is a time-consuming and error-prone process, any RE solution that could (semi)automate the process would bring precious help to the users, and thus facilitate its larger adoption.

This thesis proposes to make a step in the direction. The paradigm is largely based on the assumption that '*Everything is a model*' [110]. A whole model which defines the possible element types and structure of the systems which conform to it, similarly to the relationship between a grammar and corresponding programs in the programming field. By means of an integrated-modeling approach [111], the design problem is decomposed into a hierarchical sequence of subproblems (boxes), combining computer-aided techniques with heuristic-based experimental testing. For a specific structured system, the idea is to implement the elements, concerning mass transfer, thermodynamics, formulation process, etc. which will allow afterwards to optimize an objective function (related to release rate) in order to choose the best material (and features) for the best suited application. Thousands of alternatives (specific reverse engineering solutions) can be generated systematically and efficiently by

this approach. Expressed as a reverse design problem, the target property for the product becomes the known variable, and therefore, input for the design. This approach is the most convenient, because time and resources could be saved (compared to a simple experiment based trial-and-error approach) and more realiable results can be obtained. In addition, the combination of all these '*tools*' is useful for analyzing different scenarios including any kind of possible modification on systems.

1.7.2 A proposed reverse engineering framework

At the architecture level, the following framework (Fig. 1.25) is proposed.

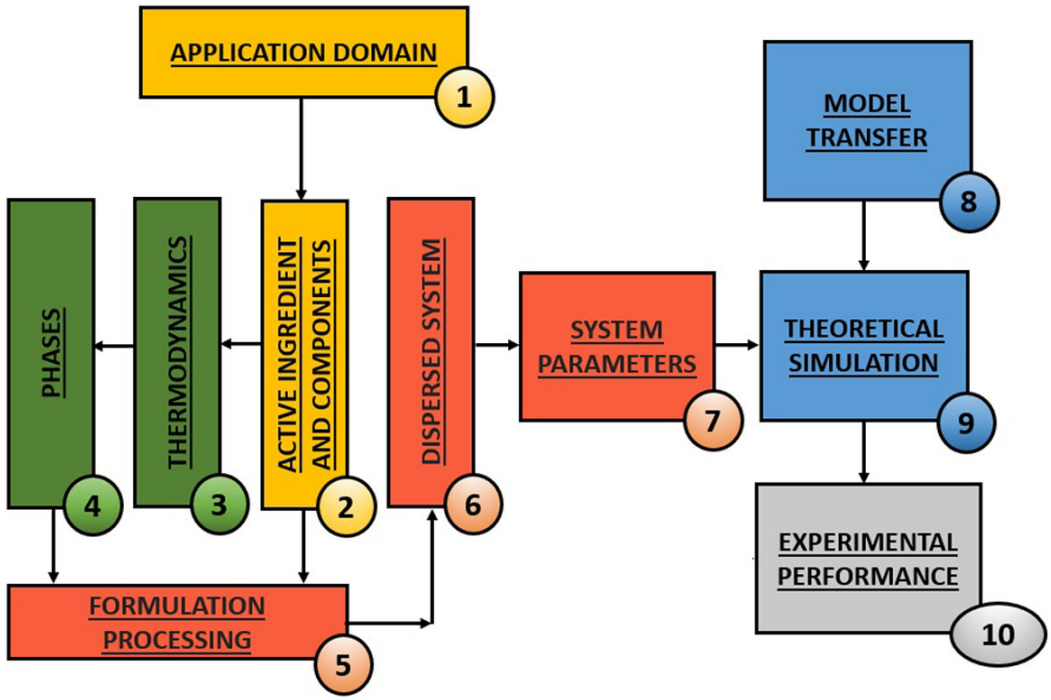

Fig. 1.25 Work-flow diagram for a reverse engineering approach to help on the design of controlled release products.

- **Application domain, active ingredient and other components;** The first boxes (1 and 2) focuse on the definition of the target product profile, what do we want to do and why. The truth is that it is the area of interest and the question being asked that will drive the metholodogy for modeling a particular system. This leads to the definition of the critical design features for the product bearing in mind the route, frequency of administration, safety or environmental considerations, as well as possibilities of secondary components included with the active ingredient in the mixture. For instance,

pharmaceutical products or drugs, apart from the active principle include excipients, solvents, etc; in food industry, products have additives so that the products last longer; in cosmetics, body creams require a proper thickness which is usually related to lotions efficiency, stability and its aceptability by the consumer with the proper absorption rate on the skin, etc.

- **Thermodynamics and phase equilibria;** Next, a reliable knowledge of the phase equilibrium behavior of the systems is required to be designed (boxes 3 and 4). During the last years, powerful thermodynamics models have been developed, which allow the calculation of the various phase equilibria of multicomponent systems. For example, group-contributions models [112] such as UNIFAC are of major interest for a computer-aided design/verification based on '*define target - match target*'. In the absence of experimental information of the mixture of interest, these models can be helpful for visualizing trends and screening of potential product candidates; the search space for alternatives can be reduced and only few product candidates can be verified against the target or best performing ingredients.

- **Formulation processing to obtain a dispersed system with specific parameters;** Boxes 5,6 and 7 concern the formulation processing of the mixture from the basic ingredients to the final product. A number of chemical and physical transformations are involved depending on the final dispersed system. Experimental testing will be helpful to test limits and feasibility of the manufacturing procedures. In addition, the needed system parameters for the following theoretical simulations will be evaluated and identified properly. As example of these parameters, the loading and concentration of active ingredient, the viscosity of the system, diffusion coefficients, phase geometries, or permeabilities through interface layers depending on thickness can be mentioned.

- **Theoretical modeling and mathematical simulation** Subsequently, boxes 8 and 9 refer to mathematical models, mechanistic realistic approaches, special correlations or numerical procedures that will be used for the target property estimation (release rate). Attention will be focused on the assessment of the mass transfer occurring in the inside/interface/outside areas of the dispersed system. Depending on the system, adapted boundary conditions as well as approaches based on one dimension or more (if necessary) could be employed.

- **Experimental performance;** Finally, the experimental resources (box 10) are applied only to test the likely best solutions and to verify or improve the former simulations.

Chapter 2

MODELING

'Everything should be as simple as possible, but not simpler', Einstein

2.1 Introduction

A development of physicochemical models is fundamentally required to quantify mass transfer as function of product composition, structural parameters and active ingredient release processes. It is important bring to mind that modeling is an iterative process and some models can take years before they become reasonably accurate. However, it is a helpful hint to start with the simplest system (even if it highly unrealistic). Then, incrementally (in small steps) add missing pieces and study the new system, comparing it to the data. With the choice of a simple system, it is possible to get quickly initial models representing the basic parts. These '*raw*' models can be sufficiently accurate to be used as a starting point of other scenarios. Eventually, in the reverse engineering framework, a subsequent increase on the abstraction or detail levels (boxes) would lead to bridge the gap between different proposed solutions for controlled delivery. These more '*processed*' models obtained at the end, could be then finally used to generate and/or display the expected views of the framework in a wide range of structured products.

At the present chapter, the main purpose is to arrive at a model conception for the mass transfer in a system model without adjustable parameters by choosing different approaches from the literature. It is the purpose of this thesis to focus only into the most '*fundamental*' and '*simple ones*'. A brief description of the different theoretical approaches will be presented. On the basis of these models, a set of different simulation tools will be developed later in a next chapter, in order to fill out the different pieces (boxes) of the reverse engineering framework previously proposed, and ultimately building a complete '*ab-initio*' model.

2.1.1 Choice of a system model for ab-initio modeling

Emusion technology is particularly suited for design and fabrication of delivery systems [113]. Traditionally, conventional emulsions consisiting of small spherical droplets of one liquid dispersed in another immiscible liquid, are used in industrial and medical applications for a variety of reasons: encapsulation and delivery of active components; modification of rheological properties; alteration of optical properties; lubrication; or modification of organoleptic attributes (among others). The two immiscible liquids are typically an oil phase and an aqueous phase, although other immiscible liquids can sometimes be used. The droplets in conventional emulsions usually have diameters in the range of 100 nm to 100 μm, and are coated by a single layer of active surface components ('*emulsifiers*') that stabilize them against aggregation. For designing conventional emulsions, there are a limited number of ways (Fig. 2.1) that droplets can be designed to provide specifical functional properties, such as stability, rheology, lubricity, optical properties, encapsulation, and delivery [15].

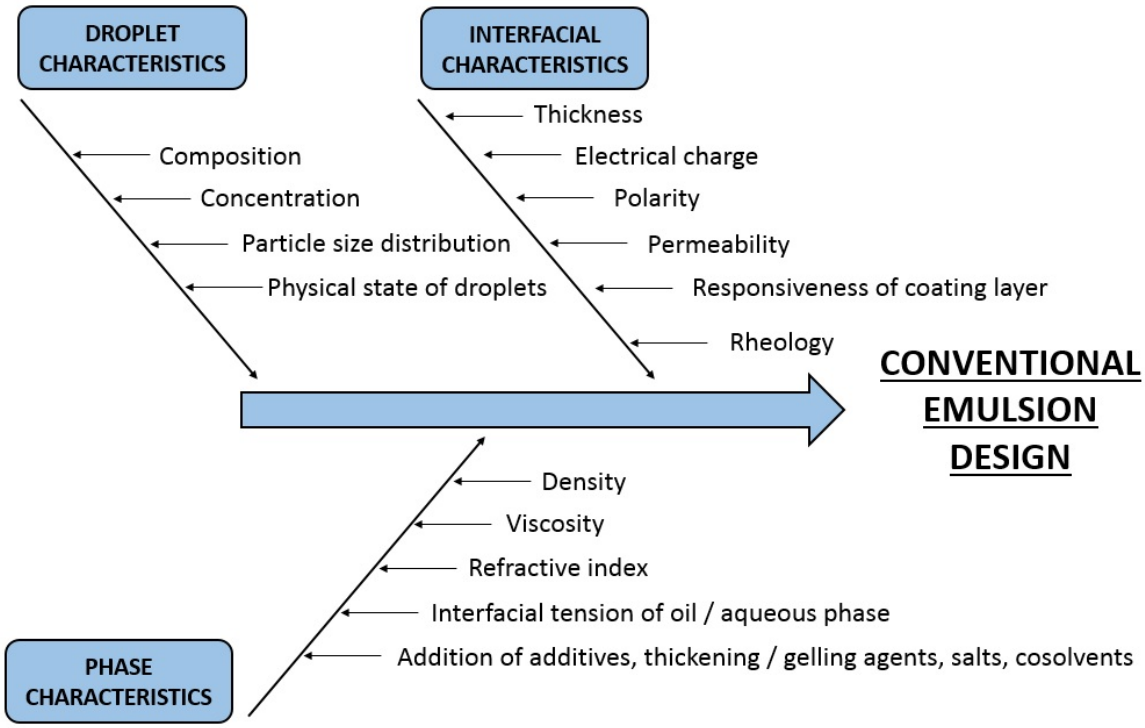

Fig. 2.1 Droplet, interfacial and phase characteristics that can be systematically altered to create building blocks of emulsions with different properties. Adapted from [15].

The major advantage of using the conventional emulsion design approach to create functional properties in emulsions is that they are relatively straightforward and inexpensive to implement, which is important for many industrial applications. On the other hand,

during the past decade, there have been major advances in the utilization of structural design principles to fabricate emulsions with novel functional properties and enhanced functionality [15], such as layering (tailor made coatings around the particles), clustering (control of the aggregation state of the droplets) and embedding (comprising droplets within larger particles of a different material). These novel approaches allow to create functional attributes that cannot be achieved using conventional emulsions (See Fig. 2.2).

Since that these emulsion-based delivery systems can potentially depict an increasing number of scenarios depending on different levels of complexity, it is forecasted that they will offer an interesting framework of possibilities in order to implement a reverse engineering.

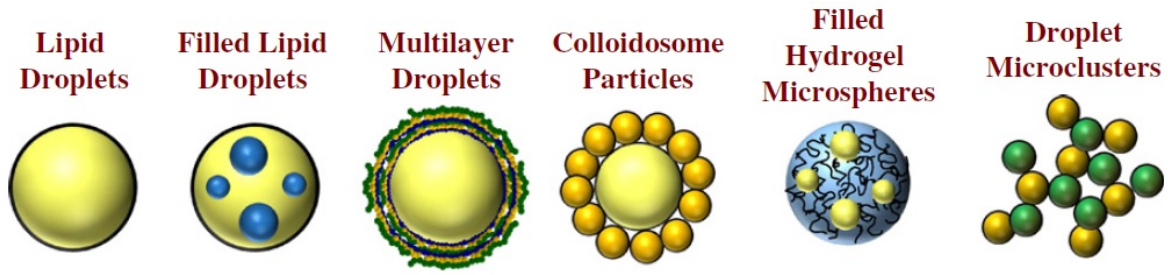

Fig. 2.2 Examples of structured emulsions that can be created by structural design principles using emulsion droplets as a building block.

Because of the enormous '*know-how*' developed in our laboratory during the last years, regarding the preparation of highly concentrated emulsions (thesis of Emilio Paruta, 2010) and also mass transfer within these systems (thesis of Hala Fersadou, 2011), we consider that they are presented as a relevant model system for the start-up of the reverse engineering that this thesis proposes.

Highly concentrated emulsions allow a high amount of dispersed phase, and a high ability to encapsulate active substances. As conventional emulsions, they can be of the oil-in-water (O/W) or water-in-oil (W/O) type. The different polarities of domains enable to solubilize hydrophilic and/or lipophilic molecules. Even though identified along as complex systems, these emulsions are very flexible regarding composition, size distribution, phase equilibria, interface type, morphology and viscosity. Therefore, they gather very good features to be applied a reverse engineering and to perform experimental validations.

A characteristic feature of these emulsions is their gel-like texture, leading to a significant improvement of emulsion stability, and offering a wide range of possibilities cocerning rheological properties and droplet size diameter. By way of illustration, in the following pages, a publication concerning the effects of formulation and processing on the rheological properties of oil-in-water highly concentrated emulsions is shown.

Colloids and Surfaces A 550 (2018) 155–166

Contents lists available at ScienceDirect

Colloids and Surfaces A

journal homepage: www.elsevier.com/locate/colsurfa

Hydrophobically modified dextrans as stabilizers for O/W highly concentrated emulsions. Comparison with commercial non-ionic polymeric stabilizers

Antonio Aguilera-Miguel[a,b], Edeluc López-Gonzalez[a,b], Véronique Sadtler[a,b,*], Alain Durand[c,d,**], Philippe Marchal[a,b], Christophe Castel[a,b], Lionel Choplin[a,b]

[a] Université de Lorraine, LRGP, UMR 7274, Nancy F-54001, France
[b] CNRS, LRGP, UMR 7274, Nancy F-54001, France
[c] Université de Lorraine, LCPM, UMR 7375, Nancy F-54001, France
[d] CNRS, LCPM, UMR 7375, Nancy F-54001, France

GRAPHICAL ABSTRACT

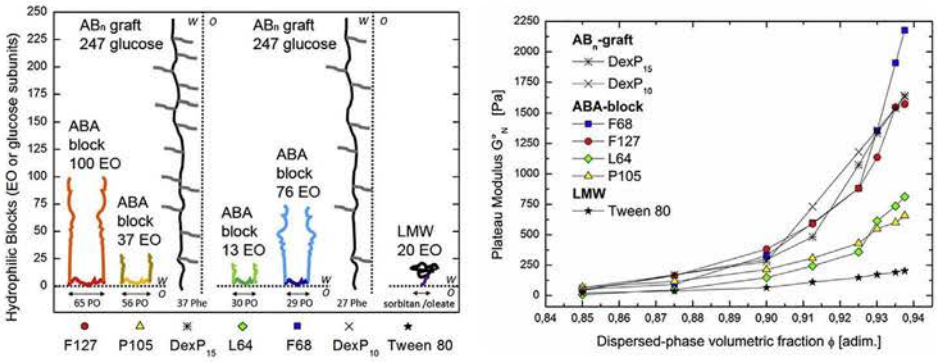

ARTICLE INFO

Keywords:
Non-ionic polymeric stabilizer
Highly concentrated emulsion
Emulsion rheology
Long-term stability

ABSTRACT

Two amphiphilic polysaccharides derived from a nonionic bacterial polysaccharide of dextran ($DexP_{10}$ and $DexP_{15}$) have been explored as emulsifiers for preparing highly concentrated oil-in-water emulsions in a semi-batch (two-step) process. A fixed amount of stabilizer (10 g/L of emulsion) was employed for preparing emulsions at dispersed-phase volumetric fractions ranging from 0.850 to 0.938. Their performances as stabilizers (interfacial tension, kinetics, droplet size distribution, rheological behavior and stability) were evaluated and compared with a group of four ABA non-ionic commercial stabilizers from Pluronic series (F68, F127, P105 and L64) and a low-molecular-weight surfactant (Tween 80). Our results demonstrate these AB_n graft amphiphilic polysaccharides can be promising stabilizers as efficient as commercial non-ionic polymeric stabilizers for preparing highly concentrated emulsions in spite of lower interfacial tensions, slower kinetics, or showing emulsions a larger droplet size and less monodispersity.

* Corresponding author at: Université de Lorraine, LRGP, UMR 7274, Nancy F-54001, France.
** Corresponding author at: Université de Lorraine, LCPM, UMR 7375, Nancy F-54001, France.
E-mail addresses: veronique.sadtler@univ-lorraine.fr (V. Sadtler), alain.durand@univ-lorraine.fr (A. Durand).

https://doi.org/10.1016/j.colsurfa.2018.04.022
Received 13 February 2018; Received in revised form 9 April 2018; Accepted 10 April 2018
Available online 12 April 2018

1. Introduction

Highly concentrated or High-internal-phase-ratio (H.I.P.R.) emulsions [22], also called gel-emulsions [35] or hydrocarbon gels [41], have many interesting applications within agrochemicals, pharmaceuticals, and personal care products. These emulsions have an extremely high content of dispersed phase volume fraction (ϕ). When ϕ is larger than the maximum packing volume fraction (ϕ^*) of about 0.74 (most compact arrangement of mono-disperse hard spheres [36], reached for a face-centered cubic packing), the drops are no longer present as spheres but are distorted into polyhedral shape. This structure gives rise to a number of peculiar and fascinating properties including high viscosities and viscoelastic rheological behavior [37].

The stability is one of the most important factor to consider in emulsions. An emulsion is stable when there is no change on the droplet size distribution or the spatial arrangement of droplets over the experimental time scale [17]. Currently, there is an increasing tendency to substitute molecular surfactants by macromolecular stabilizers to formulate emulsions because high molecular weight polymeric stabilizers have the advantage that their adsorption onto the droplet surface is much firmer than with low-molecular-weight surfactants. This occurs because polymeric surfactants attach to the droplet surface via several segments. Furthermore, they provide a thick steric barrier against flocculation and coalescence at the droplet surface, and consequently, they can be used in low concentrations and much more efficiently [28]. The most effective stabilization of oil-in-water (O/W) emulsions is generally obtained using ABA block or AB_n graft polymeric stabilizers [50].

Many polysaccharides are amphiphilic polymers that have extended flexible structures [13]. They are particularly attractive because of their good water-solubility, low toxicity and low interaction with living organisms. Some examples of AB_n graft stabilizers can be prepared by chemical modification of dextran [43]. By changing the conditions of the reaction [44], the number of the hydrophobic groups grafted onto the neutral polysaccharide chains can be controlled, giving rise to different amphiphilic dextrans of AB_n graft type, capable for emulsion stabilization. It has already been shown in the literature that amphiphilic polysaccharides can exhibit surface-active properties and to be efficient oil-in-water emulsion stabilizers for oil volume fractions up to 50 %. Nevertheless, to the best of our knowledge, there are no published studies about their use in highly concentrated emulsions ($\phi \geq 0.74$).

This paper has two purposes. On one hand, we want to shine new light on the use of these amphiphilic polysaccharide-based stabilizers for preparing highly concentrated O/W emulsions. On the other hand, we compare their performances as emulsifiers with polymeric stabilizers, and low-molecular-weight surfactants. By using a fixed mass amount of stabilizer (10 g/L of emulsion), and a two step semi-batch process, the effect of ϕ on droplet size distributions and storage moduli of the emulsions was examined. The stability of emulsions produced was also evaluated. Stabilizer concentrations were generally higher than critical concentrations determined by tensiometry and critical micelle concentrations reported on literature. This range is still largely unexplored in the literature, however is quite relevant for industrial applications [33].

2. Materials and methods

2.1. Materials

2.1.1. Dispersed and continuous phases

The dispersed phase was dodecane (Reagent Plus® 99%), obtained from Sigma–Aldrich and used as received. The continuous phase was water deionized and milli-Q filtrated by a Millipore apparatus.

2.1.2. Stabilizers

- AB_n graft – amphiphilic polysaccharide stabilizers: Two examples of phenoxy-hidrophobically modified dextrans ($DexP_{10}$ and Dex_{15}) were used. These stabilizers consist of a hydrophilic backbone within which hydrophobic units are randomly distributed (see Fig. 1a). They were synthesized as described in [44], by covalent attachment of hydrophobic groups (phenoxy groups) onto a polysaccharide backbone of dextran T_{40}. The substitution ratio or number of grafted hydrophobic groups (B) per 100 glucopyranose units (A) was 10 and 15 respectively. For comparison purposes, the backbone can be considered as a linear chain length of an average of 247 glucopyranose units (molecular weight of dextran T_{40} = 40,000 g/mol).
- ABA block – polymeric stabilizers: Four surfactants from the Pluronic series F68, F127, P105 and L64, supplied by BASF (Germany) were used as received. These water soluble polymeric stabilizers (see Fig. 1a) consist of two poly-A blocks chains of poly (ethylene oxide) (POE) and one B-block chain of poly (propylene oxide) (PPO) [1]. They were chosen as most commonly reported on literature and varying almost twice, three and four times the total average molecular weight and also their hidrophobe/hidrophile part in different proportions.
- Low-molecular-weight (LMW) stabilizer: A polyethylene sorbitol ester (Tween 80), supplied by Sigma–Aldrich was also included in this study as example of commercial surfactant of relatively low molecular weight (see Fig. 1c).

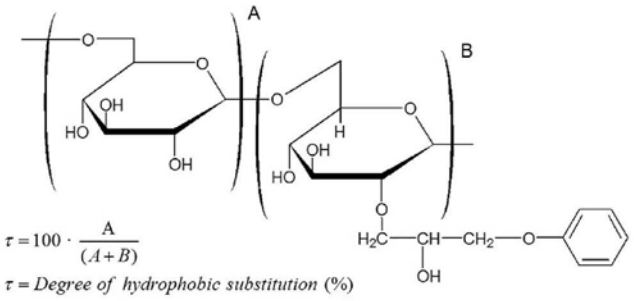

(a) AB_n-graft amphiphilic polysaccharide : DexPτ

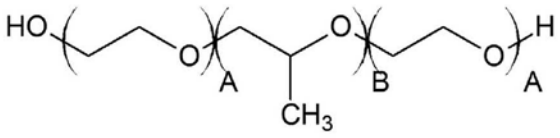

(b) ABA-block polymeric stabilizer (Pluronic)

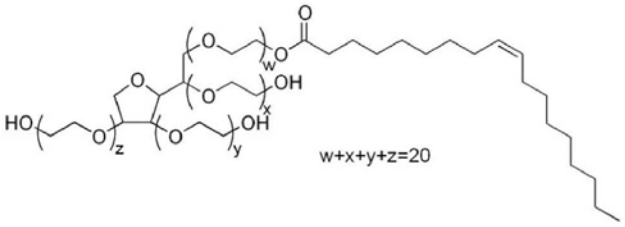

(c) Low-molecular-weight (LMW) stabilizer : Tween 80

Fig. 1. Typical molecular structures of stabilizers employed in this study.

Table 1
Properties of stabilizers employed in this study.

Stabilizer	Chemical structure[a]	MW	HLB[b]	γ_{CC}[c]	CMC
Tween 80	$C_{14}H_{34}$-COO–SR$(EO)_{20}$	1310	14.5	6.63	35.3 mg/L [55]; 57.6 mg/L [4]
L64	$(EO)_{13}(PO)_{30}(EO)_{13}$	2900	8	11.03	70 g/L [2]; 4.6 g/L (30 °C) [25]
P105	$(EO)_{37}(PO)_{56}(EO)_{37}$	6500	10	3.23	5.91 g/L in D_2O [23]
F68	$(EO)_{76}(PO)_{29}(EO)_{76}$	8400	15.6	12.26	100 g/L [27]; 25 g/L [46]
F127	$(EO)_{100}(PO)_{65}(EO)_{100}$	12600	14	4.22	2.6 g/L [48]; 9 g/L [2]
$DexP_{10}$	$H(C_6H_{10}O_5)_{247}(C_9H_{11}O_3)_{25}$	43870	19	9.95	13.16 g/L [this work]
$DexP_{15}$	$H(C_6H_{10}O_5)_{247}(C_9H_{11}O_3)_{37}$	45800	18.6	11.77	10.076 g/L [this work]

[a] EO: ethylene oxide; PO: propylene oxide; SR: sorbitan ring; Oleate: $C_{14}H_{34}$−COO−; phenoxy subunit: $C_9H_{11}O_3$.
[b] Calculated using the Beerbower and Hills equation [6] HLB = 20 × $M_H/(M_L+M_H)$ where M_H and M_L are the MW of hydrophilic and lipophilic portions of the stabilizers. It is assumed EO and glucose ($C_6H_{10}O_5$) as hydrophilic units.
[c] γ_{CC} = Interfacial tension [mN/m] for an interface dodecane – aqueous surfactant solution at C > CC.

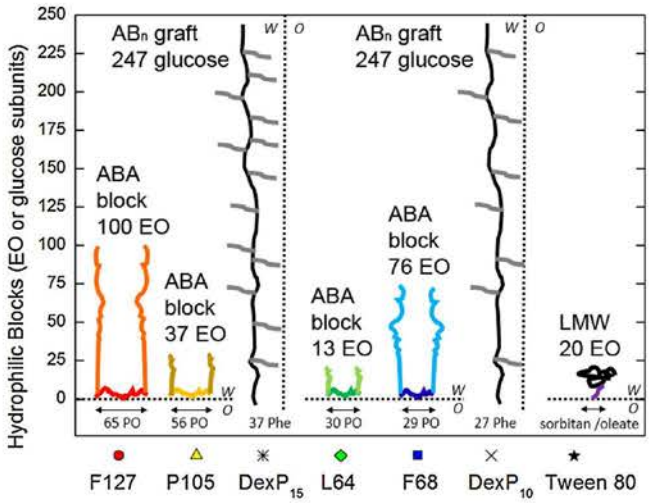

Fig. 2. Structure of the compared stabilizers. The dot line represent an interface water/oil (*W/O*). For sake of clarity, the hydrophobically modified dextrans have been depicted vertically. The number and type of hydrophobic blocks for each stabilizer are also specified on the *x* axis.

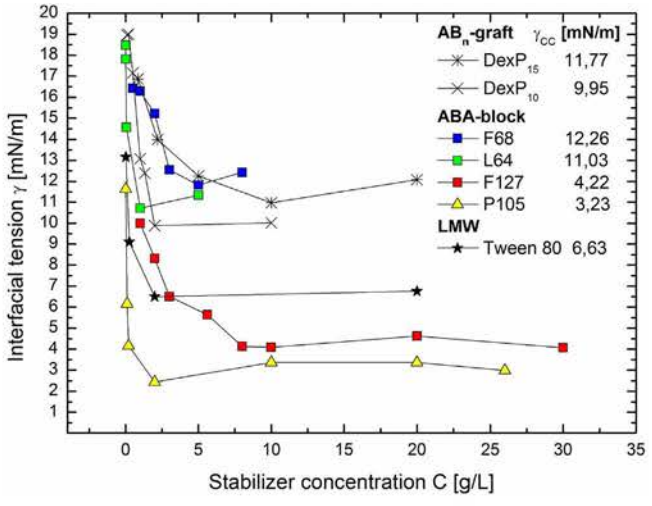

Fig. 3. Effect on interfacial tension (*W/O* interface) as function of stabilizer concentration at 25 °C. Interfacial tension values at critical concentration (γ_{CC}) are also shown.

2.2. Methods

2.2.1. Interfacial tension measurements

A drop volume tensiometer (Tracker, IT Concept) was used to measure the interfacial tension (γ) of a rising dodecane oil drop in solutions of aqueous stabilizer at 25 °C by analyzing the axisymmetric shape (Laplacian profile). The effect of the stabilizers on the interfacial tension was measured as function of the concentration. For an interface dodecane – water the value of the initial interfacial tension was around 50 mN/m. A value of 0.1 for the Bond number was set as optimum to obtain an appropriate volume of droplet and to avoid escape effects during the measurement. It took hours or even a day for more diluted solutions to obtain a stationary interfacial tension. At this moment, a representative value with a 5% accuracy was taken.

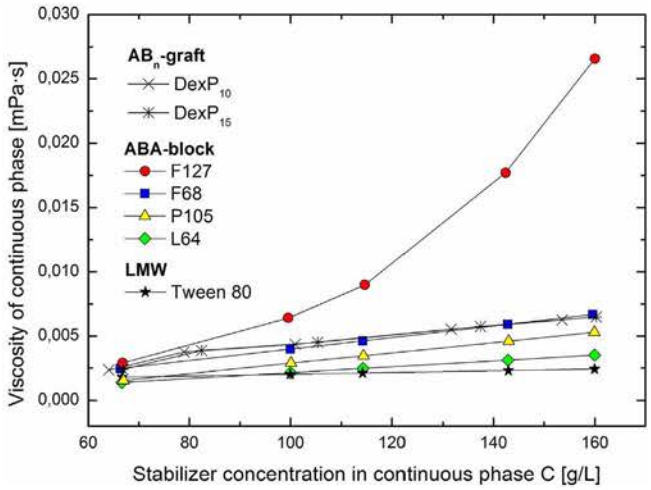

Fig. 4. Viscosity of continuous phases prior emulsification. Each point represents the initial concentration of stabilizer in the continuous phase at a given ϕ (from left to right: 0.850; 0.900; 0.913; 0.930 and 0.938).

2.2.2. Rheological measurements

The rheological characterization of the prepared emulsions was performed using a controlled stress rheometer AR-G2 (TA Instruments), equipped with a parallel plate geometry of smooth aluminum steel surfaces of 40 mm diameter. According to the literature [45], wall slip effects clearly decrease as dispersed-phase and emulsifier concentrations increases in this kind of systems. In any case, no significant influence by change of gap on the measurements was noticed.

Storage moduli (*G'*) values were determined via small amplitude oscillatory-shear tests, into the linear viscoelastic domain of the samples. Generally, it was observed for all samples that a strain of 0.1% at constant frequency of 10 rad/s was enough to remain within the linear domain. Scanning (sweep) shear rate measurements with a decreasing shear rate from 70 to 0.1 rad/s were carried out to get the characteristic viscoelastic parameter Plateau modulus, G°_N [5]. This parameter, which is considered as a measurement of the aggregation number of droplets comprising the dispersed phase, is related to the droplet interactions

and strength of the emulsion. The short-cut method proposed by Wu [54] was used to estimate G°_{N} from the loss tangent ($tan\,\delta = G''/G'$):

$$G^{\circ}_{N} = [G'] \rightarrow (\tan\delta)_{\text{minimum}}$$

The viscosity of continuous phases (prior emulsification) at different ϕ, were also measured by using a low shear viscosimeter LS300.

2.2.3. Determination of droplet size distributions

The droplet size distributions (DSD) of the emulsions were obtained using a Malvern Mastersizer 2000 (Malvern Instruments, U.K.). A beaker containing 600 mL of deionized and milli-Q filtrated water at a stirring rate of 1000 rpm was used as dilution blank for all measurements. Refraction indexes of 1.330 and 1.419 were used for water and dodecane respectively. The standard percentile $D_{0.5}$ (size in microns at which 50% of the sample is smaller and 50% is larger), was chosen as the representative diameter for the emulsion samples. Optical observations obtained by a BX51 Olympus microscope showed results from Mastersizer can be taken as the real droplet size distribution of emulsions.

2.2.4. Preparation of highly concentrated emulsions

Emulsion volumes of 40 mL were prepared in a simple two step semi-batch process, similar as described in [3]. A brief description is given below:

1. Continuous phase preparation. A fixed amount of surfactant (0.4 g) was incorporated into every aqueous phase. Different volumes of water were used depending on the ϕ to prepare; ranging from 6 mL ($\phi = 0.850$) to 2.5 mL ($\phi = 0.938$). The mixtures were allowed for thermodynamic equilibration during 24 h prior to proceeding to the next step.
2. Oil incorporation. The agitation turbine of a Turbo Test 33/750 P (Rayneri Groupe VMI), equipped with a 45° pitched agitator (4 blades) of 35 mm diameter, was positioned on the free surface of the continuous phase at a speed of 800 rpm. The oil phase was stepwise added to an emulsification vessel of 45 mm at a constant flow of 17.2 mL/min by a peristaltic pump (BVP, Ismatec). The temperature was controlled at 25 °C with a Polystat 12HT thermostatic bath (Bioblock Scientific).
3. Homogenization. After the oil incorporation, emulsions were kept stirring using the same agitation turbine and vessel during 10 min at 1000 rpm. This assured homogeneity of the dispersion. Emulsion samples were taken one hour after processing to measure their storage moduli and obtain their droplet size distributions. The remaining was transferred to a capped jar to prevent evaporation and was kept at room temperature. Properties were measured along a maximum time scale of two years.

3. Results and discussion

3.1. Characteristics of stabilizers in aqueous solutions

Table 1 summarizes the properties of the stabilizers; such as chemical structure, average molecular weight (MW), hydrophilic-lipophilic balance (HLB), interfacial tension (γ_{CC}) and critical micelle concentration (CMC) values found in the literature. In Fig. 2 their structures are depicted.

3.1.1. Interfacial tension measurements

Studies of adsorption of ABA-block polymeric surfactants at oil-water interfaces are scarce [38,39,34]. Comparison with extensive studies at air-water shows in general an analogous behavior at both interfaces [49]. We measured the effect on the interfacial tension (γ) of the stabilizers in aqueous solutions as function of the concentration. The results are plotted in Fig. 3. Generally, as the concentration of stabilizer increased, a lowering in γ occurred until a critical concentration (CC) above which no further decrease is observed. For all stabilizers, the CC values were found to be of the order of 1–10 g/L. These CC values are likely related to the formation layer at the interface, from which, further increases in the bulk concentration do not cause any more adsorption and as consequence, γ remains constant. Assuming that higher concentrations would not change this value, an average for γ using the last points (γ_{CC}) has been taken to characterize every system.

The more hydrophobic ABA block stabilizers; P105 and F127, with 56 and 65 PO units respectively, were the most effective on decreasing the interfacial tension (until 3–4 mN/m). As a general trend, longer POP blocks decrease interfacial tension to a larger extent because POP is more surface active than POE [21]. This is clearly observed when comparing these stabilizers with those of shorter POP blocks: L64 and F68, of 13 EO and 76 units respectively. Nonetheless, longer POE blocks can also result in a decrease of the interfacial tension because of an increased repulsion between the POE chains [7]. This would explain the higher reduction when using P105 instead of F127 or L64 instead of F68 in spite of having a similar number of central POP blocks. Conversely, the LMW stabilizer Tween 80, having a structure combining a single hydrocarbon group (oleate) and a bulky non-ionic polar group (sorbitan ring), led to an intermediate value of 6.63 mN/m. Surprisingly, the amphiphilic polysaccharides $DexP_{10}$ and $DexP_{15}$ with much less hydrophobic nature (25–37 phenoxy subunits) decreased γ to a same extent (up to 11–12 mN/m) than Pluronics L64 and F68. Possible interactions between the hydrophile glucose chains could also explain the higher reduction when using the less substituted $DexP_{10}$.

3.1.2. Concentration of stabilizer

The range of used concentrations at this work is shown in Fig. 4. Every point represents the initial mass concentration of stabilizer in the continuous phase at different ϕ (from 0.850 to 0.938). These values range from 60 to 180 g/L. In general, it is assumed that block copolymers and low-molecular-weight surfactants in a selective solvent form micelles via a so-called closed association process, characterized by a certain CMC, below which only molecularly dissolved stabilizer is present in solution, usually as unimers [42]. On the other hand, amphiphilic polysaccharides have shown that they can also behave like classical associative polymers [44]. Generally, it is assumed that at CMC and slightly above it, micelles are still loose but with further increase in amphiphile concentration in the medium, the unimer-micelle equilibrium shifts towards micelle formation [18]. Although the CMC is defined as a single concentration point, the micellization and micelle structure transitions can occur in a relatively broad range of concentrations in the proximity of the CMC [51]. This implies micelles become more tight and stable and decrease their size during this transition. It could be reasonable to think that previous CC determined by tensiometry should be related to those CMC reported on the literature (see Table 1). However, caution must be always applied because findings from different authors might not be transferable. In practice, a certain CMC range with some notable uncertainty could be detected, and large differences are often noted between CMC values determined by different methods [1] because their sensitivity to quantity of molecularly dispersed unimers present may vary or because of the presence of impurities. For any case, in this work, we assume and consider that all concentrations employed at this work are generally higher than these both CC and CMC. Therefore, we hypothesize that the excess of concentration above the CC, will be turned into a higher amount of micelles with probably different shapes existing in the aqueous solution.

3.1.3. Viscosity measurements

The viscosities of the stabilizer solutions employed as continuous phases at a given ϕ, were shown in Fig. 4. Identical or very close viscosity values were found when using different stabilizers at different concentrations. All aqueous solutions showed a Newtonian flow

behavior with viscosities ranging in the order of a few times the viscosity of water. The values increased with ϕ for every system. Generally, the higher the MW of the stabilizer, the higher the viscosity of the aqueous solution at a same ϕ. However, for Pluronic F127, it was observed that the viscosity was many times greater than all the others, specially at the highest ϕ. This finding reveals that the most important degree of interaction between the stabilizer molecules (micelles) within the continuous phase, likely occurs when this stabilizer is used.

3.2. Comparison of stabilizers

3.2.1. Effect of volumetric fraction (ϕ) on droplet size ($D_{0.5}$)

A set of DSD obtained at five ϕ by using the same semi-batch process at fixed total stabilizer concentration of 10 g/L emulsion can be visualized in Fig. 8. In general, the DSD of all emulsions evolve from a slightly polydispersed to a more ordered monodispersed system as ϕ increases. In Fig. 5 are shown plots of $D_{0.5}$ versus ϕ. It was noticed a linear decreasing relation between $D_{0.5}$ and ϕ for each stabilizer along the whole range of volumetric fractions studied. At a given ϕ, stabilizers with lower γ produced emulsions with smaller droplet sizes. This indicates clearly that the droplet diameter depends on the interfacial tension. However, the tendency diminishes as ϕ increases. This is explained because at high ϕ, it is the viscosity global of the emulsion which dominates the process of emulsification. This tendency corroborates ideas from previous authors [9] who argued that when the oil content increases, it is the emulsion viscosity that controls droplet size, regardless of the dispersed-phase viscosity and hydrodynamics. As authors pointed out, this implies that the efficiency of the mixing process is strongly improved by increasing the internal phase content, and less power input is necessary for a more efficient droplet rupturing process.

However, it is interesting to note that no differences were found concerning $D_{0.5}$ when employing Pluronic stabilizers F127 and L64, despite differences on viscosity of continuous phases, interfacial tension and HLB, coinciding $D_{0.5}$ lines along the whole range of ϕ. As it will be shown below, all emulsions differed in Plateau Modulus G°_N, which is generally proportional to the global viscosity of the emulsion, indicating that other dominant factors must be involved on the reduction of the droplet size. Probably, this should be understood because of the different molecular conformations adopted at the interface as a function of the surface coverage (interfacial concentration), which depends strongly on molecular packing [51]. This has been experimentally corroborated by ellipsometric [40,26], and neutron reflectivity measurements [47,52].

Our results show that in the high interfacial concentration regime, when the conformation is the most compact, there are no differences concerning final droplet size when using stabilizers of a same type though quite different characteristics. This is confirmed in Fig. 5, all lines (within a same stabilizer type; ABA or AB_n stabilizer) converged approximately at the same $D_{0.5}$ value at high ϕ. It is also worth to mention that the observed correlation between droplet size and volumetric fraction can also be explained in terms of a fixed relation between specific interfacial area created during emulsification and the concentration of stabilizer in the emulsion [53]. In other words, amount of micelles. We confirmed this fact performing additional tests. From a practical point of view, by tune-up of the stabilizer concentration in the emulsion, it is possible to spread these straight $D_{0.5}$ lines equidistantly within a wide range of droplet sizes at different ϕ.

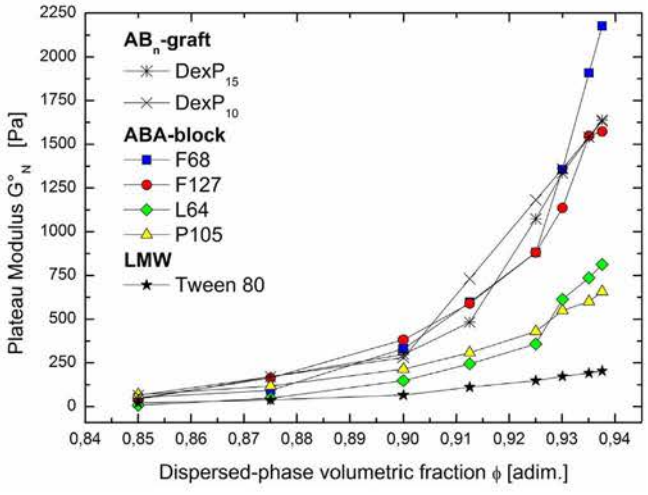

Fig. 6. Effect of volumetric fraction on plateau modulus.

3.2.2. Effect of volumetric fraction (ϕ) on plateau modulus (G°_N)

The results from scanning measurements into the linear domain of the samples can be visualized in Fig. 9. Similarly to other authors [30,8,19], it was observed the typical behavior of ideal elastic materials [14]; the elastic modulus G' was independent of frequency, covering several orders of magnitude, with G' > G in the whole amplitude domain. In Fig. 6, we show the evolution of Plateau modulus as function of ϕ. In general, all ABA-block or AB_n stabilizers showed a dramatic increase of G', specially at very high ϕ. However, for emulsions prepared by Tween 80, this fact was much more moderated. On the other hand, the amphiphilic dextrans $DexP_{10}$ and $DexP_{15}$ exhibited comparables values of G°_N to those obtained by using the commercial ABA-

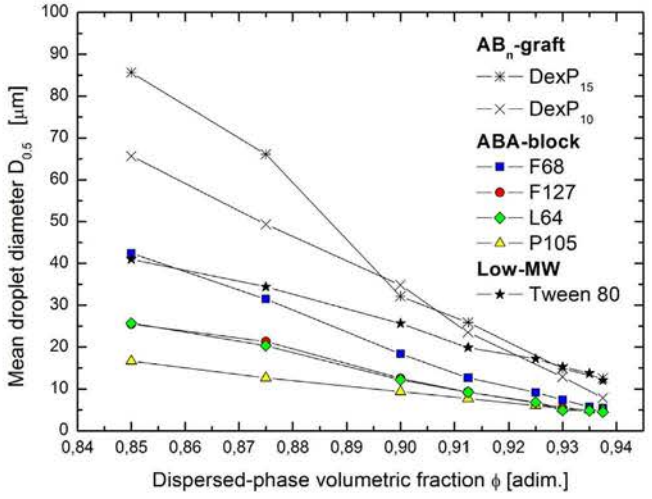

Fig. 5. Effect of volumetric fraction on mean droplet diameter.

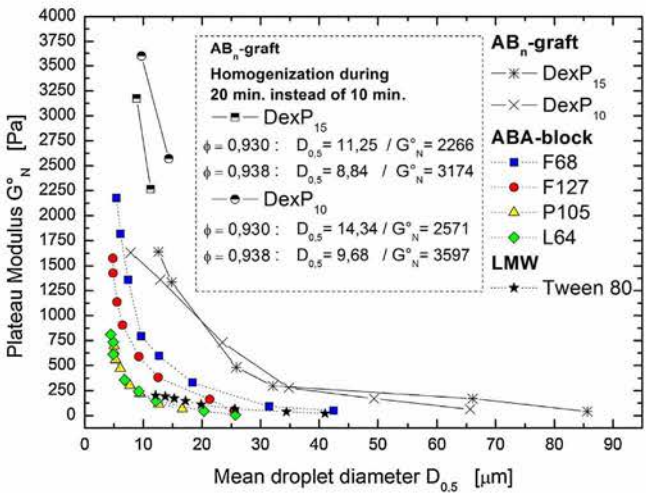

Fig. 7. Effect of mean droplet diameter on plateau modulus.

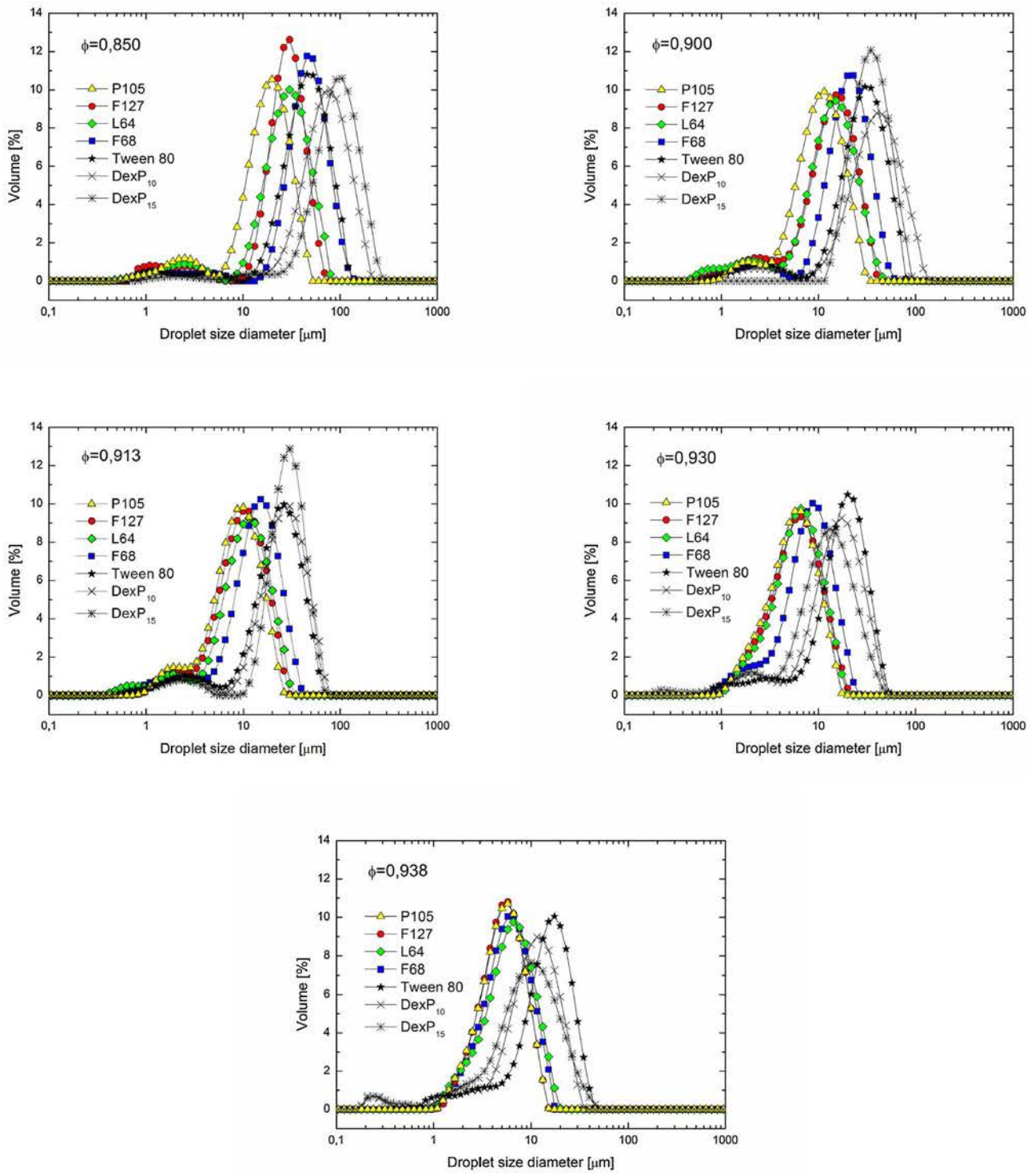

Fig. 8. DSD curves obtained for the different stabilizers of this work. All emulsions were prepared using same emulsification process conditions (10 min) at the fixed mass amount concentration of 10 g/L emulsion. Emulsions made by ABA-block Pluronic where the only to show a complete monodispersity at highest ϕ. Those prepared by DexP or Tween 80 were bidisperse. When using amphiphilic polysaccharides DexP at highest ϕ, the appearance of small population of droplets was observed. This likely could be due to the break-up of possible bridging-flocculated droplets.

block stabilizers F68 and F127 at a given ϕ. All these stabilizers have in common to be of a relatively high hydrophilic nature. On the other hand, the smallest ABA-block stabilizers, L64 and P105 showed significantly lower values.

In Fig. 7, we have shown jointly G°_N and $D_{0.5}$. A common tendency towards a critical droplet diameter with G°_N tending to infinite was observed as a lower limit for all ABA-block surfactants (around 5 μm). In previous work [31] we found a similar tendency. We argued the existence of a critical-dispersed phase volume fraction ϕ^* beyond it becomes impossible to prepare the emulsion. Normally, this is limited by the experimental conditions of emulsification. When using amphiphilic dextrans it was not clear the asymptotic increase of G°_N, therefore we allowed the time for the homogenization step to be prolonged until 20 min for emulsions of $\phi = 0.930$ and 0.938. This was performed in order to provide more energy to the process and try to keep reducing the droplet size. We did not observe significative differences concerning

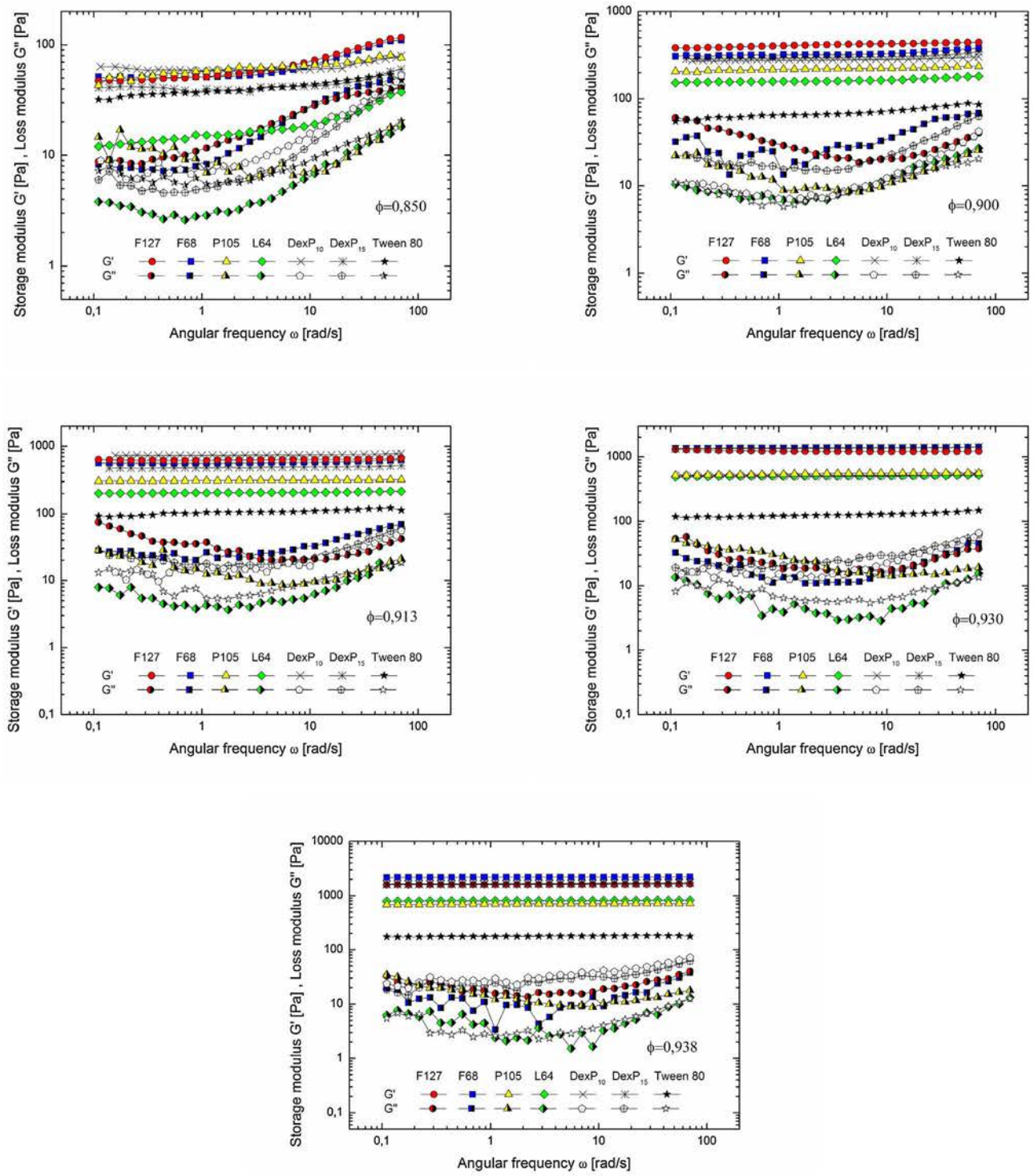

Fig. 9. Evolution of the storage, G', and loss, G'', moduli with frequency for emulsions studied as a function of oil volumetric fraction ϕ. All measurements were performed into the lineal viscoelastic domain of the samples. A strain of 0.1% at constant frequency of 10 rad/s was enough to remain within the linear domain.

G°_N or $D_{0.5}$ by using ABA-block or LMW stabilizers with a further shearing. However, when using amphiphilic dextrans (see Fig. 7), the emulsions prepared with 20 min. showed much higher values of G°_N and the critical droplet diameter was found around 10 µm. When using these AB_n graft stabilizers, it can be reasonable to think that bridging flocculation of droplets [29] occur because segments of the same polymer macromolecule can adsorb onto different droplets, thereby linking droplets together, or separate polymer chains are adsorbed onto different droplets. Therefore, one can hypothesize that a further shearing changes the structure of the flocculated network or droplet clusters. Overall, the hydrophobically modified dextrans showed higher G°_N than all the others stabilizers in spite of showing higher droplet sizes.

3.3. Follow-up of emulsification kinetics

Emulsions at $\phi = 0.930$ were prepared with all stabilizers and small sample amounts were taken at different intervals of time. They were observed by microscopy and their DSD were obtained by light scattering. As can be seen in Fig. 10, at the beginning (domain of dilute

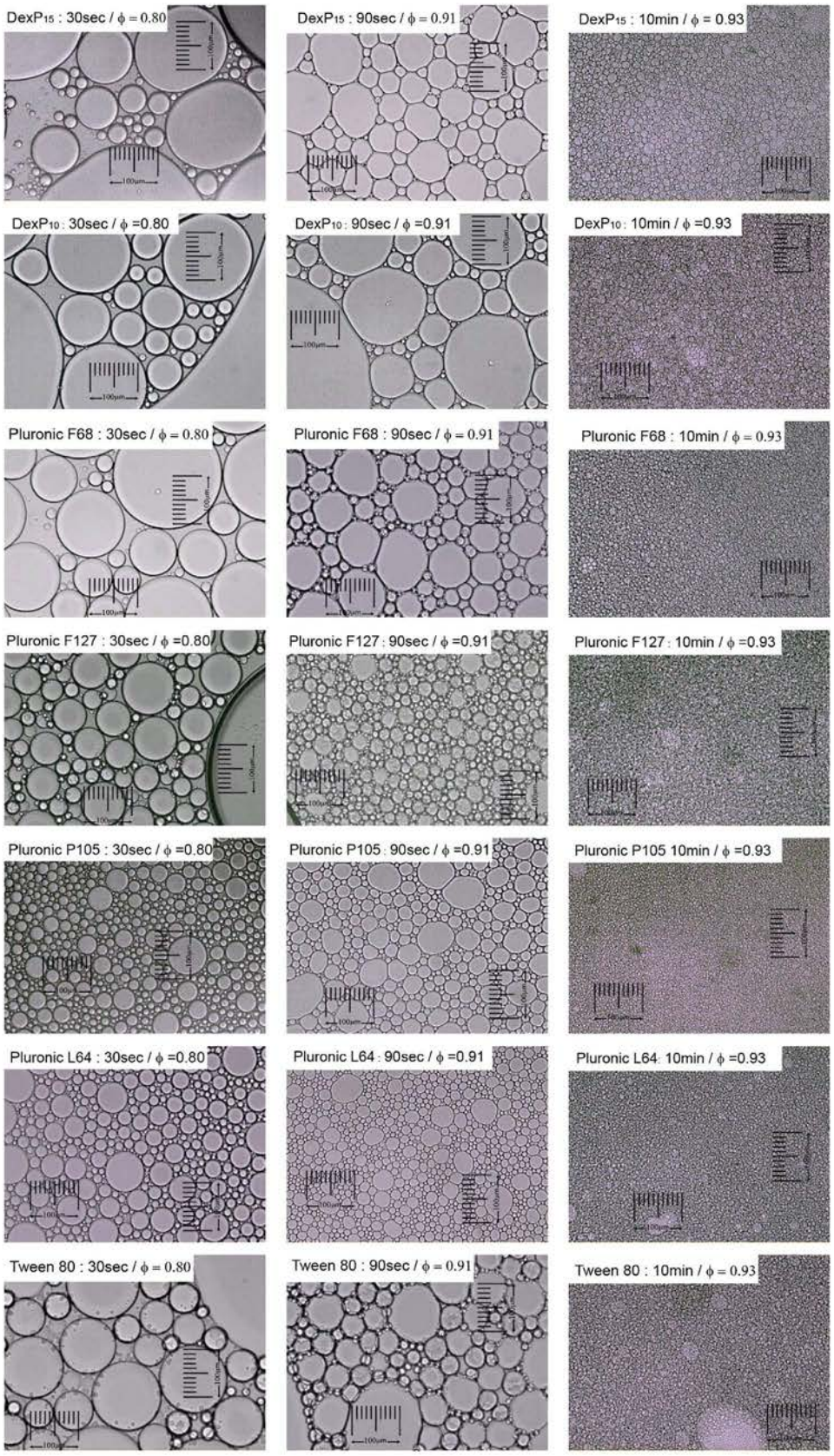

Fig. 10. Micrographs related to the oil addition (30 and 90 s) and homogenization step (10 min) when preparing highly concentrated emulsions at final $\phi = 0.93$. Microscope resolution of 20×. The dispersed-phase volumetric fractions (ϕ) were calculated considering the added volume at the respective moment.

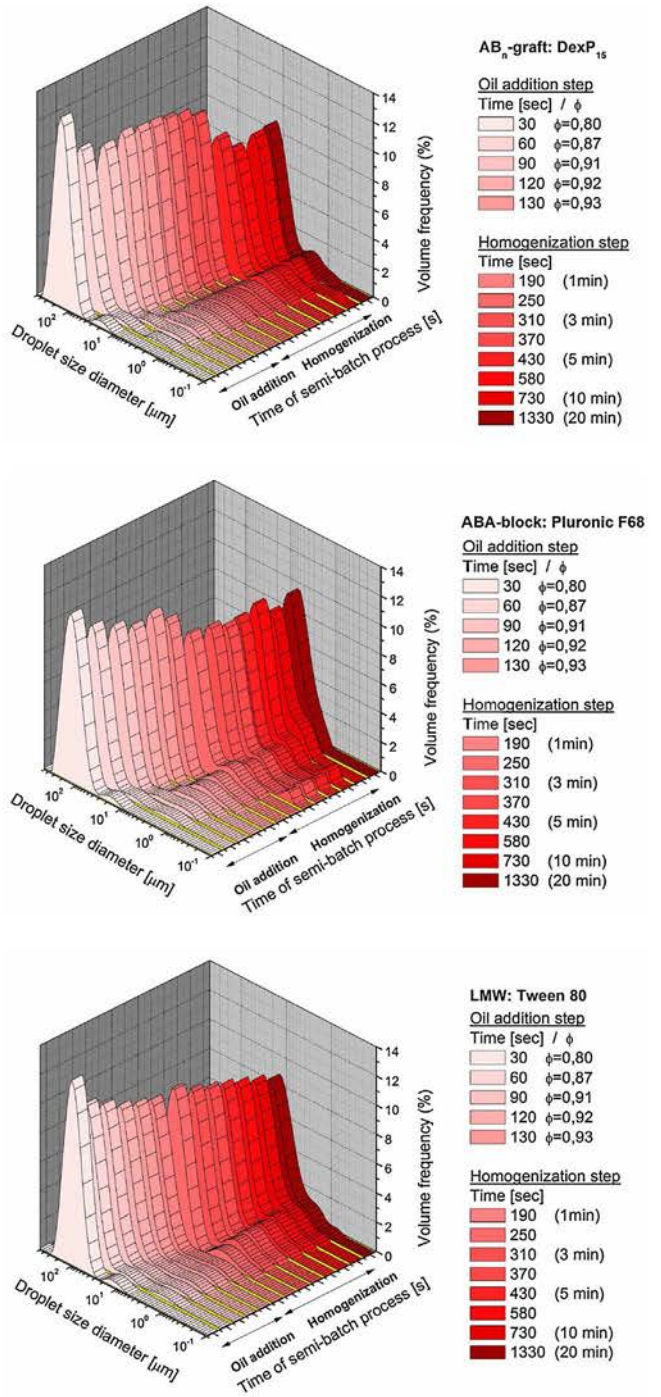

Fig. 11. Dynamic captures of DSD during emulsification processing of highly concentrated emulsions.

emulsion), droplets were spherical (without any deformation). Once the concentration of the dispersed-phase exceeded the limit of the closest packing of spherical particles in space (ϕ around 0.840 in this work), the spherical droplets started to being deformed via compression of the dispersion (domain of highly concentrated emulsion), resulting in the transformation of spherical drops into particles of different tightly packed polygonal shapes occupying the space. At the end of process, when no more reduction on droplet size was possible, a lattice or interconnected grid of tiny and deformed droplets with homogeneous nature is observed.

For sake of clarity, we have shown in Fig. 11 the evolution of the DSD for one example of each type of stabilizer. In general, the higher ϕ,

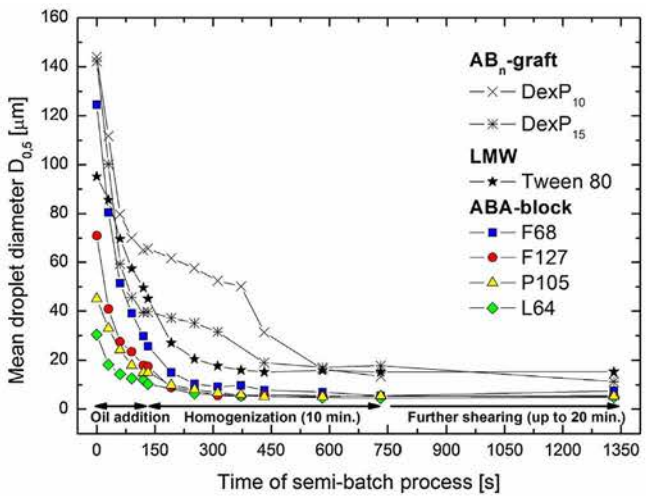

Fig. 12. Evolution of mean droplet diameter (D_{05}) during time of the semi-batch processing of emulsions at $\phi = 0.930$.

Table 2
Fitting for kinetic parameter w.

Copolymer	r^2	w_0 [s^{-1}]	$1/w_0$ [s]	HLB
L64	0.98961	0.01163	85.984	8
P105	0.97655	0.00747	133.868	10
F127	0.98266	0.00751	133.155	14
Tween 80	0.92231	0.00611	163.666	14.5
F68	0.97225	0.00536	186.567	15.6
$DexP_{15}$	0.97674	0.00518	193.050	18.6
$DexP_{10}$	0.9441	0.00326	306.748	19

the less the polydispersity. This confirms that it is relatively easy to obtain a monodisperse DSD by means of this two step semibatch process if optimal conditions and enough time are allowed for the emulsification. Fig. 12 shows the follow-up of $D_{0.5}$ for every stabilizer during the semi-batch process. First, during the oil addition step (from 0 to 130 s), all ABA-block and the LMW stabilizer presented a fast initial adsorption rate, which contributes to a rapid emulsification process. Following this, during the homogenization step, D_{05} converged to an unique asymptotic value at the end of the semi-batch process. In contrast, the amphiphilic polysaccharides show a distinctive slower linear decrease during the step of homogenization. This is probably due to the high MW of these macromolecules, which leads to a slower diffusion to the interface, as well as its particular multi-graft structure, whereby an important reorganization is required to be done. In other words, this slower decrease can also be interpreted as a very effective mechanism for the stabilization of the interface which consequently slows down the droplet size reduction.

This kind of regimes of droplet fragmentation had been observed by other authors [24,10,16,12]. They showed by microscope observations that the first regime involves deformation of drops into long cylinders which broke into aligned droplets (Rayleigh instability) [24]. During the second regime, droplet fragmentation occurred by a different mechanism with a much longer characteristic time. The authors proposed to consider, that each oil droplet is broken into $(w + 1)$ smaller droplets per unit time. As D_{05} reached an asymptotic value, w should be a function of droplet diameter $w = f(D_d)$ which canceled for any value equal to or lower than the asymptotic value. Therefore, a simple function can be postulated to describe this dependence of w:

$$w = w_0 \frac{D_d - D_f}{D_f} \text{ for } D_d > D_f \text{ and } w = 0 \text{ for } D_d < D_f$$

where D_d and D_f are initial and final asymptotic average droplet diameter respectively, and w_0 is a characteristic frequency of droplet

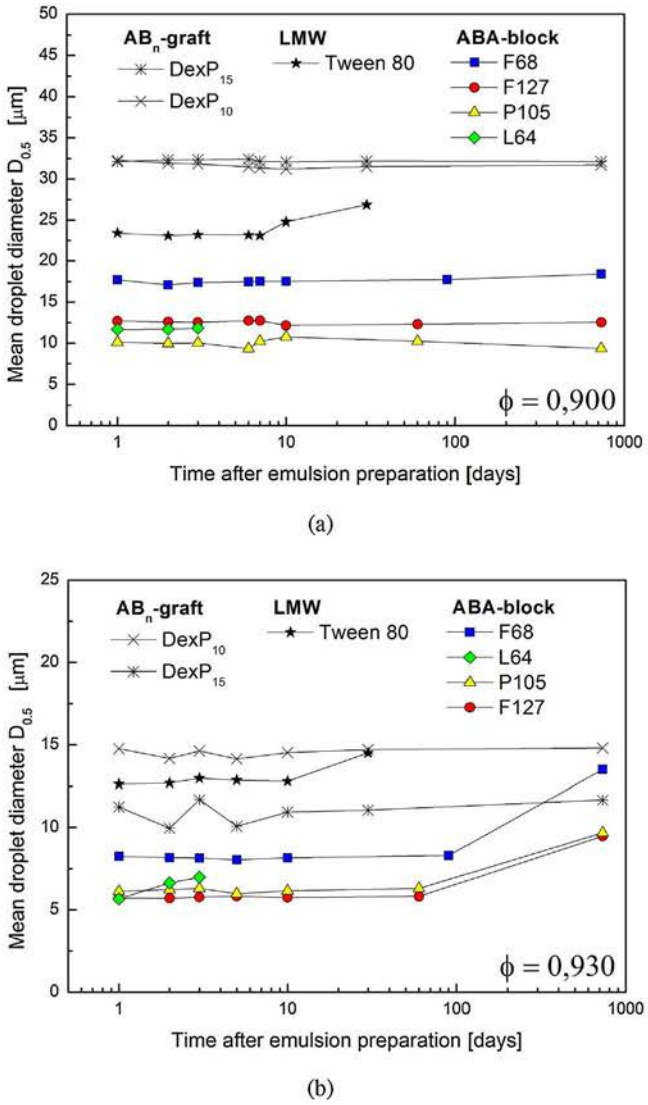

Fig. 13. Mean droplet diameter ($D_{0.5}$) of emulsions at $\phi = 0.900$ (a), 0.930 (b) along an interval of experimental time of two years.

fragmentation (s^{-1}). Combining this equation with the condition of oil volume conservation allows deriving the time variation of droplet diameter during fragmentation under shear:

$$D_d(t) = \frac{D_f}{1 - (\frac{D_0 - D_f}{D_0})\exp(\frac{-w_0 t}{3})}$$

In concordance with the results of other studies [11], we try to translate these equations to our work, but considering the presence of micelles. During the first regime or step, available monomers in equilibrium adsorb rapidly onto the freshly created interface [32]. Afterwards, additional monomers must be provided by the breakup of micelles, therefore droplet fragmentation occurs by a different mechanism with a much longer characteristic time, for which the micellar breakup time is a rate limiting step in the supply of monomers [32]. Because these two regimes could be equivalent to those observed by previous authors [24], their proposed kinetic equation could be useful to apply at this work in order to compare the different stabilizers.

For comparison purposes, our experimental $D_{0.5}$ values have been fitted to the last equation with w_0 as the only adjustable parameter. Table 2 shows the results from this fitting. The inverse w_0 corresponds to the characteristic fragmentation time of the emulsification process. As one can see, we found a proportional correlation between the HLB and the characteristic frequency of droplet fragmentation (w_0). The more the hydrophilic character of the stabilizer, the slower the fragmentation rate. Conversely, for Pluronic F127 it was observed a faster fragmentation than expected according to the HLB trend. According to the literature [51], an increase in the lengths of the POE blocks can make greater the probability of contacts of the POP units with the POE units within the core of the micelles. This effect could cause a general decrease of the hydrophobicity of the core and results in a destabilization of the micelle [1]. Likely, the viscosity measurements showed this effect. As a consequence of this, it is reasonable to think that a faster emulsification occurs when using this ABA-block stabilizer and this could justify the deviation of the tendency with HLB.

3.4. Stability of highly concentrated emulsions

We examined the change on DSD and G°_N for all emulsions in the short (a few days), middle (30–60 days) and long term (two years). Most of the HIPR emulsions did not present phase separation after two years. Only emulsions prepared with Pluronic L64 and Tween 80 broke after three days, or one month, respectively. In the same manner, emulsions prepared with $DexP_{10}$ and $DexP_{15}$ at $\phi = 0.850$ did not remain stable and separation of phases was observed in short time. This instability at low ϕ could be explained by the too big initial droplet size (around 65–80 μm). Changes or intensification on the emulsification process would be recommendable in order to get smaller droplet sizes and consequently, a better stability.

As representative examples, we show results from emulsions prepared at $\phi = 0.900$ and 0.930. Fig. 13 shows the change on $D_{0.5}$. All $D_{0.5}$ values remained almost constant for emulsions at $\phi = 0.900$. Only a variation of 4 μm was observed for the Tween 80 after 30 days. When using the ABA block L64, few hours were enough to observe clearly two transparent layer phases, on the top and the bottom of the emulsions. These layers, composed by dodecane oil in the upper part and water in the bottom are origined as a consequence of coalescence related to the bad steric stabilization between droplets. Fig. 14 the change on G°_N. For the oscillatory measurements, only the portion of the remaining emulsion was taken. After three days there was not L64 gel-emulsion enough to effectuate the characterization of G°_N. We attributed this fact to the not optimal formulation according to the HLB number. For emulsions prepared by Tween 80, this phenomena also occurred but in a longer period (approximately after one month).

Overall, the amphiphilic dextrans were the most effective stabilizers. All emulsions prepared by $DexP_{10}$ and $DexP_{15}$ showed the smallest variations on $D_{0.5}$ and G°_N along the experimental time. These findings reveal the significantly high stability when using these macromolecular stabilizers versus the other stabilizers of the study in spite of a bigger droplet size. It should be mentioned that the homogenization time for DexP emulsions at ($\phi = 0.930$) was evaluated when using 20 min (the most possible flocculated emulsion). A first decrease followed by a second increase on the moduli G°_N was observed for DexP emulsions at high ϕ. This indicates clearly that rearrangements between droplets occur along time. On the contrary, emulsions prepared by F127 and F68 showed a considerably higher decrease on G°_N. A summary of $D_{0.5}$ and G°_N values for all emulsions prepared at the different ϕ is shown in Tables 3 and 4.

Previous authors [15], had studied the thickness and disjoining pressure in O/W emulsion films stabilized with ABA Pluronic polymeric stabilizers and other graft copolymer (hydrophobically modified inulin) named INUTEC SP1. They concluded that emulsions with graft stabilizers are expected to be more stable than those stabilized with ABA polymeric stabilizers because of the strong loop-to-loop interactions and the Newton black films (NBF) that are formed. Our results corroborate conclusions of their work. Our results support steric stabilization theories in the highly concentrated regime that aim the structure in a highly concentrated emulsion refers to a big interconnected grid, with strong interaction between droplets showing a high storage moduli. The

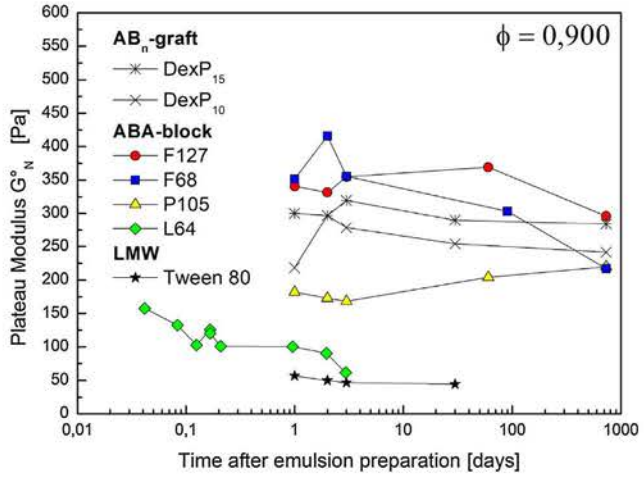

(a)

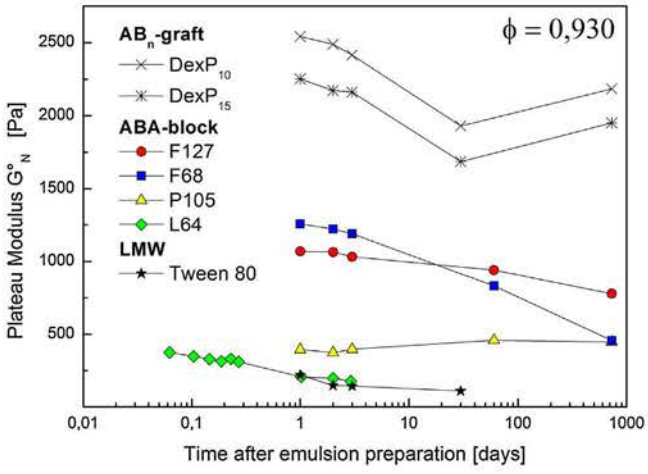

(b)

Fig. 14. Plateau Modulus (G°_N) of emulsions at $\phi = 0.900$ (a), 0.930 (b) along an interval of experimental time of two years.

change on the structure of the big interconnected grid can be easy followed up by G°_N. This parameter considers the strong interactions between droplets and in other words, the strength of the emulsion. However, a high storage moduli can be also representative of a very flocculated system. We have shown that the Plateau modulus by itself can not be always representative as indicator of stability for emulsions. It is possible that the conformation/orientation of the stabilizer in the interface evolves or for instance, it was not allowed a full total coverage of the surface droplets. Out of our scope was to consider this fact and other such as micelles by themselves were solubilizing y/o stabilizing a proportion of the droplet oils as observed by other authors [20]. Further understanding concerning the role of micelles, partition with the stabilizer on the interphase and relation to the Plateau modulus would be of interest and will be the topic for a next paper.

Table 3
Mean drople size diameter ($D_{0.5}$) of emulsions measured on the day of preparation and two years later.

ϕ	$DexP_{10}$	$DexP_{15}$	F68	F127	P105
$D_{0.5}$ [μm] on the day of preparation					
0.850	65.64	85.65	42.42	25.47	16.64
0.900	32.25	32.12	18.39	12.54	9.37
0.913	23.52	25.87	12.69	9.25	7.70
0.930	14.34	11.24	7.43	5.50	5.28
0.938	9.68	8.84	5.40	4.78	5.04
$D_{0.5}$ [μm] after two years					
0.850	–	–	44.46	27.09	18.01
0.900	36.58	33.66	21.32	14.65	12.17
0.913	24.18	26.22	18.14	12.68	10.11
0.930	15.07	11.67	13.53	9.48	9.68
0.938	10.26	9.59	14.72	9.37	9.18

Table 4
Plateau modulus G°_N of emulsions measured on the day of preparation and two years later.

ϕ	$DexP_{10}$	$DexP_{15}$	F68	F127	P105
G°_N[Pa] on the day of preparation					
0.850	63	40	50	48	67
0.900	279	297	329	381	222
0.913	730	482	596	589	303
0.930	2571	2266	1356	1136	558
0.938	3597	3174	2177	1573	696
G°_N[Pa] after two years					
0.850	–	–	36	40	63
0.900	241	284	217	296	220
0.913	719	475	283	405	243
0.930	2184	1951	458	778	446
0.938	2701	2634	500	1385	694

4. Final conclusions

- We have investigated the droplet size distributions and linear viscoelastic properties of highly concentrated O/W emulsions stabilized by different stabilizers. A typical behaviour of highly concentrated emulsions with a high degree of flocculation has been found: an increase in the emulsifier concentration leads to an increase in both viscoelastic moduli (G', G") as well as to a decrease in droplet size. This is most likely due to an enhancement of the entanglement network produced by the association of macromolecules that are surrounding oil droplets leading to a significant improvement of emulsion stability.
- Our results showed that the two step semi-batch protocol was appropriate enough to get homogenous and stable gel-emulsions for a two-year interval of time with exception of all those prepared by stabilizers Pluronic L64 and Tween 80. Emulsions prepared by hydrophobically modified dextrans $DexP_{10}$ and $DexP_{15}$ showed the highest stability in spite of slower kinetics, higher droplet sizes or higher interfacial tensions. To the best of our knowledge, there are no studies in literature showing the efficacy employing polysaccharide based graft-copolymers at these concentrations and dispersed-phase volumetric fractions.
- It looks promising the wide range of possibilities that the nonionic polymeric surfactants allow in order to prepare O/W emulsions showing different features and having long stability on the time scale. For future research on this topic, it is suggested to provide more clarity surrounding the specific role of the stabilizer on the interface, their partition with the micelles of the continuous media, and their relations to the Plateau modulus.

Acknowledgements

Financial support from the Centre national de la recherche scientifique (CNRS) and the Ministère de l'Enseignement Supérieur de la Recherche et de l'Innovation are gratefully acknowledged.

References

[1] P. Alexandridis, T. Hatton, J. Holzwarth, Micellization of poly (ethylene oxide)-poly (propylene oxide)-poly (ethylene oxide) triblock copolymers in aqueous solutions: thermodynamics of copolymer association, Macromolecules (United States) 27 (9)

(1994).
[2] P. Alexandridis, T.A. Hatton, Poly (ethylene oxide) poly (propylene oxide) poly (ethylene oxide) block copolymer surfactants in aqueous solutions and at interfaces: thermodynamics, structure, dynamics, and modeling, Colloids Surf. A: Physicochem. Eng. Aspects 96 (1) (1995) 1–46.
[3] O.A. Alvarez, L. Choplin, V. Sadtler, P. Marchal, M.-J. Stébé, J. Mougel, C. Baravian, Influence of semibatch emulsification process conditions on the physical characteristics of highly concentrated water-in-oil emulsions, Ind. Eng. Chem. Res. 49 (13) (2010) 6042–6046.
[4] A. Avranas, E. Malasidou, I. Mandrazidou, Adsorption of cetyldimethylbenzylammonium chloride on octane emulsions droplets: the effect of the presence of tween 80, J. Colloid Interface Sci. 207 (2) (1998) 363–370.
[5] M. Baurngaertel, M. De Rosa, J. Machado, M. Masse, H. Winter, The relaxation time spectrum of nearly monodisperse polybutadiene melts, Rheol. Acta 31 (1) (1992) 75–82.
[6] A. Beerbower, M. Hill, Application of the cohesive energy ratio (CER) concept to anionic emulsifiers, Am. Cosmet. Perfum. 87 (1972) 85.
[7] B.R. Blomqvist, T. Wärnheim, P.M. Claesson, Surface rheology of PEO-PPO-PEO triblock copolymers at the air–water interface: comparison of spread and adsorbed layers, Langmuir 21 (14) (2005) 6373–6384.
[8] C. Bower, C. Gallegos, M. Mackley, J. Madiedo, The rheological and microstructural characterisation of the non-linear flow behaviour of concentrated oil-in-water emulsions, Rheol. Acta 38 (2) (1999) 145–159.
[9] M. Briceno, J. Salager, J. Bertrand, Influence of dispersed phase content and viscosity on the mixing of concentrated oil-in-water emulsions in the transition flow regime, Chem. Eng. Res. Des. 79 (8) (2001) 943–948.
[10] S. Caubet, Y. Le Guer, B. Grassl, K. El Omari, E. Normandin, A low-energy emulsification batch mixer for concentrated oil-in-water emulsions, AIChE J. 57 (1) (2011) 27–39.
[11] R. Covis, C. Baravian, E. Marie, A. Durand, Kinetics of formation of polysaccharide-covered micrometric oil droplets under mechanical agitation, Colloids Surf. A: Physicochem. Eng. Aspects 466 (2015) 92–99.
[12] R. Covis, E. Marie, A. Durand, C. Baravian, Kinetics of formation of oil-in-water emulsions using in situ rheo-optical measurements? AIChE J. 61 (1) (2015) 277–284.
[13] S.W. Cui, Food Carbohydrates: Chemistry, Physical Properties, and Applications, CRC Press, 2005.
[14] S.R. Derkach, Rheology of emulsions? Adv. Colloid Interface Sci. 151 (1) (2009) 1–23.
[15] D. Exerowa, G. Gotchev, T. Kolarov, K. Kristov, B. Levecke, T. Tadros, Comparison of oil-in-water emulsion films produced using ABA or ABn copolymers? Colloids Surf. A: Physicochem. Eng. Aspects 335 (1) (2009) 50–54.
[16] S. Fournanty, Y.L. Guer, K.E. Omari, J.-P. Dejean, Laminar flow emulsification process to control the viscosity reduction of heavy crude oils, J. Dispers. Sci. Technol. 29 (10) (2008) 1355–1366.
[17] C. Gallegos, J. Franco, Rheology of food emulsions, Rheol. Ser. 8 (1999) 87L 118.
[18] Z. Gao, A. Eisenberg, et al., A model of micellization for block-copolymers in solutions, Macromolecules 26 (26) (1993) 7353–7360.
[19] K. Hyun, S.H. Kim, K.H. Ahn, S.J. Lee, Large amplitude oscillatory shear as a way to classify the complex fluids, J. Non-Newton. Fluid Mech. 107 (1) (2002) 51–65.
[20] Y. Kong, A. Nikolov, D. Wasan, Emulsion stability in the presence of nonionic surfactant micelles: role of micellar ordering and Ostwald ripening, Ind. Eng. Chem. Res. 49 (11) (2010) 5299–5303.
[21] P. Linse, T.A. Hatton, Mean-field lattice calculations of ethylene oxide and propylene oxide containing homopolymers and triblock copolymers at the air/water interface, Langmuir 13 (15) (1997) 4066–4078.
[22] K. Lissant, The geometry of high-internal-phase-ratio emulsions, J. Colloid Interface Sci. 22 (5) (1966) 462–468.
[23] J. Ma, C. Guo, Y. Tang, J. Xiang, S. Chen, J. Wang, H. Liu, Micellization in aqueous solution of an ethylene oxide-propylene oxide triblock copolymer, investigated with 1 h NMR spectroscopy, pulsed-field gradient NMR, and NMR relaxation, J. Colloid Interface Sci. 312 (2) (2007) 390–396.
[24] C. Mabille, F. Leal-Calderon, J. Bibette, V. Schmitt, Monodisperse fragmentation in emulsions: mechanisms and kinetics, EPL (Europhys. Lett.) 61 (5) (2003) 708.
[25] J. Mata, P. Majhi, C. Guo, H. Liu, P. Bahadur, Concentration, temperature, and salt-induced micellization of a triblock copolymer pluronic l64 in aqueous media, J. Colloid Interface Sci. 292 (2) (2005) 548–556.
[26] M.G. Munoz, F. Monroy, F. Ortega, R.G. Rubio, D. Langevin, Monolayers of symmetric triblock copolymers at the air–water interface. 1. Equilibrium properties, Langmuir 16 (3) (2000) 1083–1093.
[27] K. Nakashima, T. Anzai, Y. Fujimoto, Fluorescence studies on the properties of a pluronic f68 micelle, Langmuir 10 (3) (1994) 658–661.
[28] R. Pal, Rheology of emulsions containing polymeric liquids, Encycl. Emuls. Technol. 4 (1996) 93.
[29] R. Pal, Rheology of emulsions containing polymeric liquids, Encycl. Emuls. Technol. 4 (1996) (p. becher, ed.).
[30] R. Pal, Viscoelastic properties of polymer-thickened oil-in-water emulsions, Chem. Eng. Sci. 51 (12) (1996) 3299–3305.
[31] E. Paruta-Tuarez, P. Marchal, V. Sadtler, L. Choplin, Analysis of the Princen and Kiss equation to model the storage modulus of highly concentrated emulsions, Ind. Eng. Chem. Res. 50 (17) (2011) 10359–10365.
[32] A. Patist, J.R. Kanicky, P.K. Shukla, D.O. Shah, Importance of micellar kinetics in relation to technological processes, J. Colloid Interface Sci. 245 (1) (2002) 1–15.
[33] A. Perazzo, V. Preziosi, S. Guido, Phase inversion emulsification: current understanding and applications, Adv. Colloid Interface Sci. 222 (2015) 581L 599.
[34] L.M. Pérez-Mosqueda, J. Maldonado-Valderrama, P. Ramírez, M.A. Cabrerizo-Vílchez, J. Mu noz, Interfacial characterization of pluronic pe9400 at biocompatible (air–water and limonene–water) interfaces, Colloids Surf. B: Biointerfaces 111 (2013) 171L 178.
[35] R. Pons, P. Erra, C. Solans, J.-C. Ravey, M.-J. Stébé, Viscoelastic properties of gel-emulsions: their relationship with structure and equilibrium properties, J. Phys. Chem. 97 (47) (1993) 12320–12324.
[36] H. Princen, Highly concentrated emulsions. I. Cylindrical systems, J. Colloid Interface Sci. 71 (1) (1979) 55–66.
[37] H. Princen, Rheology of foams and highly concentrated emulsions: I. Elastic properties and yield stress of a cylindrical model system, J. Colloid Interface Sci. 91 (1) (1983) 160–175.
[38] P. Ramírez, J. Mu noz, V. Fainerman, E. Aksenenko, N. Mucic, R. Miller, Dynamic interfacial tension of triblock copolymers solutions at the water–hexane interface, Colloids Surf. A: Physicochem. Eng. Aspects 391 (1) (2011) 119–124.
[39] P. Ramírez, A. Stocco, J. Mu noz, R. Miller, Interfacial rheology and conformations of triblock copolymers adsorbed onto the water-oil interface, J. Colloid Interface Sci. 378 (1) (2012) 135–143.
[40] P. Ramírez, A. Stocco, J. Mu noz, R. Miller, Interfacial rheology and conformations of triblock copolymers adsorbed onto the water–oil interface, J. Colloid Interface Sci. 378 (1) (2012) 135–143.
[41] H. Rehage, G. Ebert, G. Platz, Hydrocarbon gels and their rheological properties, Abstracts of papers of the American Chemical Society, vol. 195, pages 57-Coll – Amer Chemical Soc 1155 16th st, NW, Washington, DC 20036, 1988.
[42] G. Riess, Micellization of block copolymers, Prog. Polym. Sci. 28 (7) (2003) 1107–1170.
[43] E. Rotureau, M. Leonard, E. Marie, E. Dellacherie, T. Camesano, A. Durand, From polymeric surfactants to colloidal systems (1): Amphiphilic dextrans for emulsion preparation, Colloids Surf. A: Physicochem. Eng. Aspects 288 (1) (2006) 131–137.
[44] C. Rouzes, A. Durand, M. Leonard, E. Dellacherie, Surface activity and emulsification properties of hydrophobically modified dextrans, J. Colloid Interface Sci. 253 (1) (2002) 217–223.
[45] M. Sánchez, C. Valencia, J. Franco, C. Gallegos, Wall slip phenomena in oil-in-water emulsions: effect of some structural parameters, J. Colloid Interface Sci. 241 (1) (2001) 226–232.
[46] R. Sedev, Peo-brush at the liquid/gas interface, Colloids Surf. A: Physicochem. Eng. Aspects 156 (1) (1999) 65–70.
[47] R. Sedev, R. Steitz, G. Findenegg, The structure of PEO-PPO-PEO triblock copolymers at the water/air interface, Phys. B: Condens. Matter 315 (4) (2002) 267–272.
[48] P.K. Sharma, S.R. Bhatia, Effect of anti-inflammatories on pluronic® f127: micellar assembly, gelation and partitioning, Int. J. Pharm. 278 (2) (2004) 361–377.
[49] T. Svitova, C. Radke, Aot and pluronic f68 coadsorption at fluid/fluid interfaces: a continuous-flow tensiometry study, Ind. Eng. Chem. Res. 44 (5) (2005) 1129–1138.
[50] T.F. Tadros, Applied Surfactants: Principles and Applications, John Wiley & Sons, 2006.
[51] A. Torcello-Gómez, M. Wulff-Pérez, M.J. Gálvez-Ruiz, A. Martín-Rodríguez, M. Cabrerizo-Vílchez, J. Maldonado-Valderrama, Block copolymers at interfaces: interactions with physiological media, Adv. Colloid Interface Sci. 206 (2014) 414L 427.
[52] J. Vieira, Z. Li, R. Thomas, J. Penfold, Structure of triblock copolymers of ethylene oxide and propylene oxide at the air/water interface determined by neutron reflection, J. Phys. Chem. B 106 (41) (2002) 10641–10648.
[53] P. Walstra, Formation of Emulsions, (1983).
[54] S. Wu, Chain structure and entanglement, J. Polym. Sci. B: Polym. Phys. 27 (4) (1989) 723–741.
[55] B. Zhao, L. Zhu, W. Li, B. Chen, Solubilization and biodegradation of phenanthrene in mixed anionic–nonionic surfactant solutions, Chemosphere 58 (1) (2005) 33–40.

2.1.2 Objectives

The knowledge and command of diffusion in highly concentrated emulsions may provide key information for the controlled delivery of actives [114], for the rational design of smart soft and hard materials [115], for the environmentally friendly synthesis of molecules [116], for improving the chemical or colloidal stability [117], for demulsification processes [118] or even for the understanding of structural aspects [119].

This thesis aims to apply a reverse engineering to develop a methodology for design of systems intented to controlled delivery applications, considering highly concentrated emulsions as model system, as it was aforementioned in previous section.

Because of the similarities of this model system with other dispersed colloidal systems such as multiple emulsions, nanoparticles, nano-emulsions, hydrogels, pickering emulsions, etc., it is foressen that the reverse engineering to be developed on this thesis could be subsequently expanded to others by interchange of appropriate and individualized approaches to each one of the systems.

The principles of the reverse engineering will be adopted in the approach of this work, which involve annotation, data collection, model selection, and strategic perturbations of the system, in order to build an ab-initio model that is capable of explaining and predicting its current and future behaviors [120].

The recapitulation of input and output relationships via a mechanistically inspired model will be a primary goal, followed by the prediction of behaviors under new conditions and the study and visualization of trends or influence of variables. With these goals in mind it is expected that a suitable operating model can be built, using all available information.

2.2 Diffusion in highly concentrated emulsion systems

As in Bernardo et al. (2007) model, the active ingredient vehicle for control delivery can be taken into account as a simple emulsion, consisting of an internal phase homogeneously dispersed as droplets in an external continuous phase, with the droplets being surrounded by a stabilizing layer of surfactant [16]. Both phases contain dissolved the active ingredient, usually with a higher concentration in the dispersed phase, that works as a reservoir. The active ingredient is considered to be the only transferred component, essentially in the z-direction (one-dimensional), perpendicular to the constant interfacial transfer area A. The transfer model [16] takes into account the two-phase structure of the emulsion vehicle, describing transfer out of the droplets and then diffusion across the continuous phase as a serie of inter-phase equilibria and diffusion processes. As in foams [17], the permeability of the film-forming surfactant monolayers on emulsions plays an important role for the

whole mass transfer process. If one considers a single droplet, with radius R_d, at a particular position z, within the emulsion system (see Figure 2.3), the active ingredient release to the external phase consists of two steps: (i) permeation through the surfactant layer adsorbed at the droplet surface, followed by (ii) diffusion in a thin film of continuous phase, where active ingredient concentration is higher than in the bulk of continuous phase, away from the droplet [16].

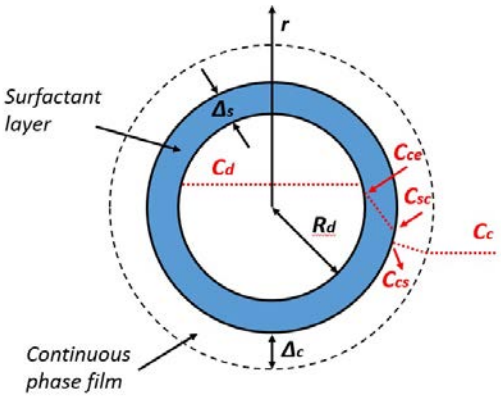

Fig. 2.3 Representation of active ingredient transfer from a spherical droplet to an external phase with an intermediate surfactant layer, where red dotted lines represent active ingredient concentration profiles. Adapted from [16].

The common view is that the total resistance to the passage of the active ingredient molecules is a sum of a series of three resistances: dispersed phase resistance, continuous phase resistance, and interfacial resistance, which arises from the adsorption of surfactant molecules to the interface. The active ingredient flux (mol/m^2s) out of the droplet, under steady state and neglecting the small variation of transfer area across the surfactant layer, is then given by:

$$J_i = k_{id}(C_d - C_{ce}) = P_s(C_{ce} - C_{sc}) = k_{ic}(C_{cs} - C_c) \tag{2.1}$$

where k_{id} (m/s) is the individual mass transfer coefficient through the dispersed phase, P_s (m/s) the surfactant layer permeability and k_{ic} (m/s) the individual mass transfer coefficient through the continuous phase film. The active ingredient concentrations can be defined as follows: C_d is the concentration in the dispersed phase, C_{ce} is an hypothetical concentration of active ingredient in equilibrium with C_d given the partition coefficient K_{cd} (between the continuous and dispersed phases, $C_{ce} = K_{cd}C_d$), C_{cs} and C_{cs} are also hypothetical concentrations in equilibrium just at the limit of the surfactant layer and just outside the surfactant film respectively, and C_c the bulk concentration in the continuous phase.

If the main issue of the mass transfer is delimited to a water-in-oil emulsion system, generally, it can be assumed that the diffusion of active ingredient through the water droplets is extremely rapid [121], in such a way that the resistance on the dispersed phase is negligible ($k_{id} = 0$). This can be verified by calculation of the Biot number ($Bi = k_{ic}(2R_d)/D_d$), where D_d refers to the diffusion coefficient of the active ingredient through the dispersed phase. According to the literature, Biot numbers smaller than 30 indicate that the diffusional resistance through the dispersed phase is negligible in relation to the one of the continuous phase [122]. Thus, one can write a global expression for the whole mass transfer process based on a global mass transfer coefficient K_g, and express C_{ce} as function of C_d by the distribution coefficient K_{cd}:

$$J_i = K_g(K_{cd}C_d - C_c) \tag{2.2}$$

where

$$K_g = \frac{1}{\frac{1}{P_s} + \frac{1}{k_{ic}}} \tag{2.3}$$

2.3 Theoretical estimation of mass transfer parameters

2.3.1 Permeability of surfactant layer

The surfactant layer permeability (P_s) of a given solute may be several orders of magnitude lower than the permeability of an isotropic liquid layer with the same thickness, essentially because the surfactant layer adsorbed to the droplet's surface is an interfacial phase more ordered than a bulk liquid [123]. The surfactant layer may comprise one or more molecular layers, the layer closer to the interface being the most ordered, with lipid chains more aligned perpendicularly to the interface. Within the first layer, the lipid chains are also more aligned close to the interface, where the polar headgroups lie (see Figure 2.4).

Solute permeation across an ordered interfacial layer has been already described by partition/diffusion models, provided that transport parameters are somehow related to the layer structural properties [124, 125]. A model of this kind was suggested for a surfactant monolayer, relating solute permeation to surfactant surface density, which is known to be proportional to the degree of chain order [123]. This model is essentially a calibration of the model of Xiang and Anderson [125], by choosing a reference state of disordered surfactant. In this way, the permeability P_s may be expressed as:

$$P_s = P_{dis} \cdot f_{ord} \tag{2.4}$$

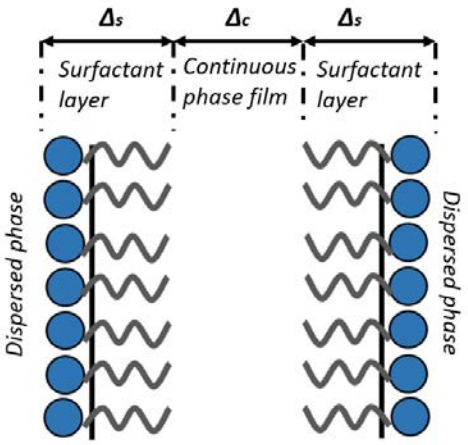

Fig. 2.4 A single continuous phase film consisting of an oily core with thickness Δ_c sandwiched between two adsorbed monolayers of surfactant with the thickness of Δ_s. In this representation the Plateau borders are neglected. The liquid layer and the surfactant monolayers are assumed to be homogeneous. Adapted from [17].

f_{ord} a factor which represents the decrease of permeability due to the interfacial order, and P_{dis} the permeability of a disorder layer. These parameters can be estimated according to relation:

$$f_{ord} = exp\left\{-\alpha\left(\frac{\lambda}{1-\lambda}-\frac{1}{2}\right)\cdot\left(\left(\frac{A_1^*}{A_2^*}\right)^{1/2}+\frac{A_1^*}{A_2^*}\right)\right\} \tag{2.5}$$

where α is a factor of free volume overlap (normally considered as 0.75), A_1^* the solute area in a compressed state, A_2^* the area per molecule of surfactant in a compressed monolayer, A_2 the actual area per molecule of surfactant, and λ the normalized surface density (ratio of A_2^*/A_2). When calculating the permeability, the starting point of the most simple models consists of depicting the surfactant layer as an homogeneous thin layer, into which the active ingredient partitions and through which it then diffuses [16]. The permeability in a disordered state P_{dis} appearing in Eq. 2.4 is thus given by

$$P_{dis} = \frac{K_{s,c}D_{s,dis}}{\Delta_s} \tag{2.6}$$

where $K_{s,c}$ is the active ingredient partition coefficient between the surfactant layer and the emulsion continuous phase, $D_{s,dis}$ an effective diffusion coefficient through the surfactant layer in a reference state (disordered state), and Δ_s the surfactant monolayer thickness. If the dispersed phase was used as reference instead [16] , the permeability would then be $P_{s,d} = K_{sd}D_s/\Delta_s$, where D_s would represent the diffusivity into bulk surfactant or an organic solvent resembling the active ingredient-surfactant interaction, and then $P_{s,d} = P_{dis}K_{cd}$.

On the other hand, as it will be shown later, for thermodynamic equilibrium estimations, it will be neccesary to know accurately the composition of the continuous phase. Generally, it is supposed that only a fraction of the surfactant participates in the adsorption at the droplet surface, and the rest, it is conceivable that remains as micelles solubilized in the continuous media. It must be here clarified, that effects such as active ingredient adsorption at the droplet's surface [126] or uptake by surfactant micelles [127], are not covered in the present model. The true is that the ideal scenario can be further complicated by the specific nature of the species in the system, limiting possible applications of this simplified model. However, we will hypothesize that these conditions are less likely to occur, at least, initially.

In this way, the total amount of surfactant $m_{s,total}$ would be the sum of the adsorbed at the droplet $m_{s,int}$ and the remaining in the continuous phase $m_{s,cont}$. Therefore, assuming a monolayer, the amount which is adsorbed comes from:

$$m_{s,int} = n_{droplets} N_{s,droplet} \frac{MW_s}{N_A} \tag{2.7}$$

where $n_{droplets}$ is the number of droplets in the emulsion, $N_{s,droplet}$ an average number of surfactant molecules per droplet surface, MW_s the surfactant molecular weight and N_A the Avogadro number. $n_{droplets}$ can be calculated according to :

$$n_{droplets} = \frac{m_{emulsion}\phi_m}{\rho_d \left(\frac{\pi}{6} {L_d}^3\right)} \tag{2.8}$$

being $m_{emulsion}$ the total mass amount prepared of emulsion, ϕ_m the mass fraction of dispersed phase, ρ_d its density, and L_d a characteristic droplet diameter. Considering the shape of a droplet as a sphere, and S_{polar} the polar surface of the surfactant. $N_{s,droplet}$ can be deduced from:

$$N_{s,droplet} = \frac{\pi {L_d}^2}{S_{polar}} \tag{2.9}$$

In this way, knowing the total emulsion mass prepared, as well as the ratio oil/surfactant $r_{o/s}$, one can obtain the following equations to characterize correctly the amount of surfactant present, considering the amount adsorbed:

$$m_{s,total} = m_{emulsion}(1-\phi_m)\frac{1}{\left(1+r_{o/s}\right)} \tag{2.10}$$

The amount of surfactant present in the continuous phase is therefore:

$$m_{s,cont} = m_{emulsion}(1-\phi_m)\frac{1}{\left(1+r_{o/s}\right)} - \frac{6 m_{emulsion} MW_s \phi_m}{S_{polar}\rho_d N_A L_d} \tag{2.11}$$

and the real value corresponding to $r_{o/s}$ can be calculated from the equation:

$$r_{o/s,real} = \frac{r_{o/s}}{1 - \frac{MW_s}{S_{polar}\rho_d N_A}\frac{6\phi_m(1+r_{o/s})}{L_d(1-\phi_m)}} \tag{2.12}$$

2.3.2 Interfacial mass transfer coefficient

The interfacial transfer coefficient k_{ic} can be calculated solving the diffusion equation for the continuous phase film, under steady state conditions [16]. Considering $\Delta_s << R_d$, with Δ_s being the thickness of the surfactant layer, and R_d the droplet radius, one obtains:

$$k_{ic} = D_c\frac{(R_d + \Delta_c)}{(R_d\Delta_c)} \tag{2.13}$$

where D_c is the active ingredient diffusion coefficient in the continuous phase and Δ_c the thickness of the continuous phase film. If thickness Δ_c is unknown, there is a minimum limiting value for k_{ic} when $\Delta_c \to \infty$, which is D_c/R_d. Therefore, $1/k_{ic}$ varies between 0 (for $\Delta_c = 0$) and R_d/D_c. Consequently, the interfacial resistance $1/k_{ic}$ falls within the following interval:

$$\frac{1}{P_s} \leq \frac{1}{k_{ic}} \leq \frac{1}{P_s} + \frac{R_d}{D_c} \tag{2.14}$$

which may be quite narrow if the resistance of the surfactant layer $(1/P_s)$ happens to be much larger than the resistance of the continuous phase film $(1/k_{ic})$ " [16].

2.3.3 Diffusion coefficient in liquids

Liquid state theories for calculating diffusion coefficients are quite idealized, and generally, none is satisfactory in providing relations for calculating D_{12} (diffusion coefficient of a molecule 1 into a solvent 2). In several cases, however, the form of a theoretical equation has provided the framework for useful prediction methods [26]. The most common basis for estimating diffusion coefficients in liquids is the Stokes-Einstein equation. Coefficients calculated from this equation are accurate to only about twenty percent [26]. Nonetheless, this equation remains the standard against which alternative correlations are judged.

The Stokes-Einstein equation is:

$$D_{12} = \frac{k_B T}{f} = \frac{k_B T}{6\pi\mu_2 R_0} \tag{2.15}$$

where f is the friction coefficient of the solute, k_B is Boltzmann's constant, μ_2 is the solvent viscosity, and R_0 is the solute radius. The Stokes-Einsten equation provides a common basis to estimate diffusion coefficients in liquids and can be applied to dilute solutions of spherical solute molecules diffusing in a solvent of considerable smaller molecules [121]. However, for molecules of similar size and low-viscosity solvents (up to 20-30 cP), reasonable estimates for predictive purposes may be obtained through empirical modifications of the Stokes-Einstein equation, such as the Wilke Chang [128]:

$$D = \frac{7.4 \cdot 10^{-8} (\Phi \overline{M}_2)^{1/2} T}{\mu_2 \overline{V}_1^{0.6}} \tag{2.16}$$

where D_{12} is the diffusion coefficient of solute 1 in cm^2/s; $\overline{M}_2$ is the mean molecular weight of the solvent 2 in daltons; T is the temperature, in K; μ_2 is the viscosity, in centipoises (cP); and V_1 the molar volume of the solute at the normal boiling point, in cm^3/mol. The empirical parameter Φ is 1 for most organic solvents, 1.5 for alcohols, and 2.6 for water. This older but useful correlation is widely used in engineering work for last estimates of D_{12} for solute concentrations of 5 to 10 mole % (limit of infinite dilution) [26].

2.3.4 Partition coefficient for a solute between two liquid phases

The knowledge of the fundamentals of equilibrium thermodynamics between phases is essential to discuss any unitary operations involving mass transfer. In fact, the mass transfer occurs due to the fact that the system is not at equilibrium and therefore, the components are transferred between the phases in contact until the equilibrium is achieved (Figure 2.5).

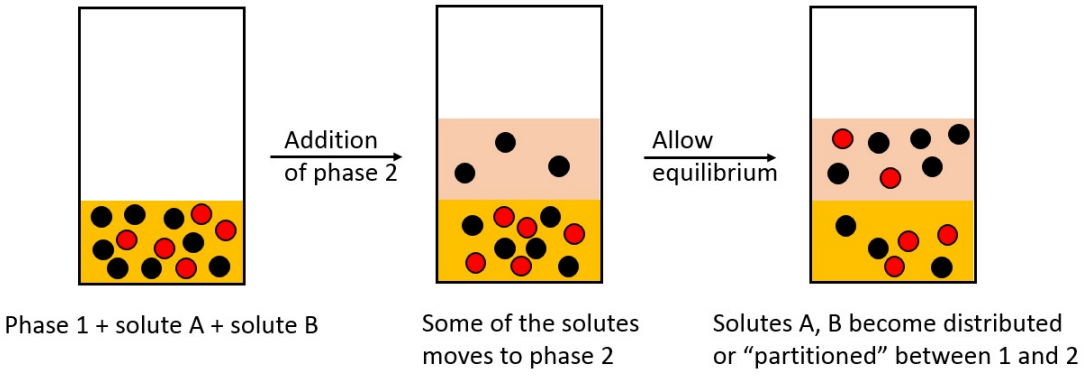

Fig. 2.5 Representation of solute mass transfer between two phases until equilibrium.

In two immiscible liquids with a common solute, the ratio between the equilibrium concentrations is given by the partition or distribution coefficient (K_{cd}). By writting the

equilibrium conditions for these systems, the expression of K_{cd} can be derived in terms of thermodynamic parameters. In fact, for a solute in two liquids (phase C and phase D), under the hypothesis of dilute and ideal solution, the equality of the chemical potentials in the two phases gives the ratio between the equilibrium concentrations C_c and C_d [129]:

$$\frac{C_c}{C_d} = \frac{V_c}{V_d} exp\left(-\frac{\mu_c^\circ - \mu_d^\circ}{RT}\right) = K_{cd} \tag{2.17}$$

where V_c and V_d are the molar volumes, μ_d° and μ_c° the standard chemical potentials, and R and T are the gas constant and the absolute temperature. Using activity coefficients γ and molar fractions x, the equilibrium equality is $\gamma_d x_d = \gamma_c x_c$. These equilibrium parameters can be estimated by using CAMD techniques as it will be shown in the next section. Converting molar fractions to volumetric concentrations, one has $\gamma_d V_d C_d = \gamma_c V_c C_c$. Hence, the partition coefficient of the solute between phases is given by:

$$K_{cd} = \frac{C_c}{C_d} = \frac{\gamma_d V_d}{\gamma_c V_c} \tag{2.18}$$

2.4 Computer-aided molecular design (CAMD) techniques

For correlating thermodynamic properties, it is often convenient to regard a molecule as an aggregate of functional groups; as a result, some thermodynamic properties of pure fluids or mixtures can be calculated by summing group contributions. Generally, CAMD techniques depend on this concept. "In any group-contribution method, the basic idea is that whereas there are thousands of chemical compounds of interest in chemical technology, the number of functional groups that constitute these compounds is much smaller. Therefore, if we assume that a physical property of a fluid is the sum of contributions made by the functional groups of the molecule, we obtain a possible technique for correlating the properties of a very large number of fluids in terms of a much smaller number of parameters that characterize the contributions of individual groups" [26].

This assumption is valid only when the influence of any one group in a molecule is not affected by the nature of other groups within that molecule. Accuracy of correlation improves with increasing distinction of groups; for example, considering aliphatic alcohols, in a first approximation no distinction is made between the position (primary or secondary) of a hydroxyl group, but in a second approximation, such distinction is desirable. Nonetheless, for practical utility, a compromise must be attained. The number of distinct groups must remain small but not so small as to neglect significant effects of molecular structure on physical properties [26].

Extension of the group-contribution idea to mixtures is attractive, because although the number of pure fluids in chemical technology is already very large, the number of different mixtures is larger by many orders of magnitude. Thousands, perhaps millions, of multicomponent liquid mixtures of interest in the chemical industry can be constituted from perhaps 30, 50, or at most 100 functional groups [130]. Group contribution methods such as UNIFAC can be utilized for predictions of liquid phase activity coefficients. However, it is also necessary to develop algorithms for calculating the equilibrium in a efficient and robust way. In addition, by means of these CAMD techniques it is possible to estimate geometric parameters such as volume or area per molecules, as well as physical properties such as viscosity. In this section, a brief description of the CAMD techniques employed in this work will be given.

2.4.1 UNIQUAC Functional-group Activity Coefficients (UNIFAC) model

The original UNIFAC, which combines the functional group concept with a model for activity coefficients, based on an extension of the quasi chemical theory of liquid mixtures (UNIQUAC), was proposed by Fredenslund et al. in 1975 [130]. The essential features are:

1. Suitable reduction of experimentally obtained activity-coefficient data in order to yield parameters characterizing interactions between pairs of structural groups in nonelectrolyte systems.

2. Use of those parameters to predict activity coefficients for other systems that have not been studied experimentally but that contain the same functional groups.

This model can be applied to predict the liquid phase activity coefficient at infinite dilution and finite concentrations of binary or multicomponent systems. The activity coefficient is expressed as functions of composition and temperature. The model has a combinatorial contribution to the activity coefficient (ln γ_i^C), essentially due to differences in size and shape of the molecules, and a residual contribution (ln γ_i^R), essentially due to energetic interactions:

$$ln\gamma_i = ln\gamma_i^C + ln\gamma_i^R \tag{2.19}$$

1. Combinatorial part.

$$ln\gamma_i^C = 1 - V_i + lnV_i - 5q_i\left(1 - \frac{V_i}{F_i} + ln\left(\frac{V_i}{F_i}\right)\right) \tag{2.20}$$

$$F_i = \frac{q_i}{\sum_j q_j x_j}, \qquad V_i = \frac{r_i}{\sum_j r_j x_j} \tag{2.21}$$

The pure component parameters r_i and q_i are, respectively, the molecular van der Waals volumes and molecular surface areas. They are calculated as the sum of the group volume and group area parameters, R_k and Q_k,

$$r_i = \sum_k \upsilon_k^{(i)} R_k, \qquad q_i = \sum_k \upsilon_k^{(i)} Q_k \tag{2.22}$$

where $\nu_k^{(i)}$, always an integer, is the number of groups of type k in molecule i. Group parameters R_k and Q_k are normally obtained from van der Waals group volumes and surfaces areas, V_k and A_k, given by Bondi [131].

$$R_k = \frac{V_k}{15.17}, \qquad Q_k = \frac{A_k}{2.5 \cdot 10^9} \tag{2.23}$$

2. Residual part.

$$ln\gamma_i^R = \sum_k \upsilon_k^{(i)} \cdot [ln\Gamma_k - ln\Gamma_k^{(i)}] \tag{2.24}$$

$ln\Gamma_k$ is the group residual activity coefficient, and $\Gamma_k^{(i)}$ is the residual activity coefficient of group k in a reference solution containing only molecules of type i.

$$ln\Gamma_k = Q_k \cdot [1 - ln(\sum_m \theta_m \psi_{mk}) - \sum_m \left(\frac{\theta_m \psi_{km}}{\sum_n \theta_n \psi_{nm}}\right)] \tag{2.25}$$

$$\theta_m = \frac{Q_m X_m}{\sum_n Q_n X_n}, \qquad X_m = \frac{\sum_i \upsilon_m^{(i)} x_i}{\sum_i \sum_k \upsilon_k^{(i)} x_i} \tag{2.26}$$

where X_m is the fraction of group m in the mixture. The group-interaction parameter ψ_{nm} is given by:

$$\psi_{nm} = exp\left(-\frac{U_{mn} - U_{nn}}{RT}\right) = exp\left(-\frac{a_{nm}}{T}\right) \tag{2.27}$$

where U_{mn} is a measure of the energy of interaction between groups m and n. The group interaction parameters a_{mn} must be evaluated from experimental phase equilibrium data. Note that a_{mn} has units of kelvins and $a_{nm} \neq a_{mn}$. Parameters a_{mn} and a_{nm} are obtained from a database using a wide range of experimental results. Equations 2.25 and 2.26 also hold for $ln\Gamma_k^{(i)}$, except that the group composition variable, θ_k, is now the group fraction of group k in pure fluid i. In pure fluid, $ln\Gamma_k = ln\Gamma_k^{(i)}$, which means that as $x_i \to 1$, $\gamma_i^R \to 1$. γ_i^R must be close to unity because as $x_i \to 1$, $\gamma_i^C \to 1$, and $\gamma_i \to 1$.

The original UNIFAC was the most widely used model before several revisions and extensions were developed. The reader is referred to Appendix A, Hansen et al (1991) for tabulated values of the fifth revised version of UNIFAC. For sake of clarity, the complete liste of matrix values (a_{mn}) has not been included in the Appendix of this thesis. However, the interested reader can easily obtain them from the literature [132].

As Lei (2008) points out, the advantages of UNIFAC over other traditional methods such as Wilson, NRTL, and UNIQUAC equations are:

1. Size and binary interaction parameters are available for a wide range of types of function groups (more than 100 function groups);

2. Extensive comparisons with experimental data are available;

3. It is an open system, and more function groups and more parameters will be filled in the UNIFAC list in the future;

4. Experimental measurements of phase equilibrium are very time-consuming and therefore expensive.

It is interesting to note that, for example, if measurements were performed for a 10-component system at just one constant pressure (e.g., atmospheric pressure), in 10% mole steps and with an average number of 10 data points being daily determined experimentally, the measurements (in total, 92378 data points) would take more than 37 years [133]. Therefore, with the insight to multicomponent mixtures, this model is more advantageous in saving the measurement time. That is why it has been very popular and desirable in the synthesis, design and optimization of separation processes over the past few years [134].

2.4.2 Modified UNIFAC (Dortmund) model

As in the original UNIFAC model, in the modified UNIFAC (Dortmund) model [27] the activity coefficient is also the sum of a combinatorial and a residual part (see Eq. 2.19). However, the combinatorial part here was changed in an empirical way to make it possible to deal with compounds very different in size. Based on the proposal of Kikic et al. [135] and Thomas and Eckert [136], the following combinatorial part is applied in modified UNIFAC (Dortmund) model:

$$ln\gamma_i^C = 1 - V_i^{'} + lnV_i^{'} - 5q_i\left(1 - \frac{V_i}{F_i} + ln\left(\frac{V_i}{F_i}\right)\right) \tag{2.28}$$

The parameter $V_i^{'}$ can be calculated by using the relative van der Waals volumes R_k of the different groups:

$$V_i^{'} = \frac{r_i^{3/4}}{\sum_j x_j r_j^{3/4}} \tag{2.29}$$

All the other parameters are calculated in the same way as in the original UNIFAC model. In comparison to the original UNIFAC model, the van der Waals properties are changed slightly (See Appendix A), and at the same time, two more temperature-dependent parameters (b and c) are introduced to permit a better description of the real behavior (activity coefficients) as a function of temperature:

$$\psi_{nm} = exp\left(-\frac{a_{nm} + b_{nm}T + c_{nm}T^2}{T}\right) \tag{2.30}$$

Thus, to calculate the activity coefficient, such parameters as R_k, Q_k, a_{nm}, b_{nm}, c_{nm}, a_{mn}, b_{mn}, c_{mn} should be predetermined. The status of the group parameter matrix during years 1993, 2000 and 2017 is shown in Fig. 2.6 and Fig. 2.7. All research concerning the modified UNIFAC model (Dortmund) is available (and the fully updtated matrix by membership) via the Internet at http://www.uni-oldenburg.de/tchemie/consortium or http://www.unifac.org. For sake of clarity, the complete list of matrix values (a_{mn}, b_{mn} and c_{mn}) has not been included in this thesis but they have been plotted in Appendix. The interested reader can easily obtain them from the literature [27]. Comparing tables (See Appendix A.1 to A.4 for UNIFAC model, and A.5 to A.6 for Modified UNIFAC, respectively) the number of main groups and available group interaction parameters is very different for both models; 50 main groups versus 45, and 108 secondary groups versus 85, for UNIFAC, and Modified UNIFAC, respectively. This means also a difference in the total number of systems that can be predicted by the different methods.

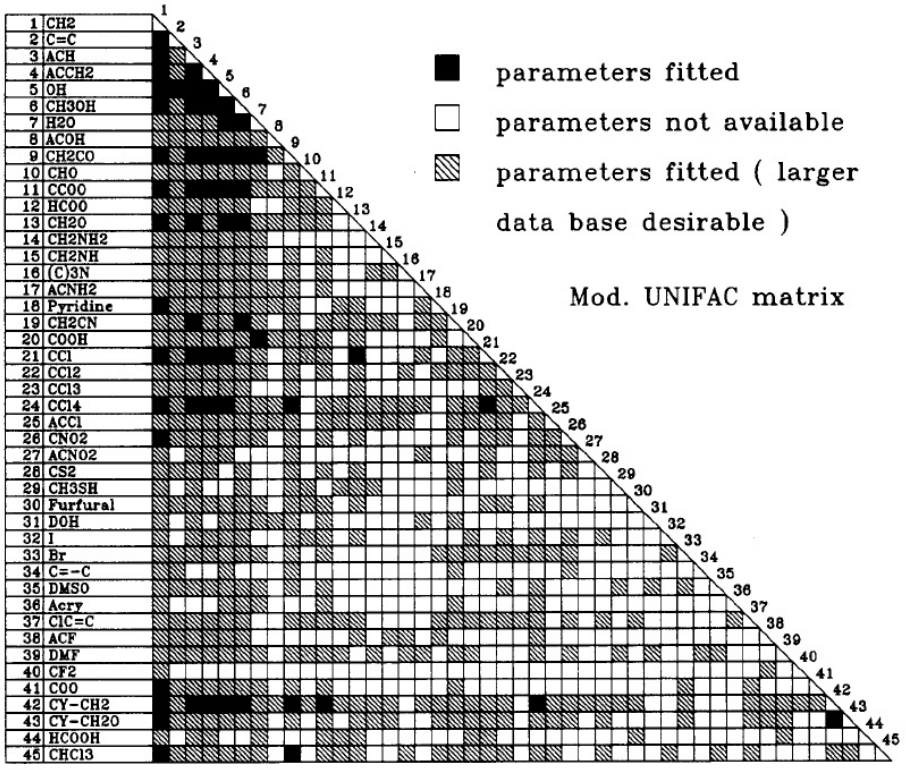

(a) Status of parameter matrix of modified UNIFAC (Dortmund) (1993) [27].

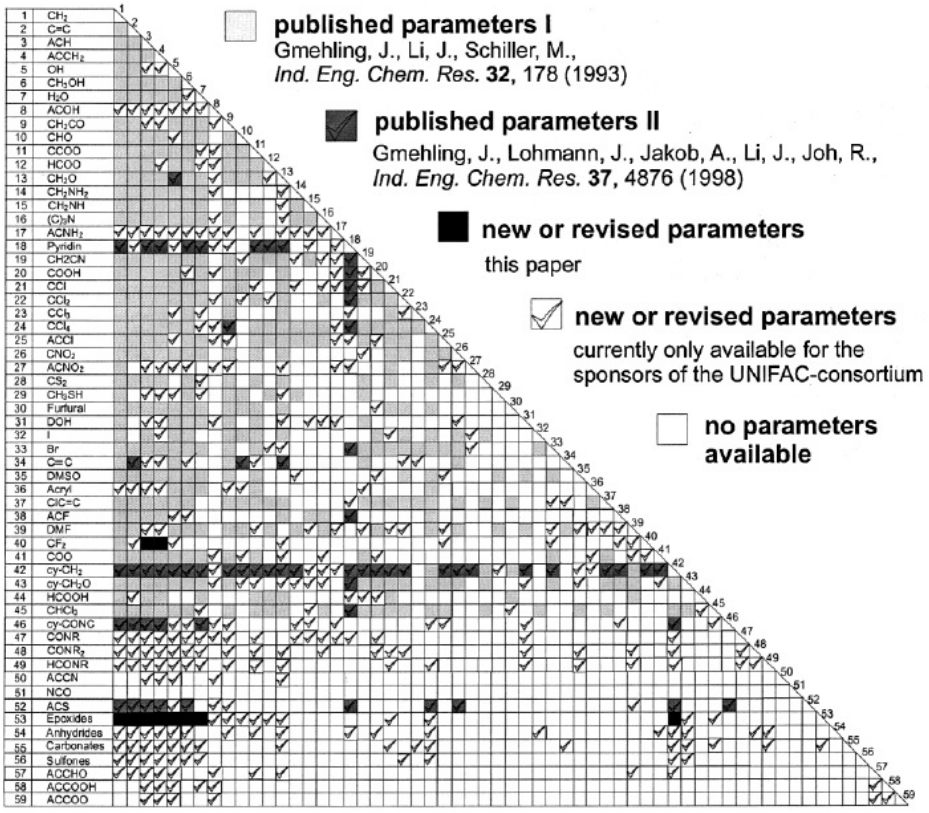

(b) Status of parameter matrix of modified UNIFAC (Dortmund) (2000) [137].

Fig. 2.6 Evolution of group interaction matrix parameters.

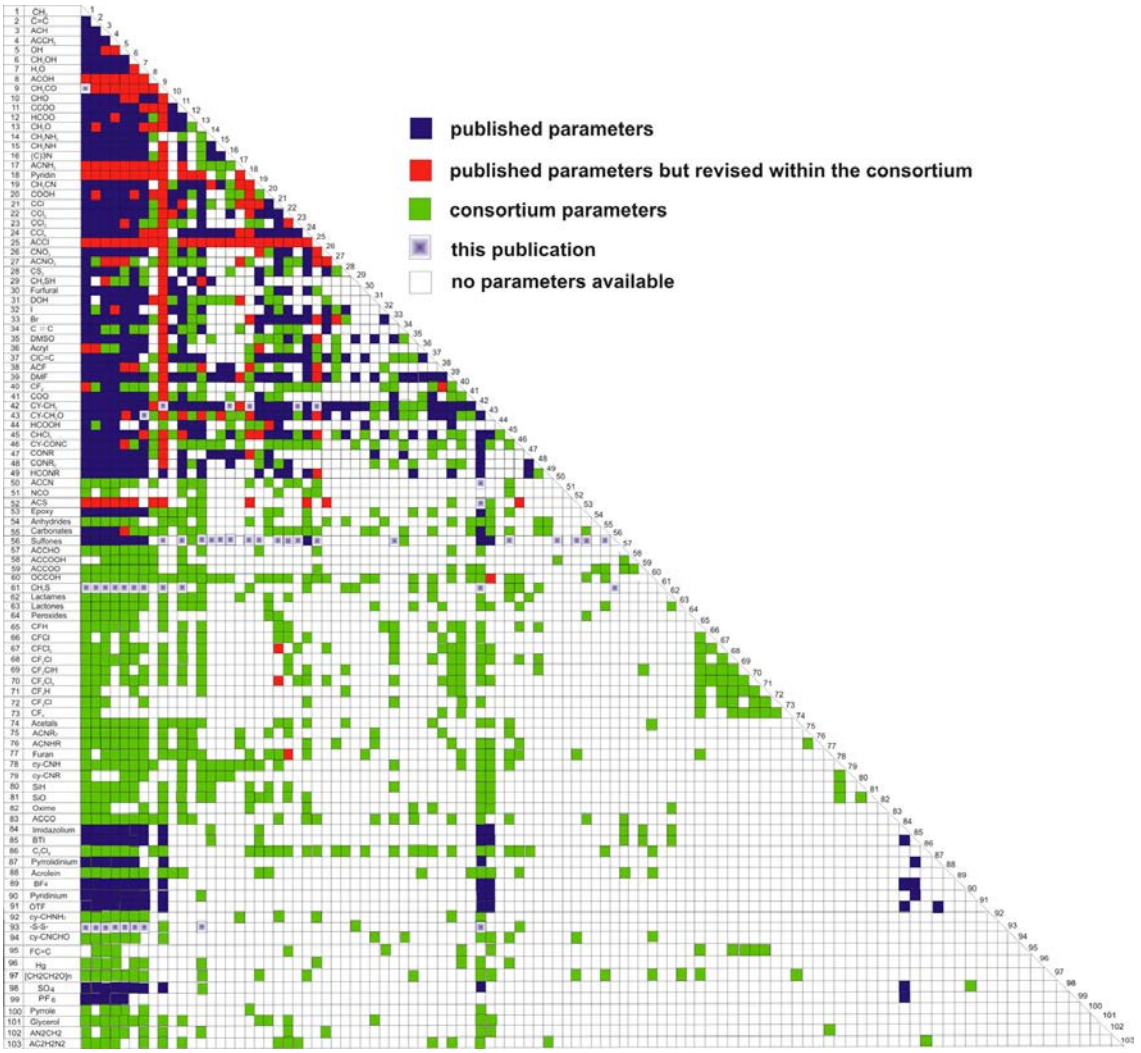

Fig. 2.7 Current group interaction parameter matrix of Modified UNIFAC (Dortmund), February 2016. Taken from [18].

2.4.3 Revision and Extension 6 of Modified UNIFAC (Dortmund) model

Despite the reliability and simple applicability of UNIFAC and Modified UNIFAC (Dortmund), there are some well-known disadvantages. For multifunctional components, the results are sometimes poor, because the interaction parameters are basically fitted to simple representatives of the main groups [134]. If one of the binary interaction parameters lacks for a determined pair of main groups, the predictions could not be so accurate and deviations from the real situation could arise. On the other hand, the fragmentation of molecules cause that group contribution models cannot distinguish among isomers, and proximity effects are also disregarded [134]. It should be also mentioned that the ions (cation and anions groups) are not complete yet in the UNIFAC menu in a really effective and practical way.

Up to date, a number of revisions [27, 138–140, 18] to the interaction parameters have been published and are freely available in the literature. These revisions were focused to overcome as possible the previous mentioned weaknesses of the UNIFAC models [137]. Currently, the most updated version of freely published interaction parameters for Modified UNIFAC (Dortmund) is the Addendum - Revision and Extension 6 of Constantinescu (2016) [18] (See Appendix A.7 to A.9). In this revision, including all previous modifications, methods such as the Conductor-like Screening Model for Real Solvents (COSMO-RS) were also applied. In the COSMO-RS model, only atom-specific parameters are required, and predictions of thermodynamic properties is made on the basis of unimolecular quantum chemical calculations that provide the necessary information for the evaluation of molecular interaction in liquids [134]. This most updated revision, including features of the COSMO-RS model, allows the prediction of '*artificial*' phase equilibrium data for selected binary systems. These artificial data are then used as pseudoexperimental data to fill gaps in the Modified UNIFAC (Dortmund) matrix. Results reported in the literature [140], show that in some cases, this version can provide reasonable results, however, in others, the quality of the artificial data derived using que quantum chemical approach is poor, which could direclty influence the accuracy of results of Modified UNIFAC.

2.4.4 Flash algorithm to predict L-L equilibrium

Liquid-liquid phase split calculations, also known as liquid-liquid flash, are typically conducted for given overall composition at constant temperature, with the compositions in the different resulting phases as unknowns [141]. For isothermal conditions at given overall system composition and pressure, the goal is to find the phase compositions corresponding to the global minimum in the total Gibbs energy of the system, which defines the stable equilibrium state [142]. The calculation of the liquid-liquid equilibrium is a problem that shows different difficulties, since the separation into two or more phases is the result of the strongly non-ideal behavior within the liquid phases.

The thermodynamic properties of the liquid phases, and more specifically, the activity coefficients, depend strongly on the composition of the phases, and this adds a strong non-linearity to the problem of equilibrium. This feature brings in the risk of obtaining trivial solutions very easily. Consequently, in order to solve problems of this nature, the algorithm leading to the solution should guarantee to achieve the correct solution in a relatively small number of iterations. In addition, because of the very strong non-linearity, the initial guess of the composition of liquid phases present in the equilibrium is crucial to achieve the correct solution [19].

An algorithm proposed on the literature [19] was used in this work for the calculation of liquid-liquid equilibrium. Its scheme is shown in Fig. 2.8. The Rachford-Rice method [143] is used as a subroutine within the flash calculation. Therefore, by means of an objective function, it is possible to calculate phase compositions for two equilibrium phases by means of an iterative bisection method where the phase molar fraction is constrained to lie in the range from 0 to 1. Equilibrium phase compositions are then calculated by mass balance from the converged phase molar fraction and the overall composition that lies inside the two-phase region, given temperature (T), and global composition (z_i) of the system.

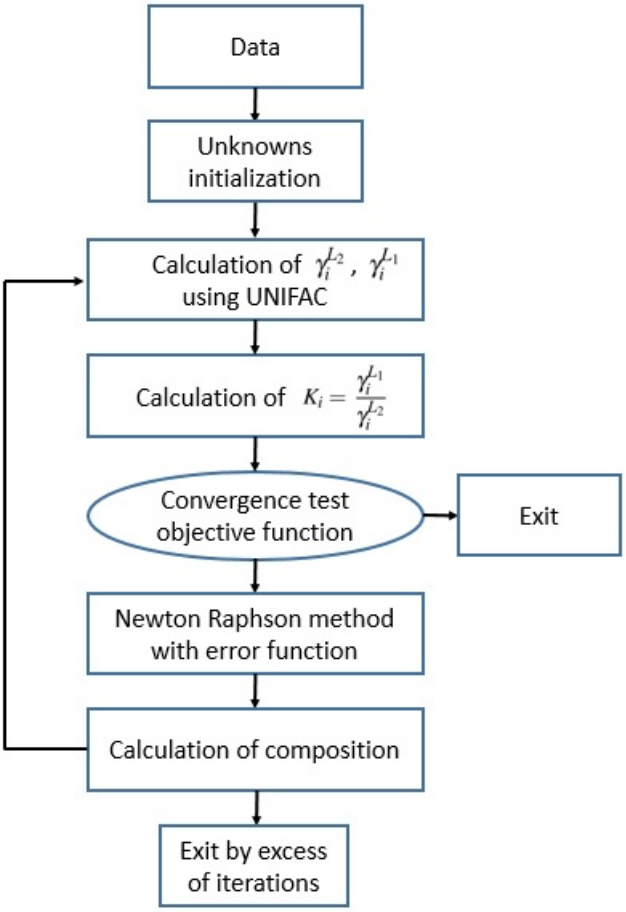

Fig. 2.8 Flux diagram showing the general structured applied in this work concerning the flash algorithm to predict L-L equilibrium. Adapted from [19].

Considering L_1 and L_2 the two liquid phases in equilibrium, F the total mole amount and z_i the global composition of the system, the unknowns are the proportion of phases (L_2/F) and the compositions of the two phases ($x_i^{L_1}$ and $x_i^{L_2}$). As it was introduced in previous section 2.3.4, the equilibrium equalities for each component i are defined as:

$$K_i = \frac{x_i^{L_2}}{x_i^{L_1}} = \frac{\gamma_i^{L_1}}{\gamma_i^{L_2}} \tag{2.31}$$

From the equations of mass balance the following expression is obtained:

$$z_i = \left(1 - \frac{L_2}{F}\right) x_i^{L_1} + \frac{L_2}{F} x_i^{L_2} \tag{2.32}$$

Combining equations 2.31 and 2.32 one obtains:

$$x_i^{L_1} = \frac{z_i}{1 + (L_2/F)(K_i - 1)} \qquad x_i^{L_2} = \frac{z_i K_i}{1 + (L_2/F)(K_i - 1)} \tag{2.33}$$

In the equilibrium conditions, the equalities appearing on Eq. 2.33 should be fulfilled simultaneously for all components present in the mixture, where the equilibrium relations (K_i) are calculated by the Eq. 2.31, and the compositions for each phase should add up to one. Since the activity coefficients in Eq. 2.31 are function of the composition of the phase, the problem is not lineal. The general strategy to solve this kind of equilibrium problems is shown in Fig. 2.8 and it is based on the uncoupling of two types of variables (L_2/F and the group of $x_i^{L_1}$ and $x_i^{L_2}$). Two cycles of convergence are established, one nested within the other. The inner cycle corresponds to the strategy of convergence of the relation L_2/F. The outside cycle is the one which handle the convergence of the compositions. Therefore, according to the structure proposed in Fig. 2.8 there are the following steps in the algorithm: (1) Convergence of the relation L_2/F; (2) Convergence of the compositions; (3) Initialization of the unknowns.

1. **Convergence of the relation** L_2/F

   In this calculation step, the equilibrium relations remain constant. Combining the equalities of Eq. 2.33, the function to find the value of the relation L_2/F is known as the Rachford and Rice equation [143]:

   $$f(L_2/F) = \sum_{i=1}^{nc} x_i^{L_2} - \sum_{i=1}^{nc} x_i^{L_1} = \sum_{i=1}^{nc} \frac{z_i(K_i - 1)}{1 + L_2/F(K_i - 1)} \tag{2.34}$$

   Because the Rachford and Rice function is monotonous in the domain of L_2/F, it is possible to employ the Newton-Raphson method to calculate the value of the independent variable in the next iteration:

   $$\left(\frac{L_2}{F}\right)_{next\ iteration} = \left(\frac{L_2}{F}\right) - \frac{f(L_2/F)}{f'(L_2/F)} \tag{2.35}$$

where the derivative of the function is calculated by:

$$f'(L_2/F) = \sum_{i=1}^{nc} \frac{z_i(K_i-1)^2}{(1+(L_2/F)(K_i-1))^2} \tag{2.36}$$

This function presents so many roots as number of components in the mixture minus one, but only those which provide positive values for the compositions are of interest. This condition establishes a maximum and a minimum value for L_2/F in order to get positive denominators in Eq. 2.34. These values are obtained becoming zero the denominator of the Eq. 2.34:

$$(L_2/F) = \frac{1}{1-K_i} \tag{2.37}$$

The maximum level, $(L_2/F)_{max}$, corresponds to the value obtained by the Eq. 2.37 employing the smallest value of K_i, as long as this value is lower than one. In the case that all K_i were greater than one, then there is not maximum level. The minimum level, $(L_2/F)_{min}$, corresponds to the value obtained by the Eq. 2.37 employing the highest value of K_i, as long as this value is bigger than one. In the case that all K_i were lower than one, then there is not minimum level. From all the above, it becomes deduced three cases:

(a) In the first case, there are both a maximum and minimum level for (L_2/F) (Fig. 2.9a). In this case, there is a root between the two levels, nevertheless, this root does not necessary comes across between zero and one, and as consequence, it can adopt either values between the minimum level (that is always lower than zero), or values between one and the maximum level (that is always greater than one). In order to find the root, the method of Newton-Raphson (Eq. 2.36) is employed allowing values greater than one or lower than zero. However, in order to provide stability to the algorithm of equilibrium, the domain of the root must be restricted in such a way to not be close to the maximum and minimum levels using the following relations:

$$(L_2/F)_{lim\,max} = 1 + 0.7\,((L_2/F)_{max} - 1) \tag{2.38}$$

$$(L_2/F)_{lim\,min} = 0.7(L_2/F)_{min} \tag{2.39}$$

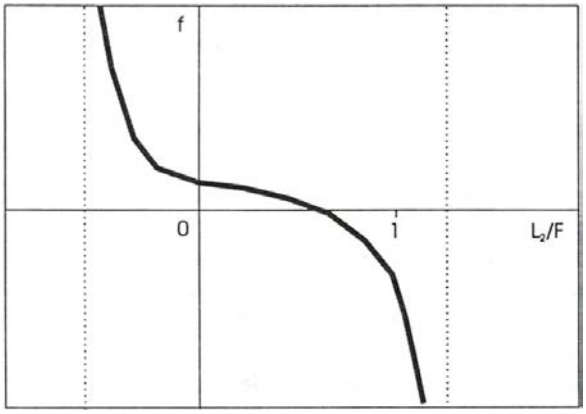

(a) Case when there is maximum level and minimum level for the domain of L_2/F and there is a root for the function.

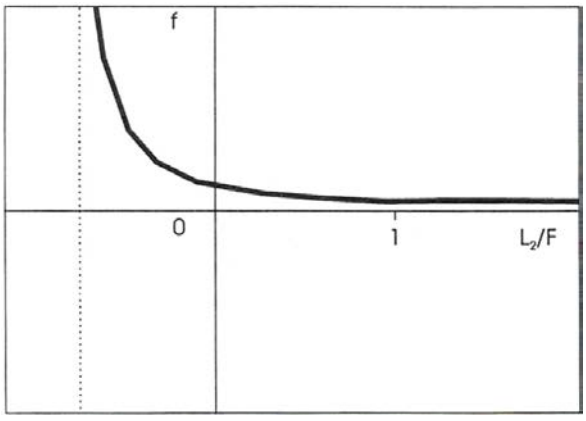

(b) Case when there is minimum level but not maximum level for the domain of L_2/F and there is not root for the function. At this case, all K_i are greater than one.

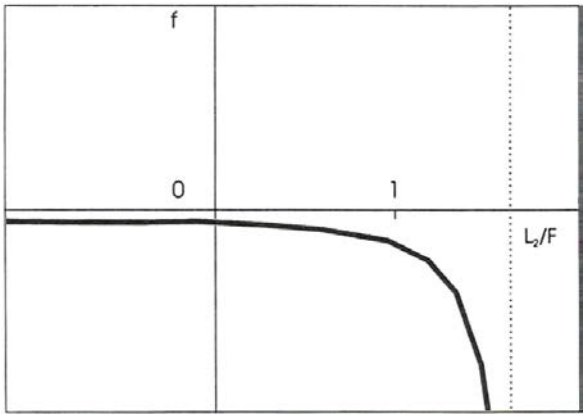

(c) Case when there is maximum level but not minimum level for the domain of L_2/F and there is not root for the function. At this case, all K_i are lower than one.

Fig. 2.9 Rachford and Rice function vs L_2/F. Taken from [19].

where $(L_2/F)_{max}$ and $(L_2/F)_{min}$ are the maximum and minimum levels given by the Eq. 2.37, and $(L_2/F)_{lim\,max}$ and $(L_2/F)_{lim\,min}$ the maximum and minimum values allowed to the roots.

(b) In the second case, there is a minimum level for the root of (L_2/F) but not a maximum, and the function given by the equation 2.34 does not have root which allows mole fractions of phases to be all positive (Fig. 2.9b). In order to provide stability to the algorithm, it should be adopted a value of (L_2/F) greater than one. When this case is found, it is not necessary to find the root of the equation and it is fixed an arbitrary value given by: $(L_2/F) = 1 - (L_2/F)_{min}$.

(c) In the third case, there is a maximum level for the root of (L_2/F) but not a minimum (Fig. 2.9c). In order to provide stability to the algorithm, it should be adopted a value of (L_2/F) lower than zero. When this case is found, it is not necessary to find the root of the equation and it is fixed an arbitrary value given by: $(L_2/F) = 1 - (L_2/F)_{max}$.

The variable L_2/F does not have physical sense out of the interval from zero to one, however, similarly to the technique of negative flash [144], it is allowed to adopt values out of this interval during the convergence course. However, the first formal iteration should be necessarily within the interval from zero to one, even if the solution of Eq. 2.34 gives a value outside. Because of this, if the first solution was lower than zero, L_2/F must adopt the value of 0.2. On the contrary, if the solution was greater than one, L_2/F must adopt the value of 0.8.

2. **Convergence of the compositions**
For compositions, the equalities on Eq. 2.33 are employed. Nevertheless, these compositions, in the moment of calculation, will not be equal to unity, thus, it is necessary to normalize them in order to satisfy the requirement. In this way, when they are utilized in the next iteration, the calculated compositions converge very fast. It should be mentioned that the compositions are the variables most difficult to converge, specially in this kind of problems, because the equilibrium relations are highly dependent of compositions, and as a consequence, the problem is strongly non-lineal. The convergence will be achieved depending on the numerical value of a specified tolerance and the following expression:

$$error = \sum_{i=1}^{nc} |x_i^{L_1}\gamma_i^{L_1} - x_i^{L_2}\gamma_i^{L_2}| \leq tolerance \tag{2.40}$$

The tolerance value is fixed arbitrarily, bearing in mind that the smaller the value, the closer to the real solution is the result when achieved the convergence by the algorithm.

3. **Initialization of the unknowns**
   The algorithm of initialization of the liquid-liquid equilibrium is based on the knowledge that exists a special responsibility for certain components of the mixture to cause the separation into phases. These components are called key components [145]. The key components concept establishes that when there is immiscibility, it is possible to identify two species responsible of the phenomenon. Additionally, it is observed that each one of the formed phases is very rich in one of the key components, while it is poor in the other key component. Thus, if the couple of key components is known for a system, a phase is assigned to each key component and it is possible to estimate initial values for the compositions, assuming that each phase will be richer in its respective key component. In this work, similarly to other algorithms, it is taken as starting point the definition of the distribution constant α_{ij} for every couple of components in the mixture:

$$\alpha_{ij} = \frac{K_i}{K_j} \tag{2.41}$$

   This constant establishes the way in which the components are distributed in the phases, and it is a good parameter to know when a component has a '*preference*' to stay mostly in one phase than other, and as a consequence, it can be a measurement of immiscibility between components. When α_{ij} is very large, this implies that molecules of the components i and j are poorly '*joined together*' between them, which can cause immiscibility. When α_{ij} is very close to unity, this indicates that molecules of components i and j are more '*allied by nature*' between them and they will not tend to separate into two liquid phases. The algorithm should take as couple of key components the one for which the distribution constant is the greatest. Once determined the key components, initial estimations for compositions of the two phases are taken; defining a phase rich in the first key component, with mole fraction of 0.98 and the other phase rich in the second key component with a mole fraction also of 0.98. To the other components, the compositions are assigned until adding up the unity. Ultimately, for the initial estimation of relation of phases L_2/F, a value within the interval 0-1 is taken. In this work, for all cases it was adopted the initial value of 0.5.

2.4.5 Atomic and Bond Contributions of van der Waals volume (VABC)

The van der Waals volume is a widely used descriptor in modeling physicochemical properties. Molecular volume is one of most popular descriptors in QSAR (Quantitative Structure-Activity Relationship) studies [146]. Traditionally, the method developed by Bondi is very popular; the volume of a molecule is calculated as the sum of volumes of mutually intersecting spheres centered on single atoms based on the bond distances, bond angles, and intermolecular van der Waals radii [131]. The UNIFAC methods from previous sections are based on this kind of approach, and in this way, parameters such as molar volume can be easily calculated. However, sometimes it could be necessary to calculate the area per molecule considering a specific polar portion, as it was shown in equations 2.5 concerning the permeability of the surfactant layer. Due to lack of experimental or theoretical partial molar surface area of components, approximations can be used based on the assumption that the molecules are spherical and the effective surface is represented by the cross-sectional area.

For this purpose, in the present work, we can use the method termed Atomic and Bond Contributions of van der Waals volume (VABC) [25], which is very simple and fast. In this method, based also on Bondi radii, the only information needed for calculating volumes of specific parts of a molecule are the atomic contributions and the number of atoms, bonds, and rings. Then, the van der Waals volume ($\text{Å}^3/molecule$) can be calculated from the following formula:

$$V_{vdW} = \sum all\,atom\,contributions - 5.92N_B - 14.7R_A - 3.8R_{NA} \tag{2.42}$$

where N_B is the number of bonds, R_A is the number of aromatic rings, and R_{NA} is the number of nonaromatic rings. The number of bonds present (N_B) can be simply calculated by $N_B = N - 1 + R_A + R_{NA}$, where N is the total number of atoms. The atomic volume contributions are shown in Table 2.1. The results on the literature have shown that the van der Waals volumes calculated from VABC are equivalent to the computer-calculated van der Waals volumes for organic compounds when generating the 3D molecular geometry [25].

Table 2.1 Bondi Radii of atoms and their volumes. Taken from [25].

atom	R_{Bondi}	V_{vdW} (Å^3)	atom	R_{Bondi}	V_{vdW} (Å^3)	atom	R_{Bondi}	V_{vdW} (Å^3)
H	1.20	7.24	Cl	1.75	22.45	As	1.85	26.52
C	1.70	20.58	Br	1.85	26.52	B	2.13	40.48
N	1.55	15.60	I	1.98	32.52	Si	2.10	38.79
O	1.52	14.71	P	1.80	24.43	Se	1.90	28.73
F	1.47	13.31	S	1.80	24.43	Te	2.06	36.62

2.4.6 Estimation of liquid mixture viscosity by UNIFAC-VISCO

Essentially, all correlations for liquid mixture viscosity refer to solutions of liquids below or only slightly above their normal boiling points; i.e., they are restricted to reduced temperatures (of the pure components) below about 0.7. At temperatures below $T_r \approx 0.7$, liquid viscosities are very sensitive to the structure of the constituent molecules. This generality is also true for liquid mixtures, and even mild association effects between components can often significantly affect the viscosity. For a mixture of liquids, the shape of the curve of viscosity as a function of composition can be nearly linear for so-called ideal mixtures [26]. But systems that contain alcohols and/or water often exhibit a maximum or a minimum and sometimes both [147]. This method is useful to estimate or correlate liquid mixture viscosities assuming that values of the viscosities of the pure components are available. Thus, it is a method interpolative. UNIFAC-VISCO method is predictive, it can be used for screening purposes in absence of experimental data, but it is limited in the types of compounds to which it can be applied (it should be utilized only with organic and not aqueous solutions).It is highly recommended if group interaction parameters are available, and particularly, for mixtures in which the components vary greatly in size [148].

Gaston-Bonhomme, Petrino and Chevalier [149] have modified the UNIFAC activity coefficient method (described in section 2.4.1) to predict viscosities. In this method, viscosity is calculated by:

$$ln\eta_m = \sum_i x_i ln(\eta_i V_i) - lnV_m + \frac{\Delta^* g^{EC}}{RT} + \frac{\Delta^* g^{ER}}{RT} \tag{2.43}$$

The combinatorial term is the same as in the UNIQUAC model and is calculated by:

$$\frac{\Delta^* g^{EC}}{RT} = \sum_i x_i ln\frac{\phi_i}{x_i} + \frac{z}{2}\sum_i q_i x_i ln\frac{\theta_i}{\phi_i} \tag{2.44}$$

where z is the coordination number, equal to 10, θ_i and ϕ_i are the molecular surface area fraction and molecular volume fraction, respectively, given by:

$$\theta_i = \frac{x_i q_i}{\sum_j x_j q_j} \qquad \phi_i = \frac{x_i r_i}{\sum_j x_j r_j} \tag{2.45}$$

where q_i, the van der Waals' surface area, and r_i, the van der Waals' volume of component i, are found by summation of the corresponding group contributions. Thus, if $n_k^{(i)}$ is the number of groups of type k in the molecule i,

$$q_i = \sum_k n_k^{(i)} Q_k \qquad r_i = \sum_k n_k^{(i)} R_k \tag{2.46}$$

Table 2.2 UNIFAC-VISCO, group volume and surface area parameters. Taken from [26].

Group k	R_k	Q_k
CH_2, CH_{2cy}	0.6744	0.540
CH_3	0.9011	0.848
CH_{ar}	0.5313	0.400
Cl	0.7910	0.724
CO	0.7713	0.640
COO	1.0020	0.880
OH	1.000	1.200
CH_3OH	1.4311	1.432

where Q_k and R_k are the constants representing the group volume and surface area parameters, which are given in Table 2.2. These values match the UNIFAC values in cases where groups are defined the same. The residual term in Eq. 2.43 is calculated by:

$$\frac{\Delta^* g^{ER}}{RT} = -\sum x_i ln\gamma_i^{*R} \tag{2.47}$$

where

$$ln\gamma_i^{*R} = \sum_k n_k^{(i)} \left(ln\gamma_*^k - ln\gamma_k^{*(i)} \right) \tag{2.48}$$

and

$$ln\gamma_k^* = Q_k \cdot [1 - ln(\sum_m \theta_m \psi_{mk}^*) - \sum_m \left(\frac{\theta_m \psi_{km}^*}{\sum_n \theta_n \psi_{nm}^*} \right)] \tag{2.49}$$

$$\theta_m = \frac{Q_m X_m}{\sum_k Q_k X_k} \tag{2.50}$$

In Eq. 2.50, θ_m is the surface area fraction in the mixture of groups and X_m is the mole fraction in the mixture of groups. Except for the minus sign in Eq. 2.47, these last four equations are identical to those in the UNIFAC method described in section 2.4.1. However, the groups are chosen differently and the interaction parameters are different and are calculated by:

$$\psi_{nm}^* = exp\left(-\frac{\alpha_{nm}}{T} \right) \tag{2.51}$$

Table 2.3 UNIFAC-VISCO, special assignements for branched hydrocarbons and substituted cyclic and aromatic hydrocarbons. Taken from [26].

Type of compound	Actual group	Representation
branched cyclic	>CH-CH_3	2 CH_2 groups
	$> CH_{cy}$-CH_3	1 CH_{2cy} + 1 CH_2
	$> C_{cy}$-$(CH_3)_2$	1 CH_{acy} + 2 CH_2
aromatic	$> C_{ar}$-CH_3	1 CH_{ar} + 1 CH_2

Values of α_{nm} are given in Table 2.4. γ_k^* is the activity coefficient of group k in a mixture of groups formed from the groups in pure component i. Groups in branched hydrocarbons and substituted cyclic and aromatic hydrocarbons are chosen as shown in Table 2.3.

Table 2.4 UNIFAC-VISCO, group interaction parameters, α_{nm}. Taken from [26].

n/m	CH_2	CH_3	CH_{2cy}	CH_{ar}	Cl	CO	COO	OH	CH_3OH
CH_2	0	66.53	224.9	406.7	60.30	859.5	1172.0	498.6	-219.7
CH_3	-709.5	0	-130.7	-119.5	82.41	11.86	-172.4	594.4	-228.7
CH_{2cy}	-538.1	187.3	0	8.958	215.4	-125.4	-165.7	694.4	-381.53
CH_{ar}	-623.7	237.2	50.89	0	177.2	128.4	-49.85	419.3	-88.81
Cl	-710.3	375.3	-163.3	-139.8	0	-404.3	-525.4	960.2	-165.4
CO	586.2	-21.56	740.6	-117.9	-4.145	0	29.20	221.5	55.52
COO	541.6	-44.25	416.2	-36.17	240.5	22.92	0	186.8	69.62
OH	-634.5	1209.0	-138	197.7	195.7	664.1	68.35	0	416.4
CH_3OH	-526.1	653.1	751.3	51.31	-140.9	-22.59	-286.2	-23.91	0

2.4.7 Estimation of liquid molar volume at the normal boiling point by Tyn and Callus Method

In this method [150], the molar volume at the normal boiling point V_b is related to the critical volume V_{crit} by

$$V_b = 0.285 V_{crit}^{1.048} \tag{2.52}$$

where both V_b and V_{crit} are expressed in cubic centimeters per gram mole. Comparisons coming from the literature [26] show that this method is somewhat more accurate than others and has a good reliability. The simplicity of the method makes it attractive.

2.4.8 Estimation of critical volume by Joback Method

One of the first successful group contribution methods to estimate critical properties was developed by Lydersen (1955) [151]. Since that time, more experimental values have been reported and efficient statistical techniques have been developed that allow determination of alternative group contributions and optimized parameters. The Joback method has the lowest error, around 3% with better results for larger substances (3 or more carbons) [26].

Joback [152, 153] reevaluated Lydersen's group contribution scheme, added several new functional groups, and determined new contribution values. His relation for the calculation of the critical volume is

$$V_{crit}[cm^3 mol^{-1}] = 17.5 + \sum_k N_k(vck) \tag{2.53}$$

where the contribution part is indicated as *vck*. The group indentities and Joback's values for contributions to the critical volume are as follows from Table 2.5.

Table 2.5 Group contributions for calculation of critical volume in Joback Method (1984). Taken from [26].

Group	*vck* [$cm^3 mol^{-1}$]	Group	*vck* [$cm^3 mol^{-1}$]
CH_3	65	O	18
CH_2	56	O (ring)	13
CH	41	C=O	62
C	27	C=O (ring)	55
$=CH_2$	56	CH=O	82
=CH	46	COOH	89
=C	38	COO	82
=C=	36	=O	36
≡CH	46	NH_2	38
≡C	37	NH	35
CH_2 (ring)	48	NH (ring)	29
CH (ring)	38	N	9
C (ring)	27	=N-	X
=CH (ring)	41	=N- (ring)	34
=C (ring)	32	=NH	X
F	27	CN	91
Cl	58	NO_2	91
Br	71	SH	63
I	97	S	54
OH	28	S (ring)	38
ACOH	-25		

2.5 Mass transfer model conception

Having defined the interfacial transfer model for a single droplet, and how to estimate theoretically and by means of CAMD techniques the required mass transfer parameters for obtaining an ab-initio prediction, a possible experimental system is now considered as a water-in-oil highly concentrated emulsion layer with thickness L and constant tranversal area S, in contact with a well stirred aqueous receptor solution (See Figure 2.10). In this section, the different assumptions and equations to model this system are described in depth.

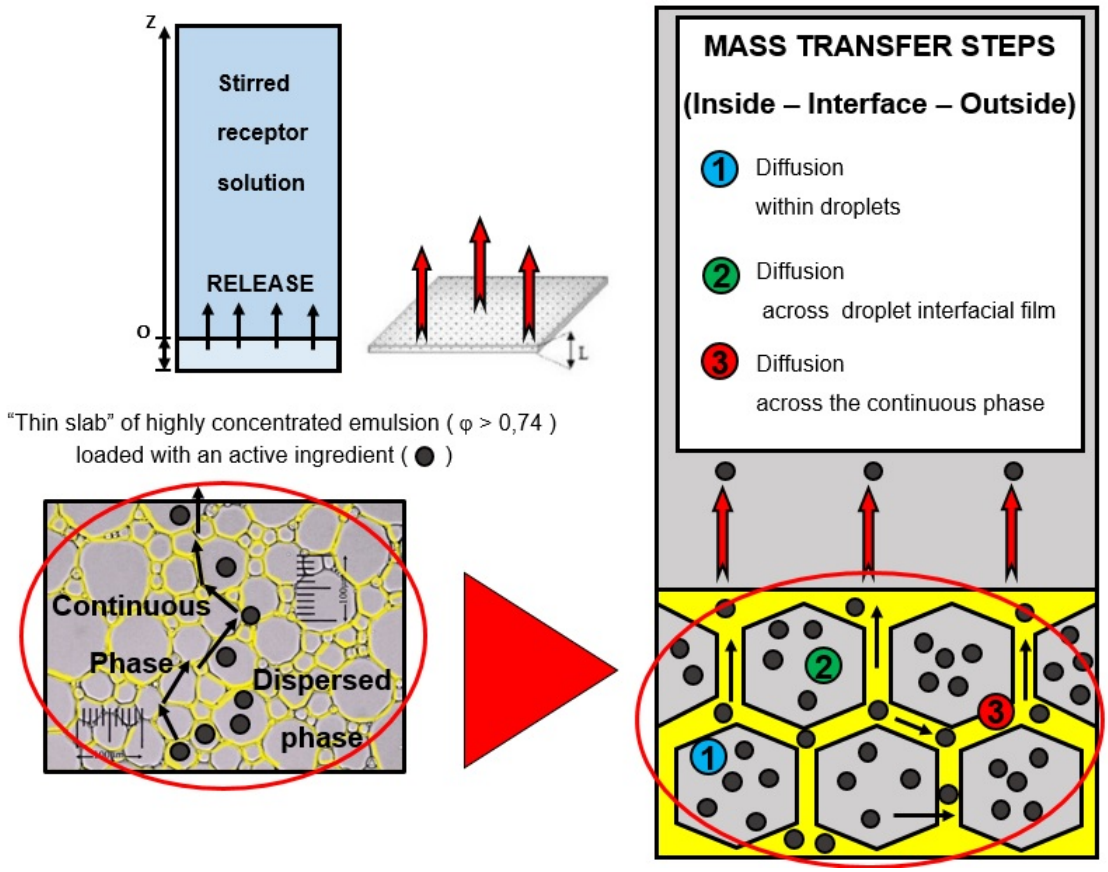

Fig. 2.10 Different steps of transfer model.

The active ingredient is transferred from the emulsion to the aqueous receptor phase according to the following continuity equation, coming from the second Fick's law:

$$\frac{\partial \overline{C}}{\partial t} = D_{eff} \nabla^2 \overline{C} \tag{2.54}$$

Where D_{eff} is an effective diffusion coefficient (m^2/s) of the active ingredient in the emulsion, $\overline{C} = (1-\phi)C_c + \phi C_d$, which presents the average active ingredient concentration

in the whole volume of the emulsion, being ϕ the volume fraction of the dispersed phase, and C_c and C_d are the concentrations (mol/m^3) in the continuous and dispersed phase respectively. Introducing the definition of $\overline{C}$ into the Eq. 2.54 and developing ∇^2, one obtains

$$\frac{\partial \overline{C}}{\partial t} = (1-\phi)\frac{\partial Cc}{\partial t} + \phi\frac{\partial C_d}{\partial t} = D_{eff}\nabla^2\overline{C} = D_{eff}\left((1-\phi)\frac{\partial^2 C_c}{\partial z^2} + \phi\frac{\partial^2 C_d}{\partial z^2}\right) \tag{2.55}$$

Now, particularizing for a water-in-oil emulsion case, it can be asusumed that diffusion inside droplets is faster than interfacial transfer [121], and the concentration can be considered uniform (C_d) in the dispersed droplets ($\partial^2 C_d/\partial z^2 = 0$). With this assumption, the effective diffusion coefficient D_{eff}, which accounts for the actual tortuous diffusion occurring in the space between droplets, can be estimated from the diffusion coefficient in the continuous phase D_c by means of the Maxwell relation [154]

$$D_{eff} = (1+3\phi)D_c \tag{2.56}$$

Therefore, with the definition of the effective diffusion coefficient and considering that the active ingredient is the only transferred component essentially in z direction, perpendicular to the transfer area S, the continuity Eq. 2.55, can be rewritten as

$$\frac{\partial Cc}{\partial t} + \frac{\phi}{(1-\phi)}\frac{\partial C_d}{\partial t} = D_{eff}\frac{\partial^2 C_c}{\partial z} \tag{2.57}$$

The previous Eq. 2.57 describes the global mass balance in transitory regime for a thin slab of emulsion volume dV, uniform section S and thickness dz. The source term ($\partial C_d/\partial t$) expressing the flux rate of the input active ingredient from the dispersed phase [155], can be easily obtained from a mass balance of the dispersed phase

$$\frac{\partial C_d}{\partial t} = -\frac{K_g\Omega}{\phi V}(K_{cd}C_d - C_c) \tag{2.58}$$

where K_g is the global mass transfer coefficient, K_{cd} the distribution coefficient between continuous and dispersed phase, Ω the total interfacial area and V the total volume of emulsion. Considering a mono-disperse population of droplets, Ω can be related to the Sauter mean diameter (volume-surface mean diameter) L_d according to the equality $\Omega = (6\phi V)/L_d$. Thus, Eq. 2.58 can be expressed as

$$\frac{\partial C_d}{\partial t} = \frac{-6K_g}{L_d}(K_{cd}C_d - C_c) \tag{2.59}$$

Now, introducing Eq. 2.59 into the global mass balance in transitory regime (Eq. 2.57), it is possible to clear up and arrive to an equation expressing the flux from the continuous phase

$$\frac{\partial C_c}{\partial t} = \frac{6K_g\phi}{(1-\phi)L_d}(K_{cd}C_d - C_c) + D_{eff}\frac{\partial^2 C_c}{\partial z^2} \tag{2.60}$$

The resolution of equations 2.60 and 2.59 permits to obtain the concentration profile evolution of active ingredient for each phase and time. The transport model in the emulsion is closed by defining initial and boundary conditions for the dependent variables C_d and C_c. At the beginning, the emulsion phases are supposed to be in their equilibrium concentrations, so that both initial concentrations $C_{0,d}$ and $C_{0,c}$ may be calculated given the initial average active ingredient concentration C_0, the previous definition of $\overline{C}$ and the distribution coefficient relation K_{cd} giving

$$C_{0,d} = \frac{C_0}{K_{cd}(1-\phi)+\phi} \quad ; \quad C_{0,c} = \frac{K_{cd}C_0}{K_{cd}(1-\phi)+\phi} \tag{2.61}$$

Concerning the boundary conditions, at $z = 0$, the concentration of active ingredient is maximum in relation to the coordinate z. In addition, assuming that the volume of the receptor solution is large enough (infinite volume), the active ingredient gets strongly diluted when it is released, the concentration in the contact surface between the emulsion and the receptor solution can be considered zero. Therefore

$$z = 0; \frac{\partial C_c}{\partial z} = 0; \quad \textit{and} \quad z = L; C_c = C_d = 0; \tag{2.62}$$

The ensemble of all equations that have been described in this chapter, allows the prediction of the active ingredient release from a highly concentrated emulsion by means of a mechanistic realistic theory based on Fick's law of diffusion, taking into account the resistances due to the interfacial layer and continuous phase, and the different equilibria present between phases. It is also considered that the diffusion of the active ingredient does not affect the structure of the emulsion, as well as all structural parameters are considered to be constant during the release.

As a remark, it should be noted that the model, although restricted here to a simple thin slab geometry and infinitely diluted solution conditions, it could be, in perspective, easily adapted to different geometries, or conditions, such as a multicomponent mass transfer (where not only an active ingredient was the transferred component) or cases of concentration dependence for diffusion coefficients.

Chapter 3

SIMULATION

'The mere act of observing something changes the nature of the thing observed', Heisenberg

3.1 Introduction

Despite of its basis on a clear scientific background, ab-initio simulations performed by model building, are an art more than a science [156]. However, fortunately, mathematical modelers share the same procedure [157], consisting in (1) delineating the phenomenon studied, (2) expressing this in mathematical terms, and finally (3) predicting experimental behavior in different conditions. This means, that if A represents a determined phenomenological manifestation of reality, model building its respective simulation means to find out, inside the mathematical world, one or more structures able to formally represent and interpret A allowing the simulation of all possible interactions [158].

In this chapter, the first subsection will consist in an overview of the ab-initio model developed in this thesis to predict the release of an active ingredient from water in oil highly concentrated emulsions, employing and connecting all the theoretical background from previous chapter. Different diagrams will try to establish the relations occuring among all the variables involved. The mathematical programming and all the work on the computer was carried out using MATLAB®.

After this, an analysis concerning molecular structures of possible candidate chemicals will be performed in order to create a cartography of materials to work with. An analysis of sensibility of variables will be performed. Thus, case studies obtained by the operation of the ab-initio model by using these materials will reveal the paramount importance for what concerns a possible experimental design on the next Chapter 4. Only with a clear knowledge about the whole system and its behaviors, it will be possible to decide later experiments, ways to perform them and check the robustness of our ab-initio model.

3.2 Logical Architecture Diagram

This section presents the formal definitions and different steps (as diagrams and relations between variables) of the computer simulation framework. Because the reverse engineering is based on CAMD techniques, it is necessary to employ some form of representation of the molecular structure information for use in physico-chemical parameter estimation. Consequently, a database is required. This database includes the representation of compounds as a collection (or vector) of groups. In this work, it has been limited to four the number of components present in the emulsion: an active ingredient, an oil acting as continuous phase, a dispersed phase (generally, water containing a small proportion of salt for stabilizing purposes) and a surfactant. However, it is expected that it could be expanded to a higher number of components (including co-surfactants, viscosity modifiers, etc.) or even to the domain of oil in water emulsions.

First, a serie of identification numbers ('*Vknumbers*') that enumerate the components of a candidate list (cartography database) are proposed. This input, will compile the number of occurrences of each atom type conforming the molecule selected ('*vk*' integers appearing in previous Eq. 2.22) to be used later for the prediction of activity coefficients by UNIFAC and mixture viscosity calculations. Following this, the cartography database has a second objective of providing respective molar volumes, molecular weights, pure compound densities/viscosities and the other required geometrical parameters for the calculations (A_1*, A_2* and A_2). It should be mentioned, that in this work, pure compound properties were taken from the free chemical structure database [20] of The Royal Society of Chemistry .

Once components and respective physico-chemical properties have been loaded from the cartography database, specifications concerning the emulsion formulation are required for a next step. These are the concentration of active ingredient (AI) in the emulsion (mass amount per mass of dispersed phase), the dispersed phase mass fraction (ϕ_m), the mass ratio between oil and surfactant ($r_{oil/surf} = m_{oil}/m_{surf.}$), the total mass prepared of emulsion, the experimental amount of emulsion utilized for the release, the volume of the receptor solution and the droplet diameter of dispersed phase. By using all these especifications, and relations appearing in Fig.3.1 concerning dispersed and continuous phases, the quantities present in a thin slab of emulsion are recalculated. Following this, the flash algorithm can be applied in order to obtain the equilibrium molar fractions and the distribution coefficient of the active ingredient between continuous and dispersed phases. After the convergence, by using the respective molar volumes and equilibrium compositions, phase volumes and the volumetric fraction of dispersed phase are calculated.

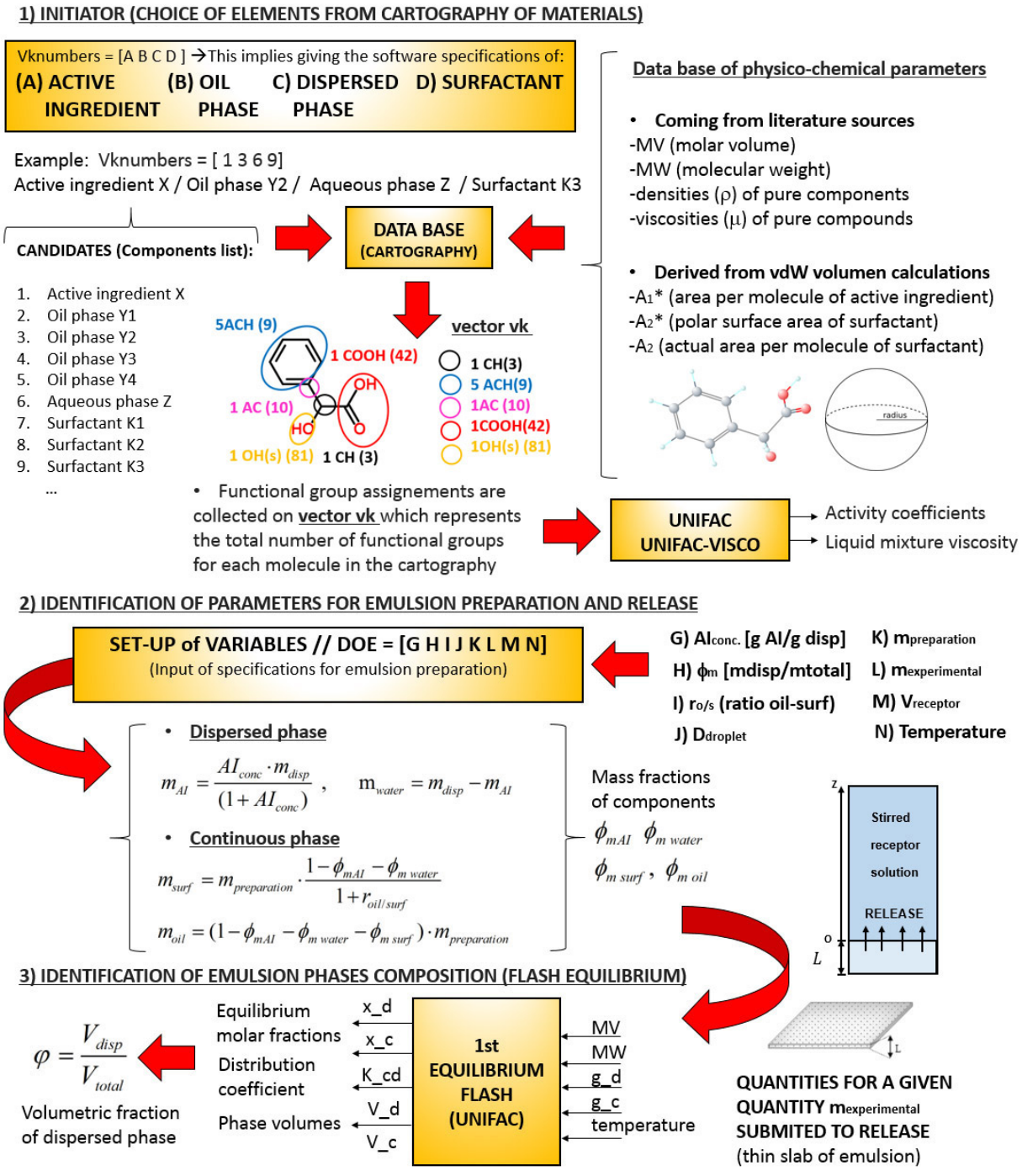

Fig. 3.1 Inital steps for selection of components from the cartography database and set-up of variables later necessary to simulate the release.

For sake of clarity, in Fig.3.2, the different steps of the flash equilibrium algorithm have been outlined, and typical snapshots given by the programming code when applied have been shown. A more detailed description is given in the following page.

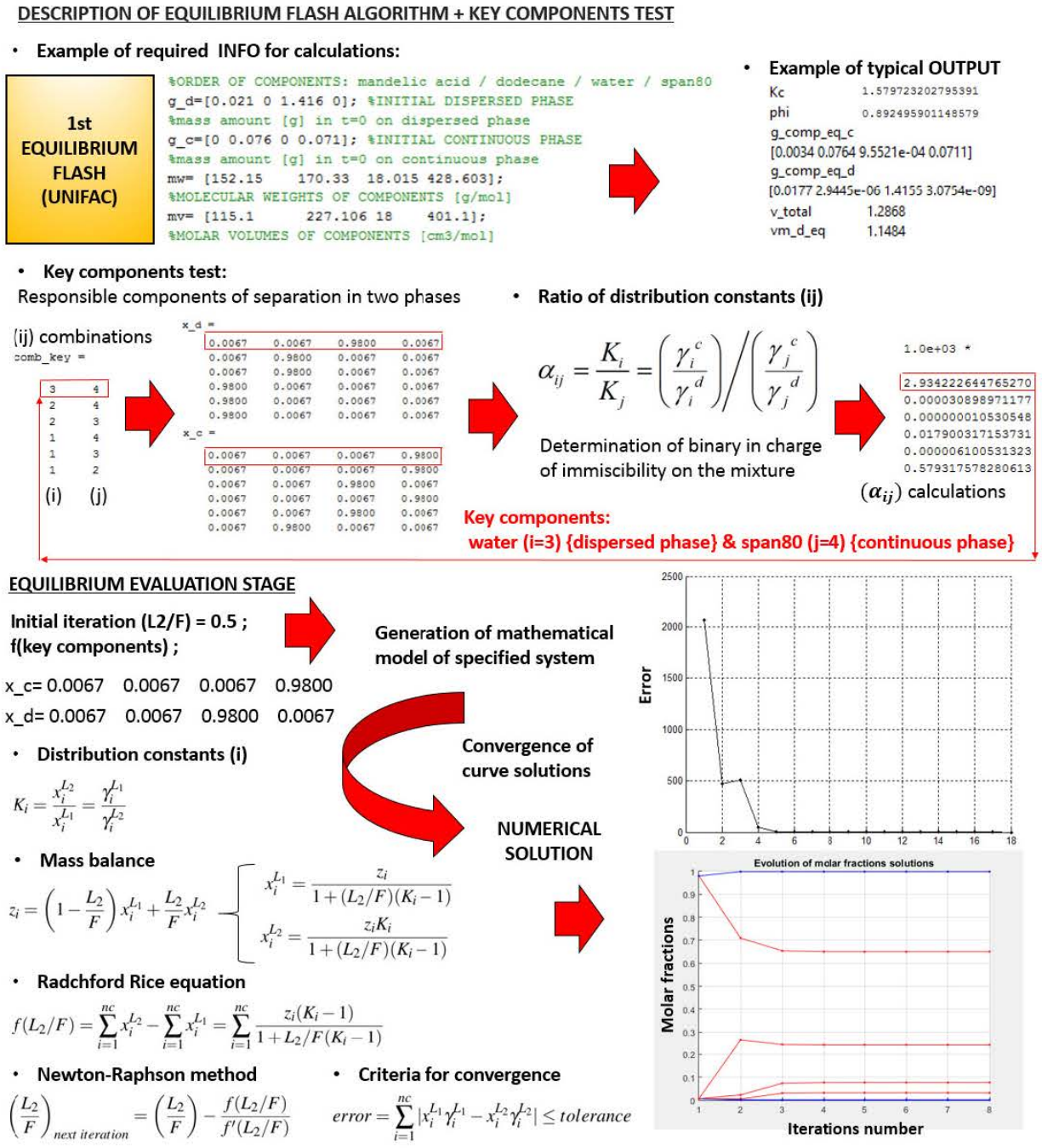

Fig. 3.2 Schematic diagram of stages of the equilibrium flash algorithm and typical response obtained when it is applied.

As one can see, the first step consisted of taking couple of components and constitute hypothetical phases, where alternately each one of the components was majority. This implied to take a mole fraction of 0.98 in the dispersed phase (mole fractions compositions represented by x_d) of a possible key component (i), and the rest of composition to be distributed between the other components, taking care the total sum to be the unity. Similarly, in the continuous phase (mole fractions compositions represented by x_c), it is taken 0.98 for the composition a component (j), which takes the rol of key component for this phase. By using these compositions, the equilibrium relations K_i can be calculated for components i and j, and with them, their respective distribution relations α_{ij}. On completion of this, it is necessary to ensure that the result will be always greater than unity (if this would not happen, it should be enough to change the order of the couple ij by ji). The procedure is performed until all possible combinations of couples in the quaternary mixture are concluded, and from this point on, the obtained values are considered as the distribution relations for every couple.

In the second step, the distribution relation values should be compared. As one can see in the graph, the couple of the first line (equivalent to components $i = 3$, water and $j = 4$, SPAN 80 in the example), showed the highest value for the ratio of distribution constant α_{34}, therefore, this couple is the candidate couple of key components of the system. Once determined the key components, the initial estimations for compositions of the two phases are taken; defining each phase rich in its respective key component, with mole fraction of 0.98. To the other components, the compositions are assigned until adding up the unity. An initial value of 0.5 was employed for the relation of phases L_2/F.

Once the equilibrium flash is applied, the presence of surfactant on the interface should be taken into account. For this purpose, the relations appearing in Fig.3.3 are used. Depending mainly on the mean droplet size of the emulsion and the surface polar head of the surfactant employed, the surfactant amount on the interface can be easily calculated. This quantity is substracted then from the continuous phase composition in equilibrium that resulted previously from the flash. Following this, a second flash equilibrium is applied, but in regards to the hypothetical equilibrium between the surfactant layer and the dispersed phase. This should be performed in order to work out the hypothetical distribution coefficient of the active ingredient between an homogeneous layer of surfactant and the dispersed phase, which is required later for the calculation of the permeability. Calculating the critical volume by the Joback method, one can use it to estimate the volume of the active ingredient at its normal boiling point by means of the Tyn and Callus relation. After this, the diffusivity in pure surfactant, given by the Wilke Chang equation can be determined. It should be noted here, that the viscosity appearing in the denominator, refers to the viscosity of pure surfactant.

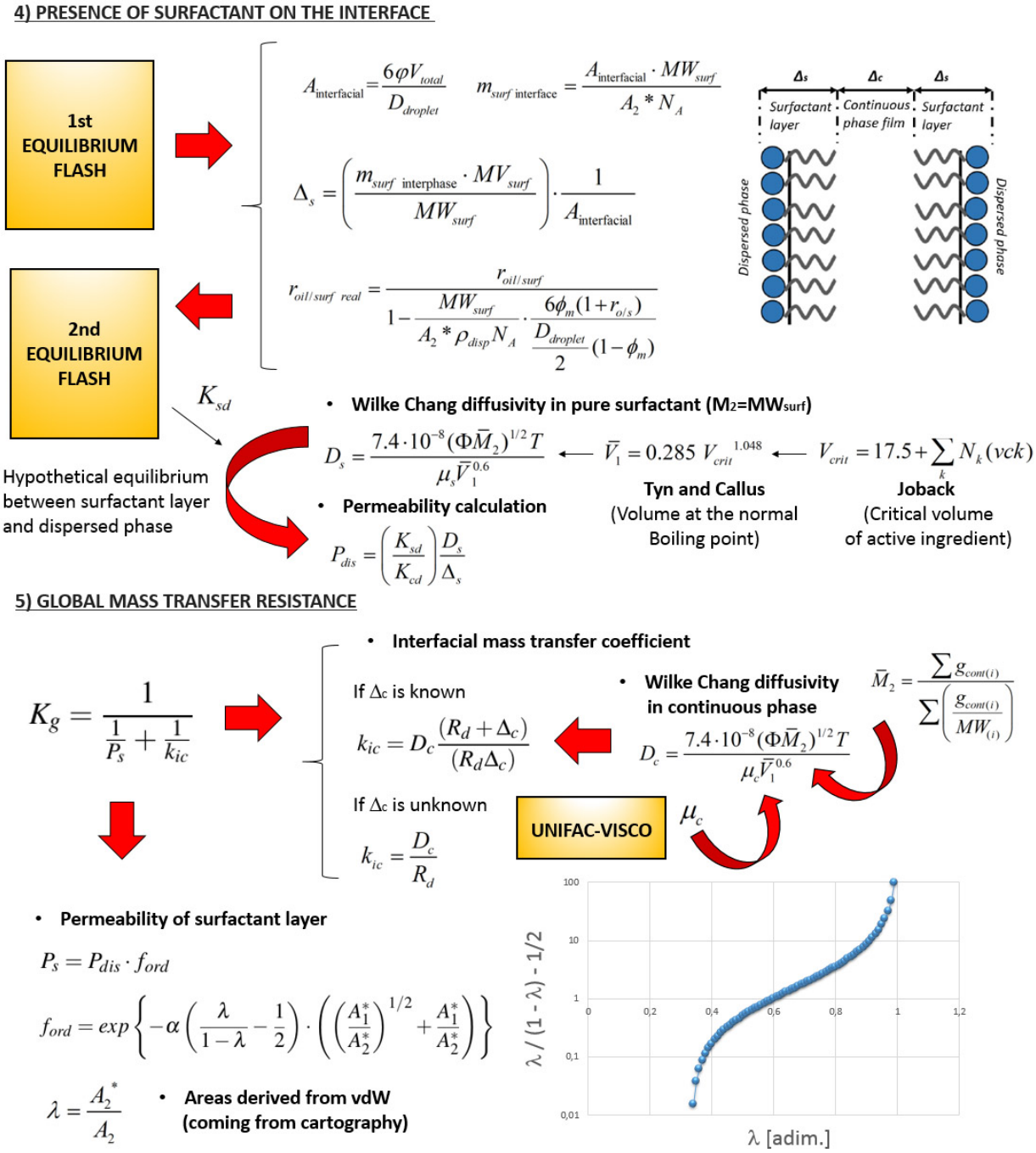

Fig. 3.3 Final steps for setting up all required variables for release simulations. Calculation of the global mass transfer resistance.

Next, the global mass transfer resistance is about to be determined. On the one hand, the interfacial mass transfer is calculated. For this purpose, the diffusivity of the active ingredient is estimated again with the Wilke Chang equation, but in this case, referring to a diffusivity

through the continuous phase. It is remarked here that the viscosity required on the equation is predicted by the UNIFAC-VISCO method. The mean molecular weight corresponding to the continuous phase, is obtained by weighting the substances present in relation to their mass amounts. On the other hand, the permeability of the surfactant layer is also calculated using the previous permeability of a disordered layer and the factor for decrease of permeability due to the interfacial order. By way of illustration, it has been shown the dominance of the normalized surface density within the exponent of the factor for decrease of permeability.

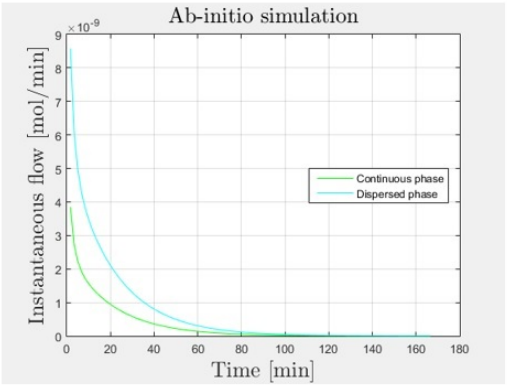

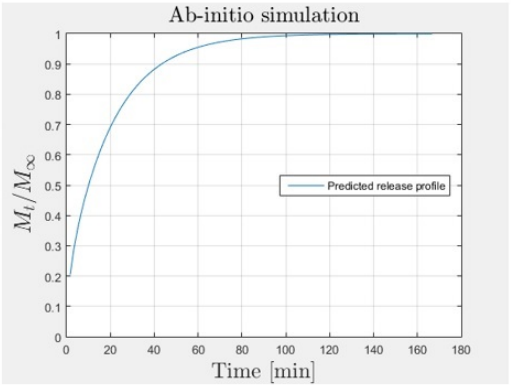

- **Initial conditions and boundary conditions**

$$C_{0,d} = \frac{C_0}{K_{cd}(1-\phi)+\phi} \qquad z=0; \frac{\delta C_c}{\delta z} = 0;$$

$$C_{0,c} = \frac{K_{cd}C_0}{K_{cd}(1-\phi)+\phi} \qquad z=L; C_c = C_d = 0;$$

- **Mass balances**

$$\frac{\delta C_d}{\delta t} = \frac{-6K_g}{L_d}(K_{cd}C_d - C_c)$$

$$\frac{\delta C_c}{\delta t} = \frac{6K_g\phi}{(1-\phi)L_d}(K_{cd}C_d - C_c) + (1+3\phi)D_c\frac{\delta^2 C_c}{\delta z^2}$$

Fig. 3.4 Sixth step and last one of the ab-initio model. The release profile is simulated.

At this point, all parameters required for the simulation of the release profile would have been estimated or calculated. Consequently, the model equations can be solved by means of the function PDEPE on MATLAB®. The ab-initio model predicts the instantaneous flow of active ingredient exiting both phases (continuous and dispersed) and its cumulative percentage profile (calculated considering a given volume of receptor solution) as function of time. An example of this prediction can be visualized in Fig.3.4. All parameters involved during each simulation are registered and this allows possible comparisons between the different cases. It is also worthy to point out that the time for the resolution of a case study is relatively fast (less than one second). Therefore, it is expected a low computational cost for the simulation of a big number of cases .

3.3 Cartography of materials

When preparing a cartography, initially, we do not know which chemicals to use in the product and in what amount they should be present but we can know the molecular structures of possible candidate chemicals. [159]. Although this is an attractive feature of CAMD techniques, it also has its drawback, the number of structures that may be generated can be very large. As a matter of '*simplicity*', and in order to build a limited cartography of materials, we have chosen 9 components that could be hypothetically used for preparing water-in-oil highly concentrated emulsions, possibly interesting as drug delivery systems for controlled release in the pharmaceutical or cosmetic industries.

In the following pages, a brief description for each component will be given and their molecular characteristics will be presented. In addition, estimations of some of their properties, which are required for later simulations will be done.

3.3.1 Active ingredient

A relatively hydrophilic molecule was chosen as the active ingredient in this work, suitable for UV determination: mandelic acid (MA). This active ingredient is an important model molecule in cosmetic and pharmaceuticals, since that yields very good results when used to treat excessive actinic keratosis, hyperpigmentation and mesh-like wrinkles, which are primarily due to sun exposure-induced aging of the skin [160]. MA is classified by the International Nomenclature of Cosmetic Ingredients (INCI) as an alpha-hydroxy acid, and it is harvested from the extract of bitter almonds via the hydrolisis of benzaldehyde. Its molecular structure, some characteristics, and group assignements according to Modified UNIFAC Dortmund (rev. 6) are shown in Fig.3.5.

- **Formule:** $C_3H_8O_3$
- **CAS number:** 90-64-2
- **Molecular weight:** 152.150 g/mol
- **Molar volume:** 115.100 cm^3/mol

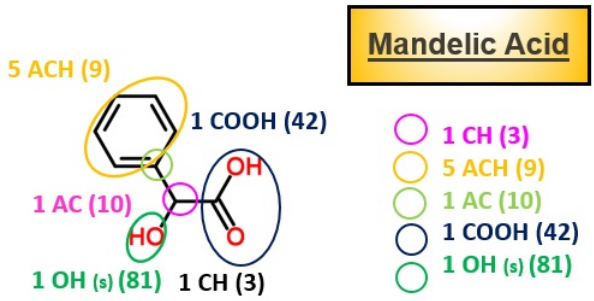

Fig. 3.5 Molecular properties for mandelic acid and group assignements.

This molecule is a weak acid (pKa=3.75 [161]), which dissociates in aqueous solution giving mandelate ions. The degree of ionization depends obviously on the pH of the medium [162]. At basic pH the formation of mandelate is favored while at acidic pH values, the nonionized species predominate (Fig. 3.6).

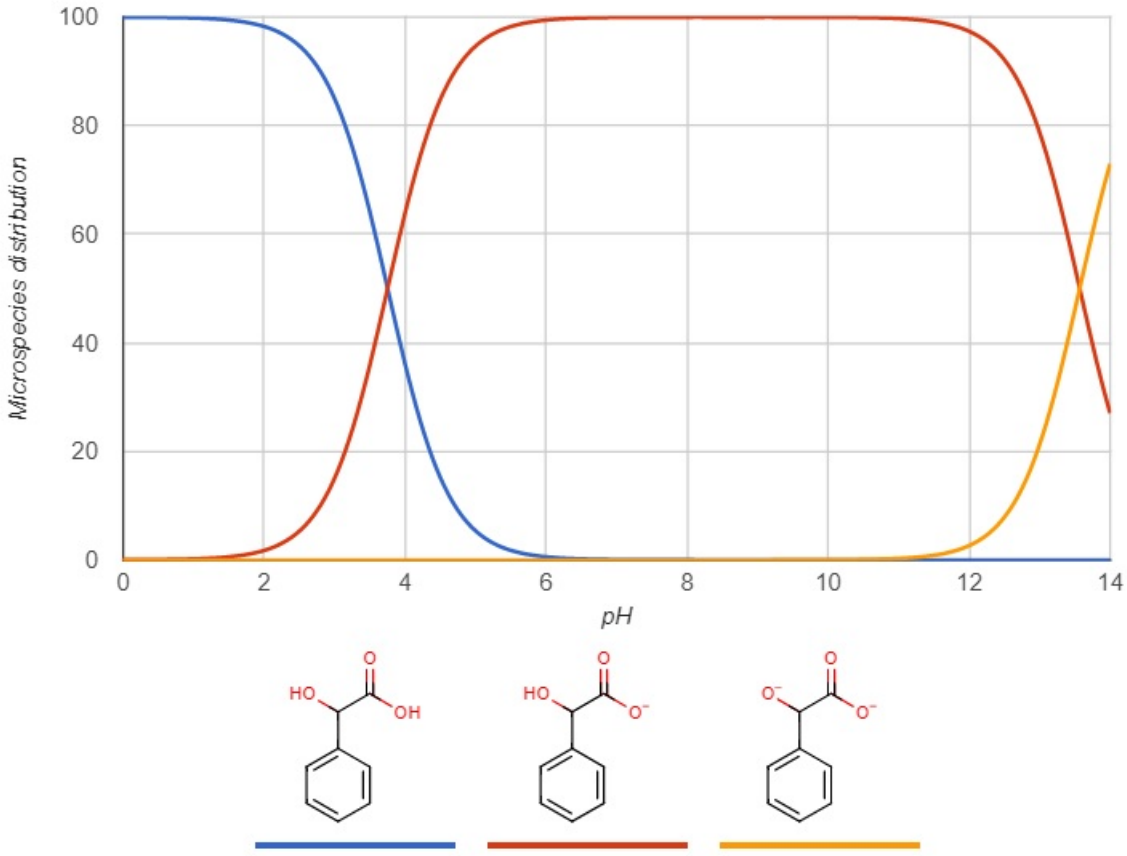

Fig. 3.6 MA microspecies distribution as function of pH. Obtained from [20].

A higher pH increases the aqueous solubility of MA, from 181 mg/mL at acidic pHs [163] to 927.81 mg/mL at pH 6.5 [20]. This is easy to understand, thinking on the typical expression used by chemists to remember how solvents work; '*Like dissolves like*', that means, that polar dissolves polar; water is polar and mandelate as ionized specie possesses a higher polarity, therefore, at higher pH will dissolve better in water.

Typical concentrations of MA employed in pharmaceutical applications, range until a max. 10% aqueous solutions [160]. For instance, the pH of a diluted aqueous solution of 1.5 g MA / 100 g H_2O (1.5 %) shows a pH of 2.7. At this pH, the corresponding distributions of microspecies are shown in Fig. 3.7.

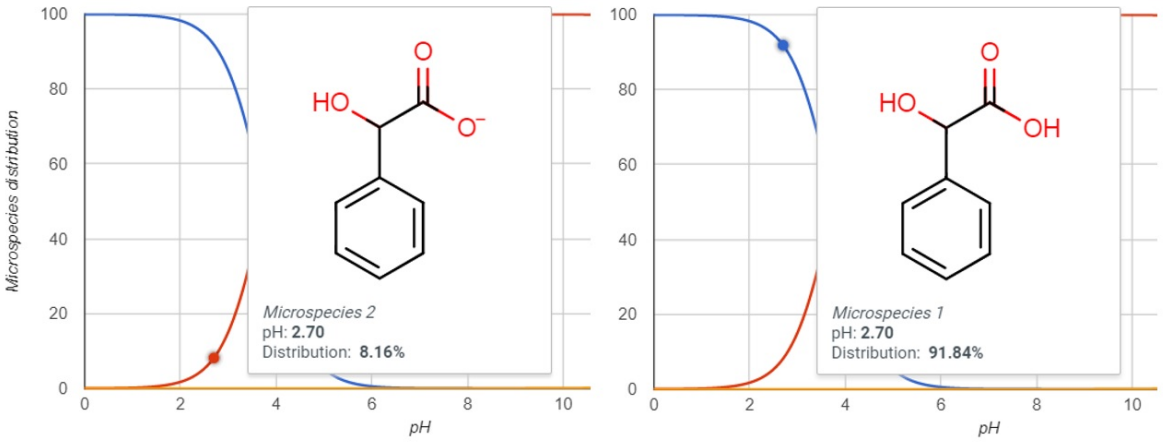

Fig. 3.7 Microspecies of MA at pH 2.7 (1.5 % aqueous solution). Obtained from [20].

The area in a compressed state (A_1^*) of MA should be estimated for permeability calculations in the ab-initio model. Taking as a reference this diluted concentration of 1.5 %, it is possible to consider that the molecule is mostly presented as nonionized form. Therefore, this area (A_1^*) was estimated by using the VABC method described in previous Section 2.4.5. Table 3.1 shows the group parameters for the vdW volume calculation of the whole molecule. Assuming a spherical shape for the whole molecule, the radius (139.51 Å^3) can be easily calculated (3.217 Å). Then, considering the cross-sectional area of this sphere, one obtains 32.521 Å^2 as the area in a compressed state (A_1^*).

Table 3.1 Calculation of area in compressed state for MA molecule by VABC method.

Type	Number	Contribution / unit [Å^3]	Total contribution [Å^3]
H	8	7.24	57.92
C	8	20.58	164.64
O	3	14.71	44.13
bonds (N_B)	19	-5.92	-112.48
aromatic rings (R_A)	1	-14.7	-14.7
nonaromatic rings (R_{NR})	0	-3.8	0
		vdW volume	139.51 [Å^3/molec]
		sphere radius	3.217 [Å]
		cross-sectional area (A_1^*)	3.217 [Å^2/molec]

In addition, the critical volume of the molecule was also estimated by using the Joback method (Section 2.4.8) for the diffusivity calculations. The following Table 3.2 shows the parameters for this calculation. Using the critical volume obtained (V_{crit} = 427.5 cm^3/mol), the molar volume (V_b) at the normal boiling point (T_b) solved by the Tyn and Callus relation (Eq. 2.52), gives a molar volume of 162.954 cm^3/mol.

Table 3.2 Estimation of critical volume for mandelic acid molecule by Joback method.

Type	Number	vck [cm^3/mol]	N(vck)
CH_2	1	56	56
=CH (ring)	5	41	205
OH	1	28	28
=C (ring)	1	32	32
COOH	1	89	89
		Critical volume (V_{crit})	427.5 [cm^3/mol]
		Normal volume at T_b (V_b)	162.954 [cm^3/mol]

3.3.2 Dispersed phase

Due to the aforementioned particularization for a water-in-oil emulsion system when the mass transfer model conception was done, the dispersed phase is automatically chosen: water. Fig. 3.8 shows the characteristics, molecular structure and group assignement for water. Nevertheless, it should be mentioned that generally a small amount of electrolytes dissolved in the aqueous phase (for example NaCl) dramatically increases emulsion stability [164]. Stability of the gel-emulsion is important, as the rupture of the gel-emulsion structure would give rise to a massive release of the active ingredient contained in the dispersed drops [162].

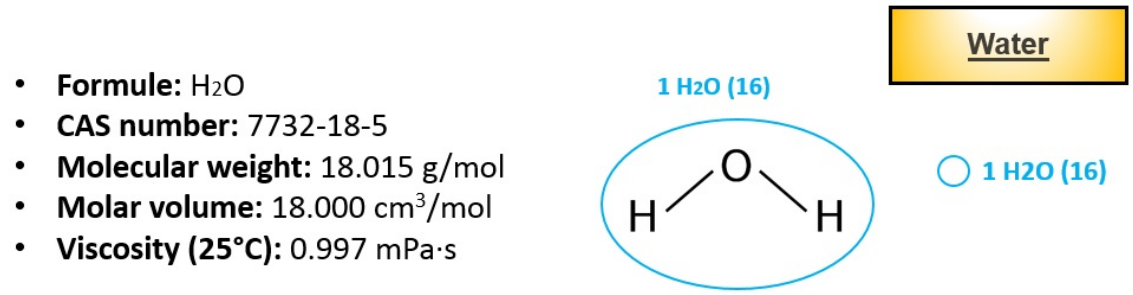

Fig. 3.8 Molecular properties for water and group assignement.

3.3.3 Continuous phase

A large number of oils are available, which can be used as components of emulsion systems, but their toxicity, irritation potential, and unclear mechanism of action sometimes limit their use. One must choose materials that are biocompatible, nontoxic, and clinically acceptable [165]. In this cartography, a group of four different oils, generally regarded as safe, have been included; two saturated n-alkanes (dodecane and hexadecane) and two fatty acid esters (isopropyl myristate and isopropyl palmitate). In Fig. 3.9, the molecular properties for the two n-alkanes and group assignements according to Modified UNIFAC Dortmund (rev. 6) are shown.

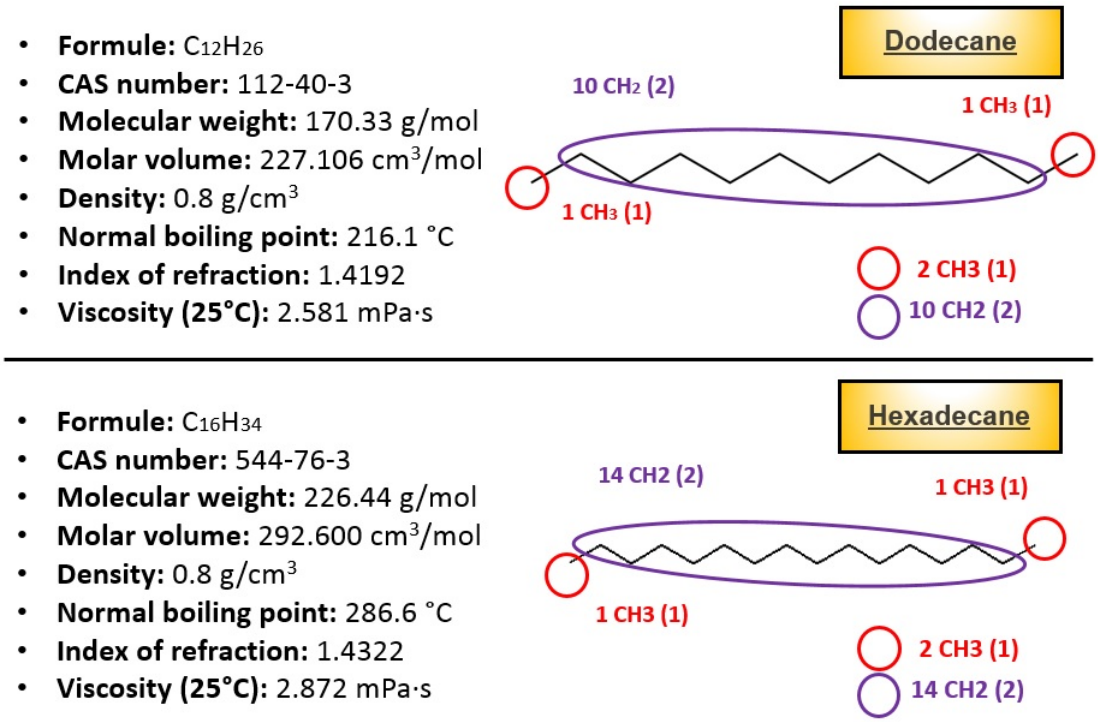

Fig. 3.9 Molecular properties for n-alkanes: dodecane/hexadecane and group assignements.

The production of dodecane and hexadecane as pure chemicals and high-purity process streams is quite small relative to the petroleum substances (i.e., kerosene, jet fuel, home heating oil, hydrocarbon solvents) that contain these these n-alkanes as constituents. Almost all (99%) of the purified n-alkane production is not as single chemicals but as process streams that contain a range of n-alkanes, typically C_{10}-C_{13}, C_{12}-C_{14}, C_{12}-C_{16} and C_{14}-C_{16} [166]. These n-alkane process streams are consumed as closed-system chemical intermediates in the manufacture of linear alkylbenzenes, which are chemical building blocks for the manufacture of detergents. In fact, a very small volume is produced in pure form. There are no known

consumer product applications for pure dodecane or hexadecane. However, they can be present in some hydrocarbon-containing products such as baby oils, sunscreens, hair oils, body and massage oils, makeup removers, some automotive chemicals, cleaning solvents, water repellents used for decks, shoes and sports equipment, and general-use household oil products [166].

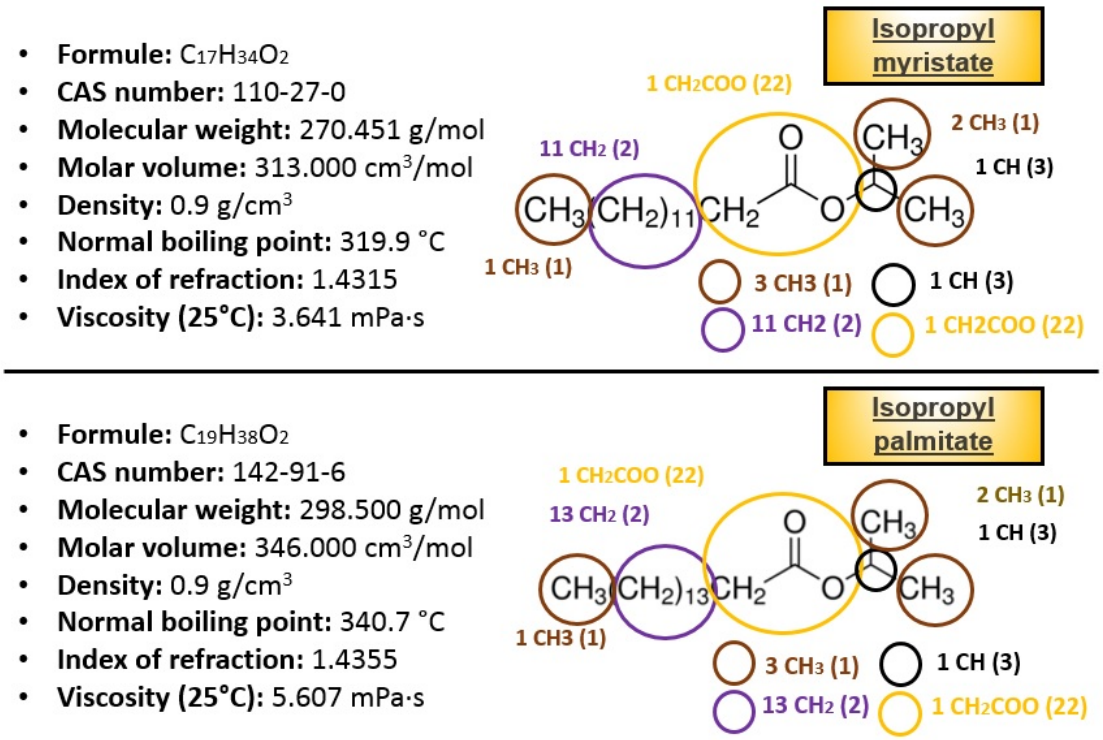

Fig. 3.10 Molecular properties for fatty acid esters: isopropyl myristate/palmitate, and group assignements.

Regards the fatty acids esters: isopropyl myristate/palmitate, they are esters of isopropyl alcohol and myristic/palmitic acid, respectively. In Fig. 3.10, their molecular properties and group assignements according to Modified UNIFAC Dortmund (rev. 6) are shown. They are commercially produced by distillation, which is preceded by the esterification of myristic/palmitic acid and isopropanol, in the presence of an acid catalyst. The product is stripped to remove excess isopropanol, alkali refined to neutralize the catalyst, and the product is then distilled to obtain isopropyl myristate/palmitate [167]. They are very important as solubilizing, spreading, and penetrating agents in anhydrous skin lubricating lotions. These esters leave the skin soft and smooth without an oily surface film. Therefore, they are typically used in bath oils, perfumes, creams, lotions, lipsticks, hair preparations, shaving lotions, aerosol toiletries, and pharmaceutical ointments.

3.3.4 Surfactants

Similarly to the oils for the continuous phase, one should use emulsifiers in an appropriate concentration range that will result in mild and nonaggressive emulsions. The surfactant chosen must be able to lower the interfacial tension to a very small value, which facilitates dispersion process during the preparation of the highly concentrated emulsion, providing a flexible film that can readily deform around the droplets. Also it must be of the appropriate lipophilic character to provide the correct curvature at the interfacial region [165].

As it is well known in the art, the terms '*hydrophilic*' and '*lipophilic*' are relative terms. To function as a surfactant, a compound must necessarily include polar hydrophilic moieties as well as non-polar hydrophobic (lipophilic) moieties; i.e., a surfactant compound must be amphiphilic. An empirical parameter commonly used to characterize the relative hydrophilicity and lipophilicity of non-ionic amphiphilic compunds is the hydrophilic-lipophilic balance (the '*HLB*' value). Surfactants with lower HLB values are more lipophilic, and have greater solubility in oils, whereas surfactants with higher HLB values are more hydrophilic, and have greater solubility in aqueous solutions [168]. The HLB of a surfactant can be an useful guide for surfactant selection. It is generally accepted that low HLB surfactants are favored for the formulation of w/o emulsions, whereas surfactants with high HLB (>12) are preferred for the formation of o/w emulsions [165].

In this work, three different types of surfactants (Fig. 3.11) have been chosen, with an appropriate HLB (at least, expected initially) in relation to the oils of the previous section: a sorbitan fatty acid ester (sorbitan monooleate, SPAN 80 ®), a polyglycerized fatty acid (polyglycerol polyricinoleate, PGPR ®) and a polyethylene glycol alkyl ether (polyoxyethylene glycol-2-oleyl ether, BRIJ 93 ®).

1. Sorbitan monooleate is a sorbitan ester of Croda, marketed under the Span product name (SPAN 80 ®). It is produced by the dehydration of sorbitol and esterification with oleic acid (mono) in a controlled chemical process. As nonionic surfactant, it offers increased stability, formulating flexibility and wider compatibility. It is stable in mild acids, alkalis and electrolytes and do not react with ionic ingredients or actives. This surfactant is a key emulsifying agent for a number of applications in household consumer products, excellent for water in oil emulsification of hydrocarbons and useful as solubiliser, wetting agent and dispersant.

2. Polyglycerol polyricinoleate (PGPR), is a food grade emulsifier consisting of polyglycerol as the hydrophilic group (mainly found a 75% as di- tri- or tetraglycerol) and interesterified ricinoleic fatty acids as the hydrophobic group. In Fig. 3.11, the typical structure of the fraction consisting of tri-glycerol tri-ricinoleate is shown. PGPR is

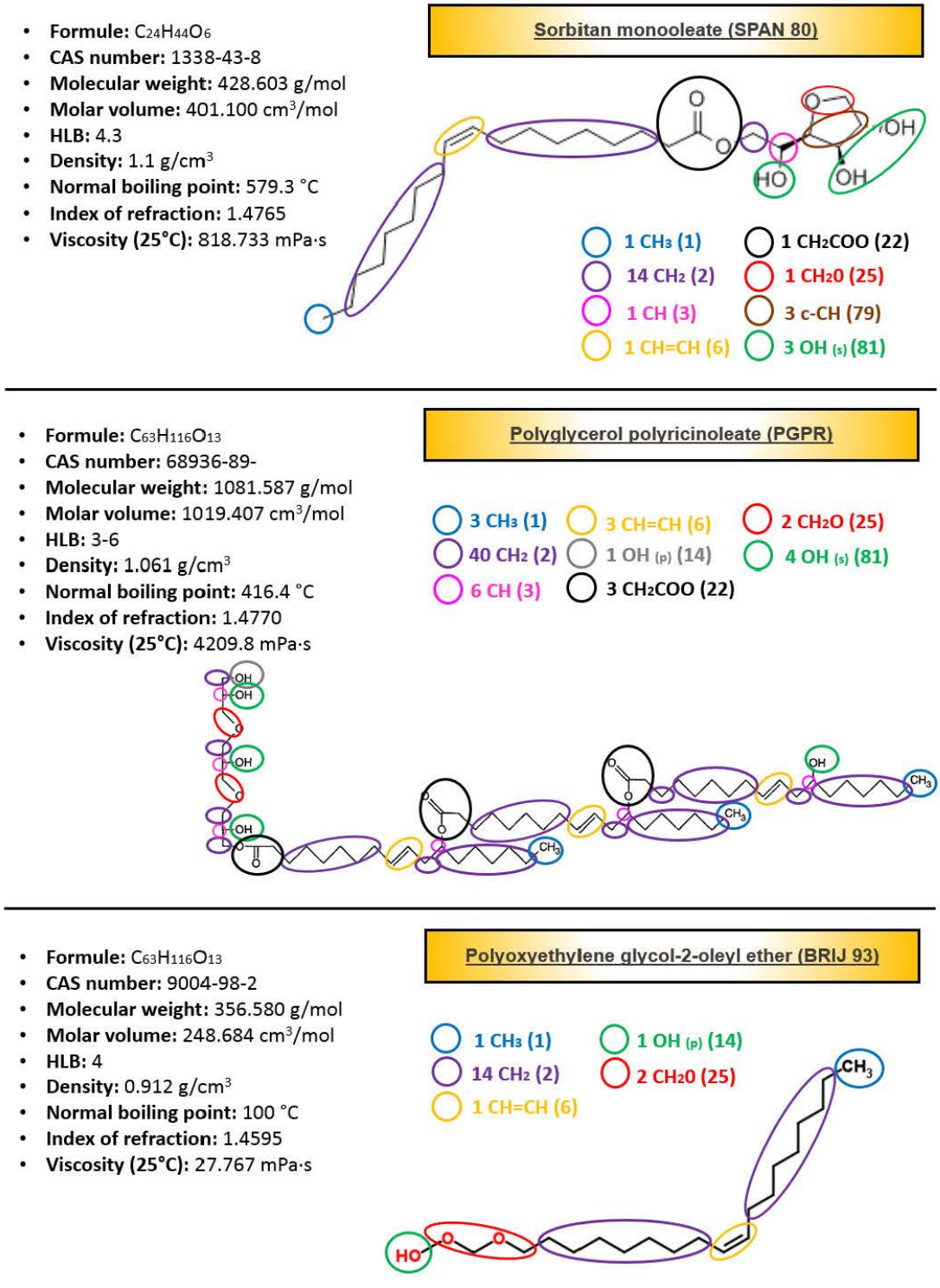

Fig. 3.11 Group assignements and molecular properties for surfactants included in the cartography.

widely known as an excellent water in oil emulsifier. It is used to manufacture stable pan release agents for the bakery industry and to stabilize low fat margarine systems with high water content. However, the main application of PGPR is in the chocolate industry, because it has the ability for improving the flow properties by lowering the friction between the particles suspended in the liquid fat phase.

3. Polyoxyethylene glycol-2-oleyl ether (also known as Oleth-2 or by its commercial name, BRIJ 93 ®, registered trademark of Croda) is an alkyl PEG ether, reaction product of an alkyl alcohol (oleyl alcohol) and two equivalents of ethylene oxide [169]. It is an exceptional nonionic water in oil emulsifier and recommended for a wide range of topical applications within cosmetic and personal care products, such as body and hand creams, hair conditioners, hair dyes, lotions and deodorants. Its nonionic nature allows flexibility in formulation and provides compatibility over a wide pH range. It acts as a wetter, co-emulsifier and solubiliser of oils.

Since it is required for permeability calculations, the area per molecule in a compressed monolayer (A_2^*), as well as the actual area per molecule (A_2) for each one of the surfactants will be estimated by using the VABC method. It should be noticed that A_2 has been worked out in a similar manner as previously done for the active ingredient mandelic acid (considering the whole molecule), but for the estimation of A_2^*, only the polar part (polar surface area) of the molecules have been taken into account. The next Fig. 3.12 emphasizes the parts considered in the calculation of polar areas (A_2^*) of surfactants. The following Tables from 3.3 to 3.5 reflect the work out of these polar areas.

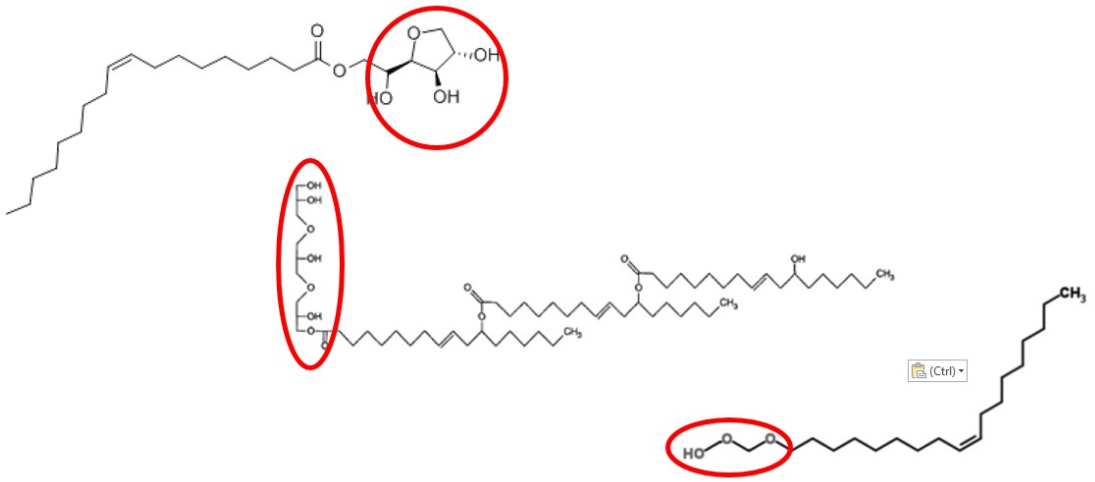

Fig. 3.12 Considered polar parts for each surfactant of the cartography in this work.

Table 3.3 Calculation of polar area (A_2^*) for SPAN80 by VABC method.

Type	Number	Contribution / unit [Å^3]	Total contribution [Å^3]
H	9	7.24	65.16
C	5	20.58	102.9
O	4	14.71	58.84
bonds (N_B)	18	-5.92	-106.56
aromatic rings (R_A)	0	-14.7	0
nonaromatic rings (R_{NR})	1	-3.8	-3.8
		vdW volume	116.54 [Å^3/molec]
		sphere radius	3.030 [Å]
		polar area (A_2^*)	28.845 [Å^2/molec]

Table 3.4 Calculation of polar area (A_2^*) for PGPR by VABC method.

Type	Number	Contribution / unit [Å^3]	Total contribution [Å^3]
H	19	7.24	137.56
C	10	20.58	205.8
O	8	14.71	117.68
bonds (N_B)	36	-5.92	-213.12
aromatic rings (R_A)	0	-14.7	0
nonaromatic rings (R_{NR})	0	-3.8	0
		vdW volume [Å^3/molec]	247.92
		sphere radius	3.897 [Å]
		polar area (A_2^*)	47.712 [Å^2/molec]

Table 3.5 Calculation of polar area (A_2^*) for BRIJ93 by VABC method.

Type	Number	Contribution / unit [Å^3]	Total contribution [Å^3]
H	9	7.24	65.16
C	4	20.58	82.32
O	3	14.71	44.13
bonds (N_B)	15	-5.92	-88.8
aromatic rings (R_A)	0	-14.7	0
nonaromatic rings (R_{NR})	0	-3.8	0
		vdW volume [Å^3/molec]	102.81
		sphere radius	2.906 [Å]
		polar area (A_2^*)	26.532 [Å^2/molec]

Now, in Tables from 3.6 to 3.8, the calculation was performed based on the whole molecule of each surfactant in order to obtain the actual area per molecule (A_2).

Table 3.6 Calculation of actual area per molecule (A_2) for SPAN 80 by VABC method.

Type	Number	Contribution / unit [Å^3]	Total contribution [Å^3]
H	44	7.24	318.56
C	24	20.58	493.92
O	6	14.71	88.26
bonds (N_B)	74	-5.92	-438.08
aromatic rings (R_A)	0	-14.7	0
nonaromatic rings (R_{NR})	1	-3.8	-3.8
		vdW volume	458.86 [Å^3/molec]
		sphere radius	4.784 [Å]
		cross-sectional area (A_2)	71.924 [Å^2/molec]

Table 3.7 Calculation of actual area per molecule (A_2) for PGPR by VABC method.

Type	Number	Contribution / unit [Å^3]	Total contribution [Å^3]
H	115	7.24	832.6
C	63	20.58	1296.54
O	13	14.71	191.23
bonds (N_B)	190	-5.92	-1124.8
aromatic rings (R_A)	0	-14.7	0
nonaromatic rings (R_{NR})	0	-3.8	0
		vdW volume	1195.57 [Å^3/molec]
		sphere radius	6.584 [Å]
		cross-sectional area (A_2)	136.190 [Å^2/molec]

Table 3.8 Calculation of actual area per molecule (A_2) for BRIJ 93 by VABC method.

Type	Number	Contribution / unit [Å^3]	Total contribution [Å^3]
H	44	7.24	318.56
C	22	20.58	452.76
O	3	14.71	44.13
bonds (N_B)	68	-5.92	-402.56
aromatic rings (R_A)	0	-14.7	0
nonaromatic rings (R_{NR})	0	-3.8	0
		vdW volume	412.89 [Å^3/molec]
		sphere radius	4.619 [Å]
		cross-sectional area (A_2)	67.036 [Å^2/molec]

Up to here, all required parameters necessary for simulations have been compiled or calculated. In Appendix B, all the data have been classified together as a cartography summary. This allows a comparison of the components and their respective parameters.

3.4 Objetives of a sensitivity analysis

Sensitivity analysis is the study of how the uncertainty in the output of a mathematical model or system can be apportioned to different sources of uncertainty in its inputs [170]. The process of recalculating outcomes under alternative assumptions to determine the impact of a variable under sensitivity analysis can be useful for a range of purposes [171], including:

1. Testing the robustness of the results of a model or system in the presence of uncertainty.
2. Increased understanding of the relationships between input and output variables in a system or model.
3. Uncertainty reduction, through the identification of model inputs that cause significant uncertainty in the output and should therefore be the focus of attention in order to increase robustness.
4. Searching for errors in the model by encountering unexpected relationships between inputs and outputs.
5. Model simplification – fixing model inputs that have no effect on the output, or identifying and removing redundant parts of the model structure.
6. Finding regions in the space of input factors for which the model output is either maximum or minimum or meets some optimum criterion.
7. In case of calibrating models with large number of parameters, a primary sensitivity test can ease the calibration stage by focusing on the sensitive parameters. Not knowing the sensitivity of parameters can result in time being uselessly spent on non-sensitive ones [172].
8. To seek to identify important connections between observations, model inputs, and predictions or forecasts, leading to the development of better models [173, 174].

Good modeling practice needs that the modeler provides an evaluation of the confidence in the model. This requires an evaluation of how much each input is contributing to the output uncertainty [170]. Sensitivity analysis addresses this issue, performing the role of ordering by importance the strength and relevance of the inputs in determining the variation in the output. In models involving many input variables, as the current being developed in this work, sensitivity analysis is an essential ingredient of model building and quality assurance. There are a large number of approaches to performing a sensitivity analysis [170]. In general, however, most procedures adhere to the following outline:

1. Identify the model output to be analyzed.
2. Quantify the uncertainty in each input.
3. Run the model a number of times using some design of experiments.
4. Using the resulting model outputs, calculate the sensitivity measures of interest.

In some cases this procedure will be repeated, for example in high-dimensional problems where the user has to screen out unimportant variables before performing a full sensitivity analysis.

3.4.1 Preparation of Virtual Design of Experiments (VDOE)

The capabilities of a design of experiments (DOE), provide a method for simultaneously investigating the effects of multiple variables on an output variable (response). These experiments consist of a series of runs, or tests, in which purposeful changes are made to input variables or factors, and data are collected at each run. In this work, by using the ab-initio model , the experiments can be conducted virtually (DOE becomes VDOE), and as a consequence, the model itself and the cartography of materials delimited in this chapter can be qualitatively and quantitatively evaluated.

It is important to recognize that virtual experiments are not the same as live experiments, they are only simulations. However, the cost of doing them is minimal compared with live experiments and the process of identifying input and output variables, decided at which level to test, sistematically reviews the interactions between them, aiming to provide clarity surrounding their roles. In addition, virtual experiments allow a great deal into the context of '*what if?*' analysis, which may stimulate creative thinking [175], and the research question of which one is the best configuration of inputs to get the optimal or desired output can also be examined.

For characterization of the response coming from the ab-initio model, the solver '*lsqcurvefit*' of MATLAB® was employed. This tool solves nonlinear curve-fitting (data-fitting) problems in least-squares sense [176], by using the Levenberg-Marquardt method [177]. Given an input data $xdata$, the observed output $ydata$, where $xdata$ and $ydata$ are vectors, and $F(x,xdata)$ is a vector-valued function of the same size as $ydata$, mathematically, *lsqcurvefit* finds coefficients x that solve the problem:

$$\min_x ||F(x,xdata) - ydata||_2^2 = \min_x \sum_i (F(x,xdata_i) - ydata_i)^2 \tag{3.1}$$

Considering $F(x, xdata_i)$ as the exact analytical solution of Fick's law for monolithic devices and thin slab geometry (Eq. 3.2), x the Fickian diffusion coefficient D, $xdata_i$ the time, and $ydata_i$ the M_t/M_∞ values coming from a virtual experiment, it is possible to fit a simulated release curve in order to obtain a representative D which characterizes the response.

$$\frac{M_t}{M_\infty} = 1 - \frac{8}{\pi^2} \sum_{n=0}^{\infty} \frac{exp[-D(2n+1)^2\pi^2 t/L^2]}{(2n+1)^2} \tag{3.2}$$

However, when using the solver lsqcurvefit one should bear in mind that the Levenberg-Marquardt method possesses a strong dependency of initial guess values in order to find the global minimum and not a local one of the problem. For this purpose, it was decided to clear up possible solution values of Fickian diffusion coefficients using the Eq. 3.2 at n = 0, employing the M_t/M_∞ values coming from a simulated response given by the ab-initio model. In this way, applying the solver *lsqcurvefit* with these possible diffusion coefficient solutions as initial guesses, one can easily obtain the best fitting of the curve by taking the value which provides the minimum residual from Eq. 3.1.

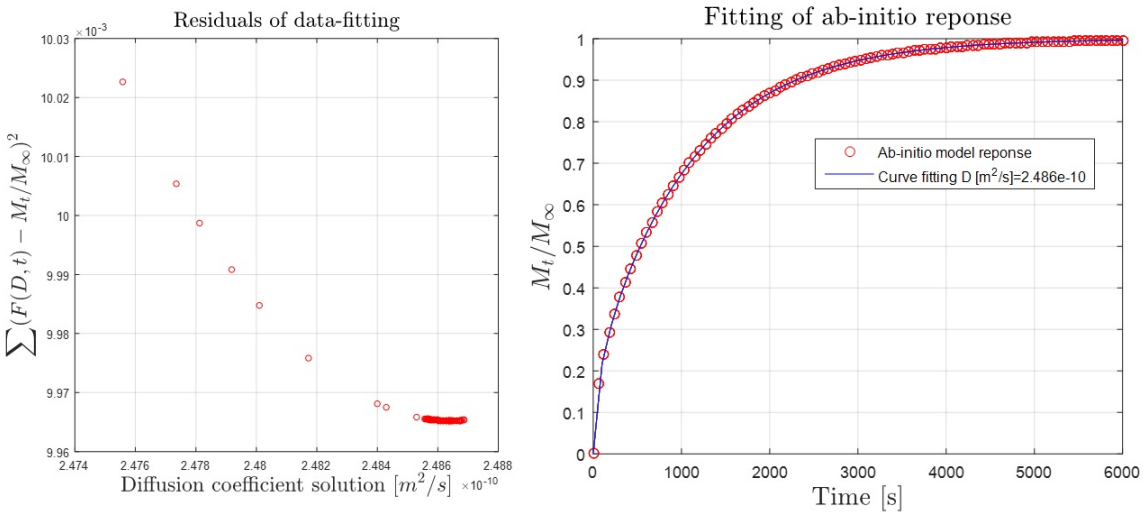

Fig. 3.13 Evolution of residuals from fitting and comparison between response and fitting curve.

By way of illustration, Fig. 3.13 shows an example of the evolution of the residual values in a data fitting. As one can see in the left graph, the fitting residuals decrease as long as the global minimum is found. The last points of possible diffusion coefficient solutions showing the lowest residual are those coming from the final time of the ab-initio model response. In the right graph, one can see the respective response curve and its fitting. Clearly, it can be seen that the fitting tool works quite good. In addition, the time for a case study fitting takes around 3 seconds.

Once the model output to be analyzed has been identified (D), the factors to test (inputs) as well as their levels need to be decided. According to the scheme showed previously in Fig. 3.1, the possible factors to be considered in the VDOE are:

- Concentration of active ingredient,
- Dispersed-phase mass fraction,
- Oil-surfactant ratio,
- Droplet diameter,
- Total mass of emulsion during preparation
- Mass employed for the release experiment,
- Volume of the receptor solution,
- Temperature during release experiment (it is considered that this temperature would be the same as the one of the preparation),
- Type of oil employed,
- Type of surfactant employed.

The design of experiments is about identifying which is the combination of the previous factors that could provide a different release curve. At a glance, some of these factors can be easily dismissed or fixed because they will not affect to the predictions of the ab-initio model or would not be practical for comparison or experimental or purposes:

- For example, the total mass of emulsion during preparation is obvious that would not give a different response whatever the amount prepared. However, this interpretation is not comparable to the mass employed for a release experiment. It is clear that the more amount employed, the more would be the delay on the release curve, but for comparison purposes, changing this variable is not useful, since that even though the curves delayed on time, all of them would give the same diffusion coefficients. For this reason it was suggested to use a basis of one gram as reference.
- On the other hand, the prediction of the ab-initio model is independent of the volume of the receptor solution, since it is considered to be maintaned at a zero constant concentration. Nevertheless, for an upcoming experimental part, it is important to bear in mind that to maintain sink conditions, the concentration of an active ingredient in

the receptor solution should be kept below 10% of its concentration in the delivery vehicle [178]. For verification purposes, change of this variable can be useful.

- Concerning the temperature, a controlled delivery device is generally considered to be designed for a specific working temperature. Therefore, it was suggested to keep it constant as variable. A reference temperature of 25°C was chosen.

After these considerations, the VDOE can be adequately planified taking into account the remaining six factors.

3.4.2 Preliminar analysis of VDOE : 64 case studies

In a two-level full factorial design, each experiment factor has only two levels. The experimental runs include all combinations of these factor levels. Although two-level factorial designs are unable to explore fully a wide region in the factor space, they provide useful information for relatively few runs per factor and can indicate major trends. Thus, it was decided to use a two-level full factorial design as a preliminar analysis to provide direction for a later full factorial design of more levels. Taking into account the six factors, this is equivalent to 2^6 = 64 possible factor combinations. The following low and high levels shown in Table 3.9 were considered for a first preliminar analysis. They were chosen as typical encountered values when preparing highly concentrated emulsions. In the case of type of oil or surfactant, variables of text type, only two representative examples from the cartography were taken.

Table 3.9 Creation of factorial design with 64 combinations. Factor level values.

Factor	Low level	High level
AI concentration [g AI / g H2O]	0.015	0.050
Dipersed-phase mass fraction [adim.]	0.75	0.95
Oil-surfactant ratio [adim.]	1	10
Droplet diameter [m]	0.000005 (5μm)	0.00002 (20μm)
Type of oil	Dodecane	Isopropyl myristate
Type of surfactant	SPAN 80	PGPR

The ensemble of the predicted release curves are shown in Figs. 3.14a. The respective Fickian diffusion coefficients obtained by fitting are represented in Fig. 3.14b. As one can see, different groups of predicted release curves were obtained, with diffusion coefficients ranging from $3.78{\cdot}10^{-11}$ to $5.82{\cdot}10^{-10}$ m^2/s. However, it appeared that some factor combinations almost did not affect to the diffusion coefficient or gave equivalent results.

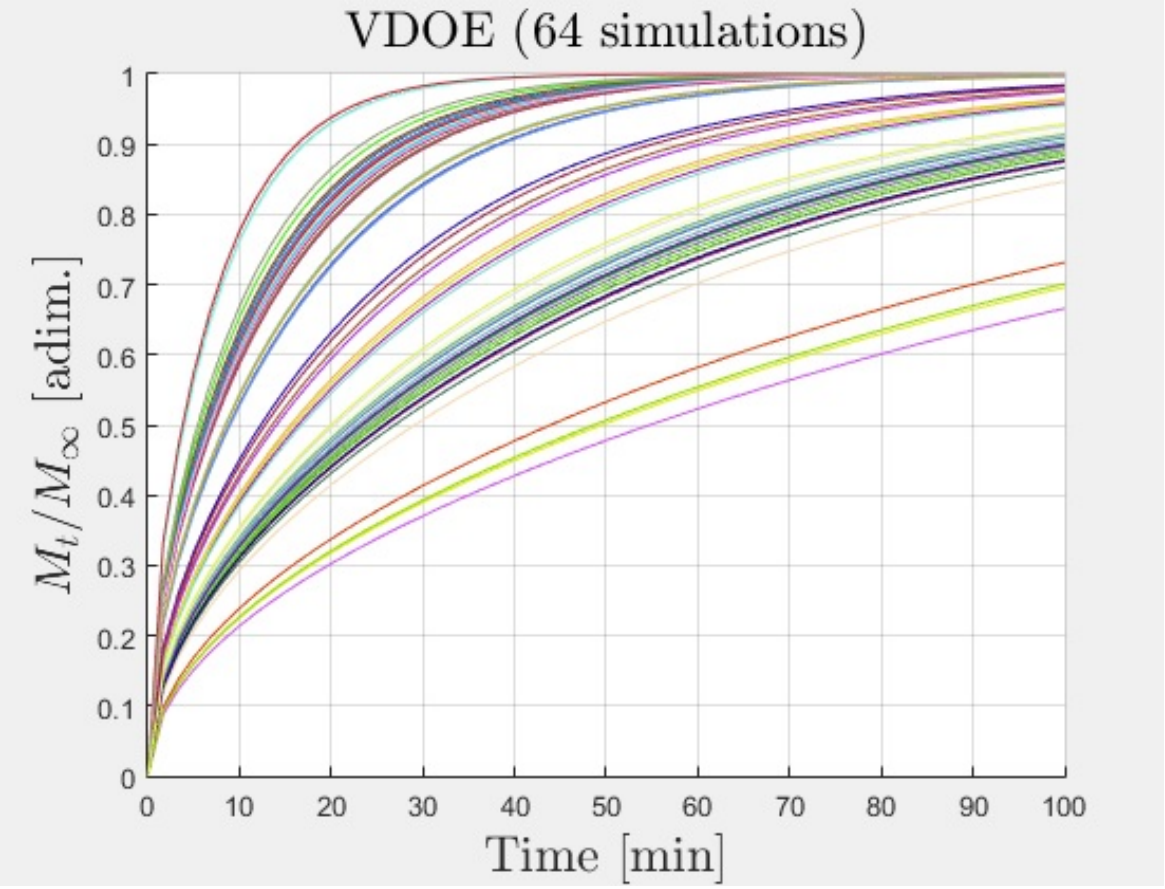

(a) Predicted release curves of two-level full factorial design.

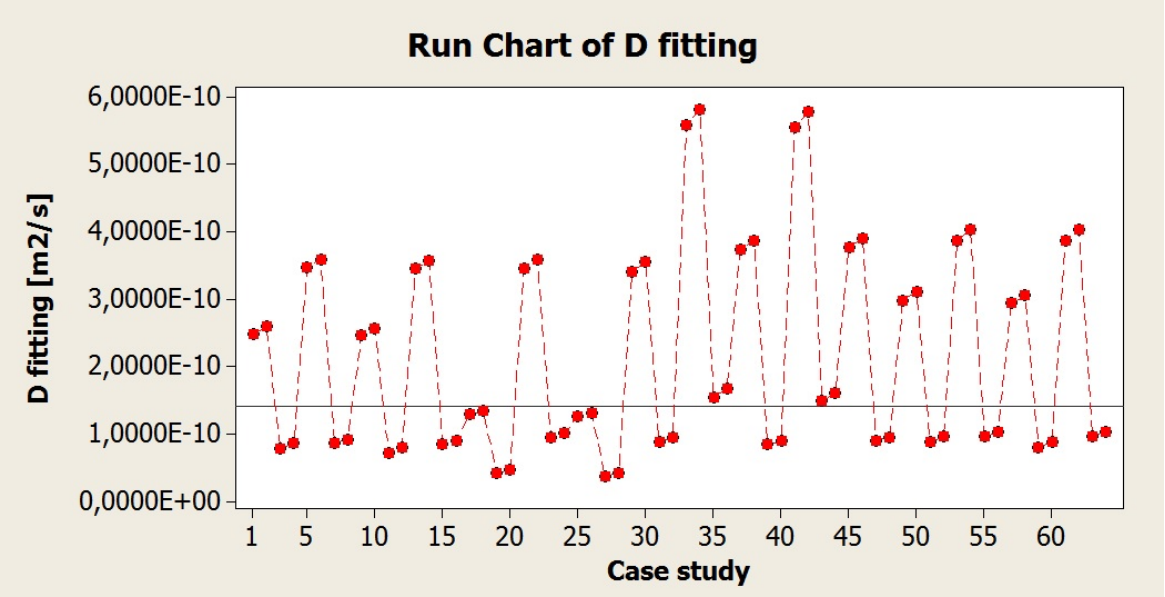

(b) Run chart of diffusion coefficients obtained by curve fitting.

Fig. 3.14 Simulation results from preliminar VDOE analysis (64 factor combinations).

For the purpose of finding the most important variables, a Pareto chart [179] was realized. The Pareto chart allows to look at both the magnitude and the importance of a factor. This chart displays the absolute value of the effects, and draws a reference line on the chart. The reference line is the limit of statistical signification corresponding to $\alpha = 0.05$. Factors on the left side of this line have a small signification, therefore, it is possible to dismiss the "null hypothesis" that they influence the response. Any effect that extends past this reference line is potentially important. Fig. 3.15 shows the Pareto chart for the preliminar 64 case study. Here, the reference line is placed vertically in the graph with an effect value of $9.0658 \cdot 10^{-13}$.

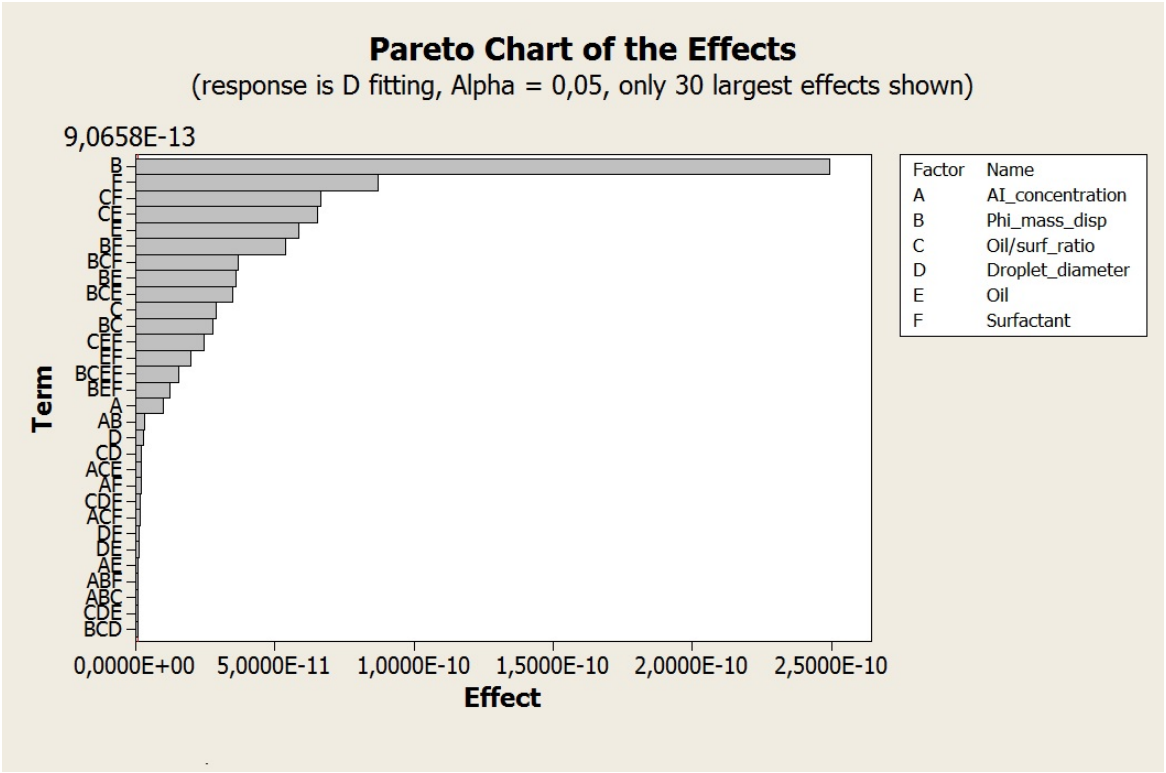

Fig. 3.15 Pareto chart of standardized effects for VDOE of 7 factors and 64 case studies.

As one can see, we have interactions at different levels. The most influencing factor is the dispersed-phase mass fraction (B), showing the highest effect. After this, it is the surfactant choice (F), but playing a much less important rol. Next, the oil-surfactant ratio (C), jointly with F or with the oil choice (E). Later, factor E by itself alone is followed by another combined interaction (BF). From now on, these factors that already showed their importance, are successively repeated until the end of the list but in different combinations. The most striking observation is that only until the sixteenth position, the concentration of active ingredient (A) does not take part, and the droplet diameter (D) occupied the eighteenth position. Thus, here a distinction can be made, the factors leading the list by themselves

alone or jointly with others (B, C, E and F), can be considered as the most important factors which really influence the active ingredient release. In contrast, the last appearing factors (A and D), can be considered as unimportant variables, since they do not influence significantly the response of the model. For this reason, they were dismissed for posterior analysis.

3.4.3 Main effects and interaction plots of VDOE : 300 case studies

After the four most important variables have been found, a more complex sensitivity analysis can be performed. From this point forward, the whole cartography of materials (4 oils and 3 surfactants) was considered. In addition, for further analysis, it was allowed more than two levels of variation per factor. The following Table 3.10 summarizes the inputs and their respective levels employed for a second VODE consisting of 300 simulations. The variables which were known that do not influence significantly the response of the ab-initio model were kept constant for every case study, such as a concentration of 0.015 g AI / g H_2O, or a 5 μm droplet diameter. The temperature was also kept at 298 K.

Table 3.10 Creation of factorial design with 300 combinations. Factor level values.

Factor	Levels
Dipersed-phase mass fraction [adim.]	0.75 / 0.8 / 0.85 / 0.9 / 0.95
Oil-surfactant ratio [adim.]	1 / 2.5 / 5 / 7.5 / 10
Type of oil	Dodecane / Hexadecane / Myristate / Palmitate
Type of surfactant	SPAN 80 / PGPR / BRIJ 93

The simulated release curves, obtained by this VDOE of 300 simulations, are depicted in Fig. 3.16a. Their respective numerical values of diffusion coefficients are shown in Fig. 3.16b. As one can see, a wider spectra was obtained in comparison with the previous one from the preliminar analysis. Apparently, it seemed that it is possible to completely cover a wide region on time by suitable manipulation of the emulsion specifications. The total time for the full simulation of 300 case studies was around 16 minutes and 20 seconds, which is equal to three seconds per case, relatively a very small amount of computational effort.

The main effects as well as the most important interactions between levels and factors of the current VDOE are plotted in Fig. 3.17. It is important to keep in mind, that values shown in these plots are not absolute values, but the mean of the respective Fickean diffusion coefficients obtained by fitting of the curves. However, they can give much information about the major tendencies.

As it is shown in the upper graph 3.17a, the dispersed-phase mass fraction is the factor which influences the most, and in a linear fashion, the value of the Fickian diffusion coefficient D. The more the value of the dispersed-phase mass fraction, the less the fitting diffusion

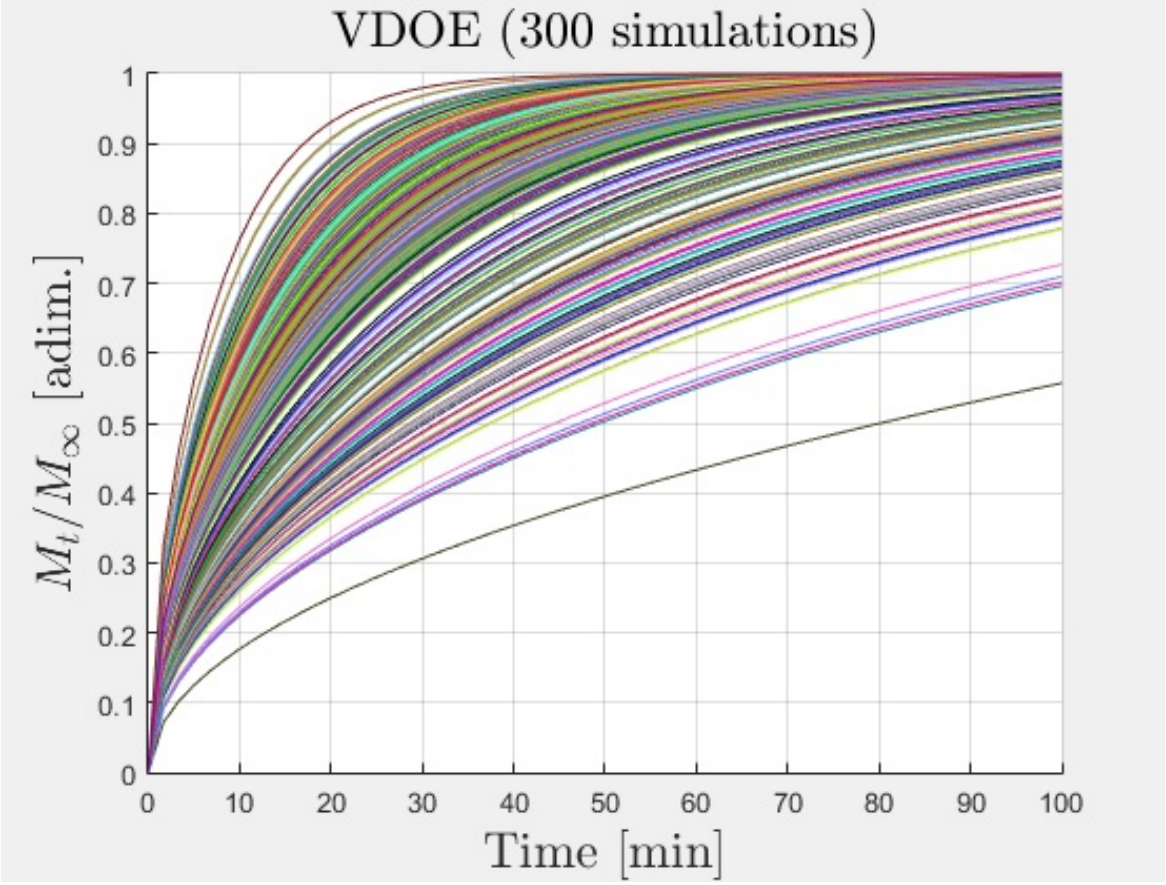

(a) Predicted release curves of two-level full factorial design.

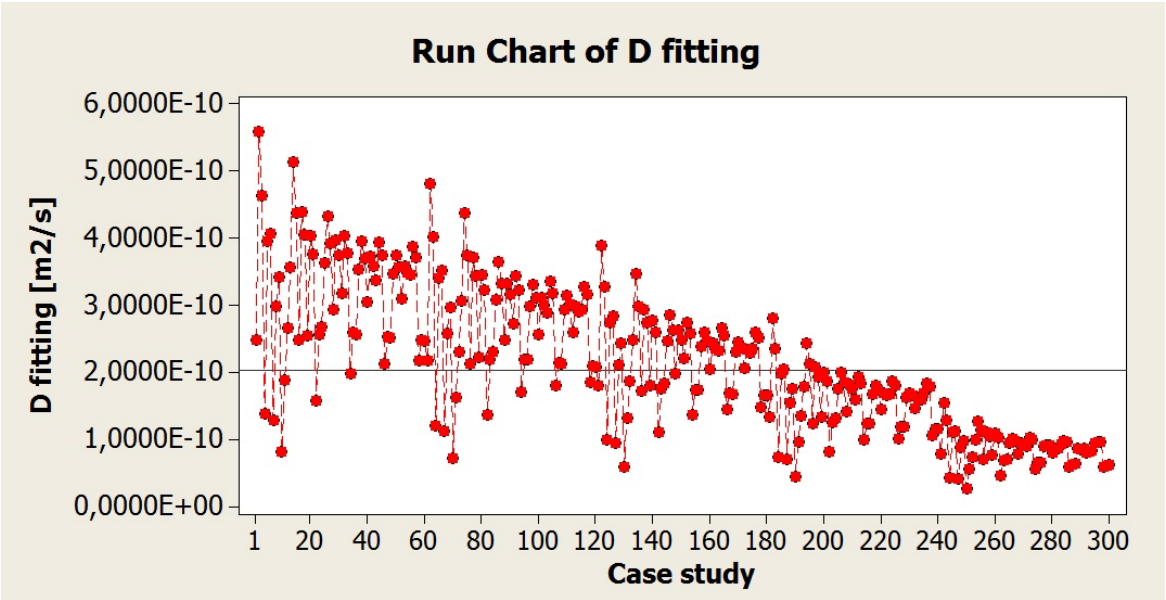

(b) Run chart of diffusion coefficients obtained by curve fitting.

Fig. 3.16 Simulation results for VDOE analysis (300 factor combinations).

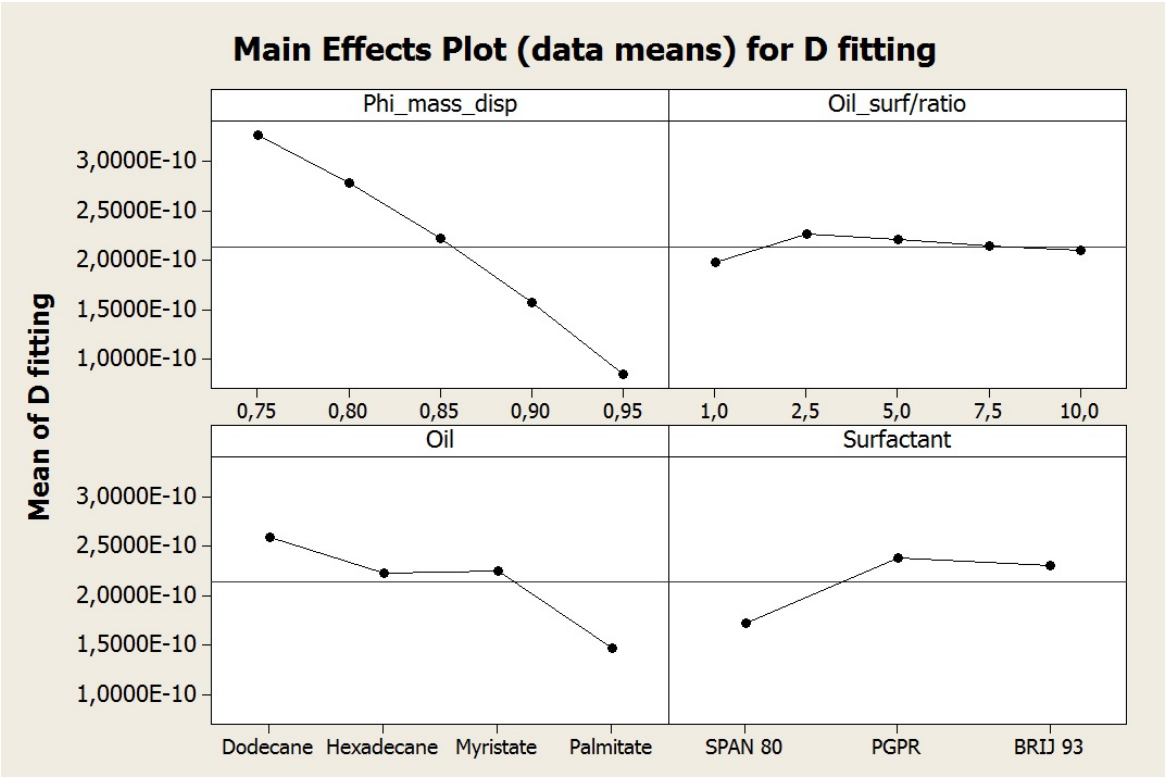

(a) Main effects plot.

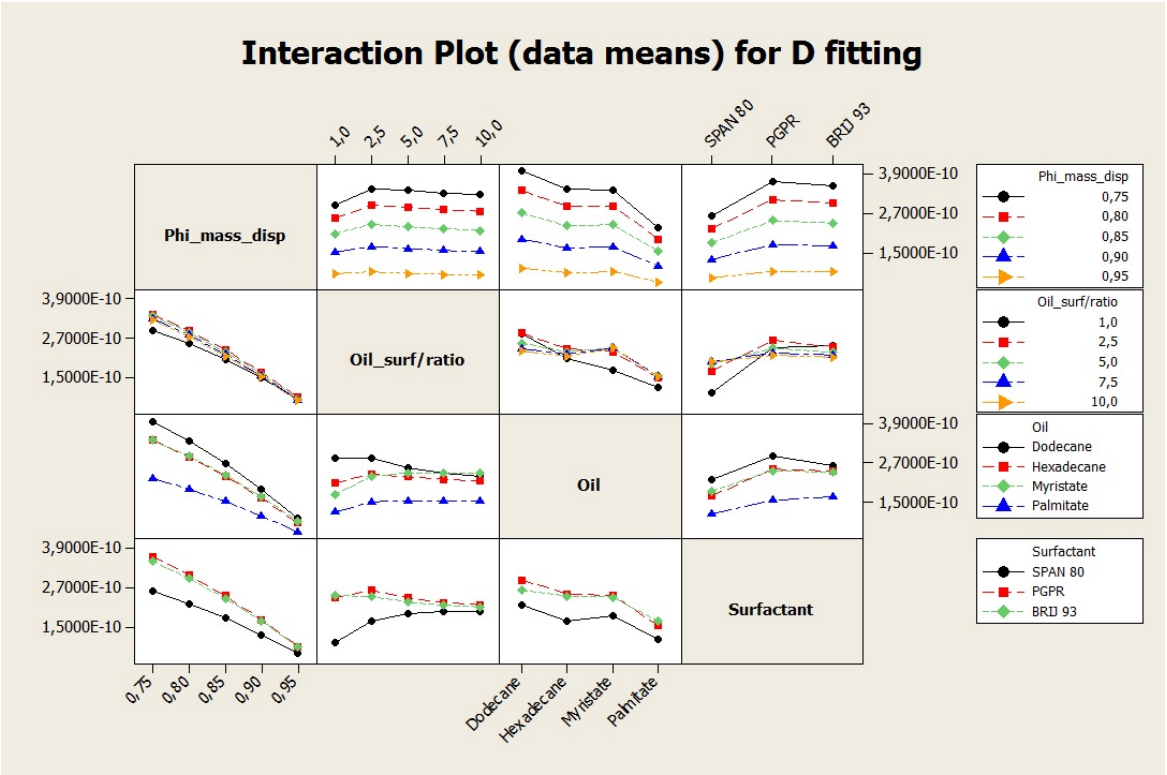

(b) Interaction plot for D fitting.

Fig. 3.17 Simulation results for VDOE analysis of 300 case studies (only the 4 most important factors are shown).

coefficient. The oil choice of hexadecane or isopropyl myristate, apparently, shows a comparable influence. This does not happen when changing from dodecane to isopropyl palmitate. Concerning the surfactant, when the surfactant SPAN 80 is employed, the D values are generally smaller than those obtained when using other surfactants. On the other hand, the oil-surfactant ratio seems like to influence very slightly the diffusion coefficient value, only small variations were observed at the lowest oil surfactant ratios.

The interactions between individual factors are presented in Fig. 3.17b. In this graph, it is possible to see some important aspects, taking into account that the more parallel the lines, the less significative interactions. Here, one can see that the most pronounced interactions of the dispersed-mass fraction are those in relation to the choice of oil or surfactant. The biggest differences are better observed when a low fraction is used. On the contrary, if the dispersed-phase mass fraction employed is relatively high, it appears that there is no significant effect on the diffusion coefficient, whatever surfactant, oil, or ratio between them is chosen. Concerning interactions related to the oil-surfactant ratio, it is interesting to note that only low ratios appear to show a significant effect on the diffusion coefficient D. In contrast, at high ratios, whatever the surfactant or oil is chosen, the effect on the diffusion coefficient is equivalent. Concerning the oil choice, generally the predicted release curves for emulsions using dodecane as oil offer the higher diffusion coefficients.

3.5 Conclusions of sensitivity analysis

All the modeling developed in previous chapter has been assembled as a complete full ab-initio model. A cartography of materials has been implemented and simulations have been performed in order to test the sensitivity of the model.

The sensitivity analysis has given an account of the possible release curves that could be obtained by using the materials composing the cartography and different specifications of a given highly concentrated emulsion formulation. This information can be used to design targetted products aimed at a desired controlled release rate, or to compare different products that could behave in a similar manner. Besides, the ab-initio model developed in this chapter could be considered as a very powerful tool that might help enormously for decision making or intensification-oriented purposes.

However, the possible results to be obtained are limited by the size of the cartography. It is very likely that the materials of the formulation will restrict the release curves aiming to obtain. In addition, future trials should assess the conclusions obtained.

Chapter 4

EXPERIMENTAL VALIDATIONS

'There are three principal means of acquiring knowledge; observation of nature, reflection, and experimentation. Observation collects facts; reflection combines them; experimentation verifies the result of that combination', Denis Diderot

4.1 Introduction

The theory developed in this work for mass transfer in highly concentrated emulsions systems, and the predictions from it must be tested with specific experiments designed to confirm or deny their truth. This is fundamental under the reverse engineering approach of this thesis. As it has been shown in the previous chapter, it is possible to obtain different release curves by using specific combinations of dispersed mass fraction, oil, surfactant and their ratios. The success of the reverse engineering of this work, will depend on the accuracy of these predictions to be considered as hypothetical design solutions depending on formulation variables.

Therefore, this chapter aims to address the following research questions:

- are the predictions by UNIFAC models accurate enough to predict the distribution coefficient of active ingredient between the phases of an emulsion?
- is it possible to predict the viscosity of oil/surfactant mixtures by UNIFAC-VISCO adequately?
- and last and most important, is the ensemble of all the modeling and simulation tools accurate enough to trust in the ab-initio model as serviceable tool for product design?

4.2 Predicted and experimental distribution coefficients

As it was seen in the modeling chapter, it is essential to evaluate and understand the partition of active ingredient in both phases. Since the active ingredient employed in this work absorbs in the UV region when solubilized in water, UV-visible spectroscopy is presented as one of the most practical techniques for determining its concentration. The interested reader may consult the Appendix C, which provides complete details about the experimental work performed. Here, only the most important results and conclusions from the tests will be presented concerning the following subjects: comparison of predictions performed by UNIFAC methods, effect of content of salt on predictions, influence of blank/dilution media, and detection limits of the technique.

4.2.1 Comparison of UNIFAC methods

A preliminar study to determine the effect of the surfactant, water, oil, active ingredient and salt amounts on the distribution coefficient was carried out. For this purpose, the system: MA + SPAN 80 + Dodecane + Water was used as a reference. Generally, they were composed by amounts and proportions imitating highly concentrated emulsions. For this reason, from now on, the aqueous phase will be named dispersed phase and the organic phase continuous phase. In Fig. 4.1 the predictions for equilibrium concentrations in the dispersed phase, as well as the distribution coefficients given by the three UNIFAC methods previously reviewed in section 2.4, are shown and compared with the experimental results:

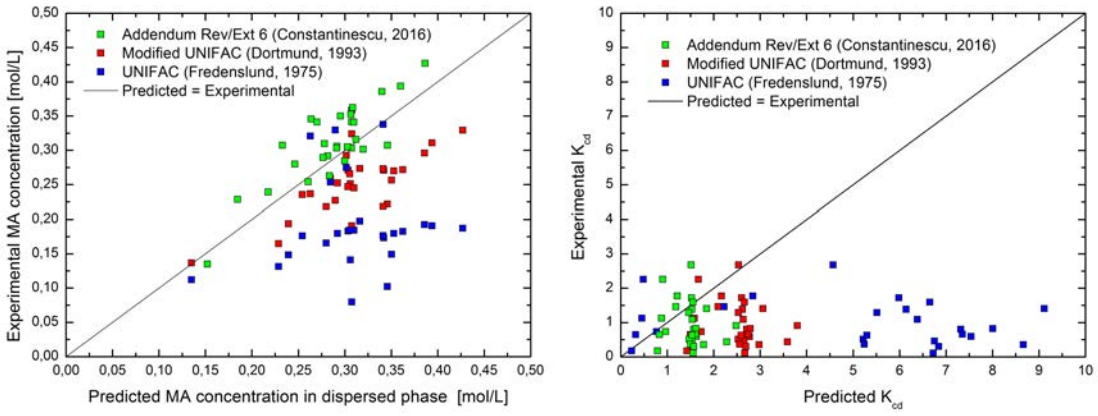

(a) (b)

Fig. 4.1 a) Predicted versus experimental concentrations in dispersed phase. b) Experimental versus predicted distribution coefficients. Samples characteristics and relative errors between predicted and experimental distribution coefficients are detailed in Table C.1 of Appendix C.0.2.

As one can see in Fig. 4.1, when using UNIFAC (Fredenslund) model, predictions were farther from experimental values. Next, in Fig. 4.2 the experimental and predicted concentrations per sample are shown. Overall, the best precision was obtained when using Modified UNIFAC models, more specifically when using the Addendum Rev/Ext 6 of Contastinescu (2016). The factors which may explain the relatively good correlation between the predicted and experimentally determined concentrations/distribution coefficients when using Modified UNIFAC are the following:

- The thermodynamic mixture data stored in the group interaction parameters of UNIFAC are mostly coming from vapor-liquid equilibrium data and not from liquid-liquid. Generally, there is an improvement for liquid-liquid equilibrium data sets when passing from UNIFAC to Modified UNIFAC. On the other hand, as it was previously seen in section 2.4.2, the combinatorial part of UNIFAC (Fredenslund) is not modified empirically to deal with compunds very different in size as it was done for the later Modified UNIFAC versions.
- In addition, the temperature dependent parameters a_{nm}, b_{nm}, and c_{nm} from the binary parameter matrix of Modified UNIFAC, allows a better description of the miscibility gap. The more updated version, the better the accuracy.

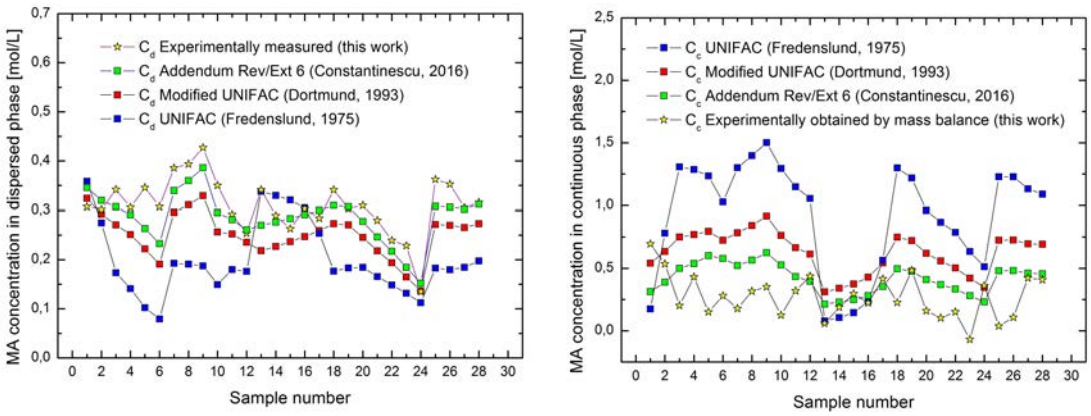

(a) (b)

Fig. 4.2 Predicted versus experimental concentrations in dispersed phase (a); and in continuous phase (b). Samples characteristics are detailed in Table C.1 of Appendix C.0.2.

It should be mentioned that the mole amounts of active ingredient in the continuous phase were worked out by mass balance of the initial weighted mass amounts. For the calculation of concentration in the continuous phase, it was considered a total continuous phase volume (volume of oil + volume of surfactant) same as the one at the moment of sample preparation.

Some important conclusions were drawn from the present study:

- The combination of results provided some support for the conceptual premise that the Modified UNIFAC method of Contastinescu (2016) is the most suitable for predicting the distribution coefficients from the three methods studied because of the better precisions obtained. For this reason, it was chosen as the UNIFAC method employed for the following experiments and later simulations.

- Generally, it was found that in samples with a less amount of surfactant, the precision obtained between experimental and predicted values was much better. This result might be related to the interference observed during the preparation of the calibration curves (See Appendix C.0.1). It is likely possible that microdroplets or microaggregates of surfactant could be transferred to the dispersed phase, in such a way that the UV-lecture could be misleading. For this reason, it was decided a new experiment in the next section contrasting the importance of employing a stock solution as blank instead of pure water.

- On the other hand, it is important to keep in mind that for all samples, a three-phase system was observed. The dispersed and continuous phases were separated by a cloudy film showing different thicknesses depending on the sample. This film, composed by surfactant in its largest part, normally assures a double role of separating agent as well as compatabilizer between the aqueous and organic domains [180]. This is not taken into account during the predictions, since only a two-phase system is considered. Therefore, this seems to be an important limitation for this experiment and source of errors; any UV-absorbance lecture of the aqueous phase could disregard analyte present within this third layer. In addition, the presence of this film could '*disturb*' compositions of equilibrium.

- Additionally, it appeared that an increase of the amount of salt improved the correlation between predicted and experimentally determined results. In fact, the films observed in samples with salt were much more narrow than those from samples without salt. Therefore, one could interpret that samples showing a less proportion of this third phase, would give a smaller margin of error. Attemps to improve quality of results were decided to be performed in the next experiment considering the reduction on the film appearing between phases by adding salt to all samples.

4.2.2 Effect of salt content and blank/dilution media.

Following conclusions from previous section, a second experiment was performed. The main goal here was to investigate the effect of adding a 2% NaCl content to the dispersed phase. This salt concentration is typically used in commercial emulsions for improving stability, nevertheless, it should be kept in mind that, a priori, the UNIFAC method employed to predict the distribution coefficients does not take into account the presence of salts. However, compensatory effects could be expected minimizing the experimental error when used.

Briefly, three orders of magnitude in the initial concentration of mandelic acid as well as three oil/surfactant ratios were evaluated. The UV lecture was also perfomed by duplicate considering pure water or stock solution as blank and as dilution media for the measurements. These respective stock solutions were prepared specifically for each range of samples; they were taken from the aqueous phase of a tube test prepared without mandelic acid, in contact with a organic phase composed by identical amounts of oil and surfactant than the sample. All sampling was done by puncture with a syringe of the bottom part of the tubes.

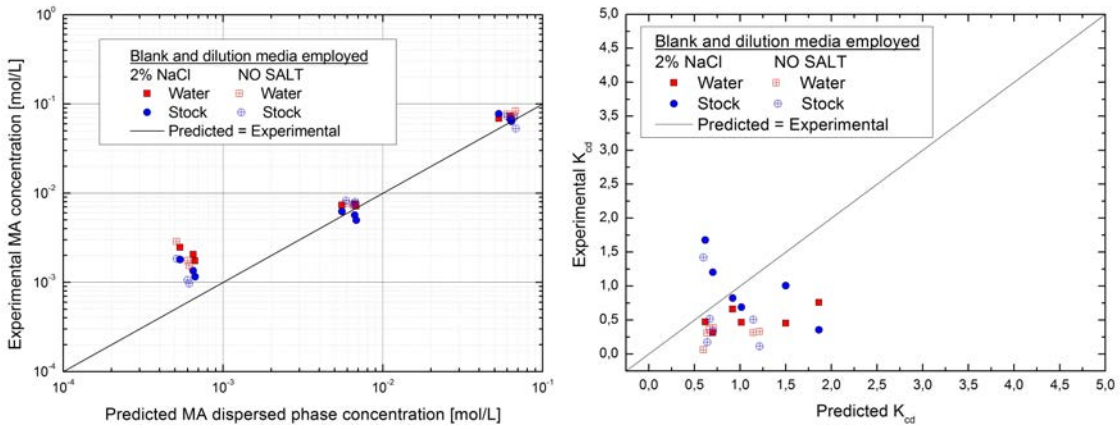

(a) (b)

Fig. 4.3 a) Predicted versus experimental concentrations in dispersed phase. b) Experimental versus predicted distribution coefficients. The reader can consult samples data in Table C.2 of Appendix C.0.3.

Once again, the effects of adding salt were observed; samples without salt showed a film between organic and aqueous phases much thicker than those prepared with salt. The reader is invited to see photos of samples in Appendix C.0.3. The predicted and experimentally determined concentrations and distribution coefficients are shown in Fig. 4.3. It was noted that samples with the lowest concentration of mandelic acid showed an absorbance signal even higher than the corresponding to the initial concentration. This lacks of physical sense, and once again, it seems possible that these results are due to a misleading UV lecture, likely

because of interferences caused by surfactant or oil molecules that were transferred to the dispersed phase (different of the analyte of interest). As a consequence of this limitation, since that samples 1, 2 and 3 yield a negative mass balance when calculating the amount present in the continuous phase of samples, they might be excluded for some of the next calculations and figures. Concerning the distribution coefficients, no appreciable differences were observed in relation to the deviations obtained from previous experiments.

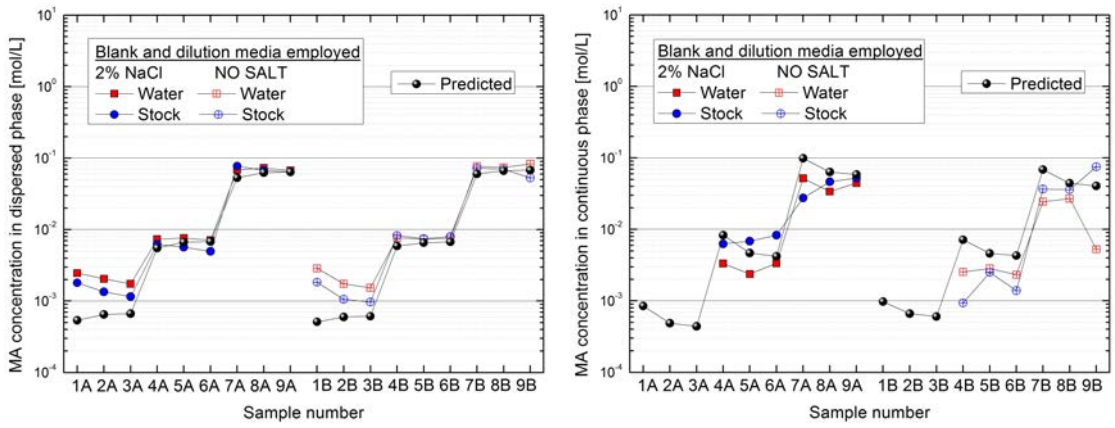

(a) (b)

Fig. 4.4 Predicted versus experimental concentrations in dispersed phase (a); in continuous phase (b). Characteristics of samples are summarized in Table C.2 of Appendix C.0.3.

Fig. 4.4 shows the concentrations of different phases per sample. For sake of clarity, sample letter A refers to a 2% NaCl aqueous solution employed as dispersed phase, and the letter B will refer to a sample prepared without salt. The oil/surfactant mass ratio depends on the sample number: for example, samples with numbers 1, 4 and 7 (low ratio group, r≈1); 2, 5 and 8 (median ratio group, r≈7); and 3, 6 and 9 (high ratio group, r≈15). Concerning the concentration, an initial molarity M≈0.0008 was used for samples 1, 2, 3; M≈0.008 for 4,5,6; and 0.08 M for 7, 8 and 9.

Apparently, no great improvements on the measurements were obtained when employing water or stock solution as blank and dilution media for the samples. As with previous experiment, it appears that the higher the ratio oil/surfactant, the better the correlation between predicted and experimentally determined concentration/distribution coefficients in the dispersed phases. This fact can be better verified in Table C.2 of Appendix C.0.3 where relative errors regarding distribution coefficients were calculated and are shown.

Overall, the experimental data were rather controversial. One would expect a much better improvement when adding salt since the observed film was much narrow, however, the results reflected that the technique might not be still sensible enough. It was noticed that

interference here could not be so easily resolved as it was managed during the preparation of calibration curves (see Appendix C.0.1) by using stock solutions as blank or dilution media. It is important to note that stock solutions employed during the preparation of the calibration curves were prepared using a separation funnel with higher area between organic-aqueous phases (4 cm diameter), and in the present test, stock solutions were prepared in tubes with smaller area (1 cm diameter). It appears that this leads to different equilibria amounts of surfactant remaining the continuous phase, as well as in the aqueous phase employed for the blank or dilution media, which could interfer significantly on the absorbance signal.

Nevertheless, the results of the present study were significant in at least three major respects; a 2% NaCl content appears to not affect to a great extent to the UNIFAC predictions, it is rather suggested to use a water solution as blank/dilution media for the measurements, since the relative errors on the distribution coefficients were slightly smaller, and the concentration of mandelic acid should be high enough to be within the detection limits of the technique, in order to avoid, as much as possible, interference effects.

4.2.3 Effect of material of the cartography and dispersed phase volume

A last experiment was carried out but considering now the whole cartography. The initial concentration of the mandelic acid solution for all samples was around 0.102 M with a 2% NaCl content. Dispersed phase volumetric fractions used here were around 0.7, 0.45 and 0.25. Dilutions prior UV-lecture were perfomed (1/15) with water ionized (2% NaCl concentration). This dilution media was also used as blank for the measurements.

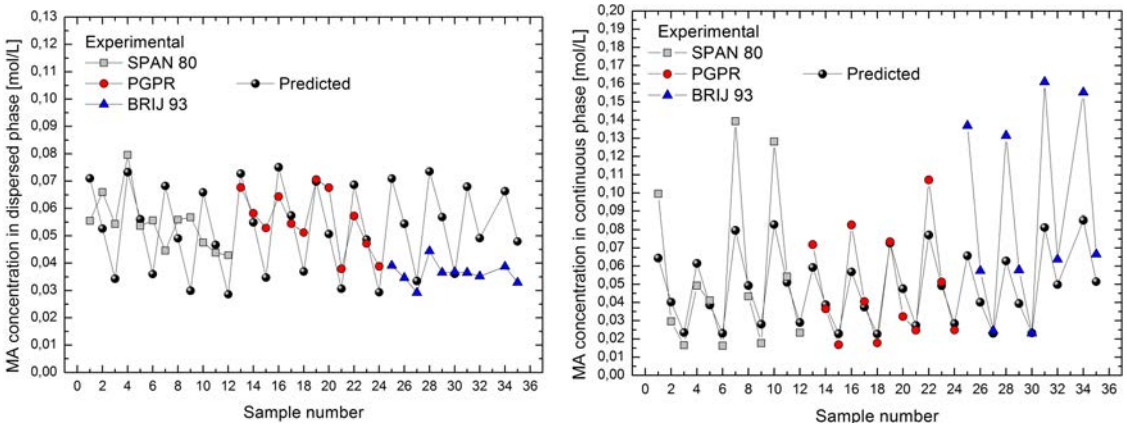

(a) (b)

Fig. 4.5 Predicted versus experimental concentrations in dispersed phase (a); in continuous phase (b). Characteristics of samples are detailed in Table C.3 of Appendix C.0.4.

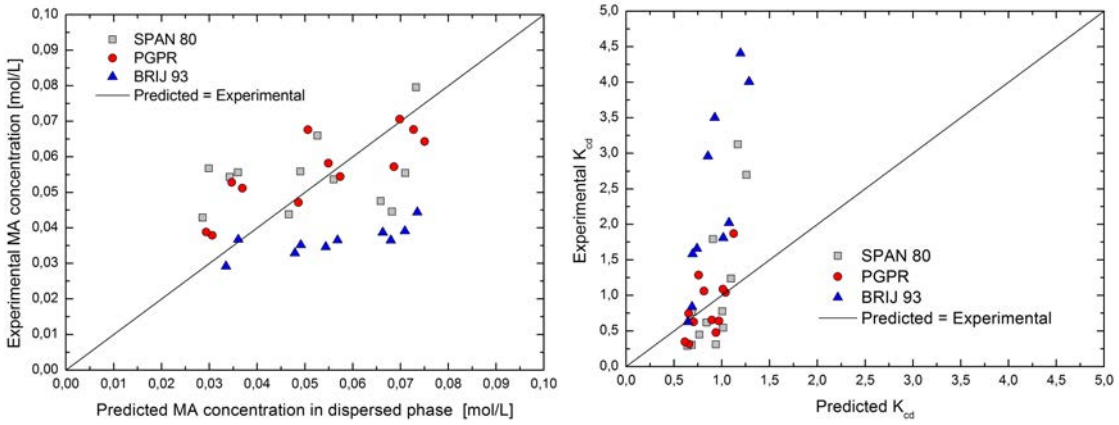

(a) (b)

Fig. 4.6 a) Predicted versus experimental concentrations in dispersed phase of samples. b) Experimental versus predicted distribution coefficients. Characteristics of samples are detailed in Table C.3 of Appendix C.0.4.

The results of predictions employing the database of Modified UNIFAC (Constantinescu) are compared in Figs. 4.5 and 4.6. The highest deviations were observed for samples containing BRIJ 93 and ester oils. One unanticipated finding was that in samples 33 and 36, the dispersed phases at the bottom of the samples showed a cloudy turbidity. It is important to mention that it was not possible to measure their concentrations due to strong interferences on the absorbance signal. For this reason, they were not included in the graphs and calculations. It is difficult to explain this observation, but it might be related to the much greater amount of oil in relation to the amount of dispersed phase present in the samples (in this test, samples with the highest oil/surfactant ratios were composed by a $\phi_v \approx 0.25$). Studies from the literature [181] suggest that in this kind of scenarios, it is eventually possible that molecules of oil could be taken up by incipient or '*budding*' micelles of surfactant belonging to the film observed between the phases. Even if this would happen at small scale, this can increase the aqueous oil solubility enough, affecting somewhat the turbidity of the dispersed phase analyzed. This explanation could justify the higher deviations observed when the oil/surfactant ratio was increased (contrary to previous experiences). The developed turbidy affects the results as an interference in the UV-absorbance signal.

The relative errors on distribution coefficients are shown in Table C.0.4 of Appendix C.0.4. Overall, comparing results, samples prepared with BRIJ93 where those which generally showed the highest deviations between experiments and predictions. As one can see, many complex phenomena and contradictory results appear to take part using this technique for the determination of distribution coefficients. Because of all the current adverse phenomena, it results very complicated to decrease the experimental error and to obtain accurate results.

4.2.4 Conclusions

Different equilibrium tests were prepared in order to check the predictions given by three UNIFAC methods for the distribution coefficient of mandelic acid between different organic and aqueous phases. The main limitations noted during the tests, as well as conclusions obtained were the following:

- The main source of weakness which could have affected the deviations on the predictions was the presence of a third phase. It is possible that a portion of the substance of interest, settled in this layer ,would have not been taken into account during the determination of concentration by UV spectrometry. Additionally, this phase can likely '*disturb*' the equilibria, and the UNIFAC methods utilized for predictions only consider a two-phase system.

- Attempts to reduce the third layer observed were performed by adding salt, but results appear to not improve significantly. Nevertheless, in spite of the experimental errors for determining the real concentration of samples in equilibrium, it could be conceivably hypothesized that in a real emulsion and since that the interfacial developed would be much greater, predictions by means of UNIFAC method would behave in an acceptable level, since the third phase observed would not exist.

- On the other hand, it is possible that microdroplets or microaggreates solubilized in the dispersed phase could have affected the measurements with experimental errors. Even though efforts were done to improve quality on results by using stock solutions as blank or dilution media for the samples, which could hypothetically eliminate this effect, no great improvements were obtained.

- All experimental studies reflected the difficulty to measure the real distribution coefficient in the emulsion-like samples by UV-spectrometry. Even so, the results confirmed that the best method with less deviation on the predictions was the Modified UNIFAC (Contastinescu, 2016) versus UNIFAC (Fredenslund, 1975) and Modified UNIFAC (Dortmund, 1993) models.

4.3 Predicted and experimental mixture viscosities

An experimental study was carried out in order to verify the predictions of viscosity performed by UNIFAC-VISCO method. As it was seen in the modeling chapter, the viscosity value is fundamental for the diffusivity calculation by means of the Wilke Chang equation.

For this purpose, oil/surfactant mixture samples composed by the components of the cartography were prepared. Their respective experimental mass ratios were calculated by simple weighting. The samples were allowed to come to equilibrium during 24h inside of closed containers left over a laboratory vibrator plate. After this, the mixture viscosities were measured in a controlled strain rheometer (ARES) equipped with a parallel plate geometry of rough steel surfaces of 25 mm diameter. Measurements were performed at 25°C by duplicate with a shear rate ranging from 50 to 500 s^{-1}. All samples showed newtonian behavior along the whole interval studied, therefore, an average from the points was taken for each sample. Results of experimental measurements and comparison with predictions performed by UNIFAC-VISCO method are shown in Fig. 4.7.

As one can see in the graphs, for all systems, a decrease on the viscosity with the increase of the oil/surfactant ratio was observed. An asymptotic value at high ratios was found for each case, corresponding to approximately the pure viscosity value of the respective oil composing the mixture. On the contrary, at small ratios, differences between viscosites of mixtures were obtained. Generally, at a given ratio, PGPR systems showed higher values, followed by SPAN 80 systems and at last, BRIJ 93 systems. It is important to bear in mind that the surfactant pure viscosities are ordered in the same manner. The differences on viscosity as the oil/surfactant ratio decreases are due to the conformational changes and solvation of molecules in the mixture.

Concerning the predictions, the most significative differences in relation to the experimental values were found for PGPR + oil systems, where values were found even 10 times higher at small oil/surfactant ratios whatever the oil combination. This behavior was not observed for the other systems. It is important to keep in mind, that UNIFAC-VISCO is a molecular-based model, taking in consideration only the functional groups conforming the molecules. The predicted viscosities are related only to a microscopic level, and possible assembly between surfactant molecules, such as micelles (macroscopic level), are not covered by this model. Therefore, it is likely possible that the divergence between experimental and predicted mixture viscosities could reveal these kind of phenomena occuring on this mixture.

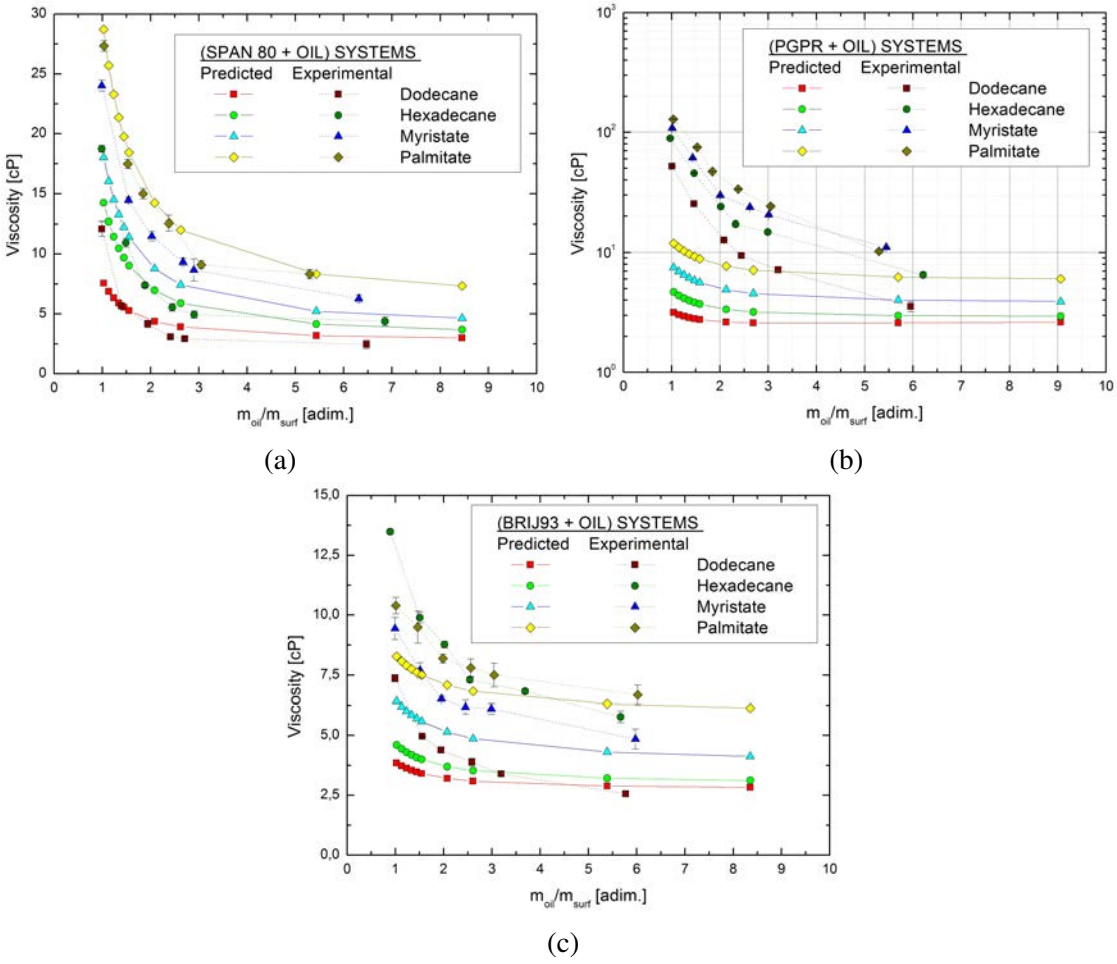

Fig. 4.7 Comparison of experimental viscosities of oil/surfactant mixtures at different mass ratios with predictions by UNIFAC-VISCO method. a) SPAN 80 systems. b) PGPR systems. c) BRIJ 93 systems.

4.3.1 Conclusions

In this study, the viscosity of surfactant and oil mixtures was determined using the group contribution method UNIFAC-VISCO. The viscosity results were compared with the experimental data. Overall, UNIFAC-VISCO method appeared to yield estimations with good agreement between predicted and experimental viscosities, with the exception of PGPR systems. In all other cases, low deviations were obtained, except cases of oil/surfactant ratios close to the unity. Regarding the results obtained with PGPR, it was found that, as the concentration of surfactant increases, the deviation of the experimentally measured viscosity of the mixture also increases, but sharply. One of the issues emerging from this finding could relate specifically to a possible macroscopic interaction between surfactant molecules, which is not considered by the molecular descriptor UNIFAC-VISCO.

4.4 Predicted and experimental release experiments

In this last experimental study, the objective was to determine if the ensemble of all modeling and simulation tools developed in this work could be employed as a reliable ab-initio model for prediction of the active ingredient release from highly concentrated emulsions. Under a reverse engineering approach, it is essential to assure that predictions correspond to reality.

4.4.1 Preparation and characterization of emulsions

All emulsions were prepared using the same equipment/procedure described in the article presented in section 2.1.1 for preparing O/W emulsions. However, the work was focused on W/O systems. This choice was justified because for the monitoring of the release of active ingredient from highly concentrated emulsions, it is generally more convenient to employ hydrophilic molecules, since they can be more easily quantified by UV-spectrometry when released into a water medium that a lipophilic molecule into an oil medium.

Fig. 4.8 Picture of the pilot plant employed for the controlled release experiments.

Therefore, experimental validations for release of active ingredient from the W/O highly concentrated emulsions systems were decided to be performed. Emulsions using all materials from the cartography were prepared at three dispersed phase mass fractions (0.9; 0.925 and 0.95) and three different oil/surfactant ratios (1; 2.5 and 5). A fixed concentration of 1.5% of mandelic acid was employed for all experiences. The reason to select these parameters was justified in advance by means of the virtual design of experiments (VDOE) performed (section 3.4.3), in order to obtain significative differences concerning release profiles. This involved doing more than 100 experiments. However, it should be mentioned that certain emulsions showed a remarkable instability (phase separation) right after the preparation. These emulsions were generally those using myristate and palmitate as oils at the highest dispersed phase mass fractions, independently of the surfactant employed. Due to this, they were excluded in the following series of experimental trials.

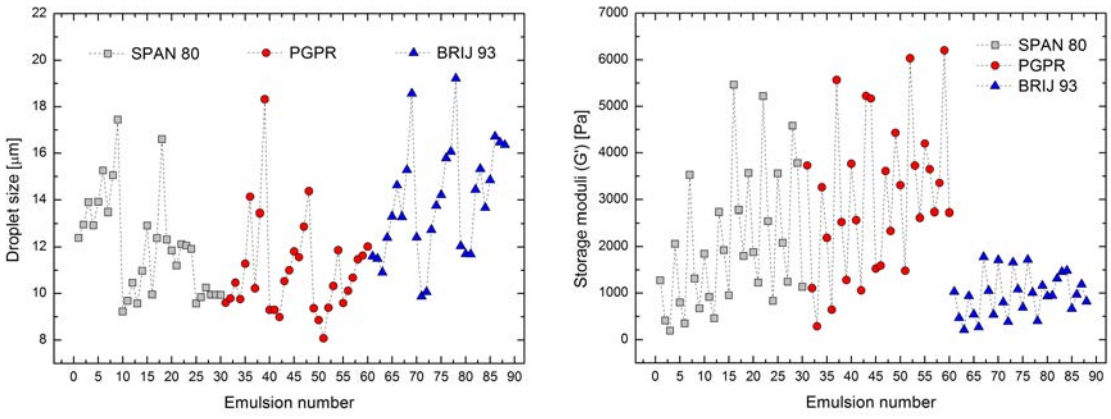

(a) (b)

Fig. 4.9 Droplet size (a) and storage moduli (G') of emulsions for release experiments.

Two main tests were performed together with the release experiments in order to characterize specific parameters of the emulsions produced:

- Firstly, the mean droplet size was determined by a technique reported in the literature [182]. The methodology, based on the coupling between the analysis of incoherent polarized steady light transport (AIPSLT) in the emulsion and a geometrical model accounting for the polyhedral arrangement of the droplets, resulted very interested for this work, since dilution steps are avoided, which could likely induce structural changes in the emulsion, and consequently, modification of the emulsion. Measurements were carried out before the release experiments. Fig. 4.9a shows the results of the measurements. The reader is referred to the Appendix C.0.5 for a more complete detail. Droplet diameters ranged from 8 to 19 μm for the whole ensemble of emulsions. For a given oil-surfactant system, generally, the maximum variation observed on the droplet size when changing the dispersed phase mass fraction or the oil/surfactant ratio was about 5 μm.

- Secondly, a rheological characterization, in the same way that was done in the article for O/W emulsions (section 2.1.1), was performed before and after the release experiment. As it was mentioned in the mass transfer model conception, our approach consider that all parameters of the emulsion remain constant during the release, therefore, the change on the storage moduli (G') becomes an excellent indicator to verify this fact. The results of the measurements are shown in Fig. 4.9b. At a given dispersed phase mass fraction, the less the oil/surfactant ratio, the less the value of the storage moduli. Emulsions prepared with BRIJ 93 showed values generally lower than the others.

4.4.2 Experimental tests of controlled release

The experimental set-up (Fig. 4.10) for the controlled release of active ingredient from emulsions consisted of a simple diffusion cell composed by a cylindrical jacketed glass vessel (75 mm diameter x 160 mm height), which acts as chamber for the receptor solution, a teflon piece for containing the emulsion sample, a magnetic stirrer to provide a perfect mixing into the whole chamber space, and a sensor, which connected to the UV-spectrometer and immersed in the receptor solution, allows the monitoring of the concentration of the receptor solution. The temperature of the jacketed vessel was controlled at 25°C. The teflon container, specifically designed for this work, fits in the vessel and it is placed on the bottom part. Its drawing can be visualized in the Appendix C.0.5. Basically, it is composed by two pieces, the first one with a void to put the emulsion, and a second one which acts as carcase. They join together by means of a thread mechanism. The upper part (carcase) possesses different holes which allow the pass of the liquid confined in the interior of the bottom part piece. A triangular shaped magnetic stirrer was placed over the carcase in order to provide movement enough for a perfect mixing in the whole receptor solution, without disturbing the emulsion.

Fig. 4.10 Picture of the pilot plant employed for the controlled release experiments.

For the release experiments, it was used a teflon disc of a 4cm diameter and 4 mm height, which fits into the inner void of the teflon container. Emulsion sample filled the remaining space between the disc and the ending part of the void (giving approximately a 1mm thickness of emulsion and a mass around 1 g). The weighted mass amount of emulsion was noted and utilized as input for the simulations. A 100 mL volume of a 2% NaCl receptor solution was used in the chamber and as blank for UV-measurements. These were performed once every minute. The determined absorbances were converted to absolute percentage released considering the constant absorbance signal at the end of the experience. In the following pages (Figs. 4.11, 4.12 and 4.12) the predicted and experimental release profiles are presented.

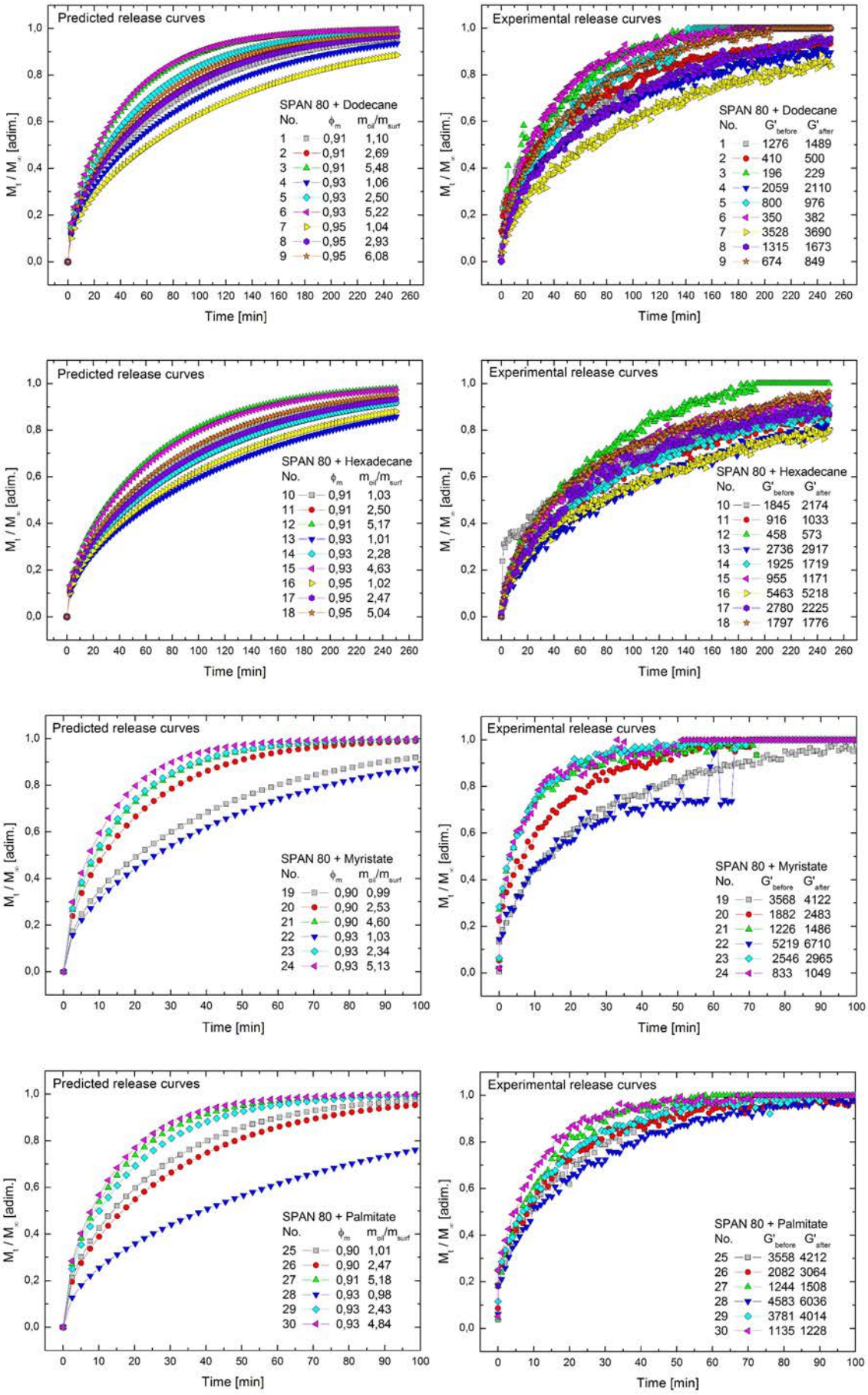

Fig. 4.11 Predicted and experimental release curves for system: SPAN 80 + Oil.

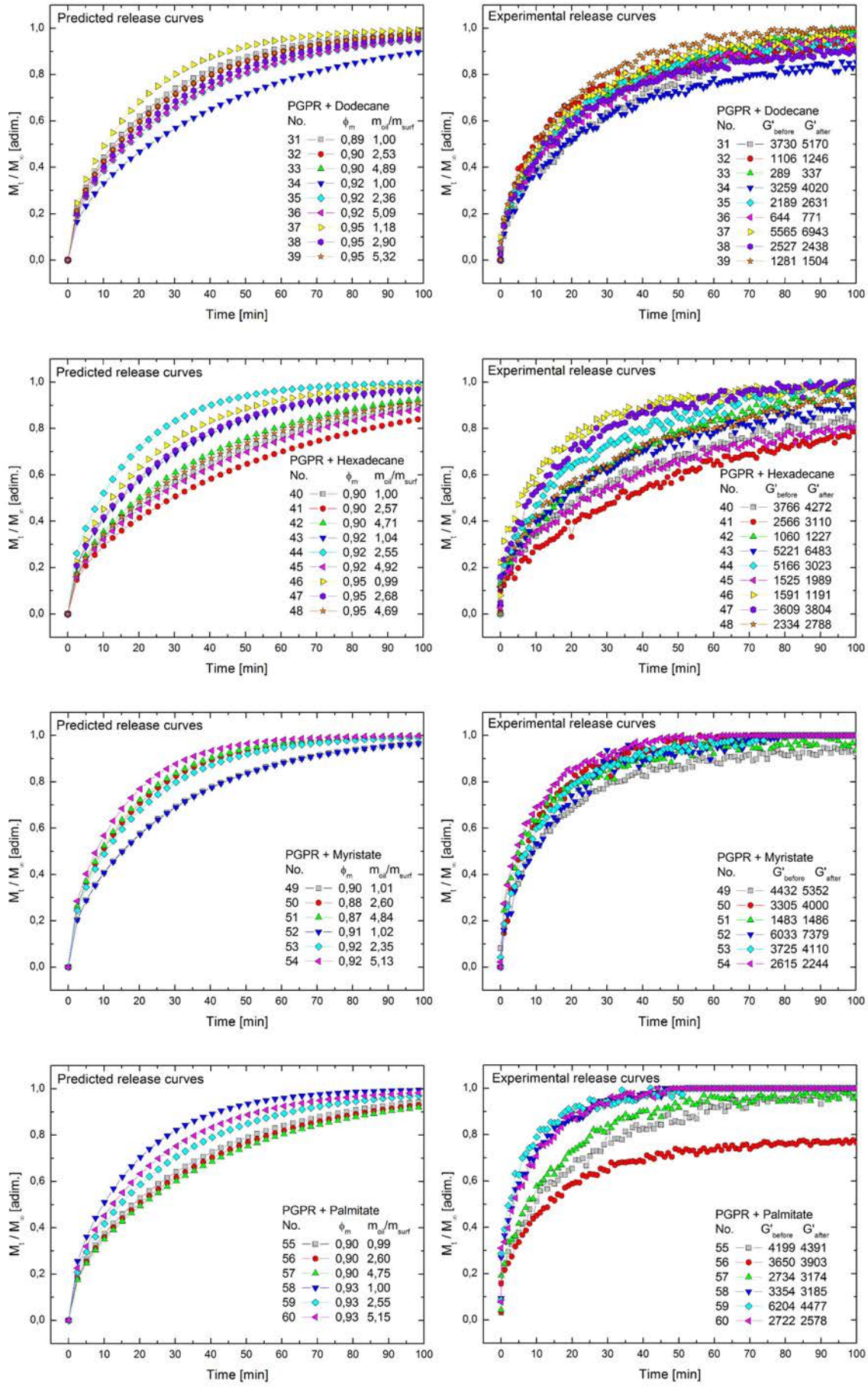

Fig. 4.12 Predicted and experimental release curves for system: PGPR + Oil.

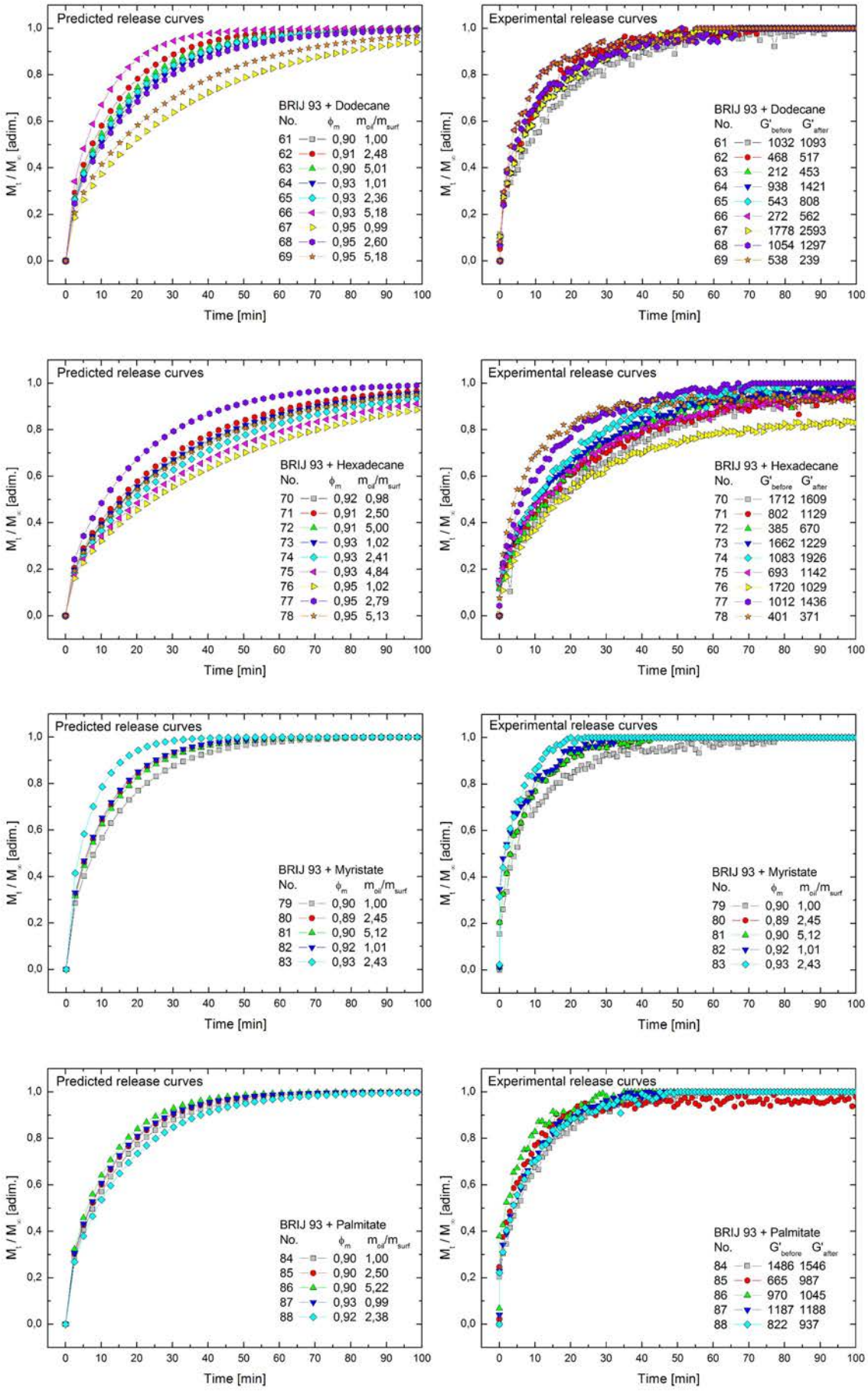

Fig. 4.13 Predicted and experimental release curves for system: BRIJ 93 + Oil.

4.4.3 Comparison of predicted and experimental diffusion coefficients

For sake of clarity, each individualized release curve is shown at the end of Appendix C.0.5. Additionally, the reader can consult a summary of the data from experiences in Tables C.4, C.5 and C.6 in the same Appendix. The simulations were successful to predict the release curves in a big number of cases. In some cases, slight deviations were found, however the variability appeared to be relatively small. In others, great divergences were observed. This aspect will be discussed more in depth during the following paragraphs. For a clearer comparison of experimental and predicted curves, they were fitted using the same procedure that was used during the VDOE (section 3.4.1) in order to obtain a diffusion coefficient characterizing each release experiment case. A comparison of the fitted diffusion coefficients for both predicted and experimental curves is shown in Fig. 4.14.

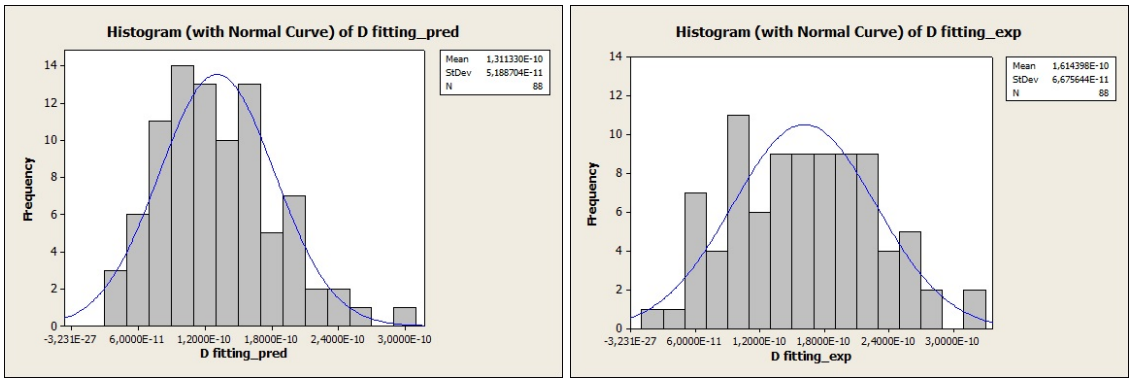

(a) (b)

Fig. 4.14 Histograms of fitted diffusion coefficients. a) Predictions b) Experiments.

The histograms showed in Fig. 4.14 allow to easily compare the variability of the diffusion coefficient data coming from predictions (a) and experiments (b). As one can see, the most part of predictions and experiments yield fitted diffusion coefficients ranging between $3{\cdot}10^{-11}$ to $3{\cdot}10^{10}$ m^2/s. However, according to the experiments, there was a significative number of experiences which surpassed the mean of the predicted values. The deviation in respect to this central tendency, could be indicating the presence of complex factors or external influences for certain experiences (or even that the simulations were not according to the reality). Now, in Fig. 4.15, the ensemble of fitted diffusion coefficients, both experimental and predicted, have been represented jointly. As one can see, generally, emulsions prepared with SPAN 80 showed the best agreement between predictions and experimental tests. On the contrary, those prepared with BRIJ 93 showed the highest divergences, showing normally experimental fitted coefficients of higher values than predicted ones. Concerning emulsions with PGPR, higher and smaller values were found.

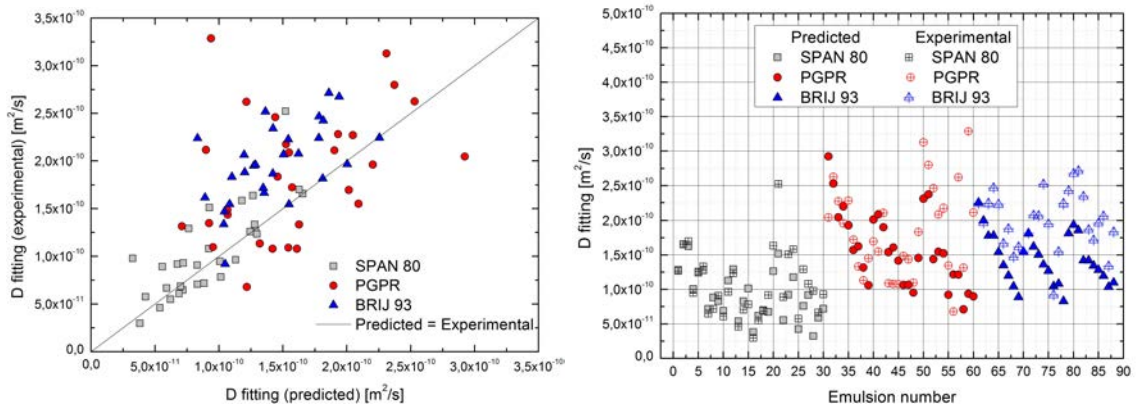

(a) (b)

Fig. 4.15 a) Comparison of fitted diffusion coefficients of experimental curves versus predicted ones. b) Comparison of fitted coefficient values per sample.

In Fig. 4.15b the value of these coefficients versus their respective identifying emulsion numbers per experience have also been represented. In order to understand easily this graph, it is important to keep in mind that the first nine emulsion numbers represented for each system (1-9, 31-39 and 61-69) are always referred to dodecane oil. Secondly, the following nine points (10-18, 40-48, and 70-78) are referred to hexadecane oil. Then, with respect to the final points, they are referred to myristate and palmitate oil in groups of six points each one for SPAN 80 and PGPR systems, but in the case of BRIJ 93 systems, in groups of five points only. This was like this because emulsions prepared using myristate and palmitate at highest dispersed phase volumetric fractions generally showed a noticeable instability and they were dismissed for the release experiments.

However, the reader is invited to see clearer interpretations in the following boxplots of Fig. 4.16. Boxplots are powerful graphs, which provide a visual synopsis of the variation patterns of the data distribution. The display consists of a rectangular box representing roughly the middle 50 % (interquartile range) of the data, and lines ('*whiskers*') extending to either side indicating the general extent of the data. It is also marked the median value inside the box and the outliers. They are specially useful for this analysis since a high number of different data are being compared. As one can see, generally, a good agreement between predicted and experimental curves was observed for emulsions prepared with dodecane or hexadecane oils when using SPAN 80 or PGPR as surfactants. However, deviations started to become important when myristate or palmitate oils where employed with these surfactants. On the other hand, when BRIJ 93 was employed, the deviations were more marked when using dodecane or hexadecane as oil. The greatest deviations from the whole study, specially occured in release experiments from emulsions prepared with PGPR and BRIJ 93.

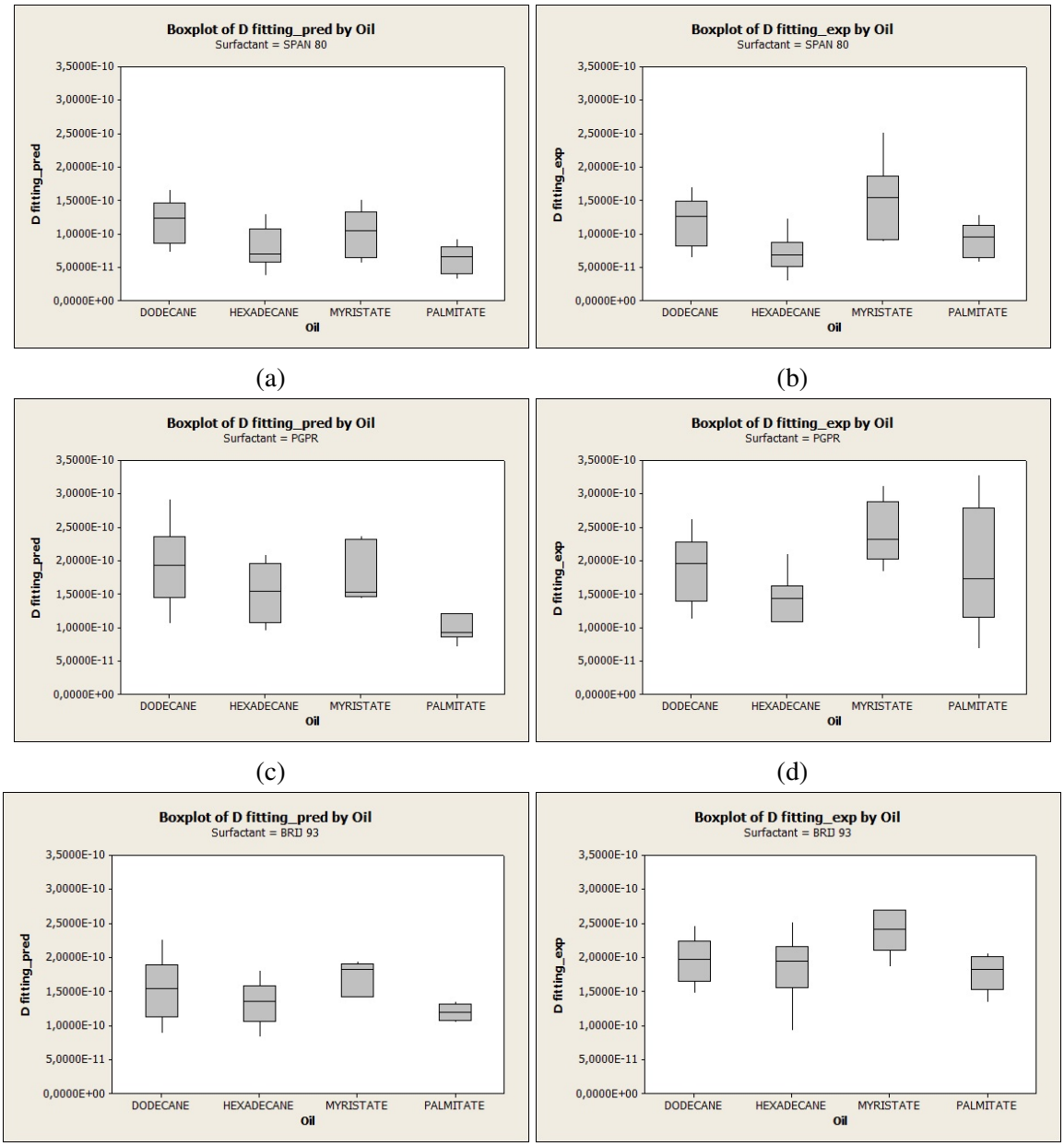

Fig. 4.16 Boxplots representing the variability of the fitted diffusion coefficients predicted (left) and experimental (right) of release experiments. They have been classified by surfactant and oil. a) and b) refer to SPAN 80 systems. c) and d) to PGPR systems. e) and f) to BRIJ 93 systems.

After having compared the fitted diffusion coefficients as function of the surfactant and oil employed, some remarks will be done in the next section regarding these results in relation to the storage moduli.

4.4.4 Analysis of storage moduli

As it was aforementioned, the storage moduli for each emulsion at the end of the release experiment was measured. In the following Fig. 4.17 the relative errors concerning the change of G' (before and after release) as well as the relative errors concerning the fitted diffusion coefficients (experimental and predicted) have been compared. Apparently, experiments which did not show significant differences on G' (less than 20 %), were those experiments generally related to a less deviation between the fitted diffusion coefficients. Since it is therefore likely that such connection exists, this kind of variations on G' can indicate that possible structural changes are happening during the release. As a consequence, it could be thought that the model would not work correctly for predicting the release at these cases.

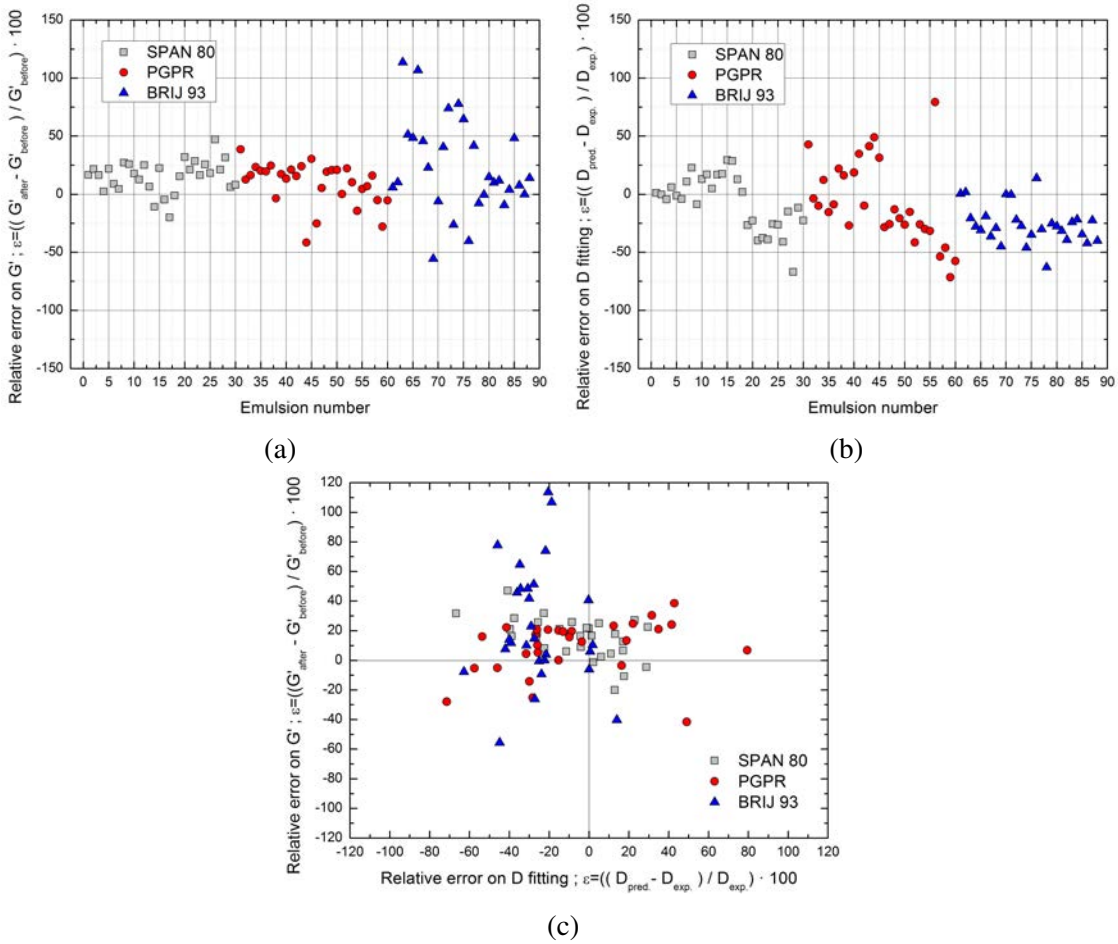

Fig. 4.17 a) Relative errors in storage moduli (G') before and after release. b) Relative errors between predicted $D_{pred.}$ and experimental $D_{exp.}$ diffusion coefficients (D). c) Jointly representation of relative errors concerning G' and D.

4.4.5 Model limitations and possible useful extensions

It is important to bear in mind that the mass transfer model developed, considers to keep constant all its parameters. During the modeling, it was supposed that there was no variation of parameters with time or position. But when the emulsion releases the active ingredient, and even considering that the active ingredient is the only transferred component, some parameters such as the droplet diameter, the thickness of the emulsion placed in the container and the dispersed phase mass fraction are likely going to decrease with time (even more rapidly if the emulsion was not stable).

The variation of time-dependent parameters may be complicated to incorporate in the mass transfer model in order to build a more rigorous nonlinear ab-initio model, which will then become it nonlinear. Nevertheless, this was not the objective of this thesis, since it was decided to consider a simple model as general as possible. But even without having a nonlinear model, it is however possible to assess the impact of some position-dependent and formulation parameters, for instance, by examination of the different release profiles at decreasing dispersed phase mass fraction or thickness of emulsion layer.

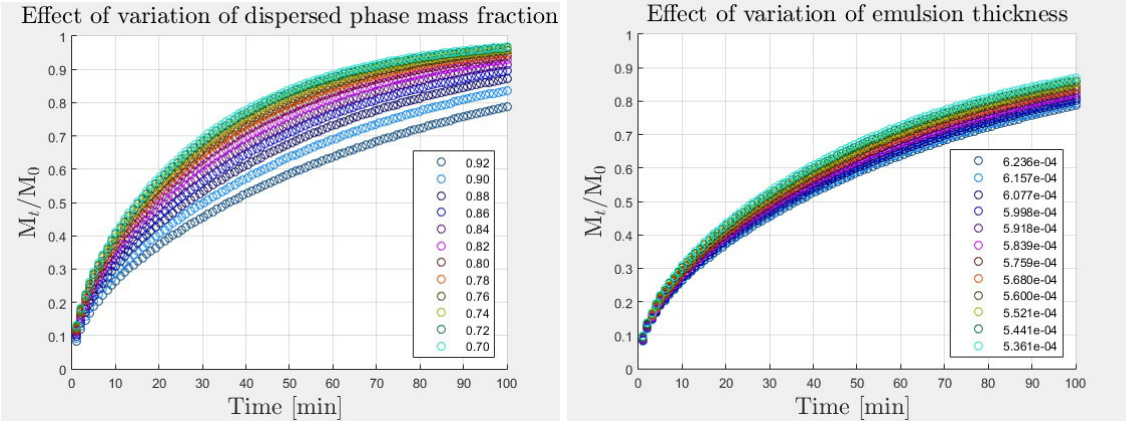

(a) Variation of ϕ_m from 0.92 to 0.70

(b) Variation of thickness L [m]

Fig. 4.18 Examples of possible variations on release curve by time-dependent parameters.

As example, in Fig. 4.18a, variations caused by a decrease of the mass dispersed phase fraction are shown. More specifically, this simulation was the one corresponding to the most extreme deviation detected in the SPAN 80 + Palmitate system (Emulsion No. 28). All input parameters for the ab-initio model were kept constant with the exception of the mass dispersed phase fraction. As one can see, a decrease on this variable caused a rising on the release curve. It could be conceivably hypothesized that in this specific case, this would be occuring and was the reason for the deviation observed. Afterwards, in Fig. 4.18b it is shown how a decrease on the thickness of the emulsion placed for the experiment could affect to the

release profile. As one can see, the effect is not so notable in comparison with the change on the dispersed phase mass fraction.

Some of these facts, individually or together with others, could have probably happened during the experimental release tests showing deviations. Specially, in some of the experiences showing a great divergence among predicted and experimental releases (typically emulsions using palmitate and myristate oils), it was visually remarked erosion-like effects on the surface of the remaining emulsions in the container at the end of the experiment. In other cases, even a part of the emulsion could had been completely detached, or even in some cases, oil droplets were observed floating on the surface of the receptor solution. One of the most extreme cases was the emulsion No. 22 (See Fig. C.6g of Appendix C.0.5). In this experience, there was a variation of approximately 1500 Pa on G' between the beginning and the end of the experience. During the initial times, a good agreement was achieved between predicted and experimental release curves, but as time increased, a divergence from the predicted profile started to appear, until arriving to the midpoint, where suddenly, a sharp increase on the absorbance signal was observed.

Additionally, it is important to bear in mind, that the model do not adress the effect of possible enhancers or reducers which could modify the permeation, neither specific reactions of the active ingredient with other substances within the system, or even interactions or association between the components. For example, the divergence between viscosity measurements and the predictions performed by UNIFAC-VISCO, suggested that it could be possibly hypothesized that more complex micelles structures could exist simultaneously in the continuous media (limit of this approach). It is clear that this phenomena could take part in the mass transfer, and this fact might justify the specific deviations observed when using PGPR as surfactant, specially the cases with a low deviation in G'. Other reasons could be an imprecise estimation of molecular volume/area parameters, bearing in mind that the nature of this surfactant is polymeric-like. A possible useful extension for the ab-initio model could be to implement the effect of the micellar transport in the diffusion coefficient [183], in order to correctly take into consideration this fact.

Given the limitations inherent to the model itself, as well as possibly uncertainty on the inputs or mass transport parameters dependent of emulsion composition such as distribution coefficients predicted by UNIFAC, diffusion coefficients, molecular volumes/areas, permeabilities, etc., the predictions in some cases could be only regarded as orientative values. Nevertheless, the findings were encouraging, and according to the satisfactory cases, we believe that the model might be still capable of providing correct or at least first approximations within a low margin of error for a big number of cases.

4.4.6 Screening of most accurate predicted scenarios

The predictions showing less experimental deviation to experimental fitted coefficients have been ploted and identified in Fig. 4.19. As one can see, checking the Table 4.1, equivalent controlled release profiles can be obtained using different formulations, o/s ratios or dispersed phase mass fractions. Therefore, the model allows to tune the emulsion properties in order to attain a given desired profile of active ingredient release.

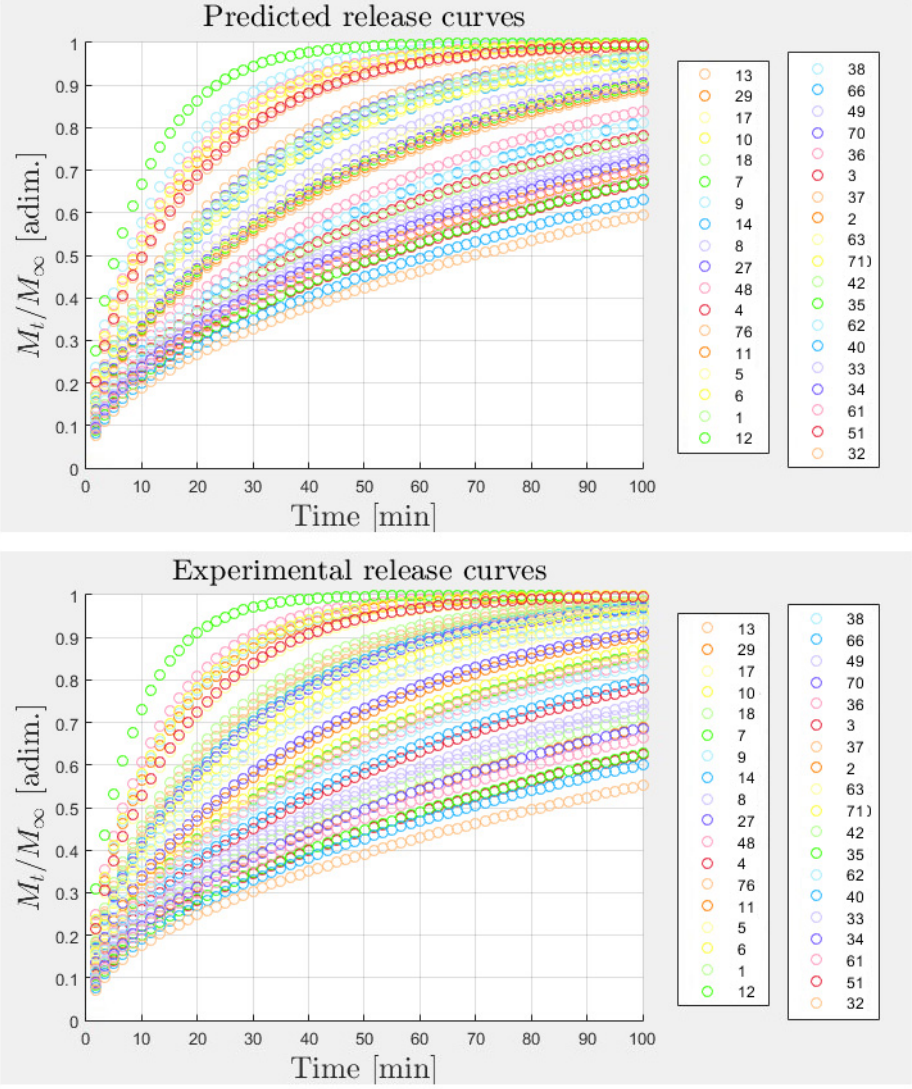

Fig. 4.19 Predicted release profiles with less deviation error ($\varepsilon \approx 20\%$) in relation to experimental tests. For the plot of these curves, $\text{Dfitting}_{(pred.)}$ and $\text{Dfitting}_{(exp.)}$ were used respectively in the exact analytical solution of Fick's law. It is important to mention that the thickness of emulsion L was calculated according to weighted mass amount and can vary slightly between experiences.

Table 4.1 Screening of predicted release curves with less experimental deviation error.

No.	Oil	Surfactant	ϕ_m	$m_{oil}/m_{surf.}$	$Dfitting_{pred.}$	$Dfitting_{exp.}$	ε (error)
13	HEXADECANE	SPAN 80	0.93	1.05	5.38E-11	4.60E-11	17.01
29	PALMITATE	SPAN 80	0.93	2.59	5.90E-11	6.67E-11	-11.48
17	HEXADECANE	SPAN 80	0.95	2.70	6.20E-11	5.49E-11	12.91
10	HEXADECANE	SPAN 80	0.91	1.06	6.88E-11	6.09E-11	13.08
18	HEXADECANE	SPAN 80	0.95	5.64	7.00E-11	6.85E-11	2.06
7	DODECANE	SPAN 80	0.95	1.04	7.18E-11	6.47E-11	10.97
9	DODECANE	SPAN 80	0.95	6.08	8.30E-11	9.08E-11	-8.58
14	HEXADECANE	SPAN 80	0.93	2.43	8.31E-11	7.07E-11	17.56
8	DODECANE	SPAN 80	0.95	2.93	8.83E-11	7.19E-11	22.87
27	PALMITATE	SPAN 80	0.91	5.66	9.21E-11	1.08E-10	-14.85
48	HEXADECANE	PGPR	0.95	5.67	9.54E-11	1.10E-10	-13.02
4	DODECANE	SPAN 80	0.93	1.06	1.01E-10	9.49E-11	5.99
76	HEXADECANE	BRIJ 93	0.95	1.05	1.05E-10	9.20E-11	13.95
11	HEXADECANE	SPAN 80	0.91	2.64	1.13E-10	9.65E-11	17.13
5	DODECANE	SPAN 80	0.93	2.50	1.24E-10	1.26E-10	-1.25
6	DODECANE	SPAN 80	0.93	5.22	1.28E-10	1.33E-10	-4.11
1	DODECANE	SPAN 80	0.91	1.10	1.28E-10	1.27E-10	1.23
12	HEXADECANE	SPAN 80	0.91	5.65	1.30E-10	1.23E-10	4.97
38	DODECANE	PGPR	0.95	3.28	1.32E-10	1.13E-10	16.33
66	DODECANE	BRIJ 93	0.93	5.59	1.35E-10	1.67E-10	-18.80
49	MYRISTATE	PGPR	0.90	1.06	1.46E-10	1.84E-10	-20.58
70	HEXADECANE	BRIJ 93	0.93	1.00	1.55E-10	1.55E-10	0.09
36	DODECANE	PGPR	0.92	5.76	1.57E-10	1.72E-10	-8.72
3	DODECANE	SPAN 80	0.91	5.48	1.63E-10	1.70E-10	-4.33
37	DODECANE	PGPR	0.95	1.29	1.63E-10	1.33E-10	22.05
2	DODECANE	SPAN 80	0.91	2.69	1.66E-10	1.66E-10	-0.19
63	DODECANE	BRIJ 93	0.90	5.38	1.78E-10	2.24E-10	-20.51
71	HEXADECANE	BRIJ 93	0.91	2.62	1.81E-10	1.82E-10	-0.28
42	HEXADECANE	PGPR	0.90	5.38	1.90E-10	2.11E-10	-9.84
35	DODECANE	PGPR	0.92	2.57	1.93E-10	2.28E-10	-15.34
62	DODECANE	BRIJ 93	0.91	2.58	2.00E-10	1.97E-10	1.78
40	HEXADECANE	PGPR	0.90	1.05	2.02E-10	1.70E-10	18.79
33	DODECANE	PGPR	0.90	5.52	2.05E-10	2.27E-10	-9.88
34	DODECANE	PGPR	0.92	1.06	2.20E-10	1.96E-10	12.34
61	DODECANE	BRIJ 93	0.90	1.02	2.26E-10	2.24E-10	0.52
51	MYRISTATE	PGPR	0.87	5.45	2.37E-10	2.80E-10	-15.25
32	DODECANE	PGPR	0.90	2.72	2.53E-10	2.63E-10	-3.64

4.4.7 Principal component analysis

Due to the complexity and the high number of parameters in the model, multivariate analysis procedures to analyze the data are extremely suggested. Similar to the Pareto chart, a principal component analysis allows to reduce the data dimension, finding out the most important variables and clear tendencies quickly. This is really interesting for reconciliation and intensification purposes, since it is possible to know the key variables (and respective weights) which most influence the response. Changes on these interrelated variables (principal components) will assure changes on the targeted release profiles.

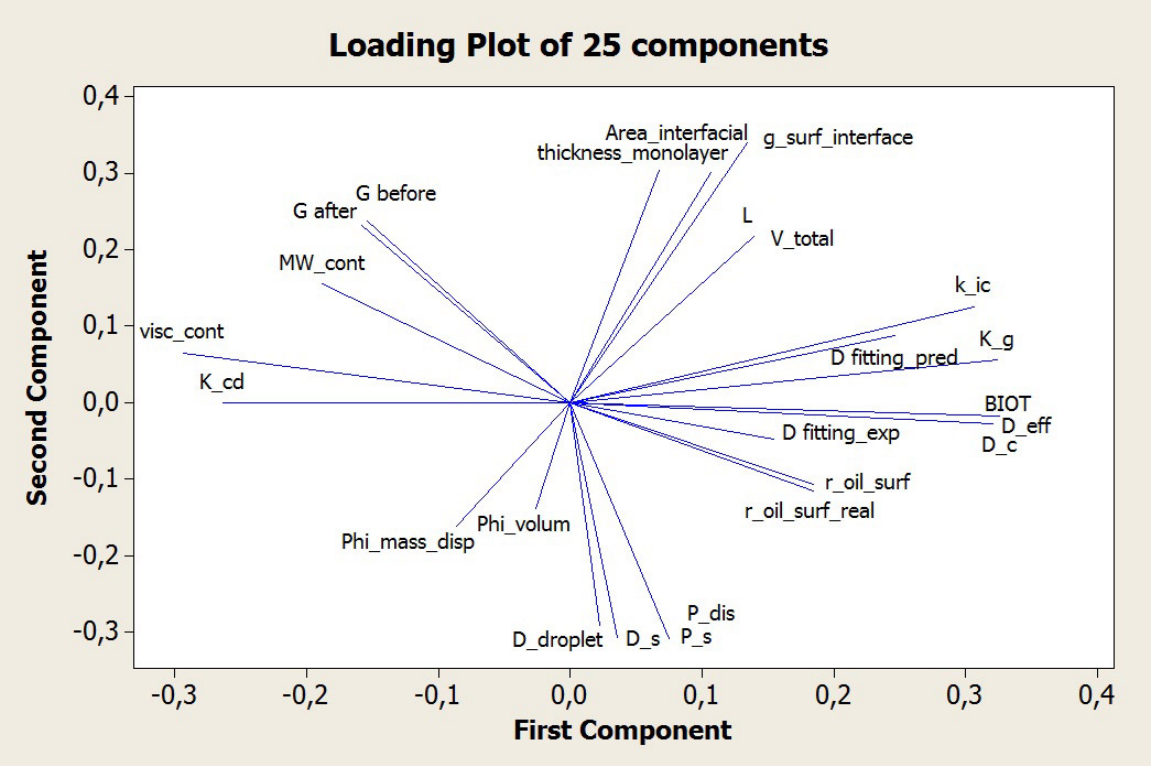

Fig. 4.20 Loading plot of principal component analysis. The study was done using all simulation and experimental results and considering 25 components to be computed.

In order to analyze the data covariance structure, the principal component analysis was performed using the statitiscal software Minitab®. An overview of principal component analysis can be found in most books on multivariate analysis, such as [184]. A total number of 25 components (variables) were chosen to compute in the analysis. The result of the loading plot for first two components is shown in Fig. 4.20. This plot checks the loadings for the second principal component (y-axis) versus the scores for the first principal component (x-axis). A line is drawn from each loading to the (0,0) point. The similarity (lineal correlation) between variables can be interpreted from the graph. The closer the components ploted in

the graph, the higher the possibilities of existing a lineal combination between them. The nomenclature for the designation of the variables is the same that was employed in the logical architecture diagram from section 3.2. A correlation matrix type was used because the variables were measured at different scales. In this way, the matrix makes sense in order to standardize variables. In order to interpret the results of the principal component analysis, the screen plot and eigenanalysis of the correlation matrix are shown in Fig. 4.21.

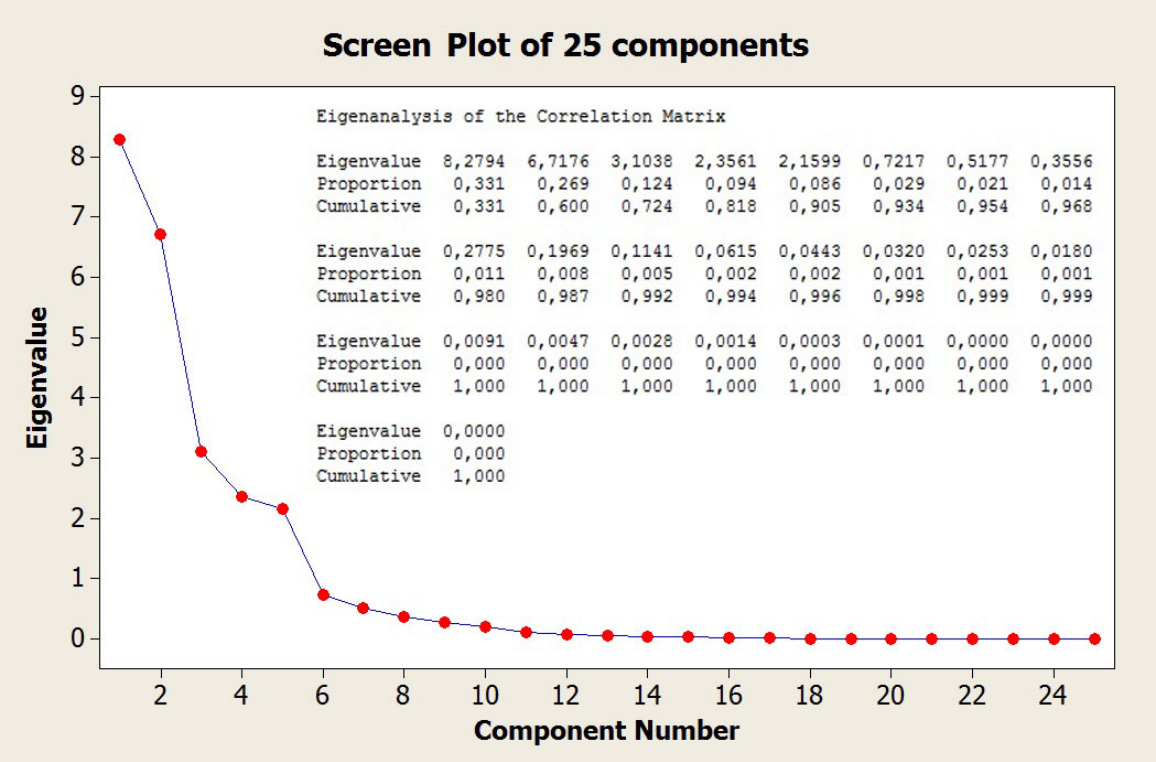

Fig. 4.21 Screen plot of principal component analysis and values resulting from the eigenanalysis of the correlation matrix.

The first principal component has a variance (eigenvalue) 8.2794 and accounts for 33.1 % of the total variance. The coefficients listed in Table 4.2 under PC1, allow to calculate the principal component score (for instance, PC1=0.154·V1+0.246·V2-0.158·V3+...). It should be noted that the interpretation of the principal components is subjective, however, obvious patterns emerge quite often. For instance, because the weights of these terms have opposite sign and are not close to zero, one could think of the first principal component as representing an effect of the distribution coefficient K_{cd} and continuous phase viscosity (μ_c) to the effective diffusivity ($D_{eff.}$) and global mass transfer coefficient (K_g). The second principal component has variance 6.7176 and accounts for 60 % of the data variability. This component could be thought of a contrasting level of the deposited surfactant amount on the

interphase ($m_{surf.}$), the interfacial area ($A_{interfacial}$) and the monolayer thickness (Δ_s) with the permeability of the surfactant layer (P_s) to some extent. For the third component PC3, as it was known beforehand from the Pareto chart, the dispersed phase mass fraction (ϕ_m) is closely linked to the representative diffusion coefficients of the curves. In the forth, PC4, it is possible to see the relationship between the volume or thickness of the emulsion tested for release (V_{total} and L respectively) with $A_{interfacial}$ and oil/surfactant ratio $r_{oil/surf.}$. In the last principal component, PC5, the storage moduli (G') appears to be specially related to ϕ_m and $r_{oil/surf.}$. Together, first four and five components represent 81.8 % and 90.5 %, respectively, of the total variability. Thus, most of the data structure can be captured in these five underlying dimensions instead. In following Figs. 4.22 to 4.23, different boxplots summarize the values of these categorical variables.

Table 4.2 Weight coefficients of correlation matrix from principal component analysis.

	Variable	PC1	PC2	PC3	PC4	PC5
V1	$D_{fitting}$ (exp.)	0.154	-0.048	-0.363	-0.189	0.081
V2	$D_{fitting}$ (pred.)	0.246	0.087	-0.331	0.01	0.083
V3	G'_{before}	-0.158	0.232	0.033	-0.148	0.347
V4	G'_{after}	-0.154	0.237	-0.001	-0.124	0.332
V5	$r_{oil/surf.}$ (real)	0.185	-0.107	0.188	-0.317	-0.331
V6	$r_{oil/surf.}$ (preparation)	0.184	-0.116	0.174	-0.308	-0.344
V7	$D_{droplet}$	0.022	-0.291	0.231	0.065	0.06
V8	ϕ_m	-0.026	-0.139	0.44	0.108	0.303
V9	ϕ_v	-0.086	-0.162	0.362	0.108	0.362
V10	D_s	0.035	-0.308	-0.262	0.165	0.129
V11	$D_{eff.}$	0.321	-0.027	0.082	-0.04	0.216
V12	D_c	0.326	-0.018	0.063	-0.044	0.199
V13	BIOT	0.326	-0.018	0.063	-0.044	0.198
V14	$m_{surf.interphase}$	0.134	0.339	-0.025	0.079	0.025
V15	Δ_s	0.067	0.304	0.132	-0.286	0.115
V16	$A_{(interfacial)}$	0.106	0.301	-0.025	0.306	-0.109
V17	V_{total}	0.139	0.217	0.105	0.416	-0.137
V18	L	0.139	0.217	0.105	0.416	-0.137
V19	$MW_{cont.}$	-0.188	0.155	-0.173	-0.277	0.121
V20	K_{cd}	-0.264	-0.001	-0.237	0.177	0.13
V21	K_g	0.324	0.055	-0.087	-0.018	0.109
V22	k_{ic}	0.306	0.125	-0.08	-0.065	0.158
V23	P_{dis}	0.074	-0.309	-0.21	0.121	0.091
V24	μ_c	-0.294	0.064	-0.043	-0.03	-0.103
V25	P_s	0.075	-0.309	-0.21	0.121	0.092

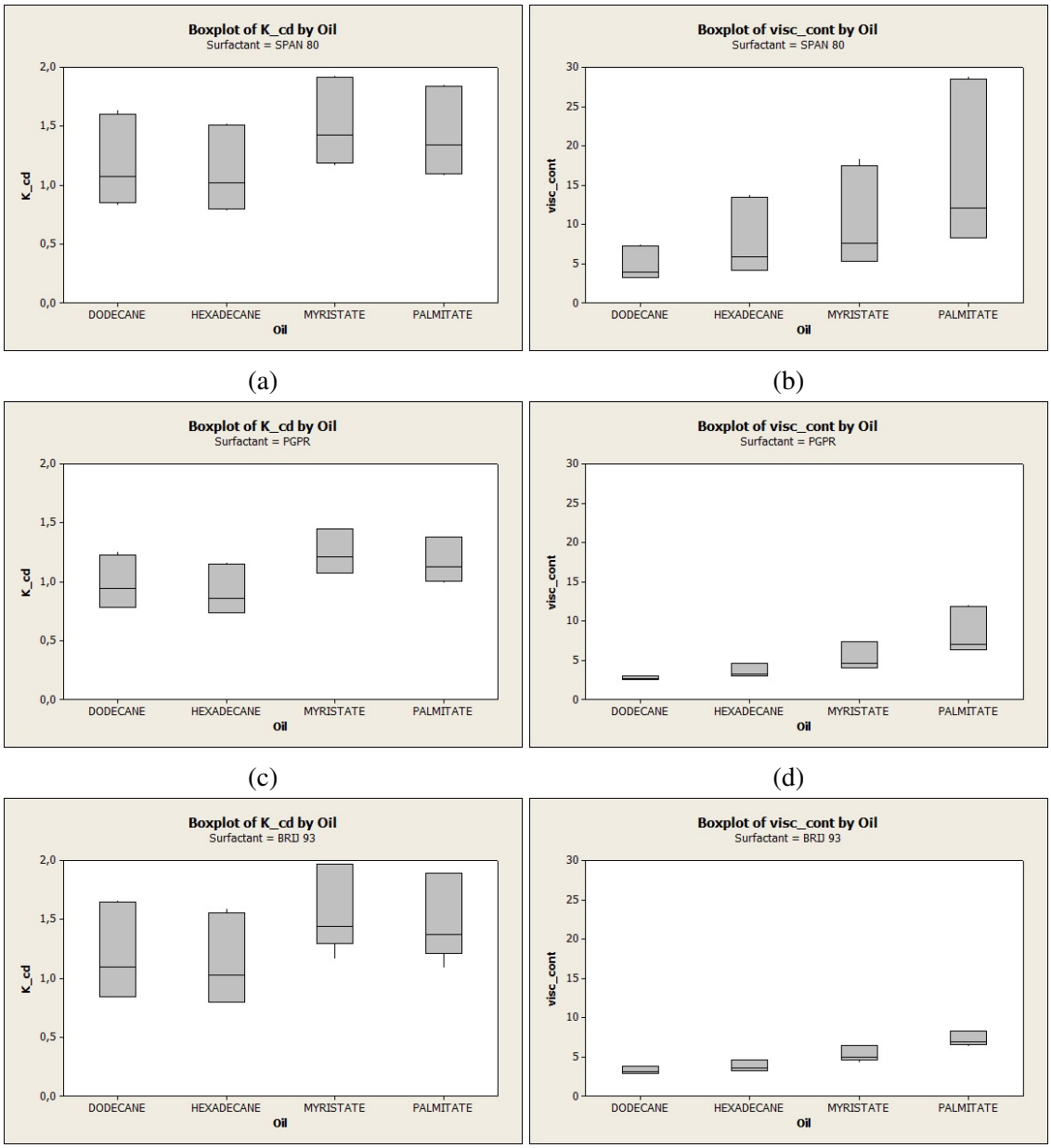

(a) (b)

(c) (d)

(e) (f)

Fig. 4.22 a) c) e) Boxplots representing the variability on distribution coefficients in the emulsions employed for release tests. b), d) and f) Boxplots representing the variability on viscosity [cP] of continuous phases predicted by UNIFAC-VISCO and used by the ab-initio model to perform the simulations.

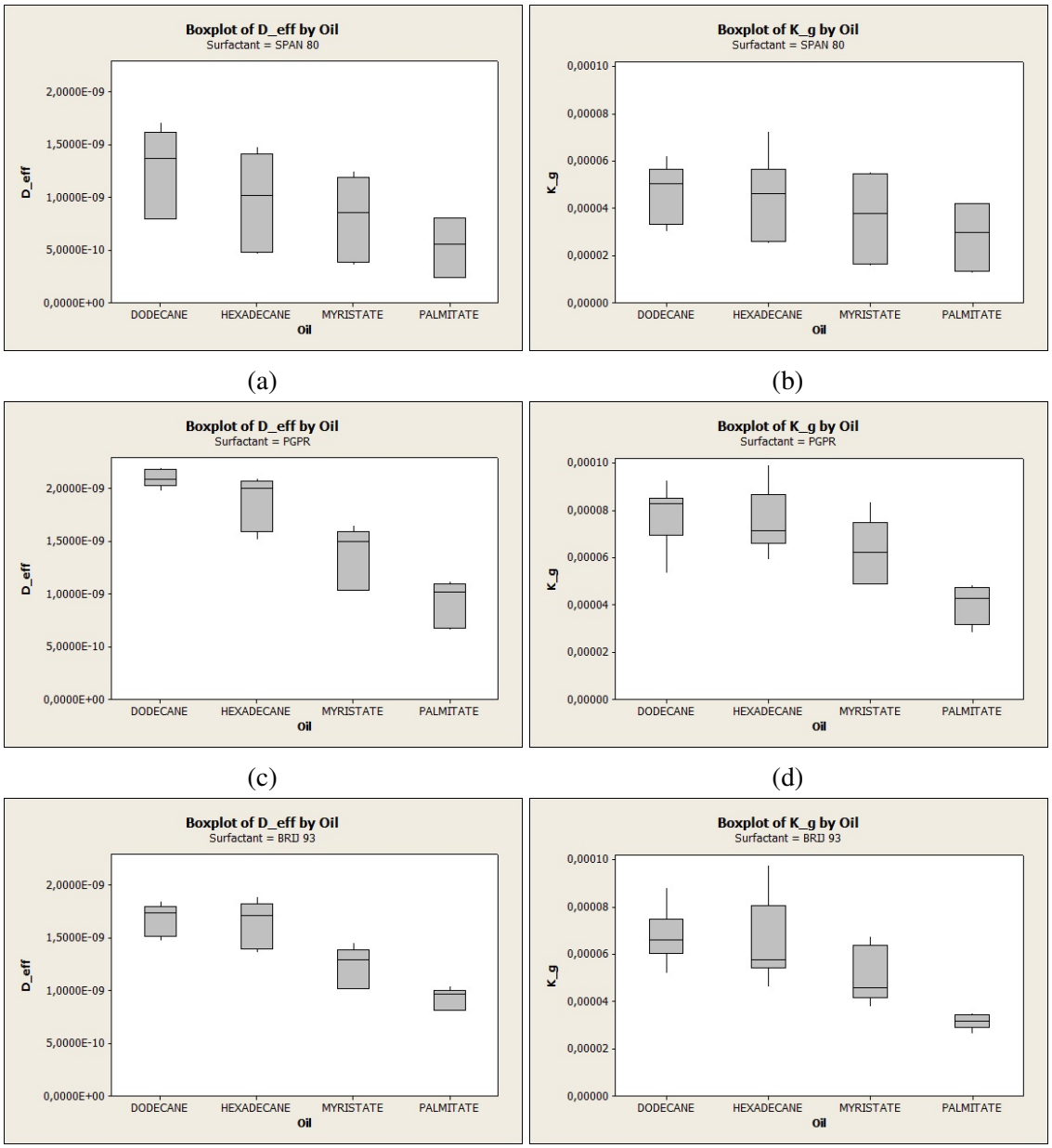

Fig. 4.23 a) c) and d) Boxplots representing the variability on the estimated effective diffusion coefficients [m^2/s] of continuous phases (after applying the Maxwell relation) by the ab-initio model. b) d) and f) Boxplots representing the values of the global mass transfer coefficients [m/s] estimated on simulations.

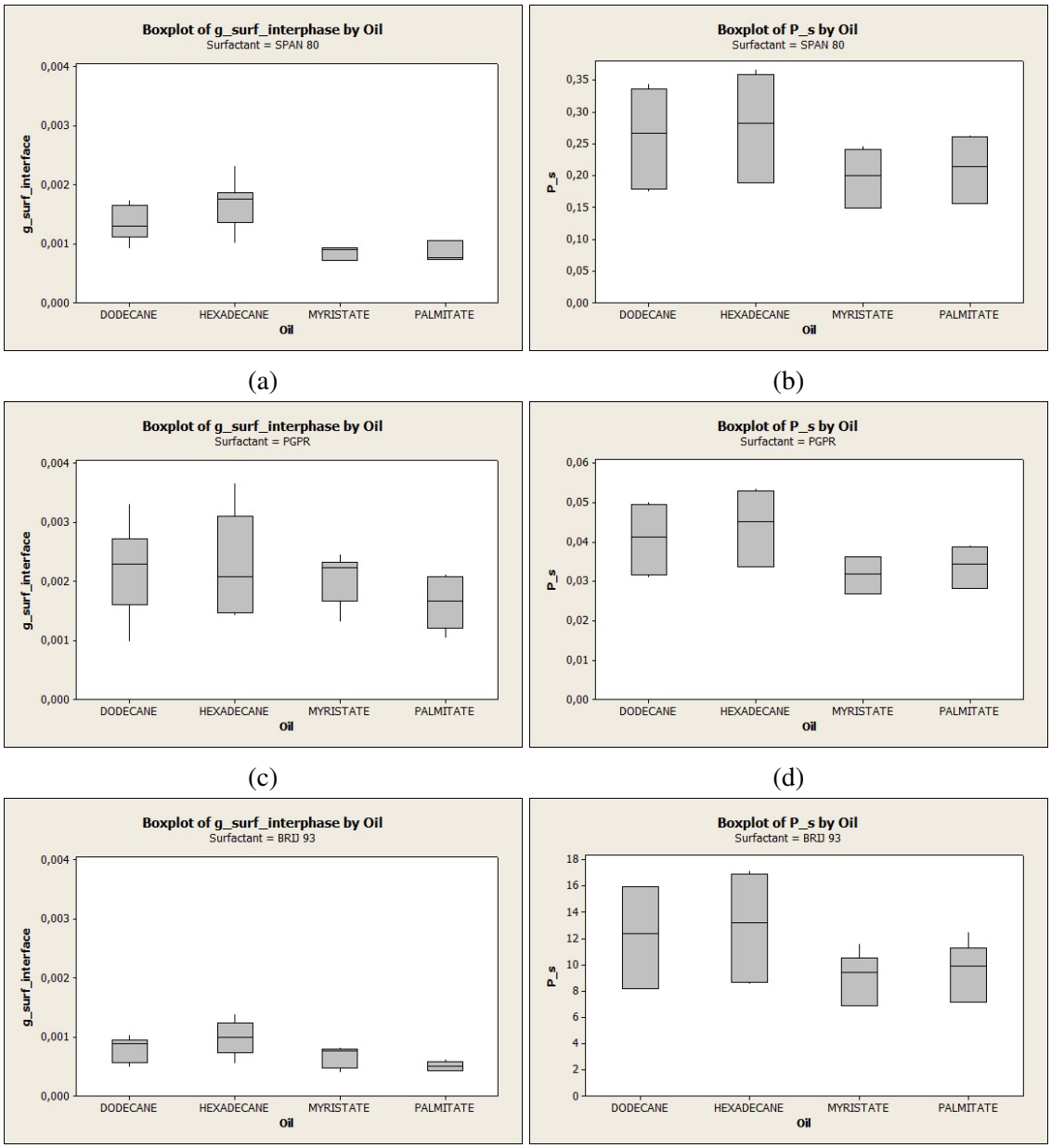

Fig. 4.24 a) c) and d) Boxplots representing the variability on the calculated mass amounts of surfactant on the droplet surfaces. b) d) and f) Boxplots representing the variabilities of the calculated surfactant layer permeabilities [cm/s].

Some of the conclusions drawn from the multivariate analysis, as well as comments in regard to the representative key variables were:

- The principal component analysis demonstrated the key role of the interfacial film as well as the partition coefficient of the diffusing molecule between the continuous and the dispersed phase on the diffusion. Overall, faster release profiles were obtained using emulsions with low partition coefficients for the diffusing molecule and low viscosities of continuous phase (see Fig. 4.22). It results interesting to note that even if distribution coefficients were close for emulsions prepared with SPAN 80 BRIJ 93, the viscosities of continuous phases for SPAN 80 emulsions were generally much higher than those prepared with BRIJ 93. This appeared to have a special impact on the release profile, giving slower diffusion rates. It can be thus suggested that the viscosity may not be negligible in terms of its impact on the diffusion coefficient: controlling the viscosity of the continuous media (for example by adding thickeners) could hypothetically lead to control slower releases.

- Regarding the estimated effective diffusion coefficient for the continuous phase, it was observed a direct and positive correlation with the global mass transfer coefficient. This fact confirmed again the importance of the dispersed phase mass fraction (as it was already seen in the Pareto chart) when applying the Maxwell relation, since its value determines to a great extent the order of the interfacial mass transfer coefficient. The higher this value, the less the resistance for the mass transfer (see Fig. 4.23).

- In some cases, it might be important to consider that surfactant permeabilities could be much greater than others and the interfacial resistance offered by the surfactant around droplets would be extremely low (for instance, when using BRIJ 93). As a consequence of this, generally faster release curves could be hypothetically obtained. However, with great permeabilities, caution must be applied, it may be the case that a rapid mass transfer through the surfactant layer could also lead to changes on the structural parameters in a shorter time. This could cause subsequent instabilities, and probably, is the reason that justifies the deviations observed between predictions and experimental tests when using BRIJ 93 (see Fig. 4.24).

- It is also important to mention that the model is very sensitive to molecular parameters such as volumes or areas. More specifically, the ab-initio model calculates the thickness of the emulsion (L) taking into account the respective molar volumes of the components. Any errors on inputs such as the weighted mass amount of emulsion for release or the oil/surfactant amounts could lead to strong miscalculations.

Chapter 5

FINAL CONCLUSIONS

'A great discovery solves a great problem, but there is a grain of discovery in the solution of any problem. Your problem may be modest, but if it challenges your curiosity and brings into play your inventive faculties, and if you solve it by your own means, you may experience the tension and enjoy the triumph of discovery', George Pólya."

5.1 Summary of results and conclusions

In this thesis, a reverse engineering framework has been proposed to design and evaluate vehicles for controlled release of active ingredients. A convenience example of structured-dispersed system: highly concentrated emulsions, was considered. The design problem was decomposed into a hierachical sequence of subproblems or boxes (see Fig. 5.1), combining:

- Constitutive models, which estimate the active ingredient mass transport as a function of formulation parameters, such as type of oil or surfactant, their mass ratio, emulsion droplet diameter, active ingredient concentration, dispersed phase mass fraction, mass employed for the release experiment, as well as receptor solution volume.
- Computer-aided techniques, such as molecular modeling descriptors for estimation of volume/area of molecules, or group-contribution models employed for equilibria predictions as well as for mixture viscosities estimations.
- Heuristic-based testing. Different simulation tools allowed to gain knowledge prior the corresponding experimental validations concerning estimations of distribution coefficients, mixture viscosities or the respective predicted release profiles.

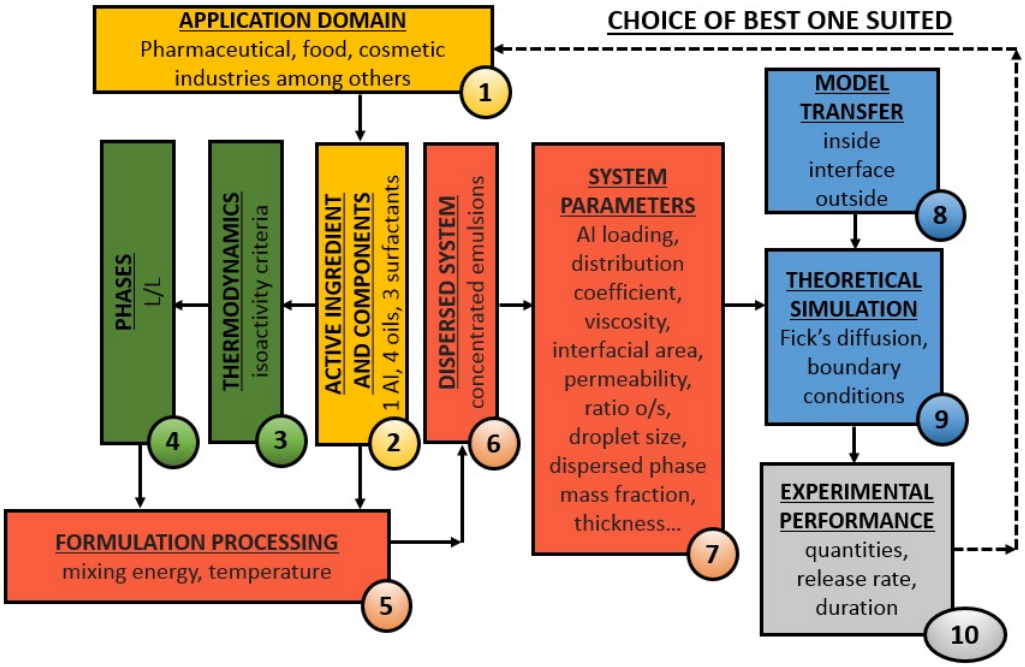

Fig. 5.1 Work-flow diagram for a reverse engineering approach to design of controlled release products.

A summary of the most important aspects covered in the reverse engineering approach of this thesis, applied for highly concentrated emulsions, were the following:

- A programming code using three UNIFAC group-contribution methods (Fredenslund, Dortmund and Constantinescu) was written using MATLAB software in order to estimate activity coefficients of liquid-liquid mixtures. An additional flash algorithm based on the Rachford and Rice equation was implemented for calculating the distribution coefficients at equilibrium of active ingredient within the emulsion phases.

- Attemps to validate experimentally the above thermodynamic descriptors were performed by determination of distribution coefficients of emulsion-like samples by UV-spectrometry. However, these validations were limited in several ways. First, a three-phase system was observed for all samples and the experimental study was not able to take into account the third phase. Adding salt seemed to reduce the amount of this third phase, however, compensatory effects could be happening simultaneously, since UNIFAC methods, a priori, do not consider the presence of salts. Secondly, it was observed that possible microdroplets or microaggregates of oil or surfactant could be misleading the UV-lecture because of interference effects. Although stock solutions were employed as blank and dilution media for the samples measurement

only slight improvements were achieved. In any case, the combinations of results provided some support for the conceptual premise that the Modified UNIFAC method of Contastinescu (2016) is the most suitable for predicting the distribution coefficients from the three methods studied because of the better precisions obtained.

- Another programming code was written using MATLAB software to estimate the continuous phase mixture viscosities by UNIFAC-VISCO method. Experimental validations were also performed to check the accuracy of the predictions. Overall, the method appeared to yield estimations with good agreement between predicted and experimental viscosities, with the exception of PGPR systems. In all other cases, low deviations were obtained, except cases of oil/surfactant ratios close to the unity.

- A full factorial design of virtual experiments has allowed to obtain a quantitative description of the release. These kind of sensitivity analysis, allowed to clearly understand the main tendencies when changing the different formulation variables prior performing any experiments. After, experimental kinetics validations have been performed.

The following conclusions can be drawn from the present thesis:

- It has been found that considering a limited cartography of 4 oils and 3 surfactants, the ensemble of tools of the proposed reverse engineering approach, generally allowed to predict the temporal profiles of active ingredient (mandelic acid) release from the emulsions in the most part of cases. The results pointed in predicted release profiles with representative Fickean diffusion coefficient values ranging from $3{\cdot}10^{-11}$ to $3{\cdot}10^{-10}$ m^2/s (one order of magnitude).

- However, the success of the predictions were significantly limited to the emulsion stability. In spite of this fact, the mean absolute relative error between predicted and experimental fitted diffusion coefficients for all release experiences performed (88 experiences) was about a 16%.

- The application of this reverse engineering results very interesting regards intensification purposes and for the development of new controlled-delivery systems. Specially, because costly trial-and-error tests can be potentially avoided and the design can be rationally facilitated when facing a set of existing possibilities.

5.2 Implications to future research

The focus of this thesis was primarily focused on highly concentrated emulsions systems, a special case of the broader material design problem in controlled release technologies. In what respects the structure of the vehicle, the system assumed was just a simple L/L emulsion on a fundamental level and appears to not show a very versatile character. A future study investigating other controlled release systems, such as nanoparticles (S/L) or gels (P/L), employing the same approach would be very interesting. Under a most global reverse engineering approach, it might be extended to address other structured-dispersed systems, such as rate-controlling membranes, or in general, any multiphasic system with multiple dispersed and continuous phases (See Fig. 5.2), to obtain more notable differences on the release rate.

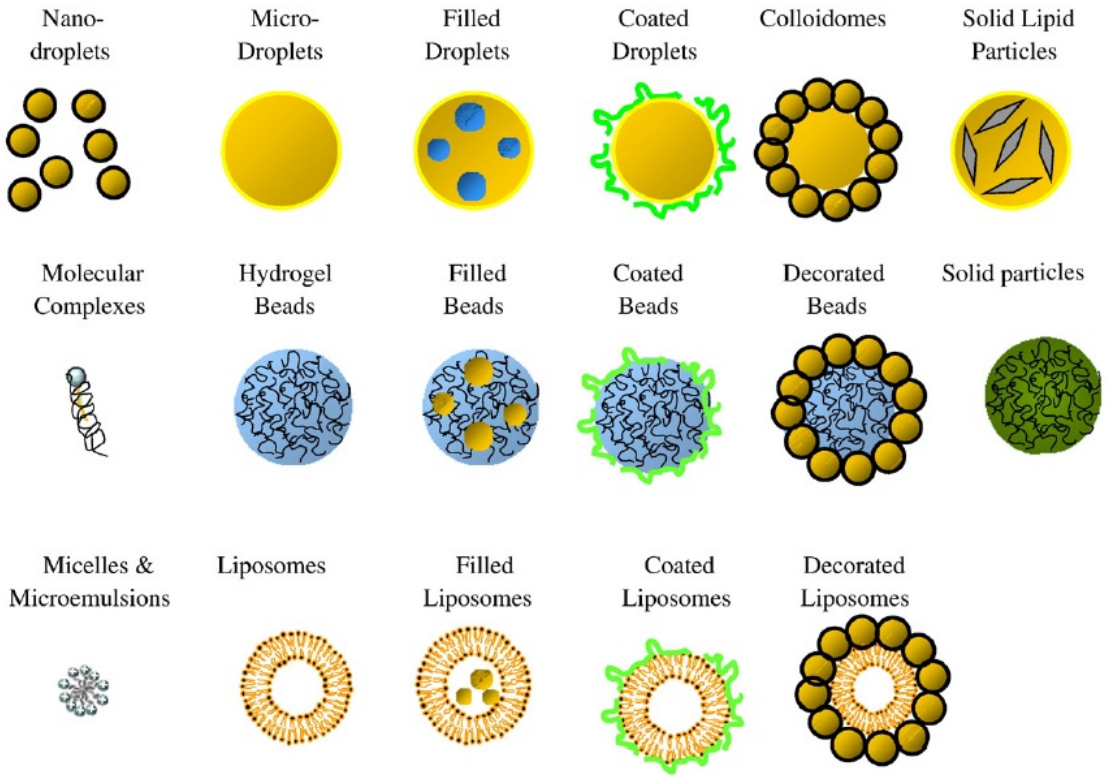

Fig. 5.2 Examples of different kinds of structured emulsion-based delivery systems that could be useful to be studied under the reverse engineering of this work. Adapted from [21].

All systems have common points: they are disperse systems. The main problem of any model of disperse system would be probably to stablish the connection between the macro-properties and micro-characteristics of the system, and take into account the above peculiarities of its behavior. Each disperse system shows a behavior complex and distinctive.

The inquiry that at any point could emerge is if a partition/diffusion description would be available or not to describe mass transfer in such more complex systems, or if specific interactions (i.e. adsorption, reaction) or phenomena at nanoscale (molecular aggregates, such as micelles) would be expressly addressed. Nevertheless, even if each disperse system possesses their own thermodynamic properties and characteristics, one expects under a reverse engineering approach that each system could be hypothetically explained by including the specific content on the adequate box.

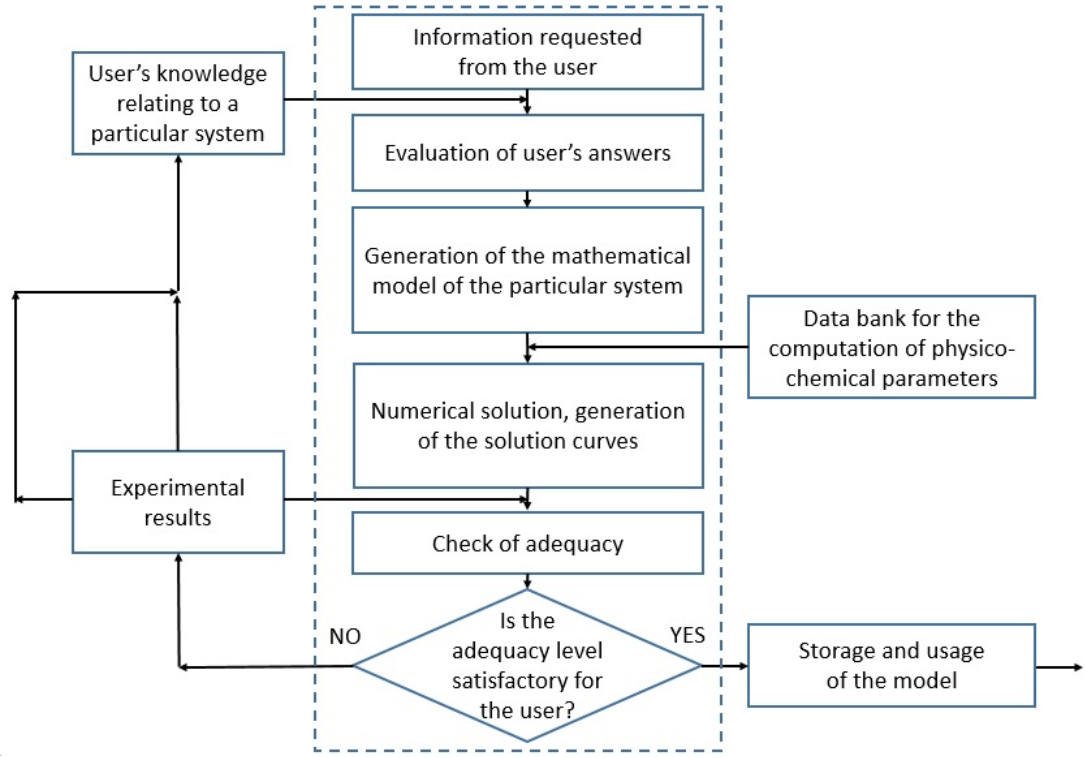

Fig. 5.3 Schematics of the computer program system used to generate, solve and verify the mathematical models of a given structured-dispersed system. Adapted from [22].

Therefore, the forward problem, which involves the computation of a controlled release for a given product would appear to be solved. However, it is also important to remind that the choice of a delivery system, rather must be driven by the nature of the active ingredient within its application domain, and the inherent properties of the respective release systems. Properties of the active ingredient, including chemistry, solubility, etc., influence on the proper selection of a desired delivery system that can achieve the desired outcomes. It is required thus, to rely on a suitable cartography database of different and adequate disperse systems (depending on the domain of application), which would allow to see significative differences or effects on the release rate.

Taken together, the results of this work support strong recommendations to explore new candidate systems in a similar way as it has been done for highly concentrated emulsions. After evaluation and verification of the different adding scenarios by the computer program and framework developed (see Fig. 5.3), one could finally apply decision making techniques and choose the best simulated formulation for a given release rate.

Additionally, it could be possible to take into consideration weight factors such as economical aspects, processing limitations, or others restraints. In this way, expressed as a reverse design problem, the target property for the product could become the known variable, and therefore input of parameters for the design (See Fig. 5.4). Ultimately, even if experimental validations were necessary to check predictions, the number of experiments would be decreased, since that only the closest solutions to the desired target would be required to be tested.

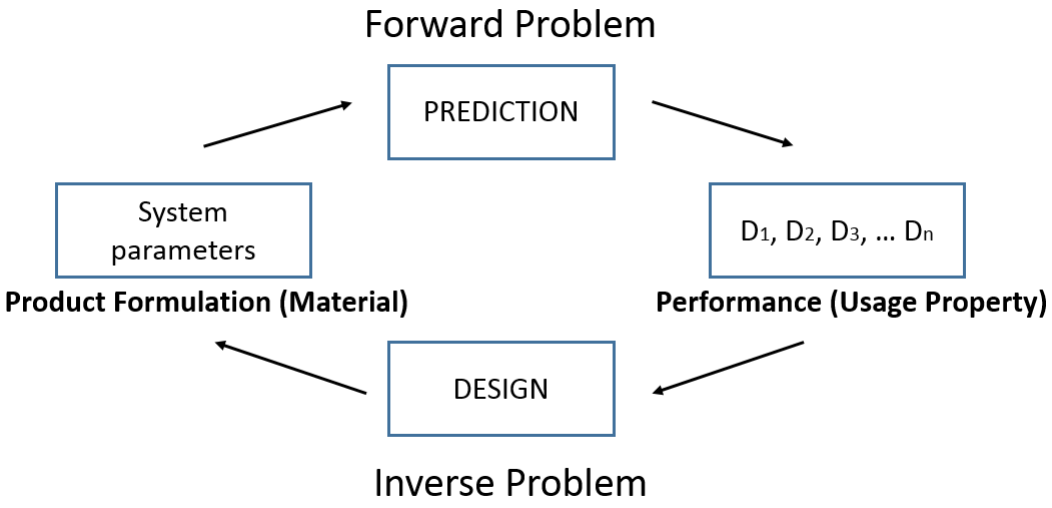

Fig. 5.4 Components of the molecular design problem. Adapted from [1].

Metaphorically, reverse engineering appears to be like working a picture puzzle: if only a few pieces (boxes of the approach) are in place, once can get a rought idea of the total picture. However, as more boxes (pieces of the puzzle) are added and completed, the picture becomes clearer. This methodology of reverse engineering has shown in this thesis to be interesting for product design and could potentially be applied to other common systems.

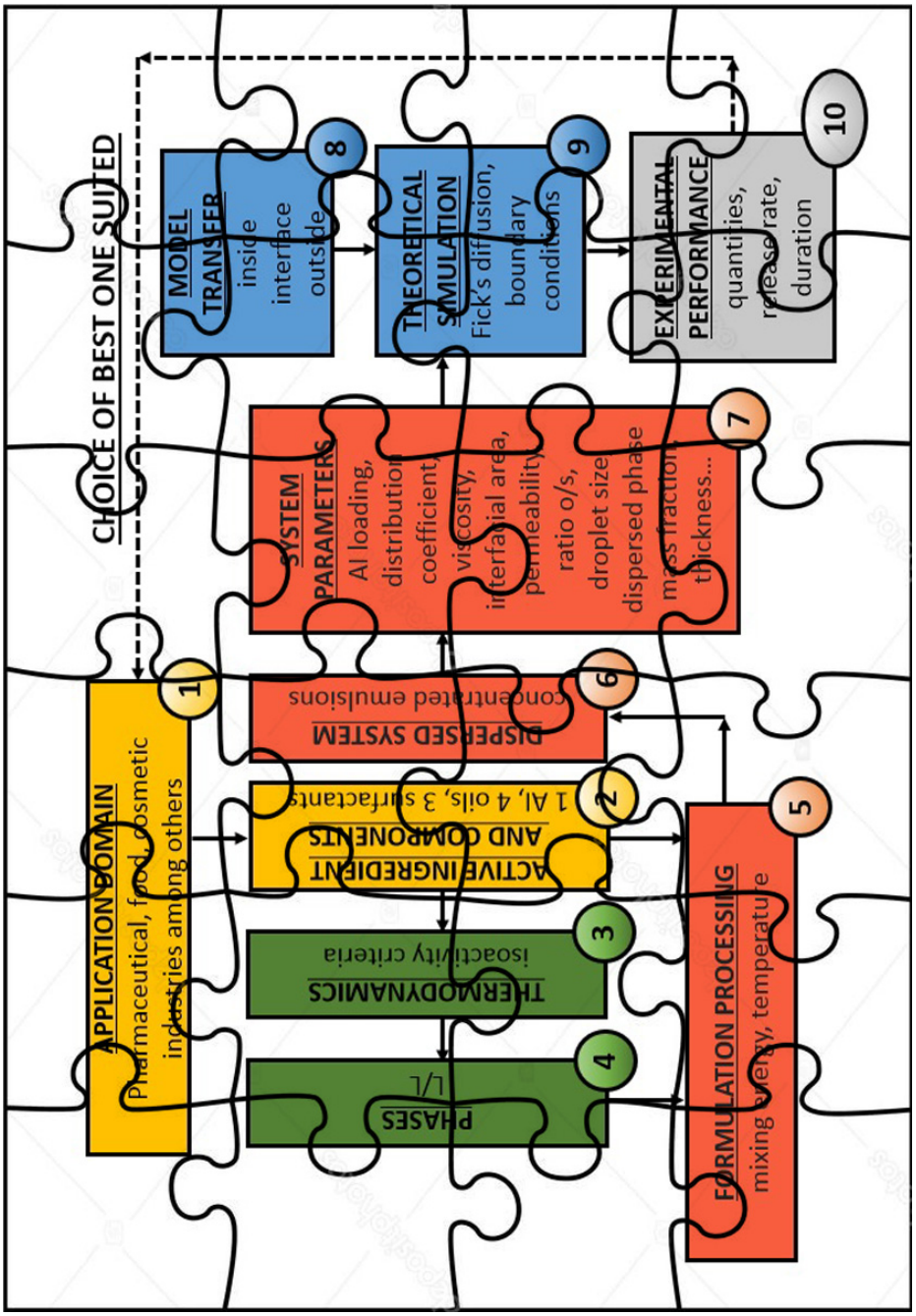

Fig. 5.5 Metaphorical puzzle representation of reverse engineering approach.

References

[1] LEK Achenie, R Gani, and V Venkatasubramanian. Genetic algorithms based camd. *Computer Aided Molecular Design: Theory and Practice*, 12:95, 2002.

[2] Jinhyun Hannah Lee and Yoon Yeo. Controlled drug release from pharmaceutical nanocarriers. *Chemical engineering science*, 125:75–84, 2015.

[3] Jennifer R Weiser and W Mark Saltzman. Controlled release for local delivery of drugs: barriers and models. *Journal of Controlled Release*, 190:664–673, 2014.

[4] Agnieszka Kowalczuk, Roza Trzcinska, Barbara Trzebicka, Axel HE Müller, Andrzej Dworak, and Christo B Tsvetanov. Loading of polymer nanocarriers: factors, mechanisms and applications. *Progress in Polymer Science*, 39(1):43–86, 2014.

[5] Nily Dan. Transport and release in nano-carriers for food applications. *Journal of Food Engineering*, 175:136–144, 2016.

[6] Martien A Cohen Stuart, Wilhelm TS Huck, Jan Genzer, Marcus Müller, Christopher Ober, Manfred Stamm, Gleb B Sukhorukov, Igal Szleifer, Vladimir V Tsukruk, Marek Urban, et al. Emerging applications of stimuli-responsive polymer materials. *Nature materials*, 9(2):101–113, 2010.

[7] David O Cooney. Effect of geometry on the dissolution of pharmaceutical tablets and other solids: surface detachment kinetics controlling. *AIChE Journal*, 18(2):446–449, 1972.

[8] Junichi Takahara, Kozo Takayama, and Tsuneji Nagai. Multi-objective simultaneous optimization technique based on an artificial neural network in sustained release formulations. *Journal of controlled release*, 49(1):11–20, 1997.

[9] J Siepmann and F Siepmann. Mathematical modeling of drug delivery. *International journal of pharmaceutics*, 364(2):328–343, 2008.

[10] Juergen Siepmann and Florence Siepmann. Modeling of diffusion controlled drug delivery. *Journal of Controlled Release*, 161(2):351–362, 2012.

[11] Paolo Colombo, Ruggero Bettini, and Nikolaos A Peppas. Observation of swelling process and diffusion front position during swelling in hydroxypropyl methyl cellulose (hpmc) matrices containing a soluble drug. *Journal of Controlled Release*, 61(1):83–91, 1999.

[12] Richard W Korsmeyer, Steven R Lustig, and Nikolaos A Peppas. Solute and penetrant diffusion in swellable polymers. i. mathematical modeling. *Journal of Polymer Science Part B: Polymer Physics*, 24(2):395–408, 1986.

[13] PI Lee. Diffusional release of a solute from a polymeric matrix—approximate analytical solutions. *Journal of membrane science*, 7(3):255–275, 1980.

[14] Juergen Siepmann, Nathalie Faisant, and Jean-Pierre Benoit. A new mathematical model quantifying drug release from bioerodible microparticles using monte carlo simulations. *Pharmaceutical Research*, 19(12):1885–1893, 2002.

[15] David Julian McClements. Advances in fabrication of emulsions with enhanced functionality using structural design principles. *Current Opinion in Colloid & Interface Science*, 17(5):235–245, 2012.

[16] Fernando P Bernardo and Pedro M Saraiva. A theoretical model for transdermal drug delivery from emulsions and its dependence upon formulation. *Journal of pharmaceutical sciences*, 97(9):3781–3809, 2008.

[17] R Farajzadeh, R Krastev, and Pacelli LJ Zitha. Foam film permeability: Theory and experiment. *Advances in colloid and interface science*, 137(1):27–44, 2008.

[18] Dana Constantinescu and Jürgen Gmehling. Addendum to "further development of modified unifac (dortmund): Revision and extension 6". *Journal of Chemical & Engineering Data*, 62(7):2230–2230, 2017.

[19] Fernando Barragán-Aroche and Enrique Bazúa-Rueda. Estrategias de convergencia para equilibrio líquido-líquido. el problema del" flash" negativo.

[20] Lutz Weber. Jchem base-chemaxon, 2008.

[21] David Julian McClements and Yan Li. Structured emulsion-based delivery systems: Controlling the digestion and release of lipophilic food components. *Advances in colloid and interface science*, 159(2):213–228, 2010.

[22] G Halász, T Virág, J Gyenis, T Blickle, and Z Csapó. Computer-aided generation of mathematical models of steady-state heat and mass transfer processes. *Computers & Chemical Engineering*, 3(1-4):519–521, 1979.

[23] Christianto Wibowo and Ka M Ng. Product-centered processing: Manufacture of chemical-based consumer products. *AIChE Journal*, 48(6):1212–1230, 2002.

[24] NA Peppas. Analysis of fickian and non-fickian drug release from polymers. 1985.

[25] Yuan H Zhao, Michael H Abraham, and Andreas M Zissimos. Fast calculation of van der waals volume as a sum of atomic and bond contributions and its application to drug compounds. *The Journal of organic chemistry*, 68(19):7368–7373, 2003.

[26] Bruce E Poling, John M Prausnitz, John P O'connell, et al. *The properties of gases and liquids*, volume 5. Mcgraw-hill New York, 2001.

[27] Jürgen Gmehling, Jiding Li, and Martin Schiller. A modified unifac model. 2. present parameter matrix and results for different thermodynamic properties. *Industrial & Engineering Chemistry Research*, 32(1):178–193, 1993.

[28] Dana Constantinescu and Jürgen Gmehling. Further development of modified unifac (dortmund): Revision and extension 6. *Journal of Chemical & Engineering Data*, 61(8):2738–2748, 2016.

[29] Elliot J. Chikofsky and James H Cross. Reverse engineering and design recovery: A taxonomy. *IEEE software*, 7(1):13–17, 1990.

[30] Hugo Bruneliere, Jordi Cabot, Grégoire Dupé, and Frédéric Madiot. Modisco: A model driven reverse engineering framework. *Information and Software Technology*, 56(8):1012–1032, 2014.

[31] Eldad Eilam. *Reversing: secrets of reverse engineering*. John Wiley & Sons, 2011.

[32] R Costa, GD Moggridge, and PM Saraiva. Chemical product engineering: an emerging paradigm within chemical engineering. *AIChE Journal*, 52(6):1976–1986, 2006.

[33] E Favre, L Marchal-Heusler, and M Kind. Chemical product engineering: research and educational challenges. *Chemical Engineering Research and Design*, 80(1):65–74, 2002.

[34] Rafiqul Gani, Kim Dam-Johansen, and Ka M Ng. Chemical product design: A brief overview. *Chemical product design: toward a perspective through case studies*, 2006.

[35] Guennadi M Ostrovsky, Luke EK Achenie, and Manish Sinha. On the solution of mixed-integer nonlinear programming models for computer aided molecular design. *Computers & chemistry*, 26(6):645–660, 2002.

[36] Jens Abildskov and GM Kontogeorgis. Chemical product design: A new challenge of applied thermodynamics. *Chemical Engineering Research and Design*, 82(11):1505–1510, 2004.

[37] JM Prausnitz. Thermodynamics and the other chemical engineering sciences: old models for new chemical products and processes. *Fluid phase equilibria*, 158:95–111, 1999.

[38] Fernando P Bernardo and Pedro M Saraiva. Value of information analysis in product/process design. *Computer Aided Chemical Engineering*, 18:151–156, 2004.

[39] Ignacio E Grossmann. Challenges in the new millennium: product discovery and design, enterprise and supply chain optimization, global life cycle assessment. *Computers & Chemical Engineering*, 29(1):29–39, 2004.

[40] Gary Blau, Bharat Mehta, Shantanu Bose, Joe Pekny, Gavin Sinclair, Kay Keunker, and Paul Bunch. Risk management in the development of new products in highly regulated industries. *Computers & Chemical Engineering*, 24(2-7):659–664, 2000.

[41] Christos T Maravelias and Ignacio E Grossmann. Simultaneous planning for new product development and batch manufacturing facilities. *Industrial & engineering chemistry research*, 40(26):6147–6164, 2001.

[42] Dharmashankar Subramanian, Joseph F Pekny, Gintaras V Reklaitis, and Gary E Blau. Simulation-optimization framework for stochastic optimization of r&d pipeline management. *AIChE Journal*, 49(1):96–112, 2003.

[43] Anna Kogan and Nissim Garti. Microemulsions as transdermal drug delivery vehicles. *Advances in colloid and interface science*, 123:369–385, 2006.

[44] Kinam Park. Controlled drug delivery systems: past forward and future back. *Journal of Controlled Release*, 190:3–8, 2014.

[45] Ronald A Siegel and Michael J Rathbone. Overview of controlled release mechanisms. In *Fundamentals and Applications of Controlled Release Drug Delivery*, pages 19–43. Springer, 2012.

[46] Sara A Abouelmagd, Hyesun Hyun, and Yoon Yeo. Extracellularly activatable nanocarriers for drug delivery to tumors. *Expert opinion on drug delivery*, 11(10):1601–1618, 2014.

[47] Miles C Braithwaite, Charu Tyagi, Lomas K Tomar, Pradeep Kumar, Yahya E Choonara, and Viness Pillay. Nutraceutical-based therapeutics and formulation strategies augmenting their efficiency to complement modern medicine: An overview. *Journal of Functional Foods*, 6:82–99, 2014.

[48] Eric Dickinson and Martin E Leser. *Food colloids: self-assembly and material science*, volume 308. Royal Society of chemistry, 2007.

[49] Inteaz Alli Catherine N. Mulligan Bernard F. Gibbs, Selim Kermasha. Encapsulation in the food industry: a review. *International journal of food sciences and nutrition*, 50(3):213–224, 1999.

[50] John N Coupland and John E Hayes. Physical approaches to masking bitter taste: lessons from food and pharmaceuticals. *Pharmaceutical research*, 31(11):2921–2939, 2014.

[51] Mahmoud Elsabahy and Karen L Wooley. Design of polymeric nanoparticles for biomedical delivery applications. *Chemical Society Reviews*, 41(7):2545–2561, 2012.

[52] Hua Wei, Ren-Xi Zhuo, and Xian-Zheng Zhang. Design and development of polymeric micelles with cleavable links for intracellular drug delivery. *Progress in polymer Science*, 38(3):503–535, 2013.

[53] Jeffrey A Hubbell and Ashutosh Chilkoti. Nanomaterials for drug delivery. *Science*, 337(6092):303–305, 2012.

[54] Ru Cheng, Fenghua Meng, Chao Deng, Harm-Anton Klok, and Zhiyuan Zhong. Dual and multi-stimuli responsive polymeric nanoparticles for programmed site-specific drug delivery. *Biomaterials*, 34(14):3647–3657, 2013.

[55] Jianbin Tang, Yuqi Sheng, Hongjie Hu, and Youqing Shen. Macromolecular mri contrast agents: structures, properties and applications. *Progress in Polymer Science*, 38(3):462–502, 2013.

[56] Tennyson L Doane and Clemens Burda. The unique role of nanoparticles in nanomedicine: imaging, drug delivery and therapy. *Chemical Society Reviews*, 41(7):2885–2911, 2012.

[57] Joaquim Miguel Oliveira, António José Salgado, Nuno Sousa, João Filipe Mano, and Rui Luís Reis. Dendrimers and derivatives as a potential therapeutic tool in regenerative medicine strategies—a review. *Progress in Polymer Science*, 35(9):1163–1194, 2010.

[58] Jae Hyung Park, Seulki Lee, Jong-Ho Kim, Kyeongsoon Park, Kwangmeyung Kim, and Ick Chan Kwon. Polymeric nanomedicine for cancer therapy. *Progress in Polymer Science*, 33(1):113–137, 2008.

[59] M Talha Gokmen and Filip E Du Prez. Porous polymer particles—a comprehensive guide to synthesis, characterization, functionalization and applications. *Progress in polymer science*, 37(3):365–405, 2012.

[60] Mikhail Motornov, Yuri Roiter, Ihor Tokarev, and Sergiy Minko. Stimuli-responsive nanoparticles, nanogels and capsules for integrated multifunctional intelligent systems. *Progress in polymer science*, 35(1):174–211, 2010.

[61] Robert Langer and Nikolaos Peppas. Chemical and physical structure of polymers as carriers for controlled release of bioactive agents: a review. *Journal of Macromolecular Science-Reviews in Macromolecular Chemistry and Physics*, 23(1):61–126, 1983.

[62] Simon Herrlich, Sven Spieth, Stephan Messner, and Roland Zengerle. Osmotic micropumps for drug delivery. *Advanced drug delivery reviews*, 64(14):1617–1627, 2012.

[63] NA Peppas, P Bures, Ws Leobandung, and H Ichikawa. Hydrogels in pharmaceutical formulations. *European journal of pharmaceutics and biopharmaceutics*, 50(1):27–46, 2000.

[64] Chien-Chi Lin and Andrew T Metters. Hydrogels in controlled release formulations: network design and mathematical modeling. *Advanced drug delivery reviews*, 58(12):1379–1408, 2006.

[65] Ping I Lee. Novel approach to zero-order drug delivery via immobilized nonuniform drug distribution in glassy hydrogels. *Journal of pharmaceutical sciences*, 73(10):1344–1347, 1984.

[66] Santanu Kaity, Jinu Isaac, and Animesh Ghosh. Interpenetrating polymer network of locust bean gum-poly (vinyl alcohol) for controlled release drug delivery. *Carbohydrate polymers*, 94(1):456–467, 2013.

[67] Soo Hyeon Lee, Hyejung Mok, Yuhan Lee, and Tae Gwan Park. Self-assembled sirna–plga conjugate micelles for gene silencing. *Journal of controlled release*, 152(1):152–158, 2011.

[68] Mani Prabaharan, Jamison J Grailer, Srikanth Pilla, Douglas A Steeber, and Shaoqin Gong. Amphiphilic multi-arm-block copolymer conjugated with doxorubicin via ph-sensitive hydrazone bond for tumor-targeted drug delivery. *Biomaterials*, 30(29):5757–5766, 2009.

[69] Hyuk Sang Yoo and Tae Gwan Park. Biodegradable polymeric micelles composed of doxorubicin conjugated plga–peg block copolymer. *Journal of controlled Release*, 70(1):63–70, 2001.

[70] Friederike von Burkersroda, Luise Schedl, and Achim Göpferich. Why degradable polymers undergo surface erosion or bulk erosion. *Biomaterials*, 23(21):4221–4231, 2002.

[71] Wen-Chuan Lee, I Chu, et al. Preparation and degradation behavior of polyanhydrides nanoparticles. *Journal of Biomedical Materials Research Part B: Applied Biomaterials*, 84(1):138–146, 2008.

[72] Susanne Fredenberg, Marie Wahlgren, Mats Reslow, and Anders Axelsson. The mechanisms of drug release in poly (lactic-co-glycolic acid)-based drug delivery systems—a review. *International journal of pharmaceutics*, 415(1):34–52, 2011.

[73] Jindřich Kopeček. Controlled biodegradability of polymers—a key to drug delivery systems. *Biomaterials*, 5(1):19–25, 1984.

[74] Scott H Medina, Maxim V Chevliakov, Gopinath Tiruchinapally, Yasemin Yuksel Durmaz, Sibu P Kuruvilla, and Mohamed EH ElSayed. Enzyme-activated nanoconjugates for tunable release of doxorubicin in hepatic cancer cells. *Biomaterials*, 34(19):4655–4666, 2013.

[75] Kyung Hyun Min, Jong-Ho Kim, Sang Mun Bae, Hyeri Shin, Min Sang Kim, Sangjin Park, Hyejung Lee, Rang-Woon Park, In-San Kim, Kwangmeyung Kim, et al. Tumoral acidic ph-responsive mpeg-poly (β-amino ester) polymeric micelles for cancer targeting therapy. *Journal of Controlled Release*, 144(2):259–266, 2010.

[76] Cong Chang, Hua Wei, Chang-Yun Quan, Yong-Yong Li, Jia Liu, Zong-Chun Wang, Si-Xue Cheng, Xian-Zheng Zhang, and Ren-Xi Zhuo. Fabrication of thermosensitive pcl-pnipaam-pcl triblock copolymeric micelles for drug delivery. *Journal of Polymer Science Part A: Polymer Chemistry*, 46(9):3048–3057, 2008.

[77] J Siepmann and NA Peppas. Modeling of drug release from delivery systems based on hydroxypropyl methylcellulose (hpmc). *Advanced drug delivery reviews*, 48(2-3):139–157, 2001.

[78] J Siepmann and A Göpferich. Mathematical modeling of bioerodible, polymeric drug delivery systems. *Advanced drug delivery reviews*, 48(2):229–247, 2001.

[79] Davis Yohanes Arifin, Lai Yeng Lee, and Chi-Hwa Wang. Mathematical modeling and simulation of drug release from microspheres: implications to drug delivery systems. *Advanced drug delivery reviews*, 58(12):1274–1325, 2006.

[80] T Higuchi. Physical chemical analysis of percutaneous absorption process from creams and ointments. *J. Soc. Cosmet. Chem*, 11:85–97, 1960.

[81] Takeru Higuchi. Rate of release of medicaments from ointment bases containing drugs in suspension. *Journal of pharmaceutical sciences*, 50(10):874–875, 1961.

[82] J Siepmann, A Ainaoui, JM Vergnaud, and R Bodmeier. Calculation of the dimensions of drug–polymer devices based on diffusion parameters. *Journal of pharmaceutical sciences*, 87(7):827–832, 1998.

[83] Balaji Narasimhan. Mathematical models describing polymer dissolution: consequences for drug delivery. *Advanced Drug Delivery Reviews*, 48(2):195–210, 2001.

[84] Göran Frenning and Maria Strømme. Drug release modeled by dissolution, diffusion, and immobilization. *International journal of pharmaceutics*, 250(1):137–145, 2003.

[85] V Lemaire, J Belair, and P Hildgen. Structural modeling of drug release from biodegradable porous matrices based on a combined diffusion/erosion process. *International journal of pharmaceutics*, 258(1):95–107, 2003.

[86] Y Zhou and XY Wu. Modeling and analysis of dispersed-drug release into a finite medium from sphere ensembles with a boundary layer. *Journal of controlled release*, 90(1):23–36, 2003.

[87] Göran Frenning, Ulrika Brohede, and Maria Strømme. Finite element analysis of the release of slowly dissolving drugs from cylindrical matrix systems. *Journal of controlled release*, 107(2):320–329, 2005.

[88] Chandrashekar Raman, Cory Berkland, Kyekyoon Kevin Kim, and Daniel W Pack. Modeling small-molecule release from plg microspheres: effects of polymer degradation and nonuniform drug distribution. *Journal of Controlled Release*, 103(1):149–158, 2005.

[89] Philip L Ritger and Nikolaos A Peppas. A simple equation for description of solute release i. fickian and non-fickian release from non-swellable devices in the form of slabs, spheres, cylinders or discs. *Journal of controlled release*, 5(1):23–36, 1987.

[90] Philip L Ritger and Nikolaos A Peppas. A simple equation for description of solute release ii. fickian and anomalous release from swellable devices. *Journal of controlled release*, 5(1):37–42, 1987.

[91] HB Hopfenberg. Controlled release from erodible slabs, cylinders, and spheres. ACS Publications, 1976.

[92] Yixin Chen, Troy W McCall, Anand R Baichwal, and Marvin C Meyer. The application of an artificial neural network and pharmacokinetic simulations in the design of controlled-release dosage forms. *Journal of controlled release*, 59(1):33–41, 1999.

[93] Svetlana Ibrić, Milica Jovanović, Zorica Djurić, Jelena Parojčić, and Ljiljana Solomun. The application of generalized regression neural network in the modeling and optimization of aspirin extended release tablets with eudragit® rs po as matrix substance. *Journal of Controlled Release*, 82(2):213–222, 2002.

[94] Abdollahi Ghaffari, H Abdollahi, MR Khoshayand, I Soltani Bozchalooi, A Dadgar, and M Rafiee-Tehrani. Performance comparison of neural network training algorithms in modeling of bimodal drug delivery. *International journal of pharmaceutics*, 327(1):126–138, 2006.

[95] Qun Shao, Raymond C Rowe, and Peter York. Comparison of neurofuzzy logic and neural networks in modelling experimental data of an immediate release tablet formulation. *European journal of pharmaceutical sciences*, 28(5):394–404, 2006.

[96] Emmanuelle Cauchetier, M Deniau, H Fessi, A Astier, and M Paul. Atovaquone-loaded nanocapsules: influence of the nature of the polymer on their in vitro characteristics. *International journal of pharmaceutics*, 250(1):273–281, 2003.

[97] John Crank. *The mathematics of diffusion*. Oxford university press, 1979.

[98] Richard William Baker et al. *Controlled release of biologically active agents.* John Wiley & Sons, 1987.

[99] Per Borgquist, Gunnar Zackrisson, Bernt Nilsson, and Anders Axelsson. Simulation and parametric study of a film-coated controlled-release pharmaceutical. *Journal of controlled release*, 80(1):229–245, 2002.

[100] Jean-Maurice Vergnaud. *Controlled drug release of oral dosage forms*. CRC Press, 1993.

[101] T Higuchi. Mechanism of sustained-action medication. theoretical analysis of rate of release of solid drugs dispersed in solid matrices. *Journal of pharmaceutical sciences*, 52(12):1145–1149, 1963.

[102] Liang-tseng Fan and Satish K Singh. *Controlled release: A quantitative treatment*, volume 13. Springer Science & Business Media, 2012.

[103] E Doelker. Water-swollen cellulose derivatives in pharmacy. *Hydrogels in medicine and pharmacy*, 2:115–160, 1987.

[104] Hiroshi Fujita. Diffusion in polymer-diluent systems. *Fortschritte Der Hochpolymeren-Forschung*, pages 1–47, 1961.

[105] Robert TC Ju, Phillip R Nixon, Mahesh V Patel, and Donald M Tong. Drug release from hydrophilic matrices. 2. a mathematical model based on the polymer disentanglement concentration and the diffusion layer. *Journal of pharmaceutical sciences*, 84(12):1464–1477, 1995.

[106] J Siepmann and NA Peppas. Hydrophilic matrices for controlled drug delivery: an improved mathematical model to predict the resulting drug release kinetics (the "sequential layer" model). *Pharmaceutical Research*, 17(10):1290–1298, 2000.

[107] Balaji Narasimhan, Nikolaos A Peppas, et al. Disentanglement and reptation during dissolution of rubbery polymers. *Journal of Polymer Science-B-Polymer Physics Edition*, 34(5):947–962, 1996.

[108] Kyriacos Zygourakis and Pauline A Markenscoff. Computer-aided design of bioerodible devices with optimal release characteristics: a cellular automata approach. *Biomaterials*, 17(2):125–135, 1996.

[109] N Faisant, J Siepmann, J Richard, and JP Benoit. Mathematical modeling of drug release from bioerodible microparticles: effect of gamma-irradiation. *European Journal of Pharmaceutics and Biopharmaceutics*, 56(2):271–279, 2003.

[110] Jean Bézivin. On the unification power of models. *Software and Systems Modeling*, 4(2):171–188, 2005.

[111] Elisa Conte, Rafiqul Gani, and Ka Ming Ng. Design of formulated products: a systematic methodology. *AIChE journal*, 57(9):2431–2449, 2011.

[112] Jens M Sørensen, Thomas Magnussen, Peter Rasmussen, and Aage Fredenslund. Liquid—liquid equilibrium data: Their retrieval, correlation and prediction part ii: Correlation. *Fluid Phase Equilibria*, 3(1):47–82, 1979.

[113] Meritxell Llinàs, Gabriela Calderó, M José García-Celma, Alessandro Patti, and Conxita Solans. New insights on the mechanisms of drug release from highly concentrated emulsions. *Journal of colloid and interface science*, 394:337–345, 2013.

[114] Gabriela Calderó, Meritxell Llinàs, María José García-Celma, and Conxita Solans. Studies on controlled release of hydrophilic drugs from w/o high internal phase ratio emulsions. *Journal of pharmaceutical sciences*, 99(2):701–711, 2010.

[115] H Maekawa, Jordi Esquena, Samuel Bishop, Conxita Solans, and Bradley F Chmelka. Meso/macroporous inorganic oxide monoliths from polymer foams. *Advanced Materials*, 15(7-8):591–596, 2003.

[116] Laia Espelt, Pere Clapés, Jordi Esquena, Albert Manich, and Conxita Solans. Enzymatic carbon- carbon bond formation in water-in-oil highly concentrated emulsions (gel emulsions). *Langmuir*, 19(4):1337–1346, 2003.

[117] Nina S Nielsen, Arni Petersen, Anne S Meyer, Maike Timm-Heinrich, and Charlotte Jacobsen. Effects of lactoferrin, phytic acid, and edta on oxidation in two food emulsions enriched with long-chain polyunsaturated fatty acids. *Journal of agricultural and food chemistry*, 52(25):7690–7699, 2004.

[118] AP Guimarães, DAS Maia, RS Araújo, CL Cavalcante Jr, and HB de Sant'Ana. Destabilization and recuperability of oil used in the formulation of concentrated emulsions and cutting fluids. *Chemical and Biochemical Engineering Quarterly*, 24(1):43–49, 2010.

[119] Carin Malmborg, Daniel Topgaard, and Olle Söderman. Nmr diffusometry and the short gradient pulse limit approximation. *Journal of Magnetic Resonance*, 169(1):85–91, 2004.

[120] Justin Ashworth, Elisabeth J Wurtmann, and Nitin S Baliga. Reverse engineering systems models of regulation: discovery, prediction and mechanisms. *Current opinion in biotechnology*, 23(4):598–603, 2012.

[121] Edward Lansing Cussler. *Diffusion: mass transfer in fluid systems*. Cambridge university press, 2009.

[122] RP Borwankar, CC Chan, DT Wasan, RM Kurzeja, ZM Gu, and NN Li. Analysis of the effect of internal phase leakage on liquid membrane separations. *AIChE journal*, 34(5):753–762, 1988.

[123] Linda R De Young and Ken A Dill. Solute partitioning into lipid bilayer membranes. *Biochemistry*, 27(14):5281–5289, 1988.

[124] Samir Mitragotri, Mark E Johnson, Daniel Blankschtein, and Robert Langer. An analysis of the size selectivity of solute partitioning, diffusion, and permeation across lipid bilayers. *Biophysical journal*, 77(3):1268–1283, 1999.

[125] Tian-Xiang Xiang and Bradley D Anderson. Permeability of acetic acid across gel and liquid-crystalline lipid bilayers conforms to free-surface-area theory. *Biophysical journal*, 72(1):223–237, 1997.

[126] Abdel-Halim Ghanem, WI Higuchi, and AP Simonelli. Interfacial barriers in interphase transport: Retardation of the transport of diethylphthalate across the hexadecane-water interface by an adsorbed gelatin film. *Journal of pharmaceutical sciences*, 58(2):165–174, 1969.

[127] Stephanie R Dungan, Beverly H Tai, and Natalia I Gerhardt. Transport mechanisms in the micellar solubilization of alkanes in oil-in-water emulsions. *Colloids and Surfaces A: Physicochemical and Engineering Aspects*, 216(1):149–166, 2003.

[128] CR Wilke and Pin Chang. Correlation of diffusion coefficients in dilute solutions. *AIChE Journal*, 1(2):264–270, 1955.

[129] Johannes Lyklema. *Fundamentals of interface and colloid science: soft colloids*, volume 5. Academic press, 2005.

[130] Aage Fredenslund, Russell L Jones, and John M Prausnitz. Group-contribution estimation of activity coefficients in nonideal liquid mixtures. *AIChE Journal*, 21(6):1086–1099, 1975.

[131] A Bondi. Physical properties of molecular liquids, crystals and glasses. *Wlley: New York*, 1968.

[132] Henrik K Hansen, Peter Rasmussen, Aage Fredenslund, Martin Schiller, and Jürgen Gmehling. Vapor-liquid equilibria by unifac group contribution. 5. revision and extension. *Industrial & Engineering Chemistry Research*, 30(10):2352–2355, 1991.

[133] Josef P Novák, Jaroslav Matouš, and Jiří Pick. *Liquid-liquid equilibria*, volume 7. Elsevier Science Ltd, 1987.

[134] Zhigang Lei, Biaohua Chen, Chengyue Li, and Hui Liu. Predictive molecular thermodynamic models for liquid solvents, solid salts, polymers, and ionic liquids. *Chemical reviews*, 108(4):1419–1455, 2008.

[135] I Kikic, P Alessi, Peter Rasmussen, and Aage Fredenslund. On the combinatorial part of the unifac and uniquac models. *The Canadian Journal of Chemical Engineering*, 58(2):253–258, 1980.

[136] Eugene R Thomas and Charles A Eckert. Prediction of limiting activity coefficients by a modified separation of cohesive energy density model and unifac. *Industrial & Engineering Chemistry Process Design and Development*, 23(2):194–209, 1984.

[137] Jürgen Lohmann, Ralph Joh, and Jürgen Gmehling. From unifac to modified unifac (dortmund). *Industrial & engineering chemistry research*, 40(3):957–964, 2001.

[138] Jürgen Gmehling, Jürgen Lohmann, Antje Jakob, Jiding Li, and Ralph Joh. A modified unifac (dortmund) model. 3. revision and extension. *Industrial & engineering chemistry research*, 37(12):4876–4882, 1998.

[139] Jürgen Gmehling, Roland Wittig, Jürgen Lohmann, and Ralph Joh. A modified unifac (dortmund) model. 4. revision and extension. *Industrial & engineering chemistry research*, 41(6):1678–1688, 2002.

[140] Antje Jakob, Hans Grensemann, Jürgen Lohmann, and Jürgen Gmehling. Further development of modified unifac (dortmund): revision and extension 5. *Industrial & engineering chemistry research*, 45(23):7924–7933, 2006.

[141] Andreas Zuend and John H Seinfeld. A practical method for the calculation of liquid–liquid equilibria in multicomponent organic–water–electrolyte systems using physicochemical constraints. *Fluid Phase Equilibria*, 337:201–213, 2013.

[142] Lee E Baker, Alan C Pierce, Kraemer D Luks, et al. Gibbs energy analysis of phase equilibria. *Society of Petroleum Engineers Journal*, 22(05):731–742, 1982.

[143] HH Rachford Jr, JD Rice, et al. Procedure for use of electronic digital computers in calculating flash vaporization hydrocarbon equilibrium. *Journal of Petroleum Technology*, 4(10):19–3, 1952.

[144] Curtis H Whitson and Michael L Michelsen. The negative flash. *Fluid Phase Equilibria*, 53:51–71, 1989.

[145] John M Prausnitz. *Computer calculations for multicomponent vapor-liquid and liquid-liquid equilibria*. Prentice Hall, 1980.

[146] Viviana Consonni, Roberto Todeschini, and Manuela Pavan. Structure/response correlations and similarity/diversity analysis by getaway descriptors. 1. theory of the novel 3d molecular descriptors. *Journal of Chemical Information and Computer Sciences*, 42(3):682–692, 2002.

[147] John Bruce Irving. *Viscosity of binary liquid mixtures: a survey of mixture equations*. National Engineering Laboratory, 1977.

[148] Y Gaston-Bonhomme, P Petrino, and JL Chevalier. Unifac—visco group contribution method for predicting kinematic viscosity: extension and temperature dependence. *Chemical engineering science*, 49(11):1799–1806, 1994.

[149] JL Chevalier, P Petrino, and Y Gaston-Bonhomme. Estimation method for the kinematic viscosity of a liquid-phase mixture. *Chemical engineering science*, 43(6):1303–1309, 1988.

[150] MT Tyn and WF Calus. Estimating liquid molal volume. *Processing*, 21(4):16–17, 1975.

[151] Aksel L Lydersen and Madison Engineering Experiment Station. *Estimation of critical properties of organic compounds by the method of group contributions*. University of Wisconsin, 1955.

[152] Kevin G Joback. *A unified approach to physical property estimation using multivariate statistical techniques*. PhD thesis, Massachusetts Institute of Technology, 1984.

[153] Kevin G Joback and Robert C Reid. Estimation of pure-component properties from group-contributions. *Chemical Engineering Communications*, 57(1-6):233–243, 1987.

[154] Charalambos G Varelas, David G Dixon, and Carol A Steiner. Mathematical model of mass transport through dispersed-phase polymer networks. *AIChE Journal*, 41(4):805–811, 1995.

[155] Charalambos G Varelas, David G Dixon, and Carol A Steiner. Zero-order release from biphasic polymer hydrogels. *Journal of controlled release*, 34(3):185–192, 1995.

[156] Mario Grassi, Gabriele Grassi, Romano Lapasin, and Italo Colombo. *Understanding drug release and absorption mechanisms: A physical and mathematical approach*. CRC Press, 2006.

[157] Jens T Carstensen. *Modeling and data treatment in the pharmaceutical sciences*. CRC Press, 1996.

[158] Paolo Freguglia. Modelli matematici nelle scienze biologiche, 1998.

[159] R Gani, LEK Achenie, and V Venkatasubramanian. Introduction to camd. 2003.

[160] Renata M Dębowska, Aleksandra Kaszuba, Iwona Michalak, Agata Dzwigałowska, Czanita Cieścińska, Elżbieta Jakimiuk, Joanna Zielińska, and Andrzej Kaszuba. Evaluation of the efficacy and tolerability of mandelic acid-containing cosmetic formulations for acne skin care. *Dermatology Review/Przeglad Dermatologiczny*, 102(3), 2015.

[161] Frank H Clarke and Natalie M Cahoon. Ionization constants by curve fitting: Determination of partition and distribution coefficients of acids and bases and their ions. *Journal of pharmaceutical sciences*, 76(8):611–620, 1987.

[162] G Calderó, MJ García-Celma, C Solans, and R Pons. Effect of ph on mandelic acid diffusion in water in oil highly concentrated emulsions (gel-emulsions). *Langmuir*, 16(4):1668–1674, 2000.

[163] David S Wishart, Craig Knox, An Chi Guo, Roman Eisner, Nelson Young, Bijaya Gautam, David D Hau, Nick Psychogios, Edison Dong, Souhaila Bouatra, et al. Hmdb: a knowledgebase for the human metabolome. *Nucleic acids research*, 37(suppl_1):D603–D610, 2008.

[164] Michael P Aronson and Michael F Petko. Highly concentrated water-in-oil emulsions: Influence of electrolyte on their properties and stability. *Journal of colloid and interface science*, 159(1):134–149, 1993.

[165] Adnan Azeem, Zeenat Iqbal Khan, M Aqil, Farhan Jalees Ahmad, Roop Kishan Khar, and Sushama Talegaonkar. Microemulsions as a surrogate carrier for dermal drug delivery. *Drug development and industrial pharmacy*, 35(5):525–547, 2009.

[166] High Production Volume HPV Challenge and EPA All. Federal register notice; voluntary children's chemical evaluation program.

[167] Myristyl Myristate. Final report on the safety assessment of myristyl myristate and isopropyl myristate. *J Am Coll Toxicol*, 1:55–80, 1982.

[168] Mahesh V Patel and Feng-Jing Chen. Solid carriers for improved delivery of active ingredients in pharmaceutical compositions, June 19 2001. US Patent 6,248,363.

[169] C Hinton. Alkoxylated nonionic surfactants. chapter: 3. *The Chemistry and Manufacture of Cosmetics*, 3:15–27, 2002.

[170] Andrea Saltelli, Marco Ratto, Terry Andres, Francesca Campolongo, Jessica Cariboni, Debora Gatelli, Michaela Saisana, and Stefano Tarantola. *Global sensitivity analysis: the primer*. John Wiley & Sons, 2008.

[171] David J Pannell. Sensitivity analysis of normative economic models: theoretical framework and practical strategies. *Agricultural economics*, 16(2):139–152, 1997.

[172] A Bahremand and F De Smedt. Distributed hydrological modeling and sensitivity analysis in torysa watershed, slovakia. *Water Resources Management*, 22(3):393–408, 2008.

[173] Mary C Hill, Dmitri Kavetski, Martyn Clark, Ming Ye, Mazdak Arabi, Dan Lu, Laura Foglia, and Steffen Mehl. Practical use of computationally frugal model analysis methods. *Groundwater*, 54(2):159–170, 2016.

[174] Mary C Hill and Claire R Tiedeman. *Effective groundwater model calibration: with analysis of data, sensitivities, predictions, and uncertainty*. John Wiley & Sons, 2006.

[175] Michael J Berry and Gordon Linoff. *Data mining techniques: for marketing, sales, and customer support*. John Wiley & Sons, Inc., 1997.

[176] Donald W Marquardt. An algorithm for least-squares estimation of nonlinear parameters. *Journal of the society for Industrial and Applied Mathematics*, 11(2):431–441, 1963.

[177] Jorge J Moré. The levenberg-marquardt algorithm: implementation and theory. In *Numerical analysis*, pages 105–116. Springer, 1978.

[178] Tapash K Ghosh and Bhaskara R Jasti. *Theory and practice of contemporary pharmaceutics*. CRC press, 2004.

[179] Leland Wilkinson. Revising the pareto chart. *The American Statistician*, 60(4):332–334, 2006.

[180] Jean-Louis Salager, RE Antón, José Maria Anderez, and Jean-Marie Aubry. Formulation des micro-émulsions par la méthode hld. *Techniques de l'Ingénieur*, 157:2001, 2001.

[181] Suwimon Ariyaprakai and Stephanie R Dungan. Contribution of molecular pathways in the micellar solubilization of monodisperse emulsion droplets. *Langmuir*, 24(7):3061–3069, 2008.

[182] Emilio Paruta-Tuarez, Hala Fersadou, Véronique Sadtler, Philippe Marchal, Lionel Choplin, Christophe Baravian, and Christophe Castel. Highly concentrated emulsions: 1. average drop size determination by analysis of incoherent polarized steady light transport. *Journal of colloid and interface science*, 346(1):136–142, 2010.

[183] Wyatt J Musnicki, Stephanie R Dungan, and Ronald J Phillips. Multicomponent diffusion in solute-containing micelle and microemulsion solutions. *Langmuir*, 30(37):11019–11030, 2014.

[184] Harry H Harman. *Modern factor analysis*. University of Chicago Press, 1976.

Appendix A

UNIFAC parameters for modeling activity coefficients

UNIFAC (Revision and Extension 5)

↘ Hansen et al (1991)

Modified UNIFAC (Dortmund) (Revision and Extension 2)

↘ Gmehling et al (1993)

Modified UNIFAC (Dortmund) (Revision and Extension 6)

↘ Constantinescu et Gmehling (2016)

Table A.1 Group Specifications and Sample Group Assignments for UNIFAC Method (Hansen, et al. 1991). Part (1/4). Taken from [26].

Group number Secondary	Main	R_k	Q_k	Name	Sample Assignments = (Number of Ocurrences) × (Secondary Group Number)
1	1	CH_3	0.9011	0.848	Hexane = (2)(1) + (4)(2)
1	2	CH_2	0.6744	0.54	2-Methylpropane = (3)(1) + (1)(3)
1	3	CH	0.4469	0.228	Neopentane = (4)(1) + (1)(4)
1	4	C	0.2195	0	2,2,4-Trimethylpentane = (5)(1) + (1)(2) + (1)(3) + (1)(4)
2	5	CH_2=CH	1.3454	1.176	3-Methyl-1-hexene = (2)(1) + (2)(2) + (1)(3) + (1)(5)
2	6	CH=CH	1.1167	0.867	Hexene-2 = (2)(1) + (2)(2) + (1)(6)
2	7	CH_2=C	1.1173	0.988	2-Methyl-1-butene = (2)(1) + (1)(2) + (1)(7)
2	8	CH=C	0.8886	0.676	2-Methyl-2-butene = (3)(1) + (1)(8)
2	70	C=C	0.6605	0.485	2,3-Dimethylbutene = (4)(1) + (1)(70)
3	9	ACH	0.5313	0.4	Benzene = (6)(9)
3	10	AC	0.3652	0.12	Styrene = (1)(5) + (5)(9) + (1)(10)
4	11	$ACCH_3$	1.2663	0.968	Toluene = (5)(9) + (1)(11)
4	12	$ACCH_2$	1.0396	0.66	Ethylbenzene = (1)(1) + (5)(9) + (1)(12)
4	13	ACCH	0.8121	0.348	Cumene = (2)(1) + (5)(9) + (1)(13)
5	14	OH	1	1.2	Ethanol = (1)(1) + (1)(2) + (1)(14)
6	15	CH_3OH	1.4311	1.432	Methanol = (1)(15)
7	16	H_2O	0.92	1.4	Water = (1)(16)
8	17	ACOH	0.8952	0.68	Phenol = (5)(9) + (1)(17)
9	18	CH_3CO	1.6724	1.488	Methylethylketone = (1)(1) + (1)(2) + (1)(18)
9	19	CH_2CO	1.4457	1.18	Ethylphenylketone = (1)(1) + (1)(19) + (5)(9) + (1)(10)
10	20	CHO	0.998	0.948	Hexanal = (1)(1) + (4)(2) + (1)(20)
11	21	CH_3COO	1.9031	1.728	Butyl acetate = (1)(1) + (3)(2) + (1)(21)
11	22	CH_2COO	1.6764	1.42	Methyl propionate = (2)(1) + (1)(22)
12	23	HCOO	1.242	1.188	Ethyl formate = (1)(1) + (1)(2) + (1)(23)

Table A.2 UNIFAC Method(Hansen, et al. 1991). Part (2/4). Taken from [26].

Group number		Volume	Area		Sample Assignments = (Number of Ocurrences) ×
Secondary	Main	R_k	Q_k	Name	(Secondary Group Number)
13	24	CH_3O	1.145	1.088	Dimethyl ether = (1)(1) + (1)(24)
13	25	CH_2O	0.9183	0.78	Diethyl ether = (2)(1) + (1)(2) + (1)(25)
13	26	CHO	0.6908	0.468	Diisopropyl ether = (4)(1) + (1)(3) + (1)(26)
13	27	THF	0.9183	1.1	Tetrahydrofuran = (3)(2) + (1)(27)
14	28	CH_3NH_2	1.5959	1.544	Methylamine = (1)(28)
14	29	CH_2NH_2	1.3692	1.236	Ethylamine = (1)(1) + (1)(29)
14	30	$CHNH_2$	1.1417	0.924	Isopropylamine = (2)(1) + (1)(30)
15	31	CH_3NH	1.4337	1.244	Dimethyl amine = (1)(1) + (1)(31)
15	32	CH_2NH	1.207	0.936	Diethylamine = (2)(1) + (1)(2) + (1)(32)
15	33	CHNH	0.9795	0.624	Diisopropylamine = (4)(1) + (1)(3) + (1)(33)
16	34	CH_3N	1.1865	0.94	Trimethylamine = (2)(1) + (1)(34)
16	35	CH_2N	0.9597	0.632	Triethylamine = (3)(1) + (2)(2) + (1)(35)
17	36	$ACNH_2$	1.06	0.816	Aniline = (5)(9) + (1)(36)
18	37	C_5H_5N	2.9993	2.113	Pyridine = (1)(37)
18	38	C_5H_4N	2.8332	1.833	2-Methylpyridine = (1)(1) + (1)(38)
18	39	C_5H_3N	2.667	1.553	2,3-Dimethylpyridine = (2)(1) + (1)(39)
19	40	CH_3CN	1.8701	1.724	Acetonitrile = (1)(40)
19	41	CH_2CN	1.6434	1.416	Proprionitrile = (1)(1) + (1)(41)
20	42	COOH	1.3013	1.224	Acetic Acid = (1)(1) + (1)(42)
20	43	HCOOH	1.528	1.532	Formic Acid = (1)(43)
21	44	CH_2Cl	1.4654	1.264	1-Chlorobutane = (1)(1) + (2)(2) + (1)(44)
21	45	CHCl	1.238	0.952	2-Chloropropane = (2)(1) + (1)(45)
21	46	CCl	1.0106	0.724	2-Chloro-2-methylpropane = (3)(1) + (1)(46)
22	47	CH_2Cl_2	2.2564	1.988	Dichloromethane = (1)(47)
22	48	$CHCl_2$	2.0606	1.684	1,1-Dichloroethane = (1)(1) + (1)(48)
22	49	CCl_2	1.8016	1.448	2,2-Dichloropropane = (2)(1) + (1)(49)
23	50	$CHCl_3$	2.87	2.41	Chloroform = (1)(50)
23	51	CCl_3	2.6401	2.184	1,1,1-Trichloroethane = (1)(1) + (1)(51)

Table A.3 UNIFAC Method (Hansen, et al. 1991). Part (3/4). Taken from[26].

Group number		Volume	Area		Sample Assignments = (Number of Ocurrences) ×
Secondary	Main	R_k	Q_k	Name	(Secondary Group Number)
24	52	CCl_4	3.39	2.91	Tetrachloromethane = (1)(52)
25	53	ACCl	1.1562	0.844	Chlorobenzene = (5)(9) + (1)(53)
26	54	CH_3NO_2	2.0086	1.868	Nitromethane = (1)(54)
26	55	CH_2NO_2	1.7818	1.56	Nitroethane = (1)(1) + (1)(55)
26	56	$CHNO_2$	1.5544	1.248	2-Nitropropane = (2)(1) + (1)(56)
27	57	$ACNO_2$	1.4199	1.104	Nitrobenzene = (5)(9) + (1)(57)
28	58	CS_2	2.507	1.65	Carbon disulfide = (1)(58)
29	59	CH_3SH	1.877	1.676	Methanethiol = (1)(59)
29	60	CH_2SH	1.651	1.368	Ethanethiol = (1)(1) + (1)(60)
32	63	I	1.264	0.992	Iodoethane = (1)(1) + (1)(2) + (1)(63)
33	64	Br	0.9492	0.832	Bromoethane = (1)(1) + (1)(2) + (1)(64)
34	65	CH=C	1.2929	1.088	1-Hexyne = (1)(1) + (3)(2) + (1)(65)
34	66	C=C	1.0613	0.784	2-Hexyne = (2)(1) + (2)(2) + (1)(66)
35	67	DMSO	2.8266	2.472	Dimethylsulfoxide = (1)(67)
36	68	Acrylonitrile	2.3144	2.052	Acrylonitrile = (1)(68)
37	69	Cl-(C=C)	0.791	0.724	Trichloroethylene = (1)(8) + (3)(69)
38	71	ACF	0.6948	0.524	Fluorobenzene = (5)(9) + (1)(71)
39	72	DMF	3.0856	2.736	N,N-Dimethylformamide = (1)(72)
39	73	$HCON(CH_2)_2$	2.6322	2.12	N,N-Diethylformamide = (2)(1) + (1)(73)
40	74	CF_3	1.406	1.38	Perfluoroethane = (2)(74)
40	75	CF_2	1.0105	0.92	
40	76	CF	0.0615	0.46	Perfluoromethylcyclohexane=(1)(74) + (5)(75)+(1)(76)
41	77	COO	1.38	1.2	Butylacetate = (2)(1) + (3)(2) + (1)(77)
42	78	SiH_3	1.6035	1.263	Methylsilane = (1)(1) + (1)(78)
42	79	SiH_2	1.4443	1.006	Diethylsilane = (2)(1) + (2)(2) + (1)(79)
42	80	SiH	1.2853	0.749	Trimethylsilane = (3)(1) + (1)(80)
42	81	Si	1.047	0.41	Tetramethylsilane = (4)(1) + (1)(81)

Table A.4 UNIFAC Method (Hansen, et al. 1991). Part (4/4). Taken from[26].

Group number Secondary	Main	Volume R_k	Area Q_k	Name	Sample Assignments = (Number of Ocurrences) × (Secondary Group Number)
43	82	SiH_2O	1.4838	1.062	
43	83	SiHO	1.303	0.764	
43	84	SiO	1.1044	0.466	Hexamethyldisiloxane = (6)(1) + (1)(81) + (1)(84)
44	85	NMP	3.981	3.2	N-Methylpyrrolidone = (1)(85)
45	86	CCl_3F	3.0356	2.644	Tricholorofluoromethane = (1)(86)
45	87	CCl_2F	2.2287	1.916	Tetrachloro-1,2-difluoroethane = (2)(87)
45	88	$HCCl_2F$	2.406	2.116	Dichlorofluoromethane = (1)(88)
45	89	HCClF	1.6493	1.416	2-Chloro-2-fluoroethane = (1)(1) + (1)(89)
45	90	$CClF_2$	1.8174	1.648	2-Chloro-2,2-difluoroethane = (1)(1) + (1)(90)
45	91	$HCClF_2$	1.967	1.828	Cholorodifluoromethane = (1)(91)
45	92	$CClF_3$	2.721	2.1	Cholorotrifluoromethane = (1)(92)
45	93	CCl_2F_2	2.6243	2.376	Dicholorodifluoromethane = (1)(93)
46	94	$CONH_2$	1.4515	1.248	Acetamide = (1)(1) + (1)(94)
46	95	$CONHCH_3$	2.1905	1.796	N-Methylacetamide = (1)(1) + (1)(95)
46	96	$CONHCH_2$	1.9637	1.488	N-Ethylacetamide = (2)(1) + (1)(96)
46	97	$CON(CH_3)_2$	2.8589	2.428	N,N-Dimethylacetamide = (1)(1) +(1)(97)
46	98	$CON(CH_3)CH_2$	2.6322	2.12	N,N-Methylethylacetamide = (2)(1) +(1)(98)
46	99	$CON(CH_2)_2$	2.4054	1.812	N,N-Diethylacetamide = (3)(1) +(1)(99)
47	100	$C_2H_5O_2$	2.1226	1.904	2-Ethoxyethanol = (1)(1) +(1)(100)
47	101	$C_2H_4O_2$	1.8952	1.592	2-Ethoxy-1-propanol = (2)(1) + (1)(2) + (1)(101)
48	102	CH_3S	1.613	1.368	Dimethylsulfide = (1)(1) + (1)(102)
48	103	CH_2S	1.3863	1.06	Diethylsulfide = (2)(1) + (1)(2) + (1)(103)
48	104	CHS	1.1589	0.748	Diisopropylsulfide = (4)(1) + (1)(3) + (1)(104)
49	105	MORPH	3.474	2.796	Morpholine = (1)(105)
49	106	C_4H_4S	2.8569	2.14	Thiophene = (1)(106)
49	107	C_4H_3S	2.6908	1.86	2-Methylthiophene = (1)(1) + (1)(107)
49	108	C_4H_2S	2.5247	1.58	2-Dimethylthiophene = (2)(1) + (1)(108)

Table A.5 R_k and Q_k Parameters and Group Assignment for Modified UNIFAC (Dortmund) Method. Gmehling et al (1993). Part (1/2) Taken from [27].

Group		Volume	Area		
Secondary	Main	R_k	Q_k	Name	Example
1	1	0.6325	1.0608	CH_3	hexane
2	1	0.6325	0.7081	CH_2	octane
3	1	0.6325	0.3554	CH	2-methylpropane
4	1	0.6325	0	C	neopentane
5	2	1.2832	1.6016	CH_2=CH	1-hexene
6	2	1.2832	1.2489	CH=CH	2-hexene
7	2	1.2832	1.2489	CH_2=C	2-methyl-1-butene
8	2	1.2832	0.8962	CH=C	2-methyl-2-butene
70	2	1.2832	0.4582	C=C	2,3-dimethyl-2-b utene
9	3	0.3763	0.4321	ACH	naphthalene
10	3	0.3763	0.2113	AC	styrene
11	4	0.91	0.949	$ACCH_3$	toluene
12	4	0.91	0.7962	$ACCH_2$	ethylbenzene
13	4	0.91	0.3769	ACCH	isopropylbenzene
14	5	1.2302	0.8927	$OH_{(p)}$	1-propanol
81	5	1.063	0.8663	$OH_{(s)}$	2-propanol
82	5	0.6895	0.8345	$OH_{(t)}$	tert-butanol
15	6	0.8585	0.9938	CH_3OH	methanol
16	7	1.7334	2.4561	H_2O	water
17	8	1.08	0.975	ACOH	phenol
18	9	1.7048	1.67	CH_3CO	2-butanone
19	9	1.7048	1.5542	CH_2CO	2-pentanone
20	10	0.7173	0.771	CHO	propionic aldhyde
21	11	1.27	1.6286	CH_3COO	butyl acetate
22	11	1.27	1.4228	CH_2COO	methyl propionate
23	12	1.9	1.8	HCOO	ethyl formate
24	13	1.1434	1.6022	CH_3O	dimethyl ether
25	13	1.1434	1.2495	CH_2O	diethyl ether
26	13	1.1434	0.8968	CHO	diisopropyl ether
28	14	1.6607	1.6904	CH_3NH_2	methylamine
29	14	1.6607	1.3377	CH_2NH_2	ethylamine
30	14	1.6607	0.985	$CHNH_2$	isopropylamine
85	14	1.6607	0.985	CNH_2	tert-butylamine
31	15	1.368	1.4332	CH_3NH	dimethylamine
32	15	1.368	1.0805	CH_2NH	diethylamine
33	15	1.368	0.7278	CHNH	diisopropylamine
34	16	1.0746	1.176	CH_3N	trimethylamine
35	16	1.0746	0.824	CH_2N	triethylamine
36	17	1.1849	0.8067	$ACNH_2$	aniline
37	18	2.5	2.1477	C_5H_5N	pyridine
38	18	2.8882	2.2496	C_5H_4N	2-methylpyridine
39	18	3.2211	2.5	C_5H_3N	2,3-dimethylpyridine

Table A.6 R_k and Q_k Parameters and Group Assignment for the Modified UNIFAC (Dortmund) Method. Gmehling et al (1993). Part (2/2). Taken from [27].

Group Secondary	Main	Volume R_k	Area Q_k	Name	Example
40	19	1.5575	1.5193	CH_3CN	acetonitrile
41	19	1.5575	1.1666	CH_2CN	propionitrile
42	20	0.8	0.9215	COOH	acetic acid
44	21	0.9919	1.3654	CH_2Cl	1-chlorobutane
45	21	0.9919	1.0127	CHCl	2-chloropropane
46	21	0.9919	0.66	CCl	tert-butyl chloride
47	22	1.8	2.5	CH_2Cl_2	dichloromethane
48	22	1.8	2.1473	$CHCl_2$	1,l-dichloroethane
49	22	1.8	1.7946	CCl_2	2,2-dichloropropane
51	23	2.65	2.3778	CCl_3	l,l,l-trichloroethane
52	24	2.618	3.1836	CCl_4	tetrachloromethane
53	25	0.5365	0.3177	ACCl	chlorobenzene
54	26	2.644	2.5	CH_3NO_2	nitromethane
55	26	2.5	2.304	CH_2NO_2	1-nitropropane
56	26	2.887	2.241	$CHNO_2$	2-nitropropane
57	27	0.4656	0.3589	$ACNO_2$	nitrobenzene
58	28	1.24	1.068	CS_2	carbon disulfide
59	29	1.289	1.762	CH_3SH	methanethiol
60	29	1.535	1.316	CH_2SH	ethanethiol
61	30	1.299	1.289	furfural	furfural
62	31	2.088	2.4	DOH	1,2-ethanediol
63	32	1.076	0.9169	I	ethyl iodide
64	33	1.209	1.4	Br	ethyl bromide
65	34	0.9214	1.3	CH≡C	1-hexyne
66	34	1.303	1.132	C≡C	2-hexyne
67	35	3.6	2.692	DMSO	dimethyl sulfoxide
68	36	1	0.92	acrylonitrile	acrylonitrile
69	37	0.5229	0.7391	Cl(C≡C)	trichloroethylene
71	38	0.8814	0.7269	ACF	hexafluorobenzene
72	39	2	2.093	DMF	NJ-dimethylformamide
73	39	2.381	1.522	$HCON(CH_2)_2$	NJ-diethylformamide
74	40	1.284	1.266	CF_3	l,l,l-trifluoroethane
75	40	1.284	1.098	CF_2	perfluorohexane
76	40	0.8215	0.5135	CF	perfluoromethylcyclohexane
77	41	1.6	0.9	COO	methyl acrylate
78	42	0.7136	0.8635	c-CH_2	cyclohexane
79	42	0.3479	0.1071	c-CH	methylcyclohexane
80	42	0.347	0	c-C	1,1-dimethylcyclohexane
27	43	1.7023	1.8784	c-CH_2OCH_2	tetrahydrofuran
83	43	1.4046	1.4	c-$CH_2O[CH_2]_{1/2}$	1,3-dioxane
84	43	1.0413	1.0116	c-$[CH_2O]_{1/2}O[CH_2]_{1/2}$	1,3,5-trioxane
43	44	0.8	1.2742	HCOOH	formic acid
50	45	2.45	2.8912	$CHCl_3$	chloroform

Table A.7 R_k and Q_k Parameters and Group Assignment for Modified UNIFAC (Dortmund) Method. Constantinescu et Gmehling (2016). Part (1/3). Taken from Addendum to "Further Development of Modified UNIFAC (Dortmund): Revision and Extension 6. [28].

Group		Volume	Area		
Secondary	Main	R_k	Q_k	Name	Example
1	1	0.6325	1.0608	CH_3	hexane
2	1	0.6325	0.7081	CH_2	octane
3	1	0.6325	0.3554	CH	2-methylpropane
4	1	0.6325	0	C	neopentane
5	2	1.2832	1.6016	CH_2=CH	1-hexene
6	2	1.2832	1.2489	CH=CH	2-hexene
7	2	1.2832	1.2489	CH_2=C	2-methyl-1-butene
8	2	1.2832	0.8962	CH=C	2-methyl-2-butene
70	2	1.2832	0.4582	C=C	2,3-dimethyl-2-butene
9	3	0.3763	0.4321	ACH	naphthalene
10	3	0.3763	0.2113	AC	styrene
11	4	0.91	0.949	$ACCH_3$	toluene
12	4	0.91	0.7962	$ACCH_2$	ethylbenzene
13	4	0.91	0.3769	ACCH	isopropylbenzene
14	5	1.2302	0.8927	$OH_{(p)}$	1-propanol
81	5	1.063	0.8663	$OH_{(s)}$	2-propanol
82	5	0.6895	0.8345	$OH_{(t)}$	tert-butanol
15	6	0.8585	0.9938	CH_3OH	methanol
16	7	1.7334	2.4561	H_2O	water
17	8	1.08	0.975	ACOH	phenol
18	9	1.7048	1.67	CH_3CO	2-butanone
19	9	1.7048	1.5542	CH_2CO	2-pentanone
20	10	0.7173	0.771	CHO	propionic aldhyde
21	11	1.27	1.6286	CH_3COO	butyl acetate
22	11	1.27	1.4228	CH_2COO	methyl propionate
23	12	1.9	1.8	HCOO	ethyl formate
24	13	1.1434	1.6022	CH_3O	dimethyl ether
25	13	1.1434	1.2495	CH_2O	diethyl ether
26	13	1.1434	0.8968	CHO	diisopropyl ether
28	14	1.6607	1.6904	CH_3NH_2	methylamine
29	14	1.6607	1.3377	CH_2NH_2	ethylamine
30	14	1.6607	0.985	$CHNH_2$	isopropylamine
85	14	1.6607	0.985	CNH_2	tert-butylamine

Table A.8 R_k and Q_k Parameters and Group Assignment for Modified UNIFAC (Dortmund) Method. Constantinescu et Gmehling (2016). Part (2/3). Taken from Addendum to "Further Development of Modified UNIFAC (Dortmund): Revision and Extension 6. [28].

Group Secondary	Main	Volume R_k	Area Q_k	Name	Example
31	15	1.368	1.4332	CH_3NH	dimethylamine
32	15	1.368	1.0805	CH_2NH	diethylamine
33	15	1.368	0.7278	CHNH	diisopropylamine
34	16	1.0746	1.176	CH_3N	trimethylamine
35	16	1.0746	0.824	CH_2N	triethylamine
36	17	1.1849	0.8067	$ACNH_2$	aniline
37	18	1.4578	0.9022	AC_2H_2N	pyridine
38	18	1.2393	0.633	AC_2HN	2-methylpyridine
39	18	1.0731	0.353	AC_2N	2,5-dimethylpyridine
40	19	1.5575	1.5193	CH_3CN	acetonitrile
41	19	1.5575	1.1666	CH_2CN	propionitrile
42	20	0.8	0.9215	COOH	acetic acid
44	21	0.9919	1.3654	CH_2Cl	1-chlorobutane
45	21	0.9919	1.0127	CHCl	2-chloropropane
46	21	0.9919	0.66	CCl	tert-butyl chloride
47	22	1.8	2.5	CH_2Cl_2	dichloromethane
48	22	1.8	2.1473	$CHCl_2$	1,l-dichloroethane
49	22	1.8	1.7946	CCl_2	2,2-dichloropropane
51	23	2.65	2.3778	CCl_3	l,l,l-trichloroethane
52	24	2.618	3.1836	CCl_4	tetrachloromethane
53	25	0.5365	0.3177	ACCl	chlorobenzene
54	26	2.644	2.5	CH_3NO_2	nitromethane
55	26	2.5	2.304	CH_2NO_2	1-nitropropane
56	26	2.887	2.241	$CHNO_2$	2-nitropropane
57	27	0.4656	0.3589	$ACNO_2$	nitrobenzene
58	28	1.24	1.068	CS_2	carbon disulfide
59	29	1.289	1.762	CH_3SH	methanethiol
60	29	1.535	1.316	CH_2SH	ethanethiol
61	30	1.299	1.289	furfural	furfural
62	31	2.088	2.4	DOH	1,2-ethanediol
63	32	1.076	0.9169	I	ethyl iodide
64	33	1.209	1.4	Br	ethyl bromide
65	34	0.9214	1.3	CH≡C	1-hexyn
66	34	1.303	1.132	C≡C	2-hexyne
67	35	3.6	2.692	DMSO	dimethyl sulfoxide
68	36	1	0.92	acrylonitrile	acrylonitrile
69	37	0.5229	0.7391	Cl(C≡C)	trichloroethylene
71	38	0.8814	0.7269	ACF	hexafluorobenzene

Table A.9 R_k and Q_k Parameters and Group Assignment for Modified UNIFAC (Dortmund) Method. Constantinescu et Gmehling (2016). Part (3/3). Taken from Addendum to "Further Development of Modified UNIFAC (Dortmund): Revision and Extension 6. [28].

Group Secondary	Main	Volume R_k	Area Q_k	Name	Example
72	39	2	2.093	DMF	NN-dimethylformamide
73	39	2.381	1.522	$HCON(CH_2)_2$	NJ-diethylformamide
74	40	1.284	1.266	CF_3	l,l,l-trifluoroethane
75	40	1.284	1.098	CF_2	perfluorohexane
76	40	0.8215	0.5135	CF	perfluoromethylcyclohexane
77	41	1.6	0.9	COO	methyl acrylate
78	42	0.7136	0.8635	c-CH_2	cyclohexane
79	42	0.3479	0.1071	c-CH	methylcyclohexane
80	42	0.347	0	c-C	1,1-dimethylcyclohexane
27	43	1.7023	1.8784	c-CH_2OCH_2	tetrahydrofuran
83	43	1.4046	1.4	c-$CH_2O[CH2]_{1/2}$	1,3-dioxane
84	43	1.0413	1.0116	c-$[CH_2O]_{1/2}O[CH_2]_{1/2}$	1,3,5-trioxane
43	44	0.8	1.2742	HCOOH	formic acid
50	45	2.45	2.8912	$CHCl_3$	chloroform
86	46	3.981	3.2	cy-CON-CH_3	N-methylpyrrolidone
87	46	3.7543	2.892	cy-CON-CH_2	N-ethylpyrrolidone
88	46	3.5268	2.58	cy-CON-CH	N-isopropylpyrrolidone
89	46	3.2994	2.352	cy-CON-C	N-tert-butylpyrrolidone
92	47	1.5	1.08	$CONHCH_3$	N methylacetamide
100	47	1.5	1.08	$CONHCH_2$	N ethylacetamide
101	48	2.4748	1.9643	$CON(CH_3)_2$	N,N diemthylacetamide
102	48	2.2739	1.5754	$CONCH_2(CH_3)$	N,N methylethylacetamide
103	48	2.0767	1.1866	$CON(CH_2)_2$	N,N-diethylacetamide
93	49	2.4617	2.192	$HCONHCH_3$	N methylformamide
94	49	2.4617	1.842	$HCONHCH_2$	N ethylformamide
104	52	1.7943	1.34	AC_2H_2S	thiophene
105	52	1.6282	1.06	AC_2HS	2-methylthiophene
106	52	1.4621	0.78	AC_2S	2,5 dimethylthiophene
110	56	2.687	2.12	$(CH_2)_2SOO$	sulfolane
111	56	2.46	1.808	CH_2SOOCH	2,4 dimethylsulfolane
122	61	1.613	1.368	CH_3S	dimethyl sulfide
123	61	1.3863	1.06	CH_2S	diethyl sulfide
124	61	1.1589	0.748	CHS	diisopropyl sulfide
201	93	1.0678	2.244	-S-S-	dimethyl disulfide

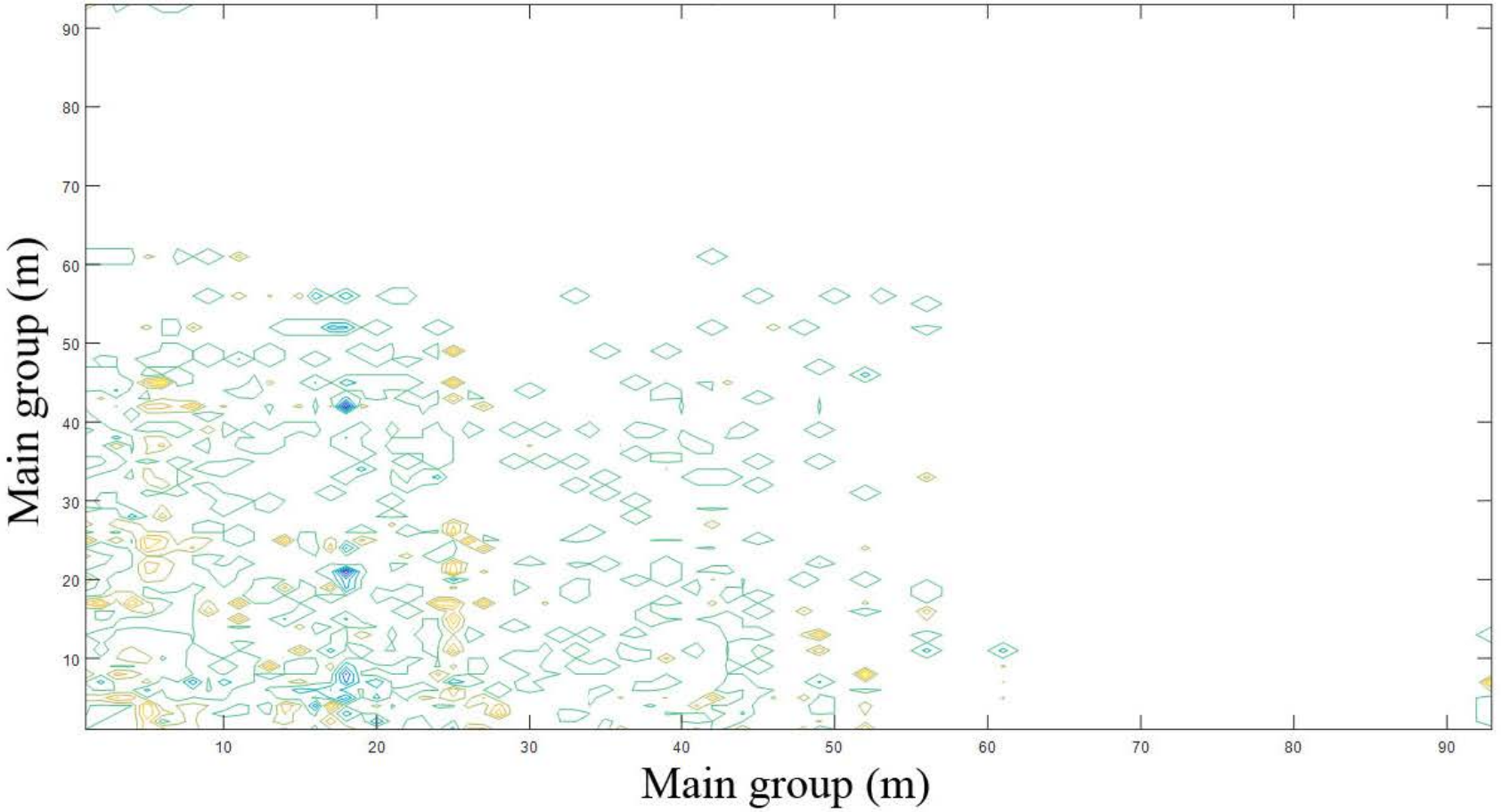

(a)

Fig. A.1 Top view of a_{nm} parameter matrix from Modified UNIFAC (Dortmund). Constantinescu et Gmehling (2016).

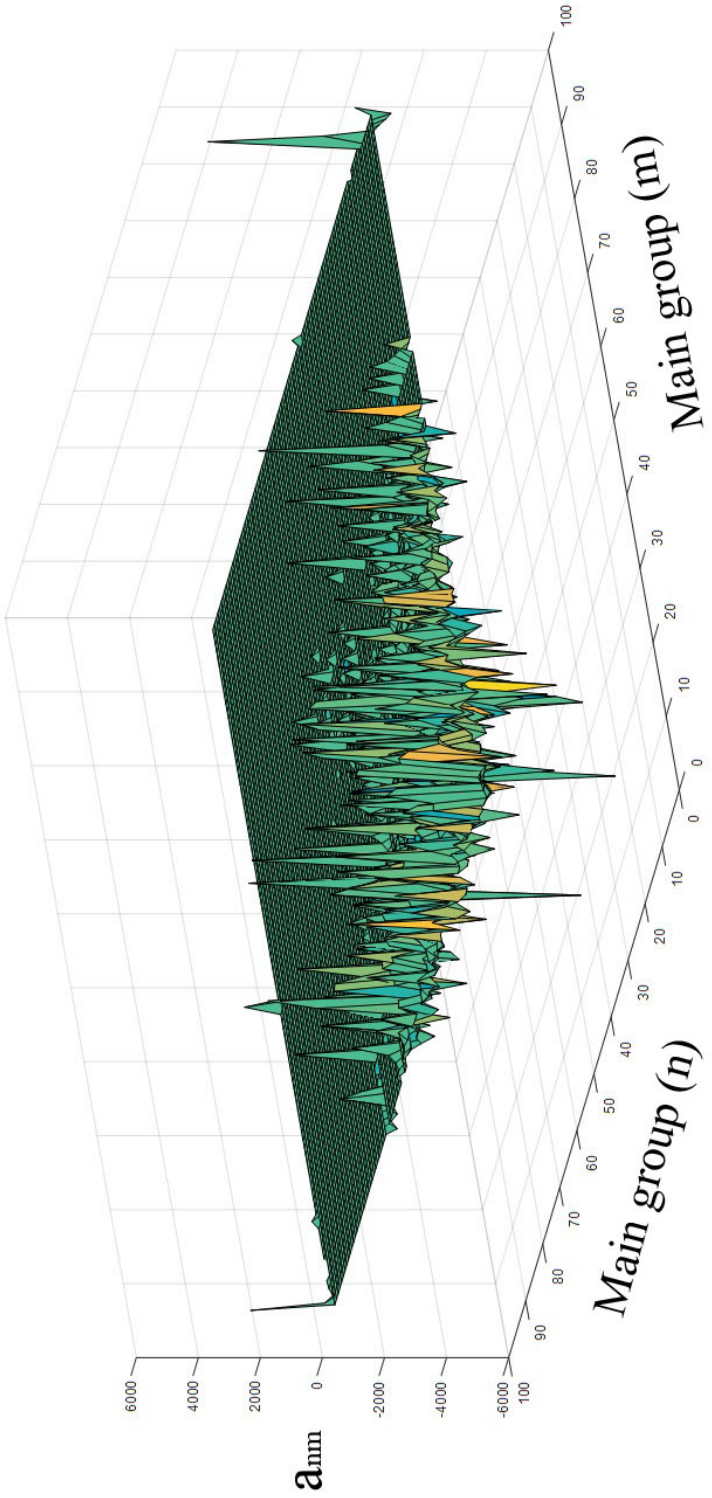

(a)

Fig. A.2 Front view of a_{nm} parameter matrix from Modified UNIFAC (Dortmund). Constantinescu et Gmehling (2016).

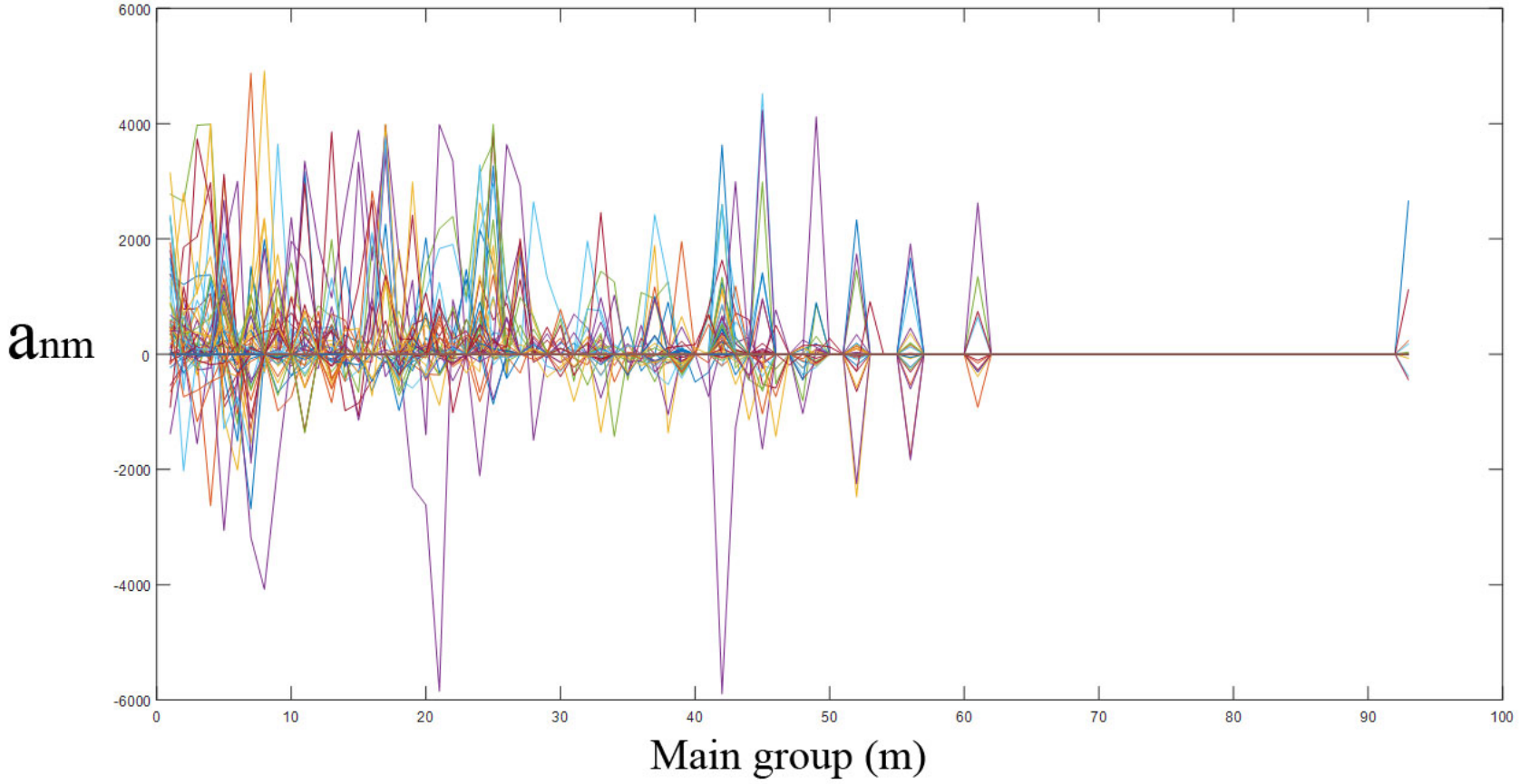

(a)

Fig. A.3 Side view of a_{nm} parameter matrix from Modified UNIFAC (Dortmund). Constantinescu et Gmehling (2016).

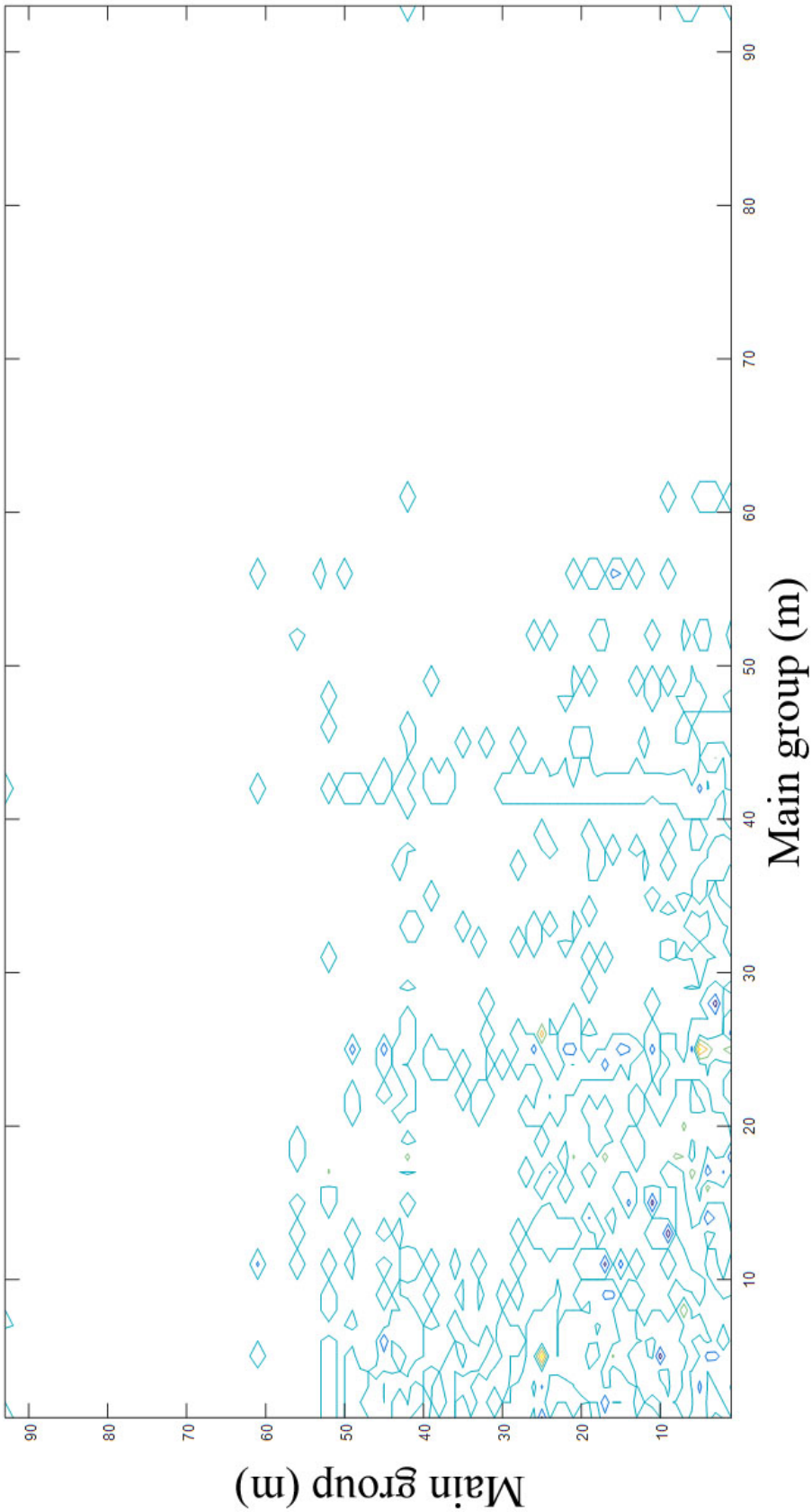

(a)

Fig. A.4 Top view of b_{nm} parameter matrix from Modified UNIFAC (Dortmund). Constantinescu et Gmehling (2016).

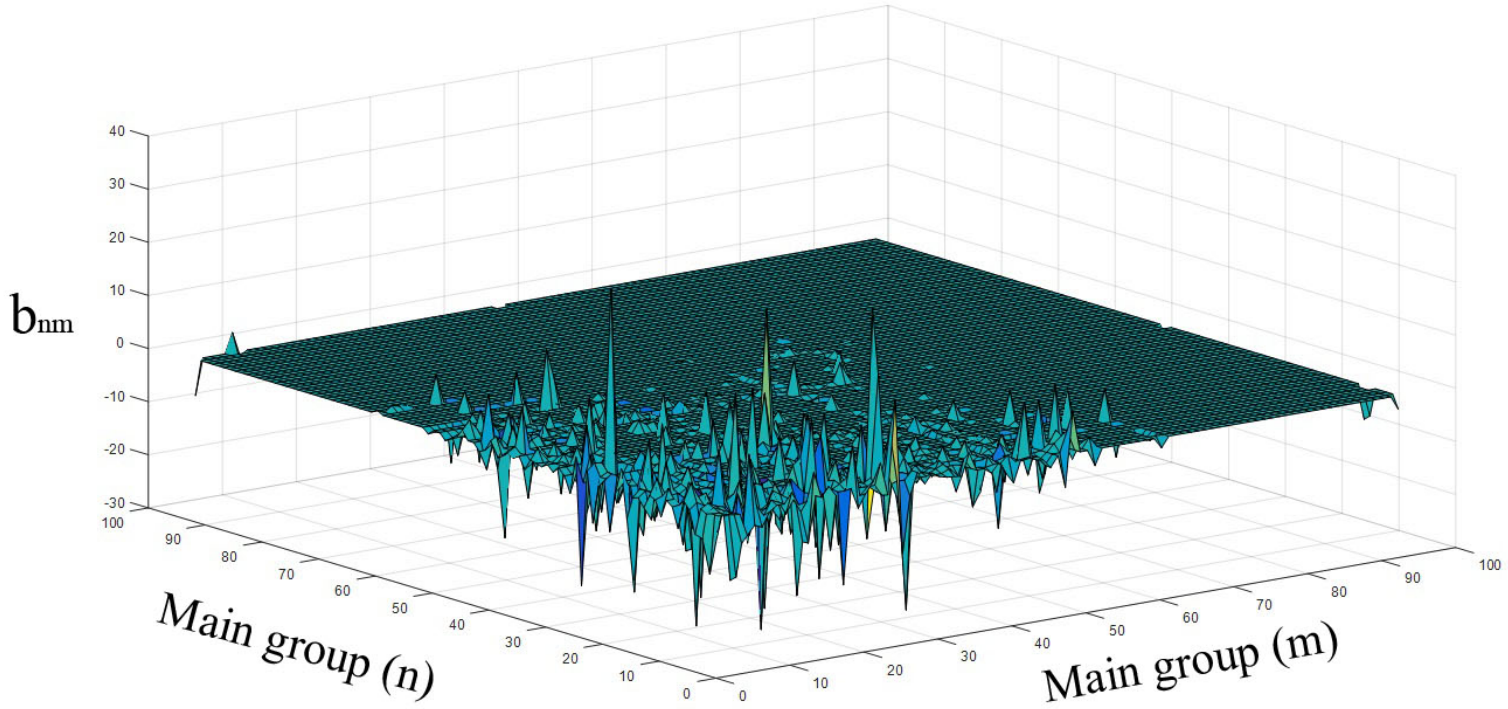

(a)

Fig. A.5 Front view of b_{nm} parameter matrix from Modified UNIFAC (Dortmund). Constantinescu et Gmehling (2016).

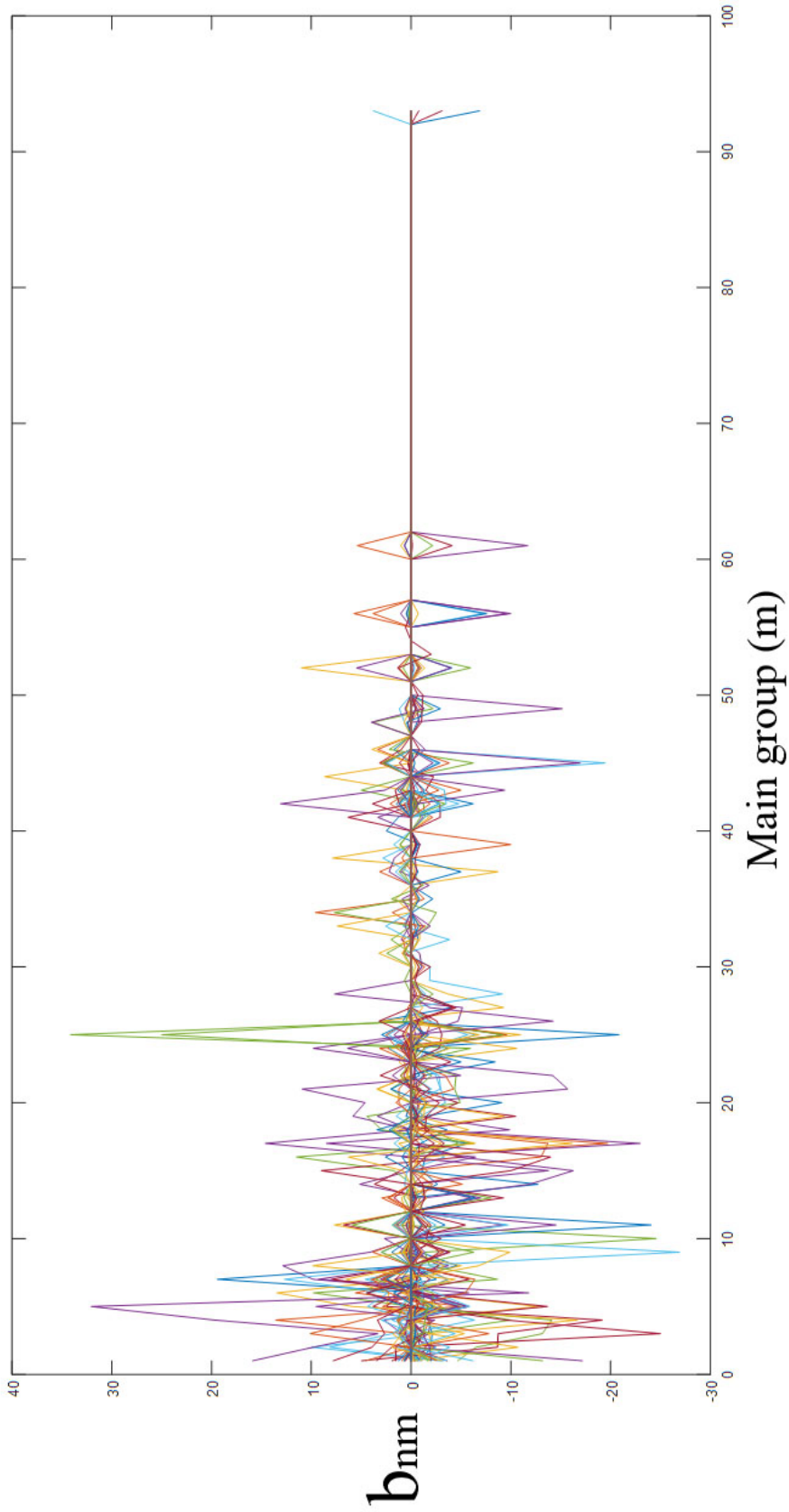

(a)

Fig. A.6 Side view of b_{nm} parameter matrix from Modified UNIFAC (Dortmund). Constantinescu et Gmehling (2016).

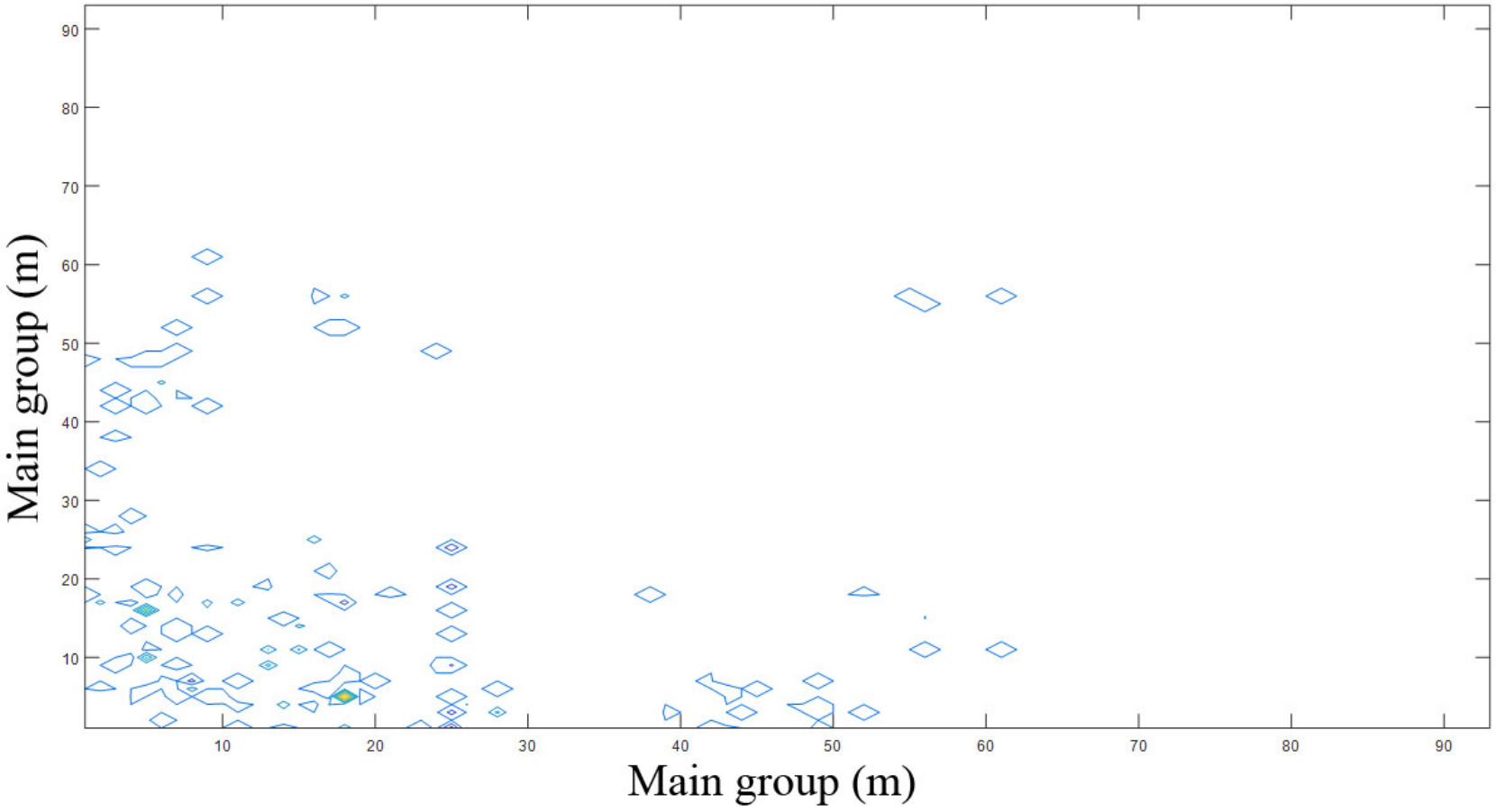

(a)

Fig. A.7 Top view of c_{nm} parameter matrix from Modified UNIFAC (Dortmund). Constantinescu et Gmehling (2016).

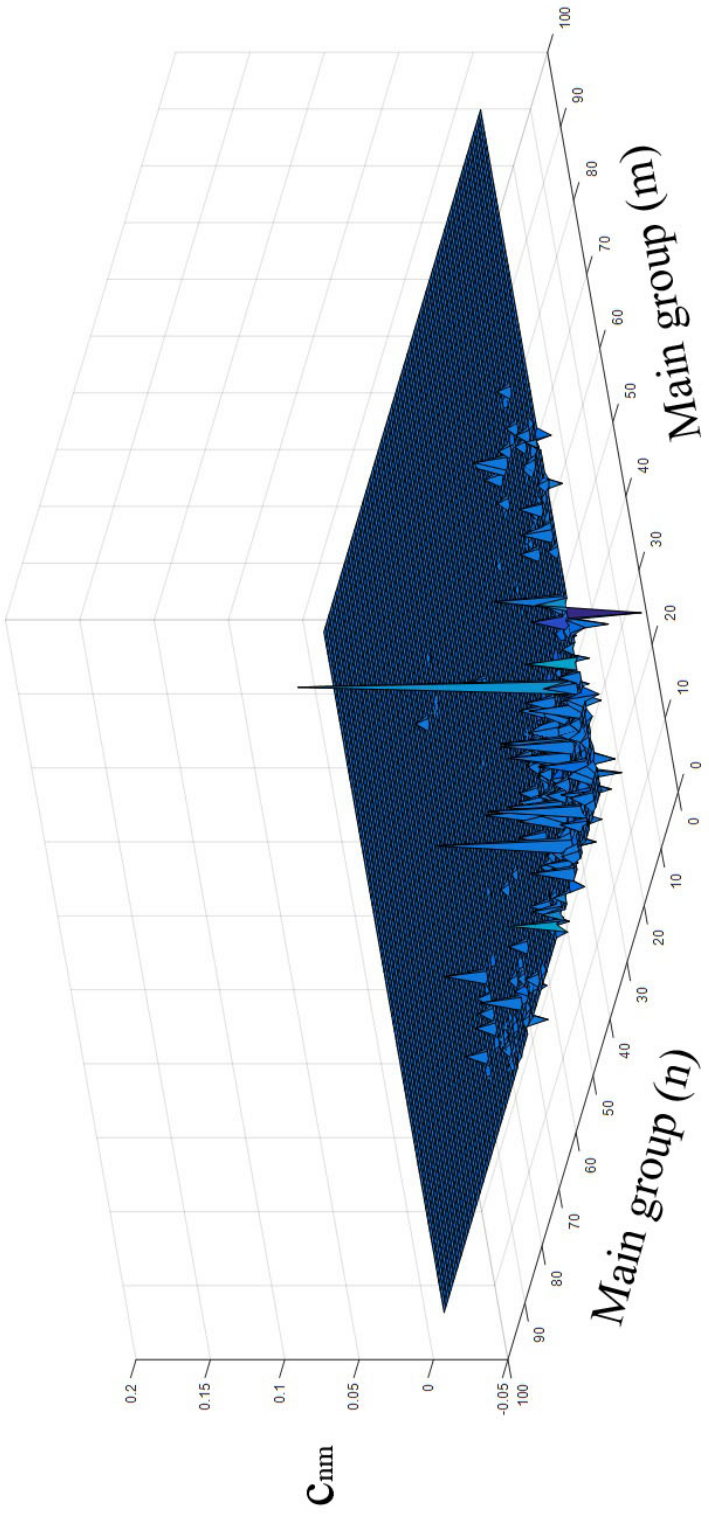

(a)

Fig. A.8 General view of c_{nm} parameter matrix from Modified UNIFAC (Dortmund). Constantinescu et Gmehling (2016).

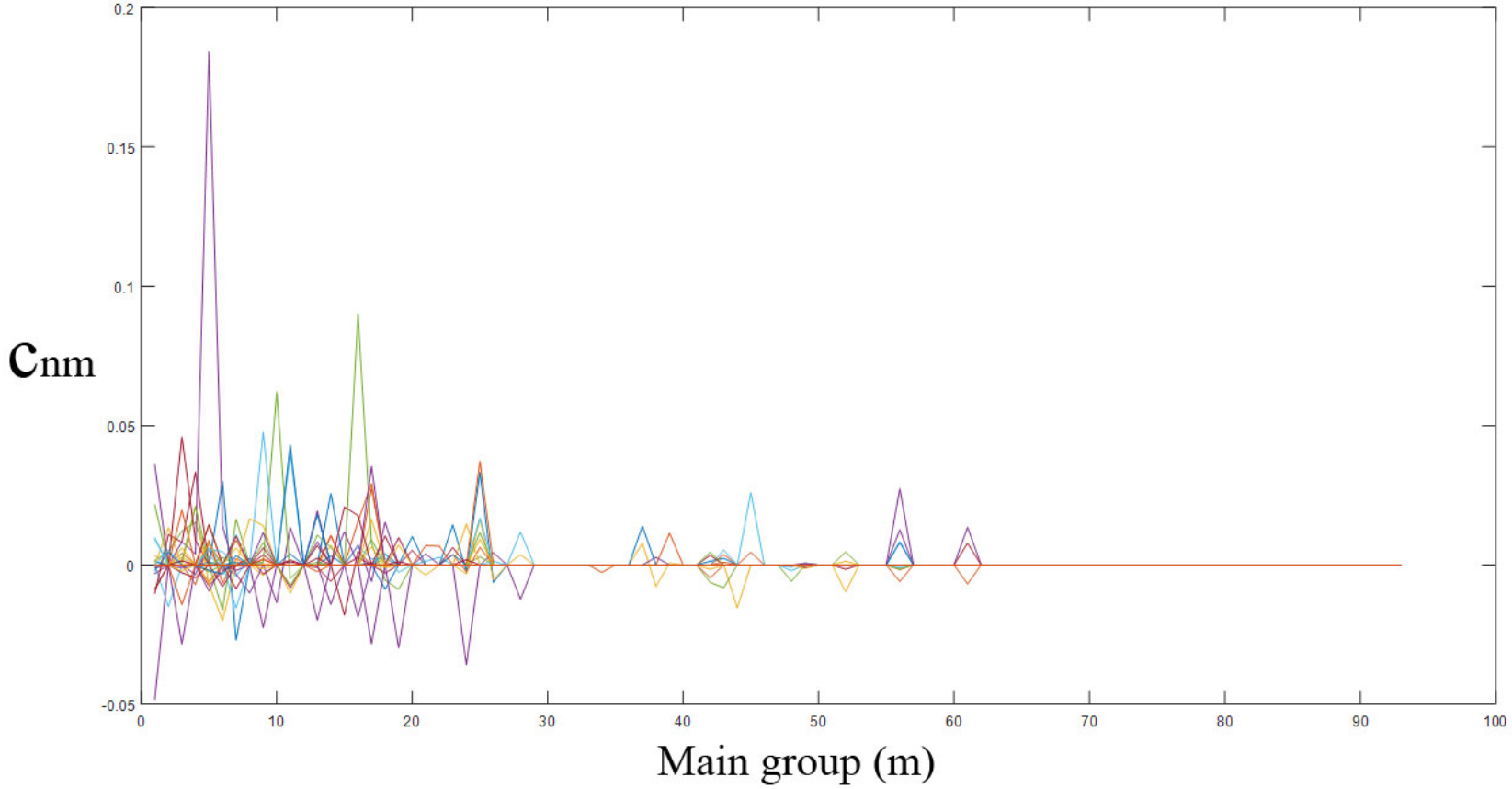

(a)

Fig. A.9 Side view of c_{nm} parameter matrix from Modified UNIFAC (Dortmund). Constantinescu et Gmehling (2016).

Appendix B

Cartography Summary

Table B.1 Characteristics of active ingredient, water and oils.

Substance	Type	Group name	Number (times)	Secondary group	Main group	η
Mandelic acid	Active ingredient	CH	1	3	1	-
		ACH	5	9	3	
		AC	1	10	3	
		COOH	1	42	20	
		$OH_{(s)}$	1	81	5	
Water	Dispersed phase	H_2O	1	16	7	1.000
Dodecane	Continuous phase	CH_3	2	1	1	2.581
		CH_2	10	2	1	
Hexadecane	Continuous phase	CH_3	2	1	1	2.872
		CH_2	14	2	1	
Isopropyl myristate	Continuous phase	CH_3	3	1	1	3.641
		CH_2	11	2	1	
		CH	1	3	1	
		CH_2COO	1	22	11	
Isopropyl palmitate	Continuous phase	CH_3	3	1	1	5.607
		CH_2	13	2	1	
		CH	1	3	1	
		CH_2COO	1	22	11	

NOTES:

-Group assignements are according to Modified UNIFAC Dortmund (rev. 6). Same groups were considered for dodecane/hexadecane when using UNIFAC-VISCO. However, for ester oils: 13 CH_2, 3 CH_3 and 1 COO (myristate) and 15 CH_2, 3 CH_3 and 1 COO (palmitate).

-η refers to the pure viscosity [mPa·s].

Table B.2 Characteristics of surfactants.

Substance	Group name	Number (times)	Secondary group	Main group	A_2^*	A_2	λ	η_s
SPAN 80	CH_3	1	1	1	28.845	71.924	0.40	818.733
	CH_2	14	2	1				
	CH	1	3	1				
	CH=CH	1	6	2				
	CH_2COO	1	22	11				
	CH_2O	1	25	13				
	c-CH	3	79	42				
	OH_s	3	81	5				
PGPR	CH_3	3	1	1	47.712	136.190	0.35	4209.8
	CH_2	40	2	1				
	CH	6	3	1				
	CH=CH	3	6	2				
	OH_p	4	14	5				
	CH_2COO	3	22	11				
	CH_2O	2	25	13				
	OH_s	4	81	5				
BRIJ 93	CH_3	1	1	1	26.532	67.036	0.39	27.767
	CH_2	14	2	1				
	CH=CH	1	6	2				
	OH_p	1	14	5				
	CH_2O	2	25	13				

NOTES

-Group assignements according to Modified UNIFAC Dortmund (rev. 6).

-A_2^* refers to the area in compressed state (polar area) [$Å^2$/molec].

-A_2 refers to the actual area per molecule (whole molecule) [$Å^2$/molec].

-λ refers to the normalized surface density ratio $\lambda = A_2^*/A_2$ [adim.]

-η_s refers to the pure viscosity [mPa·s]. -When using UNIFAC-VISCO, the group assignements were the following: 16 CH_2, 1 CH_3, 3 CH_{2cy}, 2 CH_{ar}, 1 CO, 1 COO and 3 OH (SPAN 80); 49 CH_2, 3 CH_3, 6 CH_{ar}, 2 CO, 3 COO and 5 OH (PGPR); and 14 CH_2, 1 CH_3, 2 CH_{ar}, 2 CO, and 1 OH (BRIJ 93).

Appendix C

Experimental annex

C.0.1 Preparation of experimental calibration curves

Verifications concerning the calibration standards were previously performed, in order to check if the values of of λ_{max} were influenced or not by the substances present in the experiments. All the oil substances (dodecane, hexadecane, isopropyl myristate and isopropyl palmitate), active ingredient (mandelic acid), surfactants (SPAN 80 and BRIJ 93) and salt (NaCl) were purchased in Sigma Aldrich and used as received. Concerning the surfactant PGPR, it was obtained from DANISCO. The water employed for all tests was previously deionized and mili-Q filtrated by a Millipore apparatus. On the one hand, different '*stocksolutions*' were prepared according to the following procedure using SPAN 80 and dodecane. First, a volume of water was brought into contact with a volume of pure dodecane oil in order to saturate with oil. The mixture was shaken vigorously using a magnetic stirrer during 24h. After shaking, the two-phase dispersion was added to a separating funnel and allowed to separate both organic and aqueous layers during 24h. Following this, the aqueous phase was recovered and placed in a second separating funnel with surfactant SPAN 80 in order to achieve saturation with surfactant. Again, a certain time for equilibration was allowed (3 days) and the aqueous phase was taken. The absorption curves of the aqueous phases coming from the previous steps were measured by the UV-spectrometer using pure water as blank. In addition, a diluted solution of mandelic acid was also prepared by using the aqueous phase coming from the last step (after adding surfactant). Fig. C.1a shows the typical spectras obtained when measuring these '*stocksolutions*'. Fig. C.1b shows the typical spectras obtained when only mandelic acid and water are present in the solution. As one can see, the λ_{max} for mandelic acid corresponds to a wavelength of 257 nm, however, it was evinced that oil or surfactant, likely transferred to the aqueous solution from the organic phase, can also contribute to the absorbance signal. For example, after bringing into contact

water, oil and surfactant, a λ_{max} was shown around 273 nm. After mixing water with oil, the effect was much less pronounced, no clear maximum peak was observed, but a magnification effect of 0.05 on the whole absorption curve was observed.

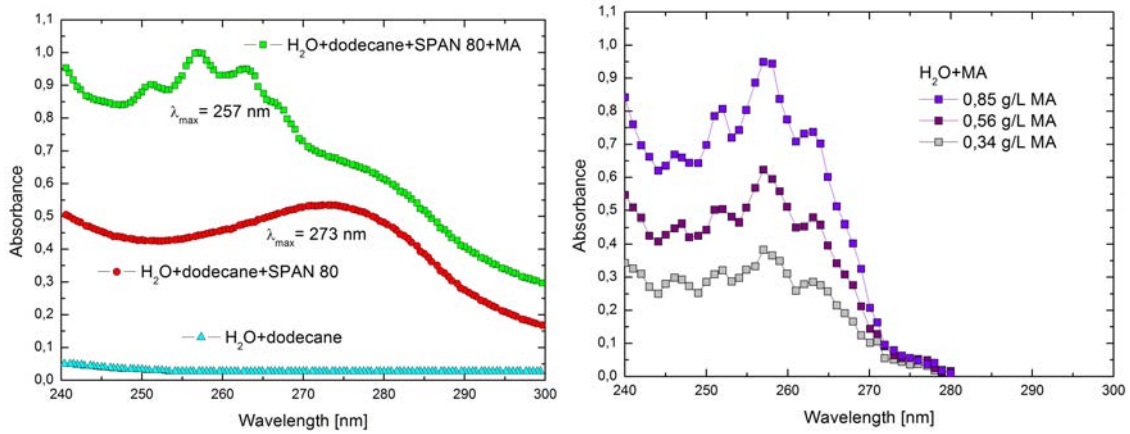

(a) (b)

Fig. C.1 a) Typical UV-spectra for liquid mixtures exmployed for calibration purposes in this work. b) UV-spectras when employing only mandelic acid and water.

These findings have important implications concerning the obtaining of a correct calibration curve, since that if there is an excessive magnification on the absorbance signal by compounds distinct from the molecule of interest, the lecture of λ_{max} could be seriously misleading. With the purpose of study and correcting these phenomena, series of calibration curves were prepared using as solvent different stock solutions containing different combinations of substances solubilized; the first one containing only water; the second, water and salt; a third one water, salt and possible oil solubilized; and a last one containing water, salt, oil and surfactant. The results of the calibration curves reading the absorbance at a wavelength of 257 nm and considering pure water as blank are shown in Fig.C.2a. As one can see, a baseline interference on the absorbance (0.4809 units) occured only when surfactant was present in the solution and the considered blank was pure water. This effect was independent of the concentration of the analyte, affecting the intercept of the calibration curve, but not its slope. All the other calibration lines agreed with a slope of approximately 1.1 with a zero intercept. Fortunately, it was observed that in order to eliminate this effect, the stock solution employed as solvent for the preparation of the calibration standards can be used as blank (Fig.C.2b). In this way, the rise of the signal produced by the concomitant substances (oil or surfactant present in the solution), can be corrected (See Fig. C.2a). As an alternative (preferable in a practical way), it was also verified that dilutions higher than 1/15 can generally decrease the baseline to zero (see Fig. C.2b). However, this would decrease

simultaneously the concentration of mandelic acid, therefore it would be only recommended if the analyte concentration was greater enough to not result out of the detection limits of the technique.

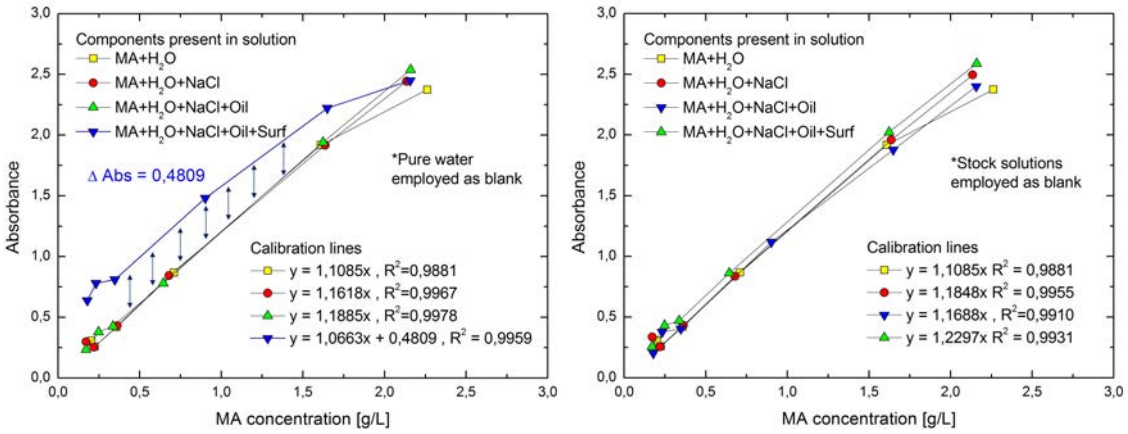

(a) (b)

Fig. C.2 a) Calibration lines employing pure water as blank for UV lectures. b) Calibration lines employing the respective stock solutions as blanks for UV lecture.

C.0.2 Preparation of samples for comparison of UNIFAC methods

The procedure for the preparation of the samples was the following. First, 6.5 mL aliquotes from a 0.5 M solution of mandelic acid were added to different labeled test tubes in order to obtain a final mass amount of 0.5 g of MA in each tube (with the exception of samples 19-24, where this mass amount was varied from 0.5 to 0.25). Subsequently, the solutions were made up with deionized water until a total volume of approximately 8.5 mL (except samples 7-12, where volumes were allowed to vary from 7.5 to 10.5). Then, 0.5 g of pure dodecane oil were weighted in every tube (besides those from 13-18, where the allowed variation was from 0.5 to 3). As a last step, approximately 0.4 g of SPAN 80 surfactant was added by using a syringe (with the exception of samples 1-6, where this amount was varied from 0.1 to 1.5). A Pasteur pippette was placed until the bottom of tubes with the intention of sampling the aqueous phase once the equlibrium was achieved. The upper part of the tube was completely sealed in order to avoid evaporation losses. It was observed that the time needed for this equilibration, in the experimental conditions of this work (298 K), was about 1 day for most of the samples used. After this time, each sample of aqueous phase obtained by the Pasteur pipettes was diluted 40 times with deionized water and the absorbance was measured at the wavelenght 257 nm by the UV-spectrometer. Table C.1 summarizes the characteristics of samples.

Table C.1 Characteristics of samples in study for comparison of UNIFAC methods. The system studied was: Mandelic acid + Water + SPAN 80 + Dodecane.

Sample	MA initial molarity	ϕ_v	$m_{oil}/m_{surf.}$	K_{cd} (pred.)	K_{cd} (exp.)	ε (error)
1	0.39	0.92	4.78	0.90	2.26	-60.08
2	0.37	0.91	2.22	1.21	1.78	-31.65
3	0.39	0.89	1.19	1.63	0.59	174.43
4	0.39	0.87	0.89	1.85	1.41	31.38
5	0.39	0.85	0.52	2.28	0.44	422.59
6	0.40	0.81	0.38	2.48	0.91	172.75
7	0.44	0.87	1.37	1.54	0.46	233.28
8	0.47	0.87	1.33	1.57	0.80	95.44
9	0.52	0.86	1.28	1.62	0.82	96.85
10	0.39	0.88	0.97	1.78	0.36	398.62
11	0.34	0.90	1.31	1.54	1.09	40.63
12	0.31	0.91	1.32	1.52	1.72	-11.49
13	0.39	0.67	7.21	0.79	0.18	348.76
14	0.39	0.70	6.02	0.83	0.65	28.08
15	0.39	0.74	4.99	0.88	1.13	-22.07
16	0.39	0.78	3.80	0.97	0.73	31.33
17	0.39	0.83	2.32	1.18	1.46	-18.98
18	0.39	0.89	1.22	1.60	0.66	142.73
19	0.39	0.88	1.31	1.55	1.59	-2.69
20	0.35	0.88	1.44	1.47	0.51	186.09
21	0.31	0.88	1.34	1.50	0.37	310.62
22	0.27	0.89	1.26	1.53	0.63	142.64
23	0.23	0.88	1.26	1.52	-	-
24	0.19	0.89	1.24	1.52	2.68	-43.44
25	0.39	0.88	1.30	1.56	0.11	1358.16
26	0.39	0.88	1.27	1.57	0.30	415.90
27	0.38	0.88	1.35	1.53	1.39	10.12
28	0.40	0.87	1.49	1.46	1.29	13.44

NOTES

-The predicted distribution coefficients K_{cd} (pred.) shown in the table were obtained by using Modified UNIFAC Dortmund (Constantinescu, 2016). For the calculation of the experimental distribution coefficient K_{cd} (exp.), it was considered a total continuous phase volume (volume of oil + volume of surfactant) same as the one at the moment of sample preparation.

-Samples 25, 26, 27 and 28 were prepared with NaCl concentrations of 1, 2, 3 and 4%.

-The relative error ε, was calculated according to the formula $\frac{K_{cd}(pred.)-K_{cd}(exp.)}{K_{cd}(exp.)}$ x 100.

-Empty values in table imply that mass balance for the continuous phase was negative.

C.0.3 Effect of salt content and blank/dilution media

The preparation of samples was carried out using a similar procedure to the one previously explained (see C.0.2). However, different mandelic acid concentrations, NaCl content, as well as oil/surfactant ratios were studied. Table C.2 summarizes the characteristics of all samples. Representative examples of the typical third layers appearing in this test, are shown in Fig. C.3. The sample letter A refers to a 2% NaCl aqueous solution employed as dispersed phase. The letter B refers to a dispersed phase without salt. In addition, Fig. C.4 shows a global picture of all samples, before and after the equilibrium was achieved.

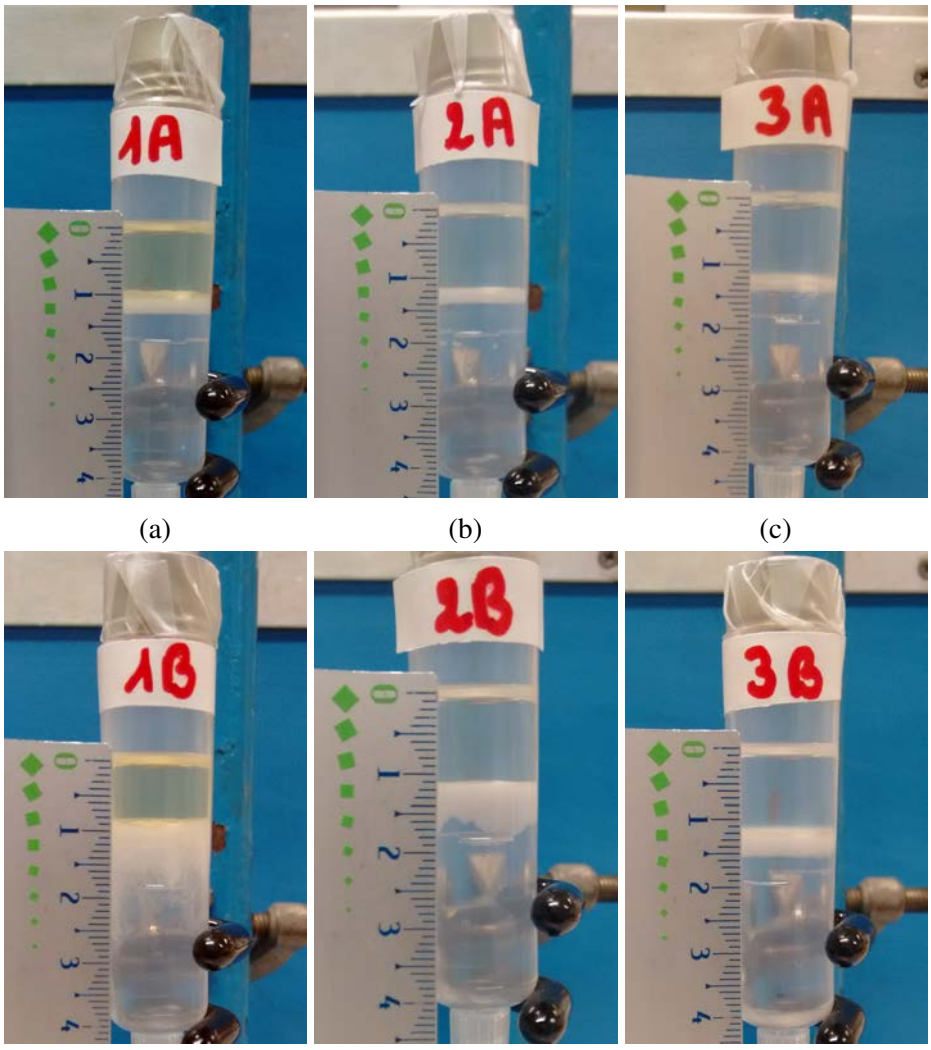

(a) (b) (c)

(d) (e) (f)

Fig. C.3 Samples at the end of equilibrium tests, $\phi_v \approx 0.7$ for all samples, oil/surfactant ratios≈1, 7 and 15 for samples number 1, 2 and 3 respectively. Letter A means a 2% NaCl content in the aqueous phase, letter B means that there is no salt.

Table C.2 Characteristics of samples in study of effect of salt content and blank/dilution media.

Sample	MA inital molarity	ϕ_v	$m_{oil}/m_{surf.}$	K_{cd} (pred.)	Water K_{cd} (exp.)	Stock K_{cd} (exp.)	Water ε (error)	Stock ε (error)
1A	8.55E-04	0.73	1.03	1.58	-	-	-	-
2A	8.60E-04	0.70	7.35	0.75	-	-	-	-
3A	8.61E-04	0.69	14.70	0.66	-	-	-	-
4A	8.56E-03	0.73	1.00	0.45	0.87	1.01	230.05	48.94
5A	8.62E-03	0.70	7.22	0.31	0.55	1.20	125.24	-41.68
6A	8.59E-03	0.70	14.61	0.47	1.40	1.68	31.17	-63.15
7A	8.75E-02	0.73	0.99	0.76	1.72	0.36	145.92	423.84
8A	8.75E-02	0.70	7.48	0.46	0.85	0.69	118.31	47.20
9A	8.69E-02	0.70	14.81	0.66	0.71	0.82	39.45	11.77
1B	8.51E-04	0.73	1.01	1.91	-	-	-	-
2B	8.57E-04	0.69	6.55	1.10	-	-	-	-
3B	8.55E-04	0.69	14.65	0.98	-	-	-	-
4B	8.59E-03	0.73	1.00	1.21	0.33	0.11	265.41	971.46
5B	8.52E-03	0.70	7.54	0.70	0.39	0.34	81.17	109.59
6B	8.58E-03	0.70	15.14	0.64	0.31	0.17	108.46	266.49
7B	8.59E-02	0.73	0.97	1.14	0.32	0.51	260.39	125.51
8B	8.55E-02	0.70	6.86	0.67	0.36	0.52	83.21	29.55
9B	8.57E-02	0.70	15.36	0.60	0.06	1.42	845.89	-57.85

NOTES

-Two measurements were performed per sample to obtain two distribution coefficients, the first one employing as a blank and dilution media, pure water (Water), and the second, employing the respective stock solution (Stock).

-The predicted distribution coefficients K_{cd} (pred.) shown in the table were obtained by using Modified UNIFAC Dortmund (Constantinescu, 2016). For the calculation of the experimental distribution coefficients K_{cd} (exp.), it was considered a total continuous phase volume (volume of oil + volume of surfactant) same as the one at the moment of sample preparation.

-The relative error ε, was calculated according to the formula $\frac{K_{cd}(pred.)-K_{cd}(exp.)}{K_{cd}(exp.)}$ x 100.

-Empty values in table imply that mass balance for the continuous phase was negative.

-The UV lecture of samples with salt and low and median concentrations of mandelic acid (from 1A to 6A), as well as samples without salt at low concentrations of mandelic acid (from 1B to 3B) were performed without dilution. A 1/15 dilution with the respective dilution media was performed for the rest of samples.

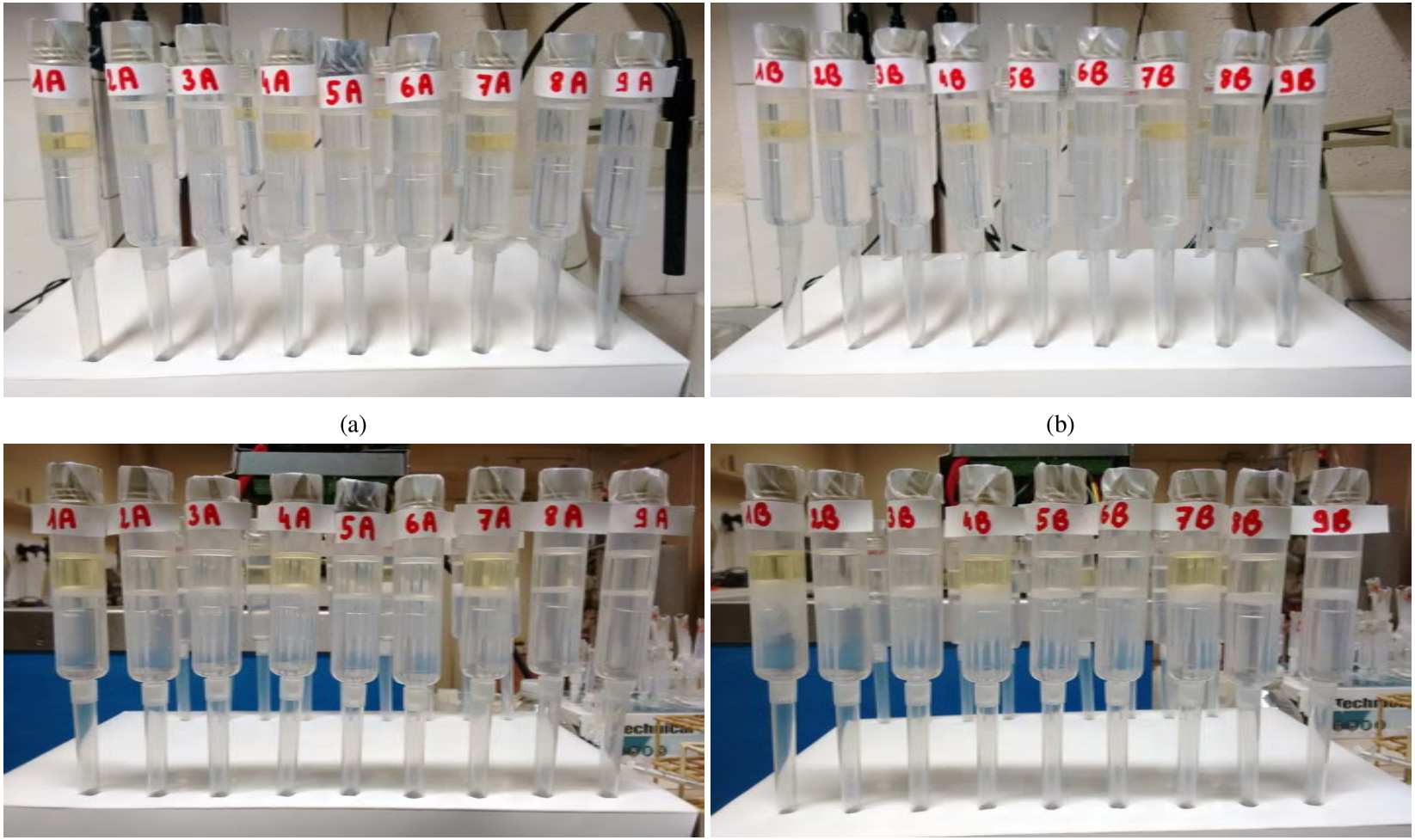

Fig. C.4 Samples for distribution coefficient determination. The sample letter A refers to a 2% NaCl aqueous solution employed as dispersed phase. The letter B refers to a sample prepared without salt. The approximate oil / surfactant ratio employed were the following: sample numbers 1, 4 and 7 (r≈1), 2, 5 and 8 (r≈7.5) and 3, 6 and 9 (r≈15). Figures a) and b) were taken right after sample preparation. Figures c) and d) after the equilibrium was achieved.

C.0.4 Effect of material of the cartography and disperse phase volume

Table C.3 Characteristics of samples in study for comparison of UNIFAC predictions using all components from cartography.

Sample	ϕ_v	$m_{oil}/m_{surf.}$	Oil	Surf.	K_{cd} (pred.)	K_{cd} (exp.)	ε (error)
1	0.68	3.94	Dodecane	SPAN 80	0.91	1.79	-49.384
2	0.45	6.99	Dodecane	SPAN 80	0.77	0.45	70.346
3	0.26	11.97	Dodecane	SPAN 80	0.69	0.30	124.758
4	0.69	3.98	Hexadecane	SPAN 80	0.84	0.62	35.610
5	0.46	8.03	Hexadecane	SPAN 80	0.69	0.77	-10.063
6	0.26	11.62	Hexadecane	SPAN 80	0.64	0.29	119.194
7	0.71	4.04	Palmitate	SPAN 80	1.17	3.13	-62.654
8	0.49	7.69	Palmitate	SPAN 80	1.01	0.78	29.488
9	0.28	11.81	Palmitate	SPAN 80	0.94	0.31	201.507
10	0.70	3.97	Myristate	SPAN 80	1.26	2.70	-53.321
11	0.48	7.25	Myristate	SPAN 80	1.10	1.24	-11.526
12	0.28	11.72	Myristate	SPAN 80	1.01	0.55	85.725
13	0.68	3.99	Dodecane	PGPR	0.81	1.06	-23.311
14	0.46	7.67	Dodecane	PGPR	0.71	0.63	12.463
15	0.26	12.08	Dodecane	PGPR	0.66	0.32	107.389
16	0.69	3.87	Hexadecane	PGPR	0.76	1.29	-41.078
17	0.46	7.73	Hexadecane	PGPR	0.65	0.75	-12.349
18	0.26	11.66	Hexadecane	PGPR	0.61	0.35	76.502
19	0.70	4.00	Palmitate	PGPR	1.04	1.04	-0.003
20	0.49	7.74	Palmitate	PGPR	0.94	0.48	96.918
21	0.28	11.96	Palmitate	PGPR	0.90	0.65	36.981
22	0.71	3.90	Myristate	PGPR	1.12	1.87	-39.930
23	0.48	7.93	Myristate	PGPR	1.01	1.09	-7.008
24	0.28	11.67	Myristate	PGPR	0.97	0.64	51.333
25	0.69	3.66	Dodecane	BRIJ 93	0.93	3.50	-73.523
26	0.46	8.07	Dodecane	BRIJ 93	0.74	1.66	-55.467
27	0.25	11.60	Dodecane	BRIJ 93	0.69	0.84	-18.161
28	0.70	3.84	Hexadecane	BRIJ 93	0.86	2.96	-71.105
29	0.47	7.94	Hexadecane	BRIJ 93	0.69	1.58	-56.179
30	0.26	11.50	Hexadecane	BRIJ 93	0.65	0.63	2.531
31	0.71	3.65	Palmitate	BRIJ 93	1.20	4.41	-72.875
32	0.49	7.24	Palmitate	BRIJ 93	1.02	1.81	-43.945
33	0.29	11.73	Palmitate	BRIJ 93	0.94	-	-
34	0.71	3.55	Myristate	BRIJ 93	1.29	4.01	-67.930
35	0.49	7.84	Myristate	BRIJ 93	1.08	2.02	-46.873
36	0.29	11.07	Myristate	BRIJ 93	1.02	-	-

C.0.5 Predicted and experimental release experiments

Table C.4 Characterization of SPAN 80 emulsions for release experiments.

No.	Oil	ϕ_m	$r_{o/s}$	$D_{droplet}$	G'_{before}	G'_{after}	D (pred)	D (exp)	ε
1	D	0.91	1.07	12.39	1276	1489	1.28E-10	1.27E-10	1.23
2	D	0.91	2.58	12.96	410	500	1.66E-10	1.66E-10	-0.19
3	D	0.91	5.13	13.90	196	229	1.63E-10	1.70E-10	-4.33
4	D	0.93	1.02	12.93	2059	2110	1.01E-10	9.49E-11	5.99
5	D	0.93	2.37	13.91	800	976	1.24E-10	1.26E-10	-1.25
6	D	0.93	4.84	15.26	350	382	1.28E-10	1.33E-10	-4.11
7	D	0.95	1.00	13.49	3528	3690	7.18E-11	6.47E-11	10.97
8	D	0.95	2.71	15.06	1315	1673	8.83E-11	7.19E-11	22.87
9	D	0.95	5.39	17.45	674	849	8.30E-11	9.08E-11	-8.58
10	H	0.91	1.03	9.22	1845	2174	6.88E-11	6.09E-11	13.08
11	H	0.91	2.50	9.69	916	1033	1.13E-10	9.65E-11	17.13
12	H	0.91	5.17	10.46	458	573	1.30E-10	1.23E-10	4.97
13	H	0.93	1.01	9.57	2736	2917	5.38E-11	4.60E-11	17.01
14	H	0.93	2.28	10.98	1925	1719	8.31E-11	7.07E-11	17.56
15	H	0.93	4.63	12.92	955	1171	1.01E-10	7.83E-11	29.50
16	H	0.95	1.02	9.96	5463	5218	3.82E-11	2.97E-11	28.77
17	H	0.95	2.47	12.38	2780	2225	6.20E-11	5.49E-11	12.91
18	H	0.95	5.04	16.61	1797	1776	7.00E-11	6.85E-11	2.06
19	M	0.90	0.99	12.32	3568	4122	6.74E-11	9.18E-11	-26.58
20	M	0.90	2.53	11.85	1882	2483	1.27E-10	1.64E-10	-22.71
21	M	0.90	4.60	11.20	1226	1486	1.52E-10	2.52E-10	-39.73
22	M	0.93	1.03	12.12	5219	6710	5.57E-11	8.91E-11	-37.52
23	M	0.93	2.34	12.06	2546	2965	9.24E-11	1.51E-10	-38.88
24	M	0.93	5.13	11.92	833	1049	1.18E-10	1.58E-10	-25.60
25	P	0.90	1.01	9.57	3558	4212	4.25E-11	5.75E-11	-26.15
26	P	0.90	2.47	9.84	2082	3064	7.63E-11	1.29E-10	-40.91
27	P	0.91	5.18	10.26	1244	1508	9.21E-11	1.08E-10	-14.85
28	P	0.93	0.98	9.95	4583	6036	3.25E-11	9.79E-11	-66.78
29	P	0.93	2.43	9.95	3781	4014	5.90E-11	6.67E-11	-11.48
30	P	0.93	4.84	9.94	1135	1228	7.21E-11	9.30E-11	-22.42

NOTES

-D=dodecane; H=hexadecane; M=myristate; P=palmitate; S=SPAN 80.

ϕ_m=dispersed phase mass fraction [adim.]; $r_{o/s}$=oil/surfactant ratio $m_{oil}/m_{surf.}$ [adim.]; $D_{droplet}$=droplet diameter [μm]; G'=storage moduli before or after experiment [Pa]; D=fitted diffusion coefficients for predicted (pred.) or experimental (exp.) curves [m^2/s]; and ε=relative error between D (pred.) and D (exp.).

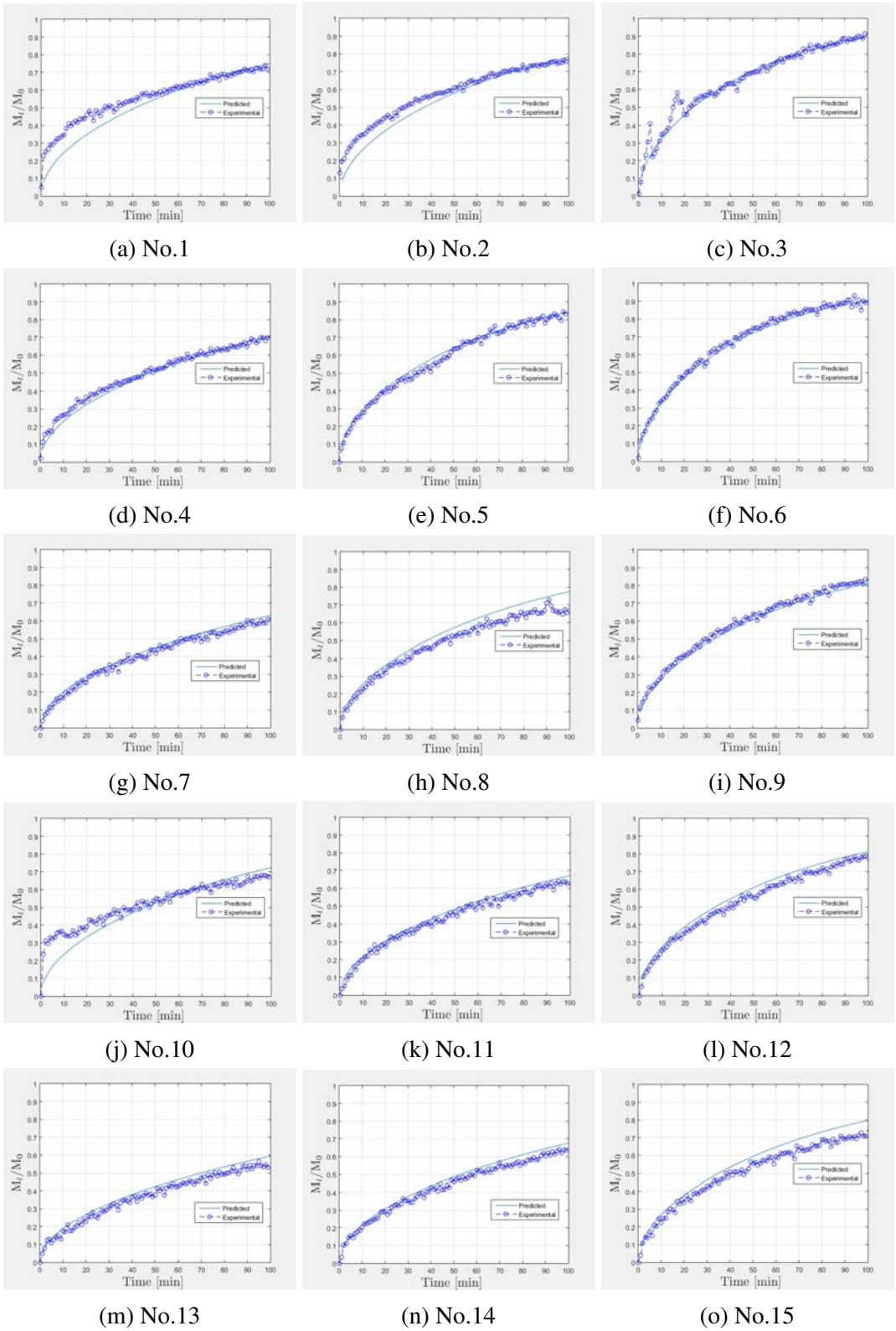

(a) No.1 (b) No.2 (c) No.3

(d) No.4 (e) No.5 (f) No.6

(g) No.7 (h) No.8 (i) No.9

(j) No.10 (k) No.11 (l) No.12

(m) No.13 (n) No.14 (o) No.15

Fig. C.5 Predicted and experimental release curves of SPAN 80 systems. Part (1/2).

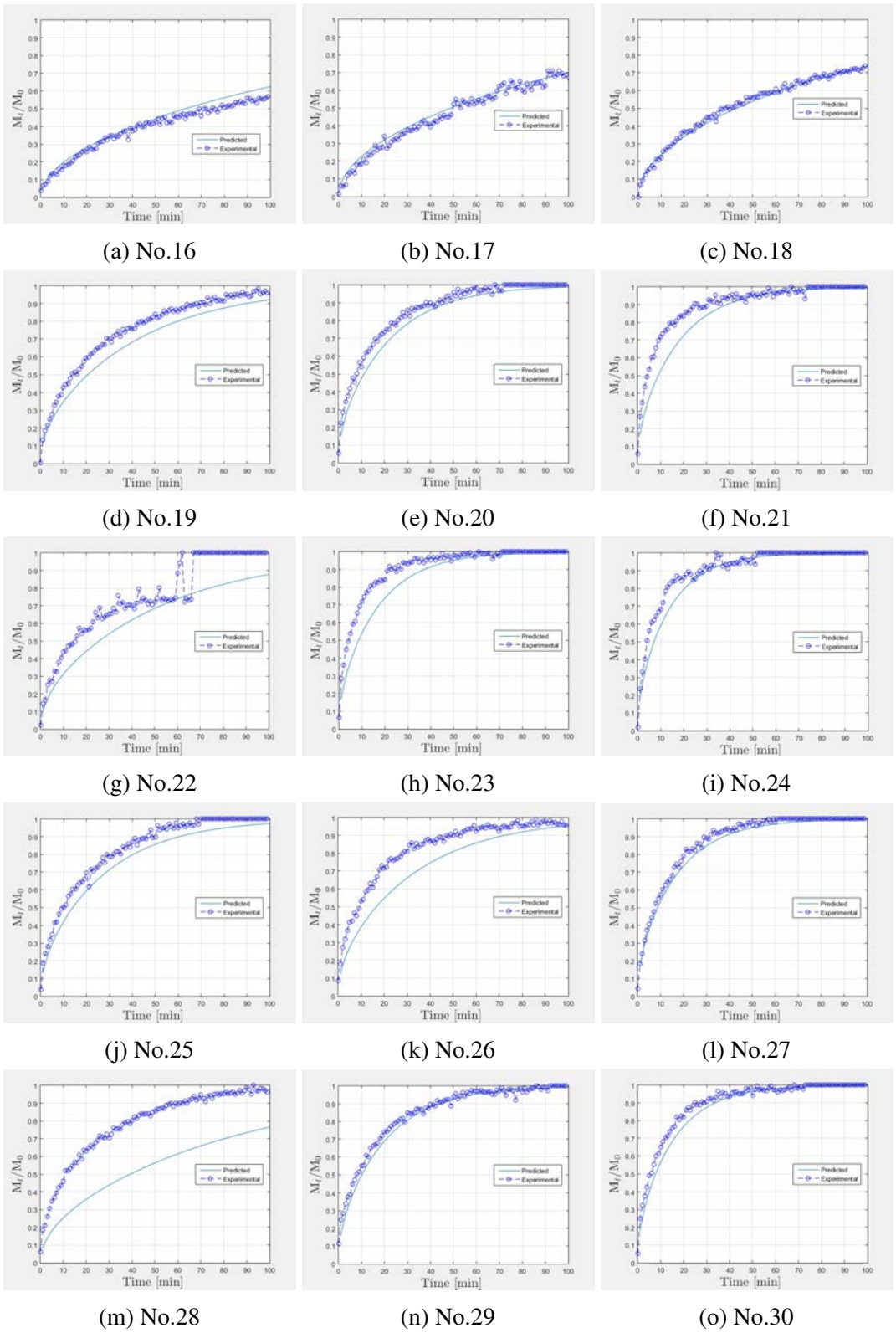

(a) No.16 (b) No.17 (c) No.18

(d) No.19 (e) No.20 (f) No.21

(g) No.22 (h) No.23 (i) No.24

(j) No.25 (k) No.26 (l) No.27

(m) No.28 (n) No.29 (o) No.30

Fig. C.6 Predicted and experimental release curves of SPAN 80 systems. Part (2/2).

Table C.5 Characterization of PGPR emulsions for release experiments.

No.	Oil	ϕ_m	$r_{o/s}$	$D_{droplet}$	G'_{before}	G'_{after}	D (pred.)	D (exp.)	ε
31	D	0.89	1.00	9.60	3730	5170	2.92E-10	2.05E-10	42.83
32	D	0.90	2.53	9.79	1106	1246	2.53E-10	2.63E-10	-3.64
33	D	0.90	4.89	10.47	289	337	2.05E-10	2.27E-10	-9.88
34	D	0.92	1.00	9.76	3259	4020	2.20E-10	1.96E-10	12.34
35	D	0.92	2.36	11.28	2189	2631	1.93E-10	2.28E-10	-15.34
36	D	0.92	5.09	14.13	644	771	1.57E-10	1.72E-10	-8.72
37	D	0.95	1.18	10.22	5565	6943	1.63E-10	1.33E-10	22.05
38	D	0.95	2.90	13.44	2527	2438	1.32E-10	1.13E-10	16.33
39	D	0.95	5.32	18.32	1281	1504	1.06E-10	1.45E-10	-26.81
40	H	0.90	1.00	9.30	3766	4272	2.02E-10	1.70E-10	18.79
41	H	0.90	2.57	9.30	2566	3110	2.09E-10	1.55E-10	34.86
42	H	0.90	4.71	8.99	1060	1227	1.90E-10	2.11E-10	-9.84
43	H	0.92	1.04	10.53	5221	6483	1.54E-10	1.09E-10	41.44
44	H	0.92	2.55	11.00	5166	3023	1.61E-10	1.08E-10	49.08
45	H	0.92	4.92	11.81	1525	1989	1.42E-10	1.08E-10	31.52
46	H	0.95	0.99	11.56	1591	1191	1.07E-10	1.49E-10	-28.29
47	H	0.95	2.68	12.87	3609	3804	1.07E-10	1.44E-10	-25.66
48	H	0.95	4.69	14.37	2334	2788	9.54E-11	1.10E-10	-13.02
49	M	0.90	1.01	9.37	4432	5352	1.46E-10	1.84E-10	-20.58
50	M	0.88	2.60	8.86	3305	4000	2.31E-10	3.13E-10	-26.15
51	M	0.87	4.84	8.08	1483	1486	2.37E-10	2.80E-10	-15.25
52	M	0.91	1.02	9.39	6033	7379	1.44E-10	2.46E-10	-41.44
53	M	0.92	2.35	10.33	3725	4110	1.55E-10	2.09E-10	-25.92
54	M	0.92	5.13	11.86	2615	2244	1.52E-10	2.18E-10	-29.93
55	P	0.90	0.99	9.59	4199	4391	9.22E-11	1.35E-10	-31.59
56	P	0.90	2.60	10.12	3650	3903	1.22E-10	6.79E-11	79.42
57	P	0.90	4.75	10.68	2734	3174	1.21E-10	2.62E-10	-53.65
58	P	0.93	1.00	11.47	3354	3185	7.10E-11	1.32E-10	-46.01
59	P	0.93	2.55	11.63	6204	4477	9.38E-11	3.29E-10	-71.47
60	P	0.93	5.15	12.02	2722	2578	8.99E-11	2.12E-10	-57.56

NOTES

-D=dodecane; H=hexadecane; M=myristate; P=palmitate; S=SPAN 80.

ϕ_m=dispersed phase mass fraction [adim.]; $r_{o/s}$=oil/surfactant ratio $m_{oil}/m_{surf.}$ [adim.]; $D_{droplet}$=droplet diameter [μm]; G'=storage moduli before or after experiment [Pa]; D=fitted diffusion coefficients for predicted (pred.) or experimental (exp.) curves [m^2/s]; and ε=relative error between D (pred.) and D (exp.).

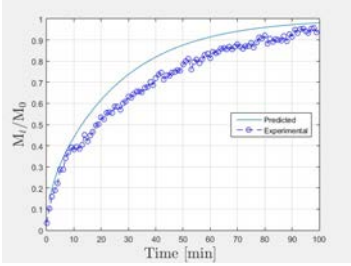

(a) No.31

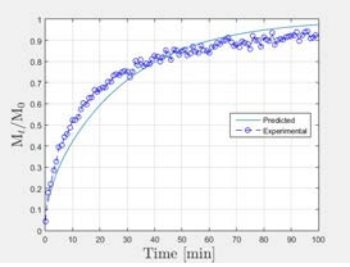

(b) No.32

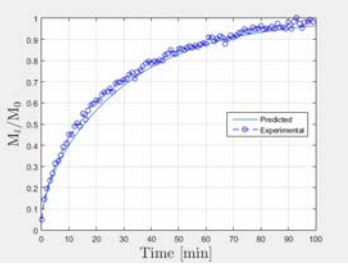

(c) No.33

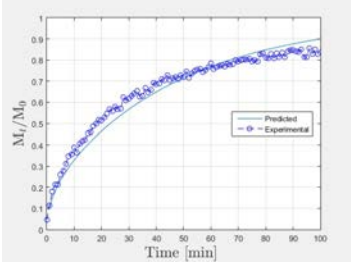

(d) No.34

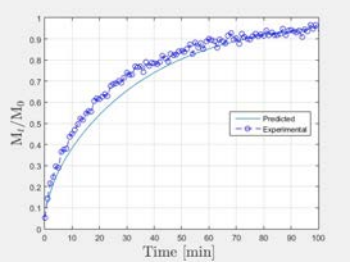

(e) No.35

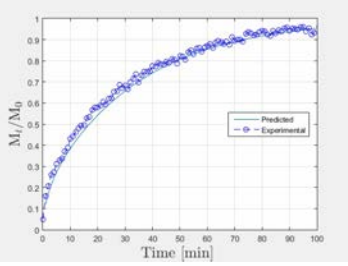

(f) No.36

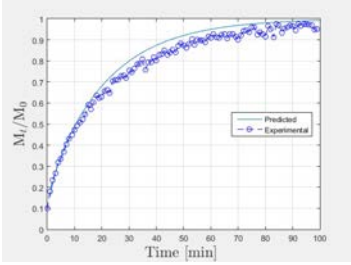

(g) No.37

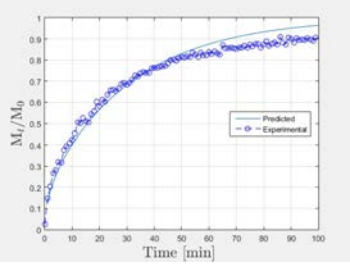

(h) No.38

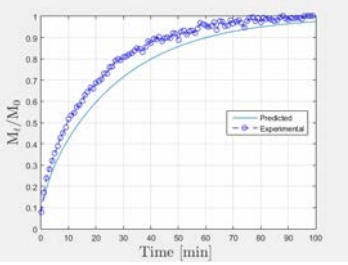

(i) No.39

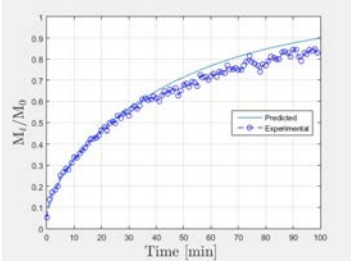

(j) No.40

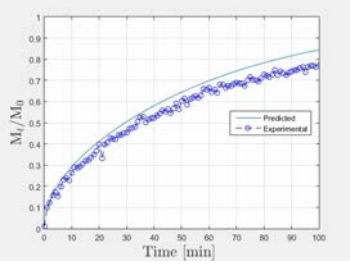

(k) No.41

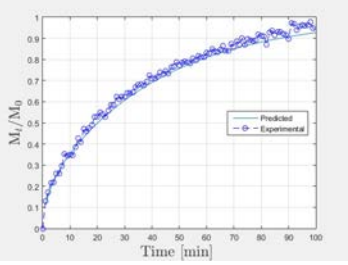

(l) No.42

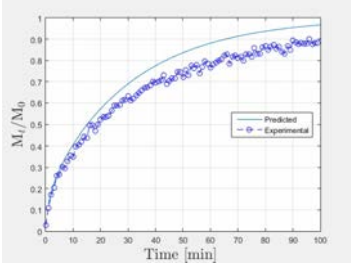

(m) No.43

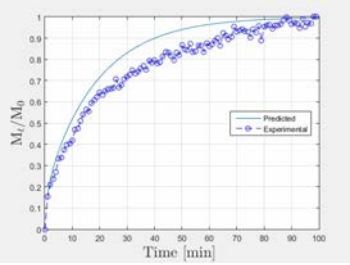

(n) No.44

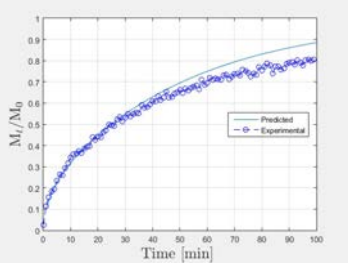

(o) No.45

Fig. C.7 Predicted and experimental release curves of PGPR systems. Part (1/2).

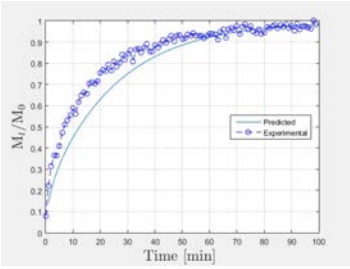

(a) No.46

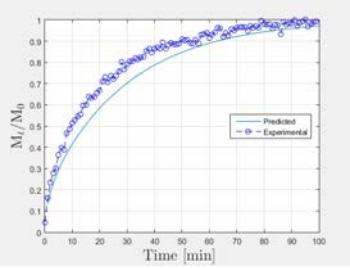

(b) No.47

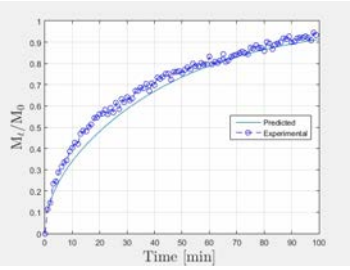

(c) No.48

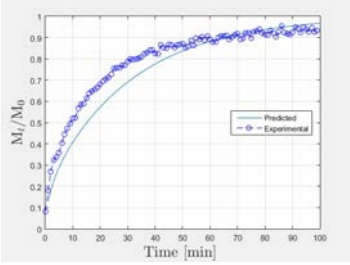

(d) No.49

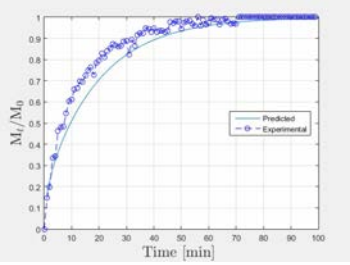

(e) No.50

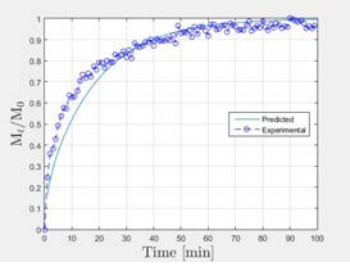

(f) No.51

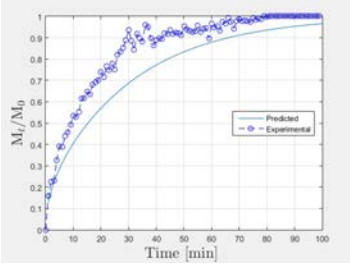

(g) No.52

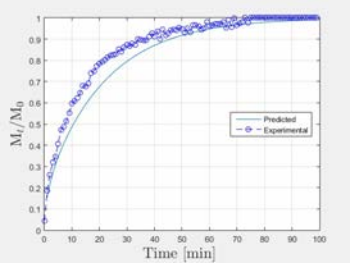

(h) No.53

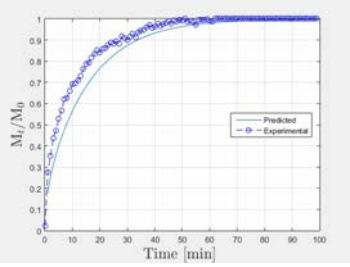

(i) No.54

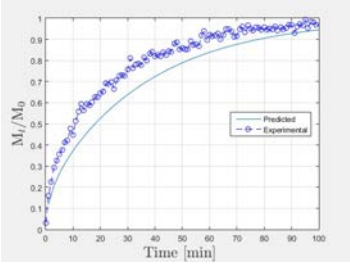

(j) No.55

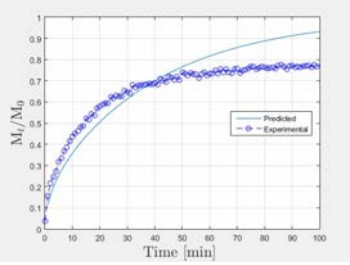

(k) No.56

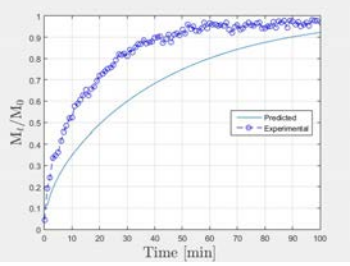

(l) No.57

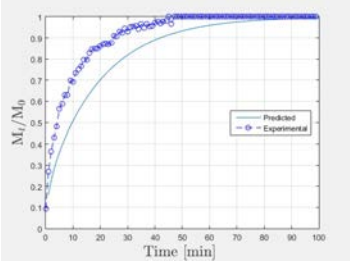

(m) No.58

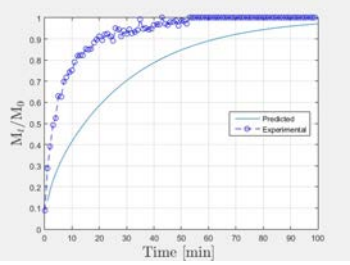

(n) No.59

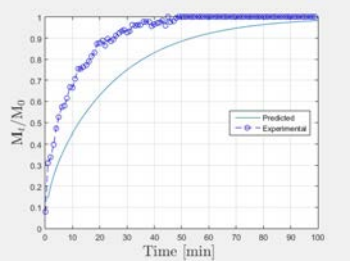

(o) No.60

Fig. C.8 Predicted and experimental release curves of PGPR systems. Part (2/2).

Table C.6 Characterization of BRIJ 93 emulsions for release experiments.

No.	Oil	ϕ_m	$r_{o/s}$	$D_{droplet}$	G'_{before}	G'_{after}	D (pred.)	D (exp.)	ε
61	D	0.90	1.00	11.60	1032	1093	2.26E-10	2.24E-10	0.52
62	D	0.91	2.48	11.50	468	517	2.00E-10	1.97E-10	1.78
63	D	0.90	5.01	10.91	212	453	1.78E-10	2.24E-10	-20.51
64	D	0.93	1.01	12.40	938	1421	1.78E-10	2.47E-10	-27.75
65	D	0.93	2.36	13.30	543	808	1.54E-10	2.23E-10	-30.81
66	D	0.93	5.18	14.63	272	562	1.35E-10	1.67E-10	-18.80
67	D	0.95	0.99	13.29	1778	2593	1.20E-10	1.88E-10	-36.19
68	D	0.95	2.60	15.28	1054	1297	1.04E-10	1.47E-10	-29.06
69	D	0.95	5.18	18.57	538	239	8.91E-11	1.62E-10	-44.92
70	H	0.93	0.98	12.41	1712	1609	1.55E-10	1.55E-10	0.09
71	H	0.91	2.50	9.88	802	1129	1.81E-10	1.82E-10	-0.28
72	H	0.91	5.00	10.07	385	670	1.62E-10	2.08E-10	-21.90
73	H	0.93	1.02	12.74	1662	1229	1.51E-10	2.07E-10	-27.28
74	H	0.93	2.41	13.75	1083	1926	1.36E-10	2.52E-10	-45.90
75	H	0.93	4.84	14.21	693	1142	1.27E-10	1.95E-10	-34.78
76	H	0.95	1.02	15.79	1720	1029	1.05E-10	9.20E-11	13.95
77	H	0.95	2.79	16.07	1012	1436	1.08E-10	1.55E-10	-30.09
78	H	0.95	5.13	19.22	401	371	8.33E-11	2.24E-10	-62.82
79	M	0.90	1.00	12.04	1162	1158	1.82E-10	2.42E-10	-25.07
80	M	0.89	2.45	11.70	935	1073	1.94E-10	2.67E-10	-27.49
81	M	0.90	5.12	11.69	949	1045	1.86E-10	2.71E-10	-31.46
82	M	0.92	1.01	14.44	1313	1468	1.42E-10	2.34E-10	-39.24
83	M	0.93	2.43	15.33	1457	1322	1.42E-10	1.87E-10	-23.92
84	P	0.90	1.00	13.66	1486	1546	1.35E-10	1.72E-10	-21.62
85	P	0.90	2.50	14.85	665	987	1.29E-10	1.96E-10	-34.45
86	P	0.90	5.22	16.72	970	1045	1.20E-10	2.07E-10	-42.06
87	P	0.93	0.99	16.47	1187	1188	1.04E-10	1.34E-10	-22.39
88	P	0.92	2.38	16.36	822	937	1.10E-10	1.83E-10	-39.98

NOTES

-D=dodecane; H=hexadecane; M=myristate; P=palmitate; S=SPAN 80.

ϕ_m=dispersed phase mass fraction [adim.]; $r_{o/s}$=oil/surfactant ratio $m_{oil}/m_{surf.}$ [adim.]; $D_{droplet}$=droplet diameter [μm]; G'=storage moduli before or after experiment [Pa]; D=fitted diffusion coefficients for predicted (pred.) or experimental (exp.) curves [m^2/s]; and ε=relative error between D (pred.) and D (exp.).

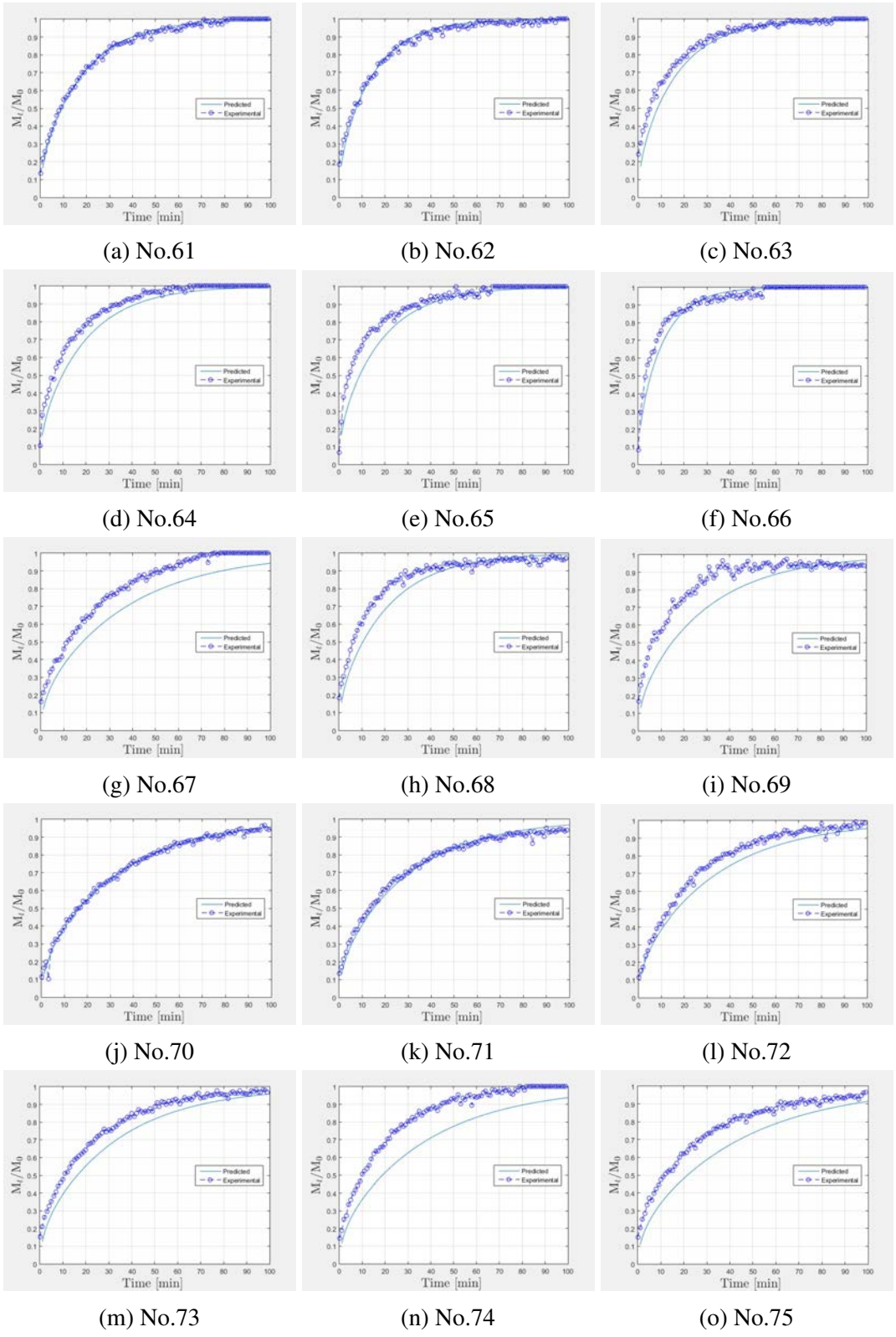

(a) No.61 (b) No.62 (c) No.63

(d) No.64 (e) No.65 (f) No.66

(g) No.67 (h) No.68 (i) No.69

(j) No.70 (k) No.71 (l) No.72

(m) No.73 (n) No.74 (o) No.75

Fig. C.9 Predicted and experimental release curves of BRIJ 93 systems. Part (1/2).

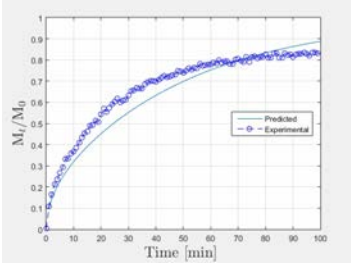

(a) No.76

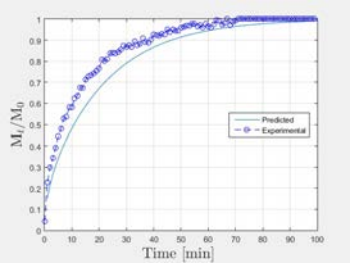

(b) No.77

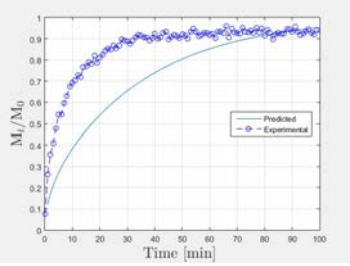

(c) No.78

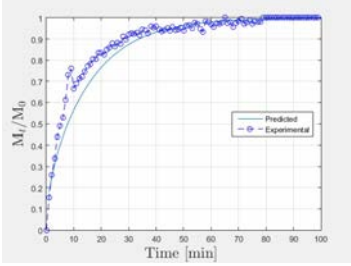

(d) No.79

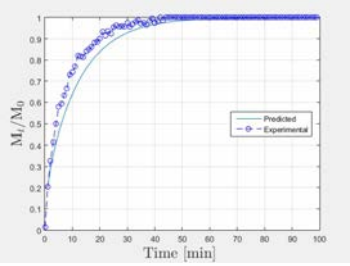

(e) No.80

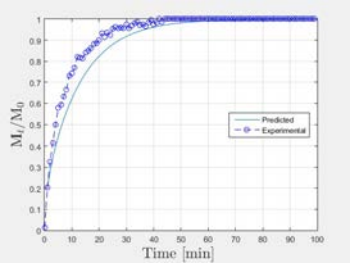

(f) No.81

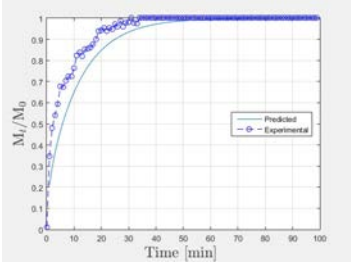

(g) No.82

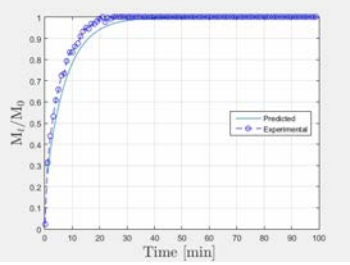

(h) No.83

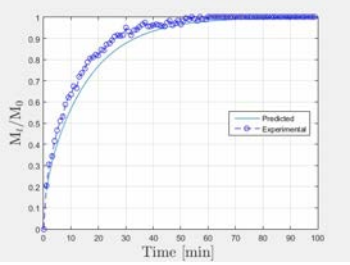

(i) No.84

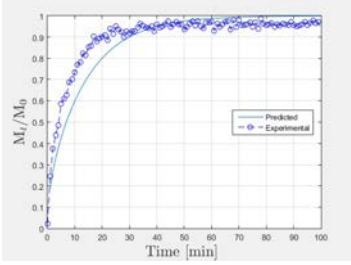

(j) No.85

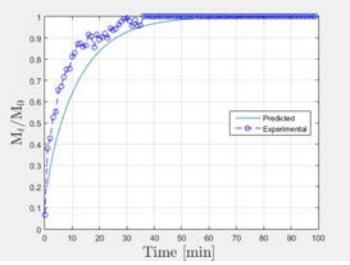

(k) No.86

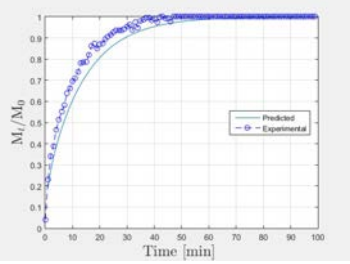

(l) No.87

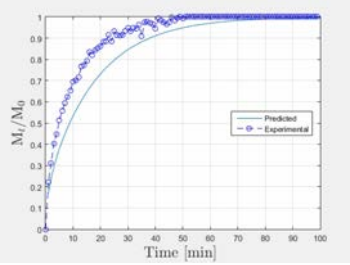

(m) No.88

Fig. C.10 Predicted and experimental release curves of BRIJ 93 systems. Part (2/2).

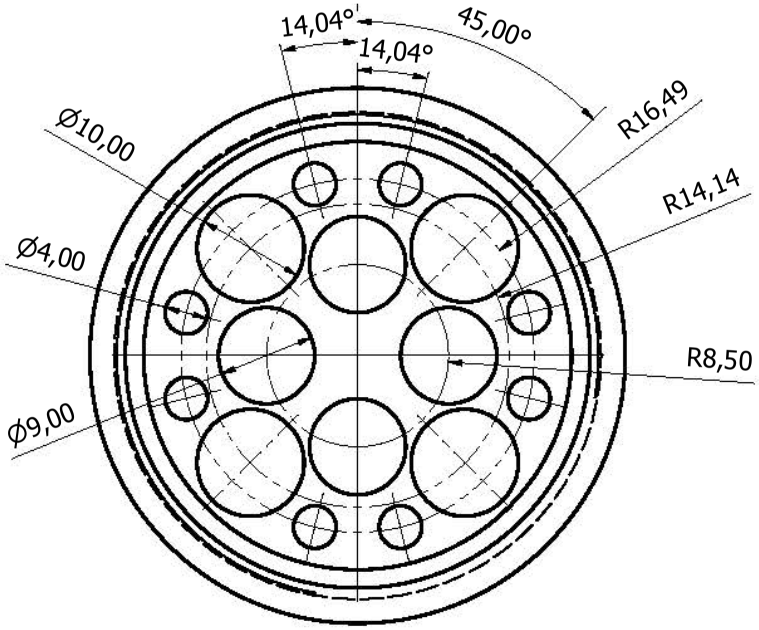

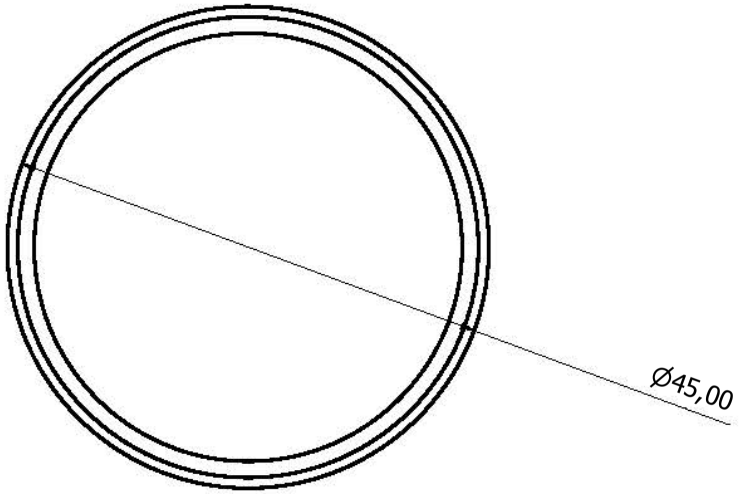

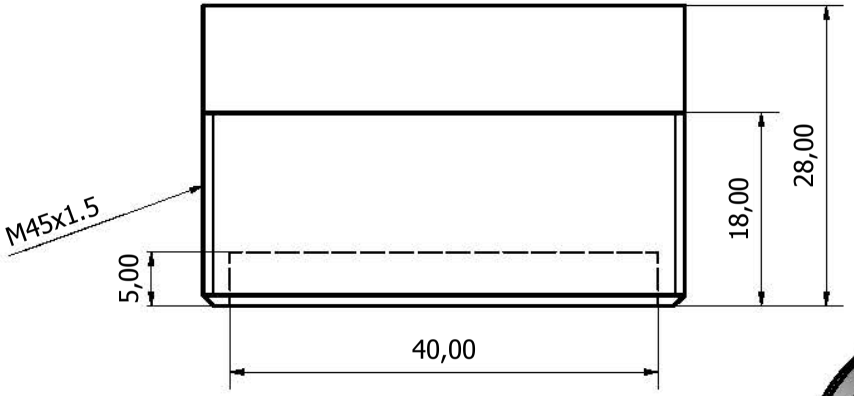

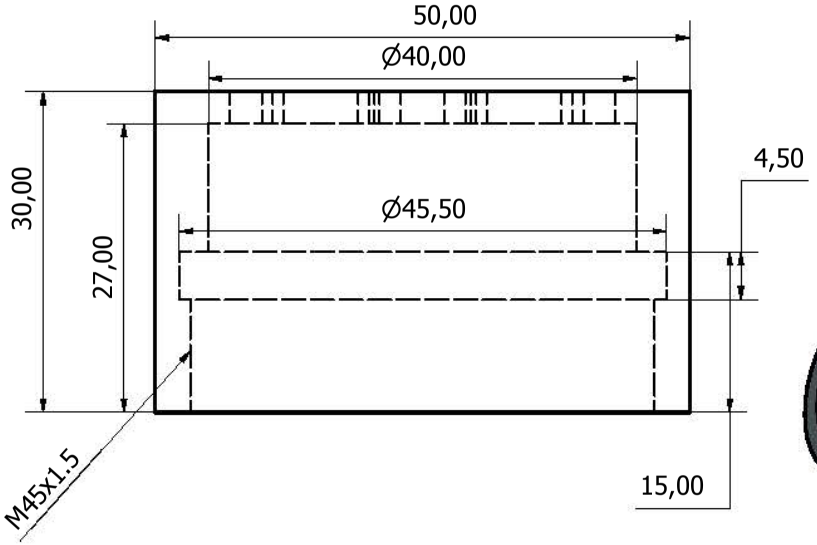

Conçu par	Vérifié par	Approuvé par	Date		Date	
Charly Koenig					13/09/2016	

4 couples en PTFE	Pot assemblé			
			Modification	Feuille 1 / 1

Transfert de matière dans les milieux complexes. Ingénierie inverse: de la propriété d'usage au matériau

Mots clés: Ingénierie inverse, emulsion hautement concentrée, diffusion, rhéologie.

Au cours de la dernière décennie, l'utilisation croissante de nombreuses nouvelles technologies comme des systèmes de livraison contrôlée a incité un développement empirique coûteux de systèmes nouveaux et efficaces. Pour faciliter une conception plus raisonnable et une optimisation, faisant face à l'ensemble de possibilités existantes, n'importe quelle solution qui pourrait semiautomatiser le développement de produits apporteraient l'aide précieuse aux utilisateurs (des scientifiques de formulation et des éducateurs). Ceci faciliterait l'importance essentielle de choisir les matériels justes pour l'application correcte. Dans cette thèse, un projet à long terme concernant une génie inverse est proposé, commençant d'une propriété d'utilisation finale (libération contrôlée), la cible mondiale est de développer une méthodologie de conception de produit qui nous permet de déterminer les caractéristiques optimales d'une formulation à préparer: les phases, la composition, le type d'interface, la taille et la distribution d'objets actuels, l'équilibre de phase, la diffusion dans des phases et le caractère évolutionnaire du matériel. Dans la considération d'un exemple de commodité de système structuré et dispersé: des émulsions fortement concentrées, le problème de design a été décomposé dans un ordre hierachical de sous-problèmes ou des boîtes, combinant les modèles constitutifs qui évaluent le transport de masse de principe actif comme une fonction de paramètres de formulation et des techniques assistées par ordinateur comme la modélisation moléculaire pour le volume/surface de molécules, ou des modèles d'UNIFAC pour des prédictions d'équilibre aussi bien que pour des évaluations de viscosités de mélange. Un ultérieur design de factoriel d'expériences virtuelles a permis d'obtenir une description quantitative de la sortie selon les paramètres modèles et une analyse composante principale a évalué l'importance des variables. En utilisant une cartographie basée sur trois tensio-actifs (pour SPAN 80, PGPR et BRIJ 93), quatre huiles (dodecane, hexadecane, isopropyl myristate et isopropyl palmitate) et l'acide mandelic comme le principe actif, le modèle ab initio physicochimique a été expérimentalement validé. Les résultats montrent que le modèle mécaniste systématiquement prévoit la diffusion du principe actif d'émulsions à un moyen récepteur dans des parfaites 'sink' conditions. Cette approche de génie inverse a montré pour être d'intérêt très élevé dans le domaine de formulation en permettant des études préliminaires examinantes rapides et robustes sur une large gamme de composants aussi bien que des outils de prédiction précis et rigoureux optimiser la sortie contrôlée d'un système identifié. On cela recommande entièrement de mettre en œuvre ses extensions à d'autre semblable systèmes.

Mass transfer within complex media. Reverse Engineering: From usage property to material

Keywords: Reverse engineering, highly concentrated emulsion, diffusion, rheology

In the past decade, the growing use of numerous novel technologies as controlled-delivery systems has prompted a costly trial-and-error development of new and effective systems. In order to facilitate a more rational design and optimization, facing the set of existing possibilities, any solution that could semiautomate the product development would bring precious help to the users (formulation scientists and educators). This would facilitate the essential importance of choosing the right materials for the correct application. In this thesis, a long-term project concerning a reverse engineering is proposed, starting from a final usage property (controlled release), the global target is to develop a product design methodology which allows us to determine the optimal features of a formulation to prepare: phases in presence, composition, interface type, size and distribution of current objects, phase equilibrium, diffusion within phases and evolutionary character of the material. Considering a convenience example of structured-dispersed system: highly concentrated emulsions, the design problem has been decomposed into a hierarchical sequence of subproblems or boxes, combining constitutive models that estimate the active ingredient mass transport as a function of formulation parameters and computer-aided techniques such as molecular modeling for volume/area of molecules, or UNIFAC models for equilibria predictions as well as for mixture viscosities estimations. A subsequent full factorial design of virtual experiments has allowed to obtain a quantitative description of the release depending on the model parameters, and a principal component analysis has assessed the importance of the variables. Using a cartography focused on three surfactants (SPAN 80, PGPR and BRIJ 93), four oils (dodecane, hexadecane, isopropyl myristate and isopropyl palmitate) and mandelic acid as an active ingredient, the ab-initio physicochemical model has been experimentally validated. Results show that the mechanistic model consistently predicts the diffusion of the active ingredient from emulsions to a release medium in perfect sink conditions. This reverse engineering approach is showing to be of very high interest in the domain of formulation by allowing fast and robust screening preliminary studies on a broad range of components as well as precise and rigorous prediction tools to optimize controlled release from an identified system. It is fully recommended to implement its extensions to other similar disperse systems.